Earth-Science Reviews
April 2022, Volume 227, Pages 103960 (56p.)
https://doi.org/10.1016/j.earscirev.2022.103960
https://archimer.ifremer.fr/doc/00751/86342/

Persistent Holocene outflow from the Black Sea to the eastern Mediterranean Sea still contradicts the Noah's Flood Hypothesis: A review of 1997–2021 evidence and a regional paleoceanographic synthesis for the latest Pleistocene–Holocene

Aksu A.E. [1,*], Hiscott R.N. [1]

[1] Department of Earth Sciences, Memorial University of Newfoundland, St. John's, NL A1B 3X5, Canada

* Corresponding author : A. E. Aksu, email address : aaksu@mun.ca

Abstract :

This review and synthesis weaves various multiproxy data into a single coherent narrative for the latest Pleistocene–Holocene paleoclimatic and paleoceanographic evolution of the Black Sea, Marmara Sea and the Aegean Sea. This narrative, referred to as the “Outflow Hypothesis” rests on several key observations and interpretations which are incompatible with the suggestion that the post-LGM reconnection of the Black Sea basin to the global ocean occurred as a catastrophic flood. The widespread occurrence of sub-storm-wavebase uppermost Pleistocene to lower Holocene sediments across the southwestern Black Sea shelf at elevations as shallow as −78 m shows that the level of the Neoeuxine Lake (today's Black Sea) between 12.3 cal ka and 9.5 cal ka was high enough to spill outward into the Marmara Sea over the shallow sill in the southern Strait of Bosphorus (−37 m today). Southwest-prograded clinoforms immediately south of the strait in the northeastern Marmara Sea record the development of an early Holocene (11.1–10.2 cal ka) mid-shelf delta (Δ1) showing ~3.3 km of aggressive progradation while its topset-to-foreset break climbed 8–9 m into a rising Marmara Sea. A streamlined south-prograded barform in the throat of the strait and giant megaflutes along its thalweg confirm the vigorous outflow from the early Holocene Neoeuxine Lake required to explain the climbing Δ1 lobe. Multiproxy data from the northeastern Marmara Sea and southwestern Black Sea shelves indicate that the post-Last Glacial Maximum (LGM) reconnection of the Black Sea with the eastern Mediterranean occurred in a gradual fashion: first, at ~10.2 cal ka, a salt wedge lifted the brackish outflow off the floor of the Strait of Bosphorus terminating Δ1 progradation; second, a more persistent density underflow introduced enough seawater strontium into the Black Sea to be taken up in mollusc shells by ~9.5 cal ka, and finally a range of euryhaline marine organisms replaced lacustrine faunas when salinity levels became favourable by ~7.5 cal ka. The onset of sapropel M1 deposition across the Marmara Sea followed the breach of the Strait of Dardanelles at 13.8 cal ka when, as originally suggested by other researchers, nutrient-rich highly saline Mediterranean waters forced lower density relict lacustrine waters to the surface and then out through the Strait of Dardanelles, initiating water-column stratification. Once the low-salinity cap was expelled, the deep waters of the fully saline Marmara Sea remained stagnant and sapropel accumulation continued. The onset of outflow from the Neoeuxine Lake at 11.1 cal ka re-established water-column stratification, induced effective deep circulation across the Marmara Sea, and created a low salinity lid across the northern Aegean Sea, initiating sapropel S1 deposition in that area.

Keywords : Bosphorus, Dardanelles, Marmara Sea, Strontium isotopes, Seismic stratigraphy, Unconformities, Density currents, Deltas, Sapropel, Catastophism

Table of Contents

1. Introduction

It has been a quarter century since geoscientists working in the eastern Mediterranean region had their core beliefs upended by a claim that the Black Sea was catastrophically inundated by marine waters in the early Holocene, rising 80–100 m in just a few years and driving Neolithic farming communities from their homes. The perceived importance of this novel hypothesis was so great that the original peer-reviewed article (Ryan et al., 1997) was accepted for publication in *Marine Geology* the day after it was received. A comprehensive book written for the general public and published one year later (Ryan and Pitman, 1998) received considerable media coverage, giving this hypothesis wide visibility. In an episode of the prestigious *Horizon* program on UK television (BBC, 1996), Walter Pitman explained how he and William Ryan focussed their attention on the Black Sea (Persian Gulf and Red Sea were also considered) in the search for a factual basis for the Gilgamesh and Noah's flood stories;

hence, their quest apparently grew from a suspicion that these flood myths had a geological explanation in the Middle East, and data were sought to support what has become known as the Flood Hypothesis. These original two publications greatly stimulated paleoceanographic and paleoclimatic research in the late 1990's across the waterways that connect the Black Sea with the global ocean through two narrow and shallow straits (Dardanelles and Bosphorus) and the intervening Marmara Sea, named the Marmara Sea Gateway by Aksu et al. (1999a). A large number of subsequent publications ensued, some supporting (e.g., Ballard et al., 2000; Çağatay et al., 2000, 2003, 2009; Algan et al., 2001, 2007; Ryan et al., 2003; Sperling et al., 2003; Dimitrov, 2003; Dimitrov and Dimitrov, 2004; Gökaşan et al., 2005a; Eriş et al., 2007, 2008; Lericolais et al., 2007a,b, 2009, 2010, 2011, 2019; Goldberg et al., 2016; Herrle et al., 2018; Yanchilina et al., 2017, 2019;) others contradicting (e.g., Aksu et al., 1999a,b, 2002a,b,c, 2016; Mudie et al., 2001, 2002a,b, 2004, 2007; Hiscott et al., 2002, 2007a,b, 2008, 2017, 2021; Marret et al., 2009; Yanko-Hombach et al., 2011; Bradley et al., 2011, 2012; Mertens et al., 2012; Lister et al., 2015; Constantinescu et al. (2015); Ankindinova et al., 2019a,b, 2020) the views expressed in the 1997 article and 1998 book.

Many former USSR, Russian and Ukrainian geoscientists, both before and after the promulgation of the Flood Hypothesis, have maintained that post-LGM base-level rise in the Black Sea basin (then occupied by the Neoeuxine Lake) was gradual and progressive, albeit with minor fluctuations (Chepalyga, 1984; Kuprin and Sorokin, 2007; Shmuratko, 2007; Shuisky, 2007; Konikov, 2007; Balabanov, 2007). These workers advocated that the rise of the Neoeuxine Lake level led to an out-spilling through the Strait of Bosphorus by the end of the Pleistocene, well before marine waters penetrating northward from the Aegean Sea and across the Marmara Sea were able to overtop the ~ –37 m sill at the southern end of the that strait, thereby gaining entry into the Black Sea basin. Several workers associated this out-spilling with an influx of glacial meltwaters into the Caspian Sea during the latest Pleistocene which then spilled into the Neoeuxine Lake via the Manych–Kerch Strait (e.g., Chepalyga, 2007; Badertscher et al., 2011; Aksu et al., 2016; Hiscott et al., 2017; Fig. 1a).

The Flood Hypothesis has been well described in reviews and extended articles since it was initially advanced (Ryan et al., 2003; Ryan, 2007; Lericolais et al., 2011; Yanchilina et al., 2017). As counterpoint, the objective of this article is to provide a comprehensive review of the seismic and core-based evidence for the persistent outflow from the Black Sea basin to the global ocean through the Marmara Sea Gateway during the entire Holocene, as first proposed by Aksu et al. (2002a) and Hiscott et al. (2002) and supported by studies in the southwestern and western Black Sea and across the Marmara Sea over the following two decades (Aksu et al., 2002a,b, 2016; Mudie et al., 2002a,b, 2004, 2007; Abrajano et al., 2002; Kaminski et al., 2002; Hiscott et al., 2002, 2007a,b, 2017, 2021; Giosan et al., 2009; Constantinescu et al., 2015; Ankindinova et al., 2020). Aksu et al. (2002c) called this the Outflow Hypothesis. This review also sythesises evidence from a number of sources and methodologies in order to address three more specific objectives: (1) to demonstrate that the Neoeuxine Lake had transgressed its lowstand shelves by the earliest Holocene and had started to spill into the Marmara Sea by ~11 cal ka, (2) to confirm that, coincident with this out-spilling, a climbing delta developed at the southern exit of the Strait of Bosphorus into the Marmara Sea and water-column stratification intensified to maintain seabed dysoxia and sapropel accumulation (M1 sapropel) in Marmara Sea, and (3) to show that downstream freshening of surface waters in the Aegean Sea also tracked the outflow (including S1 sapropel development). Objective 1 is a prerequisite for objectives 2 and 3, because direct riverine supply to the Marmara Sea is miniscule (Hiscott et al., 2021) compared with the volume supplied indirectly via the Strait of Bosphorus from major rivers entering the Black Sea basin (e.g., Danube, Dniester, Dnieper, Don, Kamchiya, Kızılırmak, Sakarya, Yeşilırmak; Fig. 1a). There not only is evidence from each sea to contradict the Flood Hypothesis, but the evidence in favour of the Outflow Hypothesis forms a single coherent story and timeline all along the gateway and its environs. In a final section of this review, we present a regional synthesis of the latest Pleistocene–Holocene paleoceanographic evolution of the gateway using maps depicting six geologically critical time slices. Events of the youngest period (i.e., transgression of shelves of the Black Sea) are critical to studies of habitation and human settlement in the region; this aspect has been the focus of IGCP Project 610 "From the Caspian to Mediterranean: Environmental Change and Human Response during the Quaternary".

The chronostratigraphy of strata imaged in high-resolution seismic reflection profiles is established in this review using 149 radiocarbon dates acquired in 24 key cores (Tables 1, 2), supplemented by six radiocarbon dates reported by Eriş et al. (2007). The chronology of sapropel S1 in the Aegean Sea is established using the age of the Z2 tephra associated with the Minoan eruption, at 3.37 ^{14}C ka (Pichler and Friederich, 1976) or 3.6 cal ka, and a further five radiocarbon dates in five cores (Tables 1, 2).

2. Regional setting

2.1. Morphology

The Marmara Sea Gateway consists of two prominent narrow and shallow straits and the intervening deep landlocked Marmara Sea (Fig. 1). The Strait of Bosphorus in the north (also known as İstanbul Boğazı in Turkish) is a very narrow naturally occurring channel which links the southwestern Black Sea with the northeastern Marmara Sea (Fig. 2). The strait is ~31 km long, 700–3400 m wide with maximum depth >110 m. The present-day sill occurs at ~ –37 m toward the southern end of the strait (Fig. 2). Channels extend basinward at each exit of the strait: (a) a prominent U-shaped, 50–60 m-deep channel extending northeastward onto the southwestern Black Sea shelf (referred to as the Saline Channel; Flood et al., 2009; Hiscott et al., 2013; Ankindinova et al., 2020) and (b) a V-shaped 50–80 m-deep channel extending south-southwest onto the northeastern Marmara Sea shelf, referred to in this review as the NE Marmara Channel (Fig. 2).

The Marmara Sea is a small (80 km × 270 km) east–west-elongated landlocked water body situated between southeastern Thrace and northwestern Anatolia (Fig. 3). The northern shelf is narrow (2–15 km), whereas the southern shelf is wider (35–50 km). The shelf-to-slope break occurs between –90 m and –110 m, from which 10º–15º slopes lead to deep basins between –1100 m and –1370 m. The four deep basins (Tekirdağ, Central, Kumburgaz, Çınarcık; Fig. 3) are separated from one another by NE–SW-trending ridges which stand 400–600 m above basin floors. A fifth basin (İmralı) is perched at shallower depths on the southeastern slope (Fig. 3).

The Strait of Dardanelles in the southwest (also known as the Çanakkale Boğazı in Turkish) is ~61 km long and 1.2–6 km wide with water depths ranging from 63–103 m. A present-day sill occurs at –63 m toward the northeastern end of the strait (Fig. 4; Aksu et al., 2016). The deeper central channel of this strait flares out toward the northeast, linking with the Şarköy Canyon in western Marmara Sea (Fig. 4). A 80–90 m-deep channel in the northeastern Aegean Sea connects to the Strait of Dardanelles at its western terminus and then takes a sharp ~90º clockwise turn, continuing NNE toward the Gulf of Saros and tightly hugging the southwestern margin of the Gallipoli Peninsula (Fig. 4).

2.2. Physical Oceanography

The physical oceanography of the modern gateway is largely controlled by the prevailing climatic conditions across the Black Sea. Precipitation at sea (P, ~300 km^3 yr^{-1}) and large freshwater input by several major rivers (R, ~350 km^3 yr^{-1}) compared with evaporative losses over the Black Sea (E, ~350 km^3 yr^{-1}) create a net water export (ΔV=R+P–E) of ~300 km^3 yr^{-1} from the Black Sea into the Aegean Sea through the gateway (Özsoy et al., 1995; Oğuz et al., 2004). The Danube, Dniester, Dnieper, Southern Bug and Don are the rivers draining into the Black Sea from the north and northwest, with the Kamchiya, Kızılırmak, Sakarya and Yeşilırmak Rivers supplying smaller quantities of freshwater primarily from the south and southwest (Fig. 1). Peak river discharges occur during the northern hemispheric spring, and the narrow constriction at the Strait of Bosphorus forces the level of the Black Sea to fluctuate ~50 cm in perfect synchroneity with the variations in seasonal and interannual river discharges (Özsoy et al., 1995, 1996). Satellite altimetry shows that the surface of the Black Sea is on average ~40 cm above the level of the Marmara Sea which, in turn, is ~30 cm above the level of the northern Aegean Sea.

The water exchange between the Black Sea and the eastern Mediterranean Sea occurs through the Marmara Sea Gateway as a two-layer flow (Fig. 5; Latif et al., 1992; Özsoy et al., 1995; Polat and Tuğrul, 1996). The cooler (5–15ºC) and lower salinity (17–20 psu – hereafter without units) surface layer originating from the Black Sea flows south-southwest at 10–30 cm s^{-1}. This watermass forms the 25–100 m-thick surface layer in the Black Sea, the Marmara Sea and the northeastern Aegean Sea. Warmer (15–20ºC) and high-salinity (38–39) Mediterranean water flows north along the eastern Aegean Sea, hugging the western Anatolian coastline (Fig. 5). This water mass plunges beneath the low-salinity surface layer (i.e., the Black Sea outflow) in the northeastern Aegean Sea immediately west of the mouth of the Strait of Dardanelles and penetrates the strait flowing northeast at 5–25 cm s^{-1}. As this water mass enters the Marmara Sea, it forms turbulent plumes which sink beneath the halocline and slowly descend into the deeper Marmara basins (Fig. 5). There are two branches of the Mediterranean watermass: (a) a shallow subsurface flow occurs at 50–100 m depth, hugging the northern margin of the Marmara Sea and flowing east and (b) a deeper flow occupies 100–500 m depth flowing along the southern margin of the Marmara Sea (Fig. 5; Beşiktepe et al., 1994). The Mediterranean watermass occupies the entire Marmara Sea below a 20–50 m-thick low-salinity surface layer. Across the northeastern sector of the Marmara Sea, this watermass penetrates the Strait of Bosphorus and flows north at 5–15 cm s^{-1}. It penetrates into the Black Sea and spreads across the southwestern shelf immediately north and west of the Strait of Bosphorus via the Saline Channel (Fig. 5; Di Iorio et al., 1996, 1999; Özsoy et al., 2001; Flood et al., 2009; Hiscott et al., 2013). Northward, the Mediterranean watermass flows into the heads of the prominent canyons which cut the shelf edge and rapidly descends along the slope forming several horizontal convective cells created by the instabilities associated with strong contrasts in temperature and salinity (Özsoy et al., 1991). A diluted Mediterranean watermass with salinity ~22 also fills the Black Sea central basins below a 100–200 m-thick surface layer.

The surface-water circulation in the Black Sea is dominated by two large central cyclonic gyres (eastern and western gyres) and several smaller, anticyclonic coastal eddies (Fig. 5; Oğuz et al., 1993). The narrow counterclockwise-rotating peripheral "Rim Current" separates the cyclonic basinal gyres from the anticyclonic coastal eddies. This current flows eastward along the Anatolian coast at ~20 cm s^{-1} and dominates the surface circulation across the narrow continental shelves (Oğuz et al., 1993). The weaker clockwise-rotating Bosphorus and Sakarya anticyclonic eddies are situated west and east of the Strait of Bosphorus, respectively. The surface circulation in the Marmara Sea is dominated by the outflow of low-salinity Black Sea watermass (Beşiktepe et al., 1994). The jet of water entering the Marmara Sea from the Bosphorus flows south-southwest as a narrow current for nearly the entire width of the basin, but curves initially west and later northwest along the edge of the southern shelf (Fig. 5). This current then crosses the Marmara Sea before it swings southwestward towards the Strait of Dardanelles, forming large meander loops with three weak anticyclonic gyres (Fig. 5; Beşiktepe et al., 1994). The bottom-water circulation in the Marmara Sea is controlled by the rate of influx of denser Mediterranean water through the Strait of Dardanelles. Today, residence times of lower-layer waters at ~ –500 m in the Marmara and Black Seas are ~12–19 years and ~625 years, respectively (Lee et al., 2002). In the Marmara Sea, saline water in the deepest basins may have a longer average residence time of ~6–7 years (Ünlüata et al., 1990; Beşiktepe et al., 1993).

2.3. Latest Pleistocene–Holocene sea-level changes in Black Sea and Marmara Sea

There are a bewildering number of latest Pleistocene–Holocene sea-level curves for the Black Sea (Fig. 6; e.g., Nevesskaya, 1970; Ostrovsky et al., 1977; Balabanov, 1981, 2007; Voskoboinikov et al., 1982; Chepalyga, 2002; Izmailov, 2005; Ivanova et al., 2007; Filipova-Marinova, 2007; Konikov et al., 2009; Nicholas et al., 2011). Many of these sea-level curves (particularly those from the former USSR) show rapid fluctuations often depicted as U-shaped or inverted U-shaped oscillations (e.g., Ostrovsky et al., 1977; Chepalyga, 2002). A perplexing issue with these curves is that radically different curves are often published by the same researchers, with no explanation for the differences in both the timing and magnitude of sea-level oscillations (cf. Chepalyga, 2002 and Ivanova et al., 2007; Ostrovsky et al., 1977 and Balabanov, 2007; Voskoboinikov et al., 1982 and Konikov et al., 2009; Fig. 6). It is conceivable that some of the dissimilarities between these curves might be the result of varying rates of local epeirogenic movements (either subsidence or emergence) which may exceed rates of eustatic sea level change (e.g., Brückner et al., 2010; Fouache et al., 2012).

Clearly, the latest Pleistocene–Holocene sea-level history of the Black Sea is in a state of flux. For this review, we have adopted the trend proposed by Lambeck et al. (2007) for the southern end of the Strait of Bosphorus (after reconnection of the Black Sea to the world ocean) and depended on our own geological data from the southwestern shelf area of the Black Sea for older times, discussed later in this review.

There is no previously published base-level curve for the Marmara Sea. In this review we adopted the curve proposed by Lambeck et al. (2007) for the Strait of Dardanelles at Cape Nara (Fig. 4), but again depended on our own geological data and observations from the Marmara basin when it was a lake disconnected from the global ocean.

2.4. Late Pleistocene–Holocene connections between the Black and Aegean Seas

During the Late Pleistocene–Holocene, the Marmara Sea Gateway existed as an interconnected waterway except when global sea level (as well as base levels in the Black and Marmara Sea basins) dropped below the sill depths in the Straits of Bosphorus and/or Dardanelles. For the Black Sea basin, lacustrine conditions prevailed from 9.5–73, 125–186, 236–282 ka and for a long period before 307 ka (Badertscher et al., 2011). Intervening times had alternating lacustrine conditions and marine (Mediterranean water) incursions. Lacustrine conditions characterised the Marmara Sea basin from ~12–30 cal ka and intermittently from ~37–55 cal ka (Yaltırak et al., 2002). During these lowstands, either the Black Sea basin alone or both the Black and Marmara Sea basins became brackish water lakes, referred to during the most recent LGM lowstand as the Neoeuxine and Propontis lakes, respectively. The full opening of the Strait of Bosphorus is a geologically young event, and is closely related to the westward advance of the North Anatolian Fault into the Marmara Sea during the Pleistocene (Le Pichon et al., 2001; Oktay et al., 2002). Syn-sedimentary folding of Middle–Late Pleistocene successions immediately south of the Strait of Bosphorus is interpreted by Oktay et al. (2002) to signal the development of the strait via near-synchronous clockwise rotations of the Istanbul and Kocaeli Peninsulas (Fig. 2). These rotations were triggered by dextral shearing between two bounding faults: a proposed E–W-striking Northern Boundary Fault situated immediately north of the Bosphorus exit in the southwestern Black Sea and the similarly trending North Anatolian Fault across the deep Marmara Sea (Fig. 2). The rotations of the two large crustal blocks (modern peninsulas), and displacements along subsidiary sinistral strike-slip faults which mark bends in the strait, may have started as late as ~115 ka (Würm glaciation; Oktay et al., 2002). The subsequent deepening and inundation of the strike-slip fault zones completed development of the Strait of Bosphorus.

A few previous studies have suggested that the Strait of Bosphorus might not have been the only waterway connecting the Black and Marmara Sea basins during the Late Pleistocene–Holocene (e.g., Pfannensteil, 1944; Meriç et al., 1995; Çağatay et al., 2000; Kerey et al., 2004; Yanko-Hombach et al., 2007). These authors have suggested that an alternative connection might have existed through the Sakarya Valley–Sapanca Lake–Izmit Bay, named the Sakarya Bosphorus by Pfannensteil (1944) (Fig. 3). Today, the Sakarya River flows north and empties into the Black Sea, draining an area of ~52,500 km^2 with an average annual water discharge of 79×10^6 m^3 (EIE 2011). Apart from core/borehole data from Sapanca Lake and Izmit Bay showing faunal and floral assemblages of Ponto–Caspian affinities (e.g., Meriç et al., 1995), no compelling information favours the former existence of this alternative route. Hence, we view this idea as speculative.

The development of the Strait of Dardanelles has been controversial, with suggestions ranging from it being a Pliocene fluvial valley (Erol, 1992), to down-dropping along a series of NE–SW-striking and NW- and SE-dipping normal faults (Alpar et al., 1996; Demirbağ et al., 1998), to the regional uplift of the Gallipoli (Gelibolu in Turkish) and Biga Peninsulas in the Pliocene and associated dextral strike-slip faulting on the Ganos Fault (Fig. 4; Yaltırak et al., 1998, 2000, 2002). The initial connection between the Marmara basin and the Aegean Sea was established following the flooding of interconnected fault-bounded valleys during the Middle–Late Pleistocene (Yaltırak et al., 2000). Yaltırak et al. (2002) further suggested that during Marine Isotopic Stage 2 (MIS2; ~12–25 ka) and MIS6 (~130–190 ka), what is now the Strait of Dardanelles was subaerially exposed because of slow ongoing tectonic uplift, while during the Holocene and most of the Pleistocene (i.e., MIS3–5, MIS7 and older) there was water exchange between the Aegean and Marmara Seas as the floor of the strait was significantly lower than today. Yaltırak et al. (2002, their figure 11) further suggested that two additional narrow connections developed over the Gallipoli Peninsula (i.e., Eceabat and Bolayır channels) during some interglacial periods.

2.5. Regional importance of the Marmara Sea Gateway

The Marmara Sea Gateway is critical to unravelling the Pleistocene–Holocene paleoclimatic evolution of Western–Central Asia and Eastern Europe, and the paleoceanographic evolution of the Black, Caspian and northern Aegean Seas, including causes of sapropel deposition in the Aegean Sea and possibly more widely across the eastern Mediterranean Sea. A number of international programs have recognised this importance (e.g., Pole–Equator–Pole Transect III of the Past Global Changes Program, PAGES; International Marine Global Change Study, IMAGES). The Black Sea has been a transient reservoir for sudden large influxes of glacial melt water through valleys of the present-day Dnieper, Dniester, Don and Volga river systems (e.g., Mangerud et al., 2004; Svendsen et al., 2004; Panin et al., 2007; Rădoane, 2021), as well as former Manych, Uzboy, Turgay and Kas-Ket channels during the catastrophic draining of ice-dammed glacial lakes (e.g., Rudoy and Baker 1993; Rudoy, 1998, 2002). During the Late Pleistocene, several giant ice-dammed lakes developed behind steep and narrow valleys of the Altay and Sayan mountains of Siberia, and cataclysmic outburst floods of these ice-dammed lakes occurred several times, most recently during the latest Pleistocene to possibly earliest Holocene, as late as 13–9 ka (Grosswald and Rudoy, 1996; Carling et al., 2002, 2011; Herget, 2005; Reuther et al., 2006; Komatsu et al., 2016). Such dramatic jökulhlaup events would have raised the Black Sea level by many metres or tens of metres (see §8.2), potentially causing it to spill into the Marmara Sea through the Strait of Bosphorus.

3. Data and methods

3.1. Data acquisition

This review is based on one of the most extensive data set that exists across the Marmara Sea Gateway, all collected by the authors using Memorial University of Newfoundland (MUN) equipment on the RV *Koca Piri Reis* of the Institute of Marine Sciences and Technology, Dokuz Eylül University, during eleven research cruises between 1991 and 2014 (Fig. 7). The data collected during these cruises are labeled with the prefix "M" (for Marmara Sea Gateway) with the last two digits of the year of acquisition as suffix. For example, M98 refers to data collected from the Marmara Sea Gateway during a 1998 cruise. Three types of primary data and several types of auxiliary data were collected. The primary data include (a) high-resolution seismic reflection profiles, (b) high-resolution multibeam bathymetry and (c) piston and gravity cores. During eight cruises (M95, M98, M00, M02, M03, M05, M08 and M11), ~10,500 line-km of

Huntec Deep Tow System (DTS) profiles were collected. During three cruises (M05, M08 and M11), ~5850 km of high-resolution multibeam profiles were collected, subsequently spliced into ~1100 km^2 of seafloor mosaics. During three cruises (M95, M00 and M02), an additional ~6000 line-km of single channel airgun and/or sparker data were collected. Finally, 155 gravity cores were collected during nine cruises (M91, M97, M98, M00, M03, M05, M08, M11 and M14) and 85 piston cores were collected during five cruises (M02, M03, M05, M11 and M14; Fig. 7). Cores relevant to this review are listed in Table 1. In addition, several types of auxiliary data were collected from the Marmara Sea Gateway, including (a) ~275 km of dual-frequency (38 kHz and 200 kHz) Simrad^{TM} ER-60 hull-mounted echo-sounder profiles (Kongsberg Maritime AS) during the M11 cruise across the Saline Channel which provided reflections from the top of the saline underflow, (b) >250 CTD (conductivity-temperature-depth) profiles during all 11 cruises using a Sea-Bird SBE 9 system, which provided *in situ* watermass structure of the gateway, (c) several tens of kilometres of high-definition video of seabed habitats during the M11 cruise using a Geological Survey of Canada underwater camera system, primarily from the Saline Channel in the southwestern Black Sea and across the eastern sector of the Strait of Dardanelles and (d) ~250 km of side-scan sonar data during the M00 cruise using a Klein 590/595 system, which provided images of the seafloor, particularly mounds interpreted by Flood et al. (2009) as mud volcanoes or fluid vents on the southwestern Black Sea shelf. Details on acquisition parameters are available as Supplementary material 1.

3.2. Radiocarbon dates and their calibration to calendar years

We have acquired 149 radiocarbon dates on shell samples (mainly molluscs and gastropods) recovered from several key cores (Table 2). Only the freshest shells were selected for dating, and in several cases bivalve shells were articulated, confirming *in situ* preservation.

Many of these dates were calibrated to calendar years for earlier papers using 2009- or 2013-vintage calibration curves. In our past and current work, we have used the Marine rather than IntCal calibration curves to benefit from the natural smoothing incorporated into Marine curves to mimic mixing of surface and deep waters in the oceans (Stuiver and Braziunas, 1993). In order to stay abreast of advances in calibration of radiocarbon dates, all MUN dates have been recalibrated using the Marine20 calibration curve (Heaton et al., 2020) and either Oxcal4.4 or Calib8.2 online utilities. Radiocarbon dates from the literature have been calibrated in the same fashion, and approximate dates of geological events published by other authors have been updated to be consistent with the Marine20 conversions (Supplementary material 2). If dates from literature sources did not have their uncertainty reported, ±50 yr was used as an approximation for Oxcal or Calib input. Throughout this review, only the Marine20 conversions of previously reported ages are provided, with the original raw ^{14}C dates and their calibrations listed in Supplementary material 2.

Conversion of raw radiocarbon dates on marine biogenic carbonate (in units of ^{14}C yrBP or ^{14}C ka) to calendar ages (in units of cal yrBP or cal ka) is challenging because the dissolved inorganic carbon (DIC) in seawater, used to build shells and other hard parts, has less ^{14}C (relative to ^{12}C and ^{13}C) than the CO_2 of the contemporary atmosphere (Stuiver and Braziunas, 1993). Hence, radiocarbon dating overestimates the age of marine shells, either because the DIC has not equilibrated with the contemporary atmosphere for decades or more, or because of the addition of old ("dead") carbon to the marine inorganic pool from weathering of limestones on land, carried to the sea by rivers. The offset, in ^{14}C years, between the radiocarbon age of a marine shell and the contemporary atmosphere is called the reservoir age (R). The Marine20 definition curve provides modelled values for R at each time step back to 55,000 cal yrBP, averaged for the global ocean (Heaton et al., 2020); local departures from the global average R are reported as a ΔR value. Local departures as a function of time [i.e., ΔR(t)] have been estimated for the Late Quaternary Black, Marmara and Aegean Sea basins (Kwiecien et al., 2008; Soulet et al., 2011; Yanchilina et al., 2017; Williams et al., 2018), but remain poorly constrained. An additional complication is that each ΔR(t) is only valid at the true age of the sample, t. If ΔR≠0, a suitable ΔR to use in individual calibrations cannot be obtained from the Marine20 definition data set using the ^{14}C raw age itself. In our work, after a target R value for a time in the past is set (see next paragraph), the calibration must be iterative because the first estimate of an appropriate ΔR will almost certainly differ from the ΔR needed to shift the default Marine20 R value (from Heaton et al., 2020) to the target value. We began each calibration with a best estimate of an appropriate ΔR, then tuned successive iterations until the ΔR value input into the Calib8.2 setup file agreed within ~±5–10 yr with the ΔR needed to shift the Heaton et al. (2020) default R value associated with the final calibrated age to the target R value. All newly converted ages, complete with R and ΔR values, are available in Table 2 and Supplementary material 2.

Our preferred (i.e., "target") reservoir ages, R(t), for the Black Sea basin are fully explained and justified by Williams et al. (2018, their §3.2); justification will not be repeated here. We do not support the large swings in reservoir age proposed by Yanchilina et al. (2017) for the early Holocene Black Sea, but do accept their innovative proposal to tune latest Pleistocene reservoir ages to data from Sofular Cave in coastal Anatolia (Badetscher et al., 2011) using trends in stable carbon and oxygen isotopes. Williams et al. (2018) presented our preferred trend in reservoir ages as a function of raw ^{14}C age, but as explained above it is better to plot reservoir ages against calibrated (i.e., true) age, as done by Soulet et al. (2011). We have transposed the Williams et al. (2018) preferred values to calendar ages using the Marine20 definition curve, and list the ΔR constraints used in this review in Table 3. A key control point is an interpolated shell age of 19,760 ^{14}C yrBP for the Y2 tephra (Kwiecien et al., 2008) which, when calibrated using the Marine20 curve and R = 1670 yr (ΔR = 800 yr), gives its correct age of 22,050 cal yrBP, determined by conversion of Y2 charcoal ages (18,130 ± 255 ^{14}C yrBP; Pichler and Friedrich, 1976; Erikson et al., 1990) using the IntCal20 data set, and consistent with Kutterolf et al. (2021). The Y2 tephra also occurs in Marmara Sea cores M02-89P and M14-16P, in the latter case 3 cm above a shell dated to 18,915±40 ^{14}C yrBP. For that situation, R = 820 yr (ΔR = –50 yr) gives a correct age of 22,055±110 cal yrBP.

The average R value from ~0–7500 cal yrBP for the Marine20 data set is ~515 ^{14}C yrBP. Therefore, after the onset of near-modern marine conditions (Marmara Sea at ~13.5 cal ka, Hiscott et al., 2021; Black Sea at ~7.5 cal ka, e.g., Ryan et al., 1997, Williams et al., 2018) we employ a fixed ΔR of –100 yr so that R = 415 yr as determined for pre-industrial shells by Siani et al. (2000). Before ~13.5 cal ka and ~7.5 cal ka, respectively, we allow R to vary as set out in Table 3 and shown graphically in Figure 8. For shells from Aegean Sea cores, we use the default Marine20 calibration curve throughout with no correction to R, because Facorellis et al. (1998) and Siani et al. (2000) concur that the reservoir age in the northern Aegean Sea is ~515 yr, indistinguishable from the middle to late Holocene average R value associated with the Marine20 calibration curve (Heaton et al., 2020).

To clarify our use of abbreviations, 'ka' is used for thousands of years before the present, whereas 'kyr' is used later in this review for time intervals which are thousands of years long, anytime in the past (North American Commission on Stratigraphic Nomenclature, 2005, Article 13c). We do not use 'a' for years in the past to avoid confusion with the indefinite article.

4. Seismic stratigraphy, allostratigraphy and chronology

We have previously published seismic stratigraphic frameworks for the southwestern Black Sea shelf (Fig. 9; Aksu et al., 2002; Hiscott et al., 2007b; Ankindinova et al., 2020), the northeastern Marmara Sea shelf (Fig. 10; Hiscott et al., 2002, 2007a, 2017; Aksu et al., 2016), and the southern and southwestern Marmara Sea shelves (Fig. 11; Aksu et al., 1999a, 2018; Hiscott and Aksu, 2002; Hiscott et al., 2021). Detailed descriptions of the seismic stratigraphic units in these three regions are not repeated here, but are summarised in Supplementary material 3.

Key seismic reflections including α0, α, α1 and α2 on the southwestern Black Sea shelf, β1, β2, β3, β4 and β5 on the northeastern Marmara Sea shelf and α1, α2 and α3 on the southern and southwestern Marmara Sea shelf (Figs. 9–11) are acoustic returns from interfaces that exhibit strong acoustic impedance contrasts (Supplementary material 3). Reflection terminations characterised by onlap, toplap, downlap and erosional truncation at these marker reflectors indicate that some of them are regional/local unconformities which laterally (and locally) pass into disconformities and/or correlative conformities. In other instances, these surfaces represent marked facies transitions with limited and/or negligible hiatuses; such transitions are characterised by local onlap surfaces primarily on the steepest flanks of pre-existing highs (e.g., delta fronts), but elsewhere are conformable surfaces. Recognition of unconformities in seismic reflection profiles is a scale issue entirely controlled by the properties of the seismic reflection system used to image the subsurface, and the geometric characteristics of the unconformities. For example, unconformities imaged using the Huntec DTS system are largely not detectable in small (40 in^3 or 656 cm^3) single-channel airgun profiles or 1.58 kJ sparker data (also see Supplementary material 1 in Ankindinova et al. 2020).

This review deals solely with the interpretation and paleoceanographic significance of the uppermost seismic stratigraphic unit (Unit 1) and its subunits, deposited above a prominent unconformity developed during the LGM lowstand and the subsequent post–LGM transgression. This surface is herein referred to as a "lowstand–transgressive surface", or L–TS. The temporal scope of this review is therefore quite limited, yet the research effort which has been expended trying to understand this short interval of geological history has been great, and there is still controversy after more than 25 years. If the genesis of such recent deposits cannot be pinned down with confidence, then one has to wonder about paleoenvironmental interpretations for Palaeozoic or even older successions for which the geological record is more fragmented.

In previous publications, we have used Greek letters to identify prominent seismic markers. These correspond to unconformities and their lateral continuations into disconformities and correlative conformities. For example, in the southwestern Black Sea, northeastern Marmara Sea and southern–southwestern Marmara Sea, the L–TS corresponds to marker horizons α (Aksu et al., 2002; Hiscott et al., 2007b; Ankindinova et al., 2020), β3 (Hiscott et al., 2002, 2007a, 2017; Aksu et al., 2016) and α1 (Aksu et al., 1999, 2018; Hiscott and Aksu, 2002; Hiscott et al., 2021), respectively (Figs. 9–11). In this paper we retain the use of Greek letters so that comparisons can be made with our earlier studies (see also Supplementary material 3). The prominent seismic markers divide the uppermost Quaternary packages into seismic stratigraphic (i.e., acoustic) units and subunits, each of which corresponds to what can be called a 'sedimentary sequence' in the geological record. According to stratigraphic practice, a 'sequence' (or unit) is defined as an unconformity-bounded succession of genetically related strata that is internally conformable (e.g., Posamentier et al., 1988; Catuneanu, 2020). Each seismic stratigraphic unit therefore corresponds to an unconformity-bounded sedimentary sequence; such units have their own special name—they are called allostratigraphic units. The North American Commission on Stratigraphic Nomenclature (2005) defines an allostratigraphic unit as "*a mappable body of rock* [or sediment] *that is defined and identified on the basis of its bounding discontinuities*". The physical, chemical and paleontological characteristics of an allostratigraphic unit may vary laterally and vertically (e.g., Bhattacharya and Posamentier, 1994; Bhattacharya, 2001). Because their definitions overlap so strongly, we use identical alphanumeric Greek identifiers for seismic stratigraphic units/subunits and their corresponding allostratigraphic units/subunits (e.g., Figs. 12–14). For brevity, we shorten the names of such deposits to allounits and allosubunits.

Dated cores establish the chronology of the seismic stratigraphic (= allostratigraphic) units and subunits (e.g., Figs. 12–14; Table 2). Three chronostratigraphic charts show the temporal and spatial arrangements of the allounits/allosubunits across the southwestern Black Sea (Fig. 15), the northeastern Marmara Sea (Fig. 16) and the southern and southwestern Marmara Sea (Fig. 17). Each stratigraphic chart is plotted alongside the relative base-level curve for the particular region. Several important observations arise from these charts. In the southwestern Black Sea (Figs. 12, 15), the hiatus at the L–TS (or the α unconformity; Fig. 8) correlates with the time when the Neoeuxine Lake had been drawn down by evaporation to ~ −100 m (Ryan et al., 2003; Major et al., 2006; Cohen et al., 2011), whereas the minor hiatuses of variable duration at the α1 and α2 discontinuities developed after the Neoeuxine Lake was reconnected with the global ocean (thereby becoming the Black Sea) and its level was above the sill at the southern end of the Strait of Bosphorus (Hiscott et al., 2002, 2017; Aksu et al., 2016). The initial development of the L–TS (or α unconformity) can be ascribed to subaerial exposure and erosion during and shortly after the LGM when the Neoeuxine Lake level was low (Ryan et al., 2003;

Major et al., 2006; Cohen et al., 2011), but it must have been modified by transgressive erosion (i.e., ravinement) during the post-glacial base-level rise (Figs. 12, 15). Accordingly, the hiatus must lie within the sand-to-gravel veneer at the L-TS level rather than at its top, even though the upper contact likely provides the impedance jump responsible for the acoustic reflection seen in seismic data. As an example, at the M02-45 core site (Fig. 12), the α hiatus is placed between the calibrated dates of 10585 and 12130 cal yrBP (Table 2), but could actually be slightly below the cored section. The α1 and α2 unconformities developed under tens of metres of water after the Holocene transgression was well under way (Figs. 12, 15). At core site M02-45, the α1 level is apparently conformable with no break in facies, no evidence for subaerial exposure (e.g., rootlets, desiccation cracks, induration), whereas upward and downward extrapolation from age-dated levels to the α2 unconformity, incorporating uncertainties, indicates a hiatus between allosubunits 1c and 1d in this area of about 3280±80 years. At core site M05-50 where α2 appears to be conformable, the same procedure provides an estimate of 2720±150 years for the duration of the hiatus at the α1 unconformity between allosubunits 1b and 1c. Flood et al. (2009) attribute these submarine unconformities to local erosion and non-deposition under ephemeral eddies associated with the Rim Current and possibly unconfined threads of the saline undercurrent as it crossed portions of the shelf in the past. The α1 unconformity potentially has special significance on the shelf seaward of the Bosphorus exit, where a network of anastomosed channels has developed beneath a persistent saline undercurrent emanating from the strait. The muddy levées of this network, on the middle to outer shelf, are younger than ~8.0 cal ka and the youngest sediments below α1 at the M05-50 site (top of allosubunit 1b; Fig. 15) have an age of ~11 cal ka so significantly pre-date the initial marine inflow from the Marmara Sea which took place at ~9.5 cal ka. A gap in the record of ~1.5 kyr before the entry of marine waters through the strait might suggest rather powerful erosion across the shelf, and perhaps a time for base level to have fallen to expose this part of the shelf. However, in places within a few hundred metres of this core site seismic profiles reveal an additional ~130 cm of allosubunit 1b sediments that escaped the amount of erosion seen at the core site itself. Using an accumulation rate of ~0.1 cm yr^{-1} based on calibrated radiocarbon dates in allosubunit 1b at the nearby core site, the youngest sediments below α1 in this area extend upward to ~9.7 cal ka (and with uncertainty to ~9.4 cal ka), just before the first saline inflow. This leaves insufficient time, we believe, for any significant base-level fall. Besides, at the M02-45 site far from the Bosphorus exit there is no facies change through the same time interval and no evidence for wave agitation at the ~9.5 cal ka seabed, demonstrating that the water depth remained at least several tens of metres on the contemporary middle shelf.

Widespread, albeit patchy, ~12.3–7.? cal ka deposition of allosubunit 1b across the entire southwestern Black Sea over the L–TS is critically important to the evolution of the region, because this confirms that base level in the Black Sea basin was higher than ~ –50 m during this period. Strong support for this conclusion comes from Constantinescu et al. (2015) who determined that the shelves of the Neoeuxine Lake were flooded at early as ~11.7 cal ka and remained flooded until the Present, because after ~11.7 cal ka the supply of coarse-grained detritus and turbidity currents to the Danube submarine fan ceased. Hiscott et al. (2007b) argued that base level had probably risen as high as the sill in the Strait of Bosphorus because of the lack of wave-generated structures in allosubunit 1b sediments. A multibeam mosaic of the central Bulgarian shelf (Fig. 18) reveals a ~9–9.5 km-long and ~0.9–1.1 km-wide arcuate body identical in shape to a typical recurved spit (Ashton et al., 2016). Its top is at ~ –30 to –35 m elevation below which there is a 20–30 m-thick Holocene deposit known to be sand-prone (Krastev et al., 1990; Ankindinova et al., 2020). The inferred spit occurs immediately south of Cape Emine at a sharp change in orientation of the coastline, and it is interpreted as an abandoned structure from a time when base level was at ~ –30 to –35 m. It is unlikely that the subaerial crest of a beach-dune complex would survive transgressive erosion, so the paleo-shoreline elevation was probably closer to –30 m than to –35 m. The development of this sediment body would require (a) south-directed longshore transport away from the Danube Delta when the Neoeuxine Lake was at its spill depth into the Marmara Sea (i.e., ~ –30m elevation), and (b) a stillstand a few metres above the elevation of the spill depth lasting hundreds of years to account for uninterrupted growth of such a large feature (Ankindinova et al., 2020). The Outflow Hypothesis includes a lengthy early Holocene (~11.1–9.5 cal ka) stillstand at ~ –30 to –35 m (Hiscott et al., 2007a; Ankindinova et al., 2019a, 2020) as the Neoeuxine Lake spilled into a rising, but lower Marmara Sea. Unimpeded along-shelf transport could only have operated if the level of the Neoeuxine Lake was above ~ –40 m to –35 m through the entire Holocene (see also Giosan et al., 2009). The transport pathway did not end offshore Bulgaria; based on sediment thicknesses and mineralogy, this pathway apparently continued southeastward to the vicinity of the Strait of Bosphorus (Lister et al., 2015; Ankindinova et al., 2020), and possibly along the strait itself to the delta Δ1 lobe in the northeastern Marmara Sea (Aksu et al., 2016; Hiscott et al., 2017) that is contemporary with the lower portion of Black Sea allosubunit 1b and presumably with the morphological spit south of Cape Emine. These independent lines of evidence point to a high and potentially out-spilling Neoeuxine Lake by ~11.5–12.0 cal ka.

In the northeastern Marmara Sea just beyond the southern exit of the Strait of Bosphorus, there are several prominent shelf-crossing unconformities, two of which are particularly well expressed near the shelf edge, where they cut significantly into older successions: these are designated as β5 and β3 in Fig. 19. Hiscott et al. (2002, their figure 4) identified five seismic units (Units 1–5) beneath the northeastern Marmara Sea shelf over a prominent regional shelf-crossing unconformity which they called Q1 and which is identical to our β5. Those authors argued that β5 (Q1) is an erosional angular unconformity which truncates deposits likely older than ~160 ka, and that might have developed during the prolonged MIS6 lowstand. Hiscott et al. (2017) suggested an age of ~17.2 cal ka for the sediments immediately below the key reflector β4, which is the surface directly above the uppermost Pleistocene set of clinoforms called delta Δ2 by Hiscott et al. (2002). Delta Δ2 itself rests on the β5 unconformity. Therefore, β5 appears to be a composite unconformity possibly originally developed during MIS6, but significantly reworked during the LGM, some 24–18 cal ka (ages consistent with Lambeck et al., 2014). Unconformity β3 is an irregular, locally rutted, surface of truncation, and is identified based on age and depth of erosion as the lowstand to transgressive surface (L–TS) in this area. It began to form when the Propontis Lake had been drawn down by evaporation to below –85 m (Aksu et al., 1999a; Çağatay et al., 2009; Eriş et al., 2011), exposing much of the shelf to subaerial erosion during the LGM (Fig. 13, 16). How is it that β5 and β3 could have formed during the same glacial lowstand, yet be separated by a progradational unit of clinoforms (Δ2)? Although yet to be tested by coring, we believe that there were two intervals of vigorous Black Sea outflow and delta development at the southern exit of the strait, the first during Late Pleistocene early deglaciation and the second during early Holocene establishment of an increasingly humid and wet climate swelling the rivers entering the Neoeuxine Lake to the north (i.e., Δ2 and Δ1, respectively; Fig. 20; Hiscott et al., 2002; Aksu et al., 2016). In the case of the β3 unconformity, it is interpreted that base level temporarily rose to ~ –64 m (5 m above the topset-to-foreset elevation of the youngest Δ2 clinoforms) and stayed at that depth long enough for subaerial erosion to leave a mark landward of the contemporary shoreline. Aksu et al. (2016) have shown that Δ1 developed during the early Holocene (~11.1–10.2 cal ka) and not during ~6.5–3.7 cal ka (see Supplementary material 2 for calibration) as claimed by Eriş et al. (2007) and Çağatay et al. (2021) using incorrect ties between vintage seismic profiles and a RV *Marion Dufresne* core site MD04-2750. Hence, a positive link exists between evidence for a high Neoeuxine Lake and evidence that the resultant outflow reached the northeastern Marmara Sea, and of course must have penetrated farther along the gateway to the Aegean Sea.

Using the strictest definition of a stratigraphic sequence (Posamentier et al., 1988; Catuneanu, 2020), there are two unconformity-bounded sequences across the northeastern Marmara Sea shelf (as opposed to the five proposed by Hiscott et al. 2002). Unit 1 occurs between the prominent shelf-crossing unconformity β3 and the present-day seafloor, whereas Unit 2 occurs between the shelf-crossing unconformities β5 and β3 (Fig. 10). These two seismostratigraphic units correspond to two allostratigraphic units (i.e., allounits 1 and 2; Fig. 10). Allounit 1 and its three allostratigraphic subunits, 1a–1c, was deposited above the L–TS (i.e., the β3 unconformity), and incorporates seismic stratigraphic units 3–1 of Hiscott et al. (2002; blue circled numbers in Fig. 10). Allounit 2 was deposited over the β5 unconformity and includes the uppermost Pleistocene delta Δ2 (unit 5 of Hiscott et al., 2002; Fig. 20) and deposits over the β4 marker which accumulated following abandonment of delta Δ2 (unit 4 of Hiscott et al., 2002). Following a brief interval of sedimentation over the L–TS (i.e., allosubunit 1a) a second prominent, climbing delta prograded over the mid-shelf region. It was sourced from the Neoeuxine Lake between 11.1–10.2 cal ka (allosubunit 1b; Figs. 10, 13, 16; Aksu et al., 2016). This delta was abandoned at 10.2 cal ka as a salt wedge is inferred to have advanced up the Strait of Bosphorus, leading to eventual penetration of marine waters into the Black Sea basin by ~ 9.5

cal ka, initiating its salination (Fig. 16). Allosubunit 1c constitutes deposition across the northeastern Marmara Sea shelf during and following the establishment of two-way flow across the Strait of Bosphorus (Fig. 10).

In the southern and southwestern Marmara Sea, the development of the L–TS (i.e., the α1 unconformity; Fig. 11) can also be ascribed to subaerial exposure and erosion during the LGM when the Propontis Lake level was low, and to the subsequent transgression and associated ravinement (Figs. 14, 17; Aksu et al., 1999a, 2018; Hiscott and Aksu, 2002; Hiscott et al., 2021). Allounits 1 and 2 across the southwestern Marmara Sea are not subdivided, but correlate temporally with allosubunits 1a+1b+1c and allosubunits 2a+2b of the northeastern Marmara Sea, respectively.

Bioherm colonies across the eastern sector of the Strait of Dardanelles (e.g., Hiscott et al., 2007a; Aksu et al., 2018), above the L–TS, are an indicator of saline bottom water, and are inferred to share their environmental requirements with older bioherms along the β3 unconformity in the northeastern Marmara Sea. Hiscott et al. (2021) calculated that the replacement of fresh/brackish waters of the Propontis Lake by saline waters from the Aegean Sea took no more than a few hundred years because of the small volume required, so bioherms formed by marine organisms should have started to develop on submerged shelves of the Marmara Sea as early as ~13.2–13.5 cal ka, given proper nutrient supply and sunlight penetration (cf. Aksu et al., 2018).

All three water bodies along the gateway have experienced sapropel accumulation, the timing of which can provide clues to water-mass exchange. Organic-rich sediments called sapropels and sapropelic muds are widespread across the Aegean Sea (e.g., Aksu et al., 1995a,b,c; Triantaphyllou et al., 2009; İşler et al., 2016a,b,c; Giamali et al., 2019) and the

Marmara Sea (Çağatay et al., 2000, 2009; Abrajano et al., 2002; Aksu et al., 2002b), containing 1.5–24% total organic carbon, TOC. Although there are several hypotheses on the formation of sapropels, including basin anoxia and enhanced surface water productivity leading to the augmented export of organic matter to the seafloor, their development simply requires that the supply of total organic carbon to the seafloor exceeds its consumption by fauna and oxidation through the water column and at the sediment-water interface (e.g., Rohling et al., 2015).

In this review we only address the development of the most recent sapropel S1 in the Aegean Sea (Aksu et al., 1995b; İşler et al. 2016b) and M1 in the Marmara Sea (Çağatay et al., 2000, 2009). The Black Sea also hosts a laminated sapropel with age 7.7–2.0 cal ka (Dean and Arthur, 2011), but this unit is not relevant to the history of Black Sea outflow, so it is not considered here. Mediterranean sapropel S1 was dated by Aksu et al. (1995b) to 10.3–6.65 cal ka in the Aegean Sea, revised to 10.75–6.9 cal ka by İşler et al. (2016b). In the Marmara Sea, sapropel M1 consists of two units: the older and younger units were initially dated to 11.9–6.7 cal ka and 5.0–3.0 cal ka, respectively (Çağatay et al., 2000; see Supplementary material 2 for calibration). *Calypso* core MD01-2430 (580 m water) fully recovered M1, but key papers are inconsistent on the position of the lower M1 unit in this core (230–320 cm for Vidal et al., 2010; 242–360 cm for Çağatay et al., 2015; 220–360 cm for Londeix et al., 2009). We therefore evaluated the MD01-2430 TOC trend (Vidal et al., 2010; Çağatay et al., 2015, their figure 9), picked boundaries for sapropelic mud (1.5–2.0% TOC) and sapropel (>2.0% TOC but including a small peak on the side of the main M1 peak), then reconverted the ages to conform with our procedures (Marine20 calibration using R values of Fig. 8). Sapropelic muds occur from 13.85–12.8 cal ka and again from 6.65–6.25 cal ka (see Supplementary material 2 for calibration). Sapropel bridges the gap from 12.8–6.65 cal ka (its main peak, entirely >2.0% TOC, spans 11.7–

6.65 cal ka). The onset of sapropel M1 deposition post-dates the onset and termination of latest Pleistocene Black Sea outflow (Tudryn et al., 2016) by ~4400 years and ~2900 years, respectively, and pre-dates the onset and termination of the early Holocene (Δ1) outflow by ~1700 years and 2600 years, respectively.

5. Key elements of Flood and Outflow Hypotheses

5.1. Flood Hypothesis (Fig. 21a)

Ryan et al. (1997) and Ryan and Pitman (1998) proposed that the post-glacial reconnection of the Black Sea occurred as a catastrophic flooding of the Neoeuxine Lake by Mediterranean waters, and speculated that this was the basis for the story of Gilgamesh and the biblical story of Noah's Flood. During the last 20–25 years, several studies have been published lending support to the Flood Hypothesis or have taken the chronology of the Flood Hypothesis as the starting point for interpretations (e.g., Ballard et al., 2000; Çağatay et al., 2000, 2003, 2009; Algan et al., 2001; Dimitrov 2003; Major et al., 2002, 2006; Eriş et al., 2007; Lericolais et al., 2009, 2019; Yanchilina et al., 2017, 2019). The Flood Hypothesis rests on the following key premises:

- during the early-mid Holocene the Black Sea (and Caspian Sea) had become freshwater lakes maintained by large influxes of fluvial runoff and glacial meltwaters,
- during this time the drainage patterns of the major Eastern European rivers were modified during deglaciation and some rivers that presently drain into the Black Sea were diverted toward the North Sea,
- an arid climate during the early-mid Holocene across Eastern Europe and river diversion resulted in the dramatic lowering of the level of the Neoeuxine Lake through excess evaporation compared to fluvial inflow and precipitation,

- a dramatic lowering of the lake level to –150 m coincided with the post-glacial rise in global sea level,
- at 9.1 cal ka (8.4 ^{14}C ka; Ryan et al., 2003, revised from 7.15 ^{14}C ka or 7.55 cal ka in Ryan et al., 1997; see Supplementary material 2 for calibrations), the rising Marmara Sea, which was connected to the global ocean, breached a shallow sill in the Strait of Bosphorus, creating a catastrophic inflow of Mediterranean waters into the Neoeuxine Lake to create the Black Sea,
- the flooding caused a very rapid transgression across the modern Black Sea shelves, profoundly affecting prehistoric human settlements across eastern Europe and environs.

5.2. Outflow Hypothesis (Fig. 21b)

We have argued since 2002 that the post LGM salination of the Black Sea occurred in a gradual fashion during the Holocene, following the second of two Late Quaternary periods of outflow from the Neoeuxine Lake (today's Black Sea) into the Marmara Sea (Aksu et al., 2002a,b, 2016; Hiscott et al., 2007a,b, 2017; Mudie et al., 2002a,b, 2007). The key elements of the Outflow Hypothesis are supported by several former USSR/Russian and Ukrainian geoscientists (e.g., Fedorov, 1982; Chepalyga, 1984, 2002; Yanko-Hombach, 2006; Kuprin and Sorokin, 2007; Shmuratko, 2007; Shuisky, 2007; Balabanov, 2007). The Outflow Hypothesis rests on the following key observations and interpretations:

- allostratigraphic subunit 1b is widespread across the southwestern Black Sea shelf, dated in cores from 12.3–7.2 cal ka (Ankindinova et al., 2020), showing that the shelf was transgressed and inundated long before the first entry of marine (i.e., saline) water through the Strait of Bosphorus,

- water depth at key core sites such as M02-45 (–69 m today) and M11-23 (–77 m today) in the southwestern Black Sea was several tens of metres by ~12.3 cal ka (Hiscott et al., 2007b; Marret et al., 2009), and these sites communicated freely with the open Black Sea,
- two intervals of brackish-water export from the Neoeuxine Lake into the Marmara Sea occurred during the latest Pleistocene–Holocene at ~17.2–15.7 cal ka and 11.1–10.2 cal ka (Aksu et al., 2016), both creating deltas immediately south of the Strait of Bosphorus (i.e., Δ1 and Δ2; Fig. 20),
- the 3.3 km progradation of the early Holocene mid-shelf delta (Δ1) into at least an 8 m rise in the base level of the Marmara Sea could only have resulted from vigorous outflow through the Strait of Bosphorus, as even rapidly transgressed deltas worldwide are unable to advance under such conditions and instead backstep or are drowned,
- interpretation of benthic foraminiferal data (Kaminski et al., 2002) and dinoflagellate cyst data (Mudie et al., 2002a) from Holocene deposits of the Marmara Sea suggests a persistent surface layer of brackish water that can only have been provided by Black Sea outflow,
- an abrupt climb in $^{87}Sr/^{86}Sr$ in mollusc shells at 9.42–9.46 cal ka (Ankindinova et al., 2019a) marks the first significant intrusion of saline water into a previously isolated Neoeuxine Lake, but $^{87}Sr/^{86}Sr$ data also prove that the M02-45 core site was not in a perched coastal pond (liman) before this (cf. Yanchilina et al., 2017), but was open to the central Black Sea because the Ankindinova et al. (2019a) Sr-isotopic trend is identical (both values and timing) to lower-resolution trends for the open sea published by Major et al. (2006) and Yanchilina et al. (2017).

6. Evaluation of the LGM level of the Neoeuxine Lake

Ryan et al. (1997, 2003) suggested that the level of the Neoeuxine Lake stood at –150 m during the LGM. In a more recent paper, Yanchilina et al. (2017, p. 27) suggested that "*the lake surface stood at least below 120 mbsl at 9300 calendar years (8200 corrected ^{14}C years)*". These authors based their interpretation on a prominent shelf-crossing unconformity (also identified in previously studies, e.g., Nevesskaya (1965); Federov (1971); Evsylekov and Shimkus, 1995) across the northern and northeastern Black Sea shelves, truncating the underlying Pleistocene successions, and extending beyond the shelf edge to depths exceeding –150 m. Ryan et al. (1997, 2003) described the sediments at the unconformity as gravel, sand and clay. The gravel contains *Dreissena rostriformis* eroded from underlying coquina-bearing layers and the stiff clay is characterised by abundant leafy plant material, fluvial gastropods *(Viviparus viviparus),* desiccation cracks and roots indicative of former alluvial to coastal marsh environments. Ryan et al. (1997) dated intact valves of *D. rostriformis* in the coquina below the gravel to 16.1–12.0 cal ka (14.7–10.4 ^{14}C ka; Supplementary material 2), with reworked molluscs in the overlying gravel as young as 8.87 cal ka (8.25 ^{14}C ka). These authors compared their findings with prior descriptions of sediments beneath the unconformity as being loess soils (Kuprin et al., 1974), alluvium (Popov, 1973; Skiba et al., 1975; Scherbakov et al., 1978), littoral deposits (Kuprin et al., 1974; Shimkus et al., 1975; Scherbakov et al., 1978; Dimitrov, 1982; Scherbakov, 1983) and beach terraces (Shimkus et al., 1980), all part of a lowstand landscape developed between 21.57 cal ka and 11.0 cal ka (17.78–9.66 ^{14}C ka; Supplementary material 2). Subsequent studies by Ballard et al. (2000), Algan et al. (2007) and Lericolais et al. (2007a,b, 2010, 2011) interpreted wave-cut terraces and coastal paleo-dunes at various depths ranging from –90 m on the Romanian shelf to –155 m on the northern Turkish shelf, in support of the presence of a submerged coastline which existed during the latest Pleistocene.

However, there are several difficulties with the base-level proposals noted above: (a) Badyukova (2010) suggested that unconsolidated dunes could not survive transgression, a conclusion supported by core data from the northern and northwestern Black Sea where no lithological fingerprint of drowned wind-blown dunes has been detected (Yanko-Hombach et al., 2013) and (b) the lowstand landscape originally described by Ryan et al. (1997) is proposed by them to have existed during the 17.2–15.7 cal ka interval of time when Tudryn et al. (2016) demonstrated major ice-sheet melting, leading to swelling of the Neoeuxine Lake, and providing an explanation for its outflow to form the lower strait delta (i.e., A2; Hiscott et al., 2007a; Aksu et al., 2016). Clearly, the Neoeuxine Lake cannot have been at a lowstand and overtopping the Bosphorus sill at the same time. We use the elevation of radiocarbon dated shells from our cores to evaluate this clear inconsistency between Ryan et al. (1997) and Tudryn et al. (2016; Figure 22). There are 13 shells in southwestern Black Sea cores with calibrated radiocarbon ages between 17.7 and 11.1 cal ka. The shells include the gastropods and molluscs *Dreissena rostriformis*, *D. polymorpha*, *Turricaspia spica*, and other *Dreissena* and *Turricaspia* species. Most are in allosubunit 1b so based on arguments above lived on the margins of the Neoeuxine Lake and not in limans or rivers. Relative to modern sea level and accounting for their current depths of burial, these shells occur at elevations of –78 m to –99 m (red-filled circles in Figure 22). There is a gap between ~15.5 and ~13 cal ka, but from 13 cal ka onward there are sufficient dates to exclude the possibility of a base level below ~ –78 m, demonstrating that significant portions of the southwestern Black Sea shelf were already inundated by a rising Neoeuxine Lake by this time (Figure 22). There are 11 additional samples in our southwestern Black Sea cores with calibrated radiometric ages from 10.7–9.5 cal ka at –78 m and –97 m elevations, similarly suggesting that the inundation of the Neoeuxine shelf persisted until the time of the purported catastrophic flooding of the Neoeuxine Lake, reaching elevations at least as shallow as –78 m (yellow-filled circles in Figure 22). This, of course, is a minimum requirement because in other work (Hiscott et al., 2007b) we have explained that allosubunit 1b was deposited below storm wave base and beyond a near-shore region which, like today, must have been devoid of muddy sediments because of persistent wave suspension. The modern seabed on the southwestern shelf is without a mud veneer to water depths of ~40 m, so recovery of lacustrine shells in allosubunit 1b at an elevation of –78 m could mean that contemporary base level was close to –78+40 = –38 m. This matches the modern elevation of the sill in the Strait of Bosphorus, and therefore is consistent with the onset of outward spilling into the Marmara Sea by 11 cal ka at the latest.

The Neoeuxine Lake level dropped by evaporative drawdown during the LGM; however high-resolution seismic reflection studies across shelf-edge deltas provide evidence that the drawdown never reached below –110 m (e.g., Panin, 1989; Aksu et al., 2002; Popescu et al., 2004; Larchenkov and Kadurin (2011); Yanko-Hombach et al., 2017b). Across the northern and northwestern Black Sea, the shelf is very wide (100–200 km) and a number of prominent rivers, such as the Danube, Dnieper, Dniester and Southern Bug, enter the sea (Jipa and Panin, 2020). Beneath a thin veneer of Holocene sediments, former fluvial channels which developed during the LGM when base level was lower are preserved (e.g., Giosan et al., 2005; Radoane, 2021). Farther seaward these channel networks link with canyons along the upper slope (Jipa and Panin, 2020). In these areas, the shelf-to-slope break occurs at elevations of –100 m to –140 m. The magnitude of the LGM drawdown is well constrained by these shelf-edge deltas. For example, Panin (1989) showed that the LGM delta fronts across the northwestern Black Sea shelf are limited to <100 m water depth. Similarly, Popescu et al. (2004) confirmed the position and depth of the paleo-coastline during the last lake-level lowstand, with a prominent wave-cut terrace occurring at 100–110 m water depth in the vicinity of the Danube Canyon. Two regions characterised by networks of buried channels associated with paleo-drainage system do not extend beyond the paleo-coastline at 100–110 m depth (Popescu et al. (2004).

Similarly, seaward off the Dnieper and Dniester river mouths and across the northeastern Black Sea shelf Yanko-Hombach and Motnenko (2011), Larchenkov and Kadurin (2011) and Yanko-Hombach et al. (2017b) place the 17.01–16.45 cal ka (15.5–15 ^{14}C ka; Supplementary material 2) paleo-shoreline between the present-day –50 and –60 m isobaths, well onto the shelf. These authors further placed the 12.7–11.29 cal ka (11–10 ^{14}C ka) and 9.9 cal ka (9 ^{14}C ka) paleo-shorelines at the present-day –40 m and –30 m isobaths, respectively (Larchenkov and Kadurin (2011); Yanko-Hombach et al., 2017b). Small lowstand shelf-edge delta lobes are described from the southwestern Black Sea shelf (Aksu et al., 2002a). These successions consist of a number of stacked, laterally overlapping, north-prograding packages, characterised by distinct sets of oblique-prograding clinoforms along the present-day shelf edge where they form seaward thickening wedges reaching thicknesses of 55–135 m. Individual wedges are 20–40 m thick and 1500–3000 m long in the dip direction, and are separated from one another by local unconformities, which merge in the landward direction with the shelf-crossing unconformity, α (Aksu et al., 2002a). The transition from the upper to middle segments of the oblique-prograding clinoforms represents the topset-to-foreset transition (offlap break of Myers and Milton, 1996). The topset-to-foreset transition of the youngest delta 1 of Aksu et al. (2002a), interpreted as the combined lowstand lobe of the Bulanık, Pabuç Kazan and Çilingöz streams now in Turkish Thrace (Fig. 1c) occurs at –116 m. Assuming that the topset-to-foreset transitions of deltas in the Neoeuxine Lake occurred at 5–10 m water depth and that there has been little subsequent subsidence, base level during the last phase of progradation of delta 1 would have been at an elevation of –106 to –111 m, very similar to interpretations in the Danube delta area and at odds with any suggestion that the ancient lake level stood between –150 m and >–120 m during the LGM.

The bounding envelope plotted on Figure 22 shows that as shell ages become younger, they are progressively found closer to the modern shoreline. This is consistent with encroachment of the Holocene shoreline during a gradual base-level rise rather than over only a few decades following a catastrophic inundation as proposed by proponents of the Flood Hypothesis.

7. Supporting evidence for the Outflow hypothesis

7.1. Allosubunit 1b across the southwestern Black Sea shelf

Allosubunit 1b is bounded at its base and top by the L–TS (or α unconformity) and α1 unconformity (including its correlative conformity), respectively (Fig. 9). Several well dated cores show that it was deposited from 12.3–7.2 cal ka (Fig. 12; Hiscott et al., 2007b; Ankindinova et al., 2020). A dense grid of high-resolution seismic reflection profiles demonstrates a patchy but widespread distribution across the southwestern shelf (Fig. 23). Previous studies showed that the base of subunit 1b onlaps the L–TS (α unconformity), and fills depressions along that surface (e.g., Fig. 9; Hiscott et al., 2007b; Ankindinova et al., 2020). As accumulation continued, the onlapping basin fill overstepped highs and created a shelf-wide blanket of sediments (Fig. 9). Allosubunit 1b is interpreted as the lowermost portion of a transgressive systems tract.

The proponents of the Flood Hypothesis have argued that older sediments like allosubunit 1b of Ankindinova et al. (2020) might have accumulated in perched depressions on today's middle-inner shelves which were isolated from the contemporary open Neoeuxine Lake, as is the case for some present-day limans (Major et al., 2006; Ryan et al., 2007; Yanchilina et al., 2017). Limans are large lagoons that develop seaward of river mouths (thus are estuaries) which often have a bar or spit along the seaward side, leaving a small narrow entrance which restricts water communication between the lagoon and the sea. Major et al. (2006, p. 2041) suggested that multiproxy data arising in cores retrieved from such limans (perched saline ponds) would not reflect the properties of the Neoeuxine Lake/Black Sea, because "*the chemistry of such a small water body is sensitive to the local conditions, driven by evaporation, algal blooms, and groundwater leakage*". The MUN Sr-isotopic data clearly demonstrate that the M02-45 site was not in a geochemically isolated setting, but instead must have been open to the central basins of the Neoeuxine Lake. Hence, the core site must have been below base level as early as ~12.3 cal ka. This is consistent with evidence provided by Constantinescu et al. (2015) that the shelf seaward of the Danube Delta was transgressed to at least –70 m elevation by 11.7 cal ka (see Supplementary material 2 for calibration), and by Giosan et al. (2009) and Yanko-Hombach et al. (2014) that water depth in the northwestern Black Sea basin was above –30 to –40 m elevation by no later than ~9.0 cal ka and perhaps as early as ~9.9 cal ka (Larchenkov and Kadurin, 2011). Lister et al. (2015) presented three additional arguments for an unimpeded connection between a transgressed southwestern shelf and the open Neoeuxine Lake since at least 11.9 cal ka. They showed that there is a serious discrepancy between the annual flux and therefore integrated volume of sediment available from small local rivers of northwestern Turkey and the much larger volume of allosubunit 1b (their lithologic Unit C) around the M02-45 core site. For sources outside the immediate area to have contributed the majority of the sediment in this portion of allosubunit 1b, the shelf would need to have been accessible to major currents and waves capable of advecting sediment from larger rivers. Lister et al. (2015) further demonstrated a similar clay and silt mineralogy and trace-element content (Sc, Fe, Co, Ce, La, Th, Y) between the oldest Holocene deposits at the M02-45 site and its uppermost Holocene muds (allosubunit 1d), and argued that the Danube and perhaps the Kamchiya Rivers are the strongest candidates for this detritus, with erosion of calcareous loess from their floodplains accounting for calcitic silt (~30% of the silt fraction in lower allosubunit 1b at site M02-45; Lister et al., 2015). Finally, a significant contribution from river systems in general is supported by the dominance of terrestrial organic carbon in the TOC of allosubunit 1b (Hiscott et al., 2007b) and the considerable amount of coarse plant debris, pollen and fern spores in palynology samples from the allosubunit (Mudie et al., 2007). Allosubunit 1b has relative abundances of aquatic pollen taxa, algal spores, *Pediastrum ceonobia*, and fungal remains similar to those which characterise modern sediments of the Danube delta front and prodelta (Frail-Gauthier and Mudie, 2014).

Six paleobathymetry/paleotopography maps constructed between the α and α1 surfaces at the base and top of allosubunit 1b show that core site M05-50 near the Bosphorus exit was always open to the Neoeuxine Lake/Black Sea (Figs. 24–26 panels a–f). Core site M02-45 was also open to the Neoeuxine Lake during the latest Pleistocene with water depth of ~5 m at 12.5 cal ka, increasing to ~12 m at 11.5 cal ka (Fig. 24). The depression containing a greater thickness of allosubunit 1b around the M02-45 site remained open to the lake/sea and shows progressive increases in water depth between 10.5 cal ka and 7.5 cal ka (Figs. 25, 26 panels c–f). These maps and the dense grid of high-resolution seismic reflection data suggest no barrier islands, bars or spits to close or otherwise restrict communication between this depression and the open lake/sea.

The onset of lacustrine sedimentation of allosubunit 1b coincides with the time when the Neoeuxine Lake was purportedly experiencing an evaporative drawdown (§6). Lericolais et al.

(2007a, 2011) also argued for a deep regression at this time, interpreting that the contemporary Romanian shelf to –100 m elevation was covered by a field of aeolian dunes, recovered as sandy deposits in cores. The time of dune abandonment was dated to ~9.05 cal ka (see Supplementary material 2 for calibration) at a different site, several hundred metres away, where the entire Holocene section is only ~70 cm thick (compared with 1028 cm at key MUN site M02-45). A slight miscorrelation of seismic reflections over the intervening distance, leading to an error of as little as 10–15 cm, could make the top of the dunes considerably older (i.e., late lowstand, perhaps >12 cal ka).

7.2. Allosubunit 1b across the northeastern Marmara Sea shelf

Across the northeastern Marmara Sea immediately south of the Strait of Bosphorus (Fig. 20), the lower Holocene allosubunit 1b (equivalent to seismic stratigraphic Unit 2 of Hiscott et al., 2002) is bounded at its base and top by the β2 and β1 marker reflectors, respectively (Figs. 10, 27). It is interpreted as a south-prograded delta (i.e., Δ1; Hiscott et al., 2002; Aksu et al., 2016). Along the top of Δ1, irregularly stratified, flat-lying deposits are interpreted as delta-top fluvial and wetland deposits, whereas strata toward the distal portion of the depositional lobe are interpreted as prodeltaic silts and muds (Fig. 27).

The interpretation that Δ1 was fed by vigorous Black Sea outflow via the Strait of Bosphorus through 11.1–10.2 cal ka is one of the strongest arguments against the Flood Hypothesis. Eriş et al. (2007) used several radiocarbon dates from the *Calypso* core MD04-2750 to suggest that Δ1 developed from 6.55–3.7 cal ka, so had nothing to do with Neoeuxine Lake outflow. They instead attributed the delta to a small nearby stream, the Kurbağalıdere. However, Aksu et al. (2016) used three independent seismic and multibeam data sets and re-plotting of navigational fixes for the 1992/1993-vintage survey lines used by Eriş et al. (2007) to correctly align the MD04-2750 core with seismic profiles, and demonstrated that Eriş et al. (2007) misplotted the location of the MD04-2750 core site on their seismic profiles by a minimum of 200 m, using seismic data acquired by the Turkish Navy, Office of Navigation, Hydrography and Oceanography in Istanbul (SHOD for short) with navigation tied to navigation tied to ED50 (Turkish) ellipsoid, and plotting the core site with navigation tied to WGS84 ellipsoid. As a consequence, MD04-2750 does not date Δ1 to the middle Holocene, but rather to 11.1–10.2 cal ka (Aksu et al., 2016), precisely when evidence from the Black Sea suggests that the Neoeuxine Lake had risen to a height sufficient for brackish water to spill southward along the Strait of Bosphorus and into the Marmara Sea. Although Çağatay et al. (2021) have offered no challenge to the clear demonstration that the MD04-2750 site was incorrectly tied to seismic profiles in Eriş et al. (2007), they have retained a narrative that Δ1 is of late Holocene age. We categorically dismiss that narrative.

Both Gökaşan et al. (2005a) and Eriş et al. (2007) proposed that Δ1 was sourced by the small Kurbağalıdere stream which enters the northeastern Marmara Sea immediately east of the southern exit of the Strait of Bosphorus, but which is now largely buried beneath the southeastern Anatolian sector of the greater city of Istanbul between Fenerbahçe and Kadıköy (Fig. 27). However, four lines of evidence refute this suggestion: (a) calculations based on the sediment-yield model of Syvitski and Milliman (2007) indicate that the Kurbağalıdere stream could not have provided even 5% of the sediment contained in the delta lobe over the available time interval Hiscott et al. (2008); (b) there is no shelf-edge precursor to this delta at the LGM, suggesting that it was not formed by a pre-existing water course, but instead by a special set of circumstances which occurred after the Holocene transgression was underway (Hiscott et al., 2002, 2008); (c) the topset-to-foreset transition of the delta shows 3.3 km of progradation and at least 8–9 m climb into the rising Marmara Sea, unlike nearby deltas of larger rivers (e.g., Kocasu River; Fig. 3) which retreated landward during the early stages of the post-glacial transgression (Hiscott et al., 2002, 2007b; Aksu et al., 2016), and (d) source-to-sink tracing of very fine sand supplied to the delta (using SEM backscatter mapping and quantitative "mineral liberation analysis") suggests 50% contribution from Oligo–Miocene successions of the southwestern Black Sea coast and inner shelf, 20% contribution from the Göksu stream mid-way up the strait, and only minor contributions from other sources including the Kurbağalıdere stream (Aksu et al., 2016; Hiscott et al., 2017). The Kurbağalıdere sand fraction also contains far too little K-feldspar (relative to plagioclase) and lacks compatible amphiboles based on the Na, Mn and Ti contents of 152 separate crystals determined by energy dispersive X-ray analysis.

The topset-to-foreset transition of lowstand deltas along the southern shelf of the Marmara Sea occurs at a modern elevation of –100 m (Aksu et al., 1999a). There are two mid-shelf deltas across the northeastern Marmara Sea south of the Strait of Bosphorus, but there are no shelf edge precursor deltas (Hiscott et al., 2002, 2007a). The oldest and youngest topset-to-foreset transitions of the latest Pleistocene delta (i.e., Δ2 of Hiscott et al., 2002) occur at –77 m and –69 m, respectively. Similarly, the oldest and youngest topset-to-foreset transitions in the early Holocene delta (i.e., Δ1 of Hiscott et al., 2002) occur at –48 m and –40 m, respectively (Aksu et al., 2016). Assuming that the topset-to-foreset transition of deltas in the Marmara Sea occurs at 5 m water depth, the presence of two deltas believed to have been fed by Neoeuxine Lake outflow through the Strait of Bosphorus requires that the level of the Neoeuxine Lake reached and exceeded the elevation of the Bosphorus sill of the day. The breach depth of the Strait of Bosphorus during the Late Pleistocene is not known. The modern sill elevation is –37 m. The youngest delta Δ1 formed as base level in the Marmara Sea rose from –43 to –35 m, consistent with the earliest Holocene outflow over the sill having its water surface at or a few metres above ~ –40 m to maintain a hydraulic head *en route* to the delta top. A Neoeuxine Lake lowstand at this time (Ryan et al.,2003) cannot satisfy this requirement.

The only way that a small marine delta like Δ1 can aggressively prograde 3–4 km for 900 years into a regionally transgressing sea is if the short-term rates of sediment supply were remarkably high. There is no known source along the northeastern shores of Marmara Sea that could have provided this sediment supply, except the Strait of Bosphorus itself. It is also important to note that if deltas Δ1 and Δ2 were river deltas (as opposed to strait deltas), it would be difficult to explain the absence of precursor lowstand shelf-edge deltas, or what process(es) might have abruptly initiated and then abruptly terminated delta development to leave only a ~1000 yr record. If the strait itself provided detritus to the two delta lobes, it might be expected that the crest of the sill might have experienced erosion and temporal changes in elevation. Today, the elevation of unconformity β2 in the vicinity of the sill is ~ –55 m and the reflection we have correlated to the oldest Δ1 clinoforms is at ~ –50 m elevation (Fig. 35, although this cross section is not along the shallowest –37 m crest of the sill). If water-surface elevation was –40 m at 11.1 cal ka and only 5 m of water submerged the topset-to-foreset break, then it is possible that the sill was perhaps 5 m higher before the onset of Δ1 advance (so at –50+5 = –45 m elevation). The contemporary sill cannot have been lower than the –55 m β2 elevation, and after 10.2 cal ka it cannot have been lower than ~ –40 to –45 m (Fig. 35). The β1 surface is believed to be older than the ~9.5 cal ka first entry of Mediterranean water into the Black Sea basin (Aksu et al., 2016), so there appears to have been little erosion into the unconsolidated sediments in the vicinity of the sill when this northward flow passed through the strait.

The elevation of the sill during Late Pleistocene development of delta Δ2 must have been as low as –55 m or perhaps lower, because β2 is at that elevation near the sill (Fig. 35) and β2 post-dates the development of the Δ2 lobe. A second sill at the northern end of the Strait of Bosphorus has an elevation of –58 m today and only meager sedimentary cover over volcanic bedrock (Çağatay et al., 2021), so the elevation of the Neoeuxine Lake probably exceeded –58 m to permit outflow into the Propontis Lake at delta Δ2 time. If the lake surface was ~3–5 m higher than the northern sill, then the level of the Neoeuxine Lake would have been ~ –55 m. We use this value in §7.4 when considering conditions for evaporative drawdown of the Neoeuxine Lake. Note that setting water-surface elevation over the oldest delta Δ2 topset to –77 + 5 = –72 m and the level of the Neoeuxine Lake to –55 m results in an energy slope of ~0.0006 along the ~30 km-long strait. Stretches of rapids would have ensued, mostly downstream of the southern sill because it was probably no lower than ~ –60 m. For comparison, the energy slope of the Niagara River in North America, neglecting its famous waterfall, is ~0.0008.

7.3. Sr-isotopic measurements

Sr-isotopic measurements previously have been used by Major et al. (2006) and Yanchilina et al. (2017) to support the Flood Hypothesis, with shells coming mainly from coquina layers in short, low-resolution cores collected along the modern shelf edge and upper slope rather than from long, conformable stratigraphic successions. These coquina layers are transgressive lags created by wave action and contain shells of variable ages. One major issue in using coquina layers in Sr-isotopic work is that shells might have been transferred basin-ward during transgressive reworking; thus, the "principle of superposition" cannot be used to judge the true sequence of events whenever the error bars of radiocarbon-dated shells overlap. An additional problem with low-resolution cores is the difficulties associated with establishing accurate ties to nearby seismic profiles. In a low-resolution core, a 10 cm error in the tracing of a seismic reflection to the core site might lead to an error of several hundred years (if not more) in the assignment of an age to the seismic event.

Instead, Ankindinova et al. (2019a) obtained Sr-isotopic measurements on mollusc shells extracted from a 10 m-long composite core from the southwestern Black Sea shelf. Their data provide a detailed and unambiguous temporal trend with resolution ranging between <200 years in sediment older than 5.5 cal ka and 20–25 years for the early Holocene time of reconnection between the Black Sea (formerly the Neoeuxine Lake) and the global ocean (Fig. 28; Ankindinova et al., 2019a). These authors delineated four stages of $^{87}Sr/^{86}Sr$ increase and salination associated with the reconnection. From 12.04–9.53 cal ka (stage A), before first Mediterranean inflow, the Sr-isotopic ratio varied from 0.708847–0.708881 (Fig. 28). For 100 years immediately before reconnection (9.53–9.48 cal ka, stage B), $^{87}Sr/^{86}Sr$ values dropped to their lowest levels: 0.708841–0.708843, but then in stage C abruptly began to climb starting at 9.48–9.45 cal ka and reached a quasi-steady-state "plateau" with ratios 0.708965 by 9.42 cal ka (Fig. 28). The sharp $^{87}Sr/^{86}Sr$ increase marks the first significant intrusion of saline water into a previously isolated Neoeuxine Lake. The quasi-steady-state condition lasted ~500–550 years. Subsequently, starting 8.87 cal ka and proceeding to the present day, there was a step-wise rise of $^{87}Sr/^{86}Sr$ to modern levels (stage D; Fig. 28), during which a salinity threshold was passed that allowed widespread replacement of brackish-water faunas by Mediterranean species (Fig. 29; Williams et al., 2018). In the original Ankindinova et al. (2019a) paper, two critical $^{87}Sr/^{86}Sr$ values in stage B are missing in the table of isotopic measurements, so a full complete list of Sr-isotopic ratios and their newly recalibrated ages are provided here as Supplementary material 4.

Modelling by Ankindinova et al. (2019a) suggests that the lake/sea level likely did not, and could not, rise from −120 m to −30 m between 9.48 cal ka and 9.42 cal ka unless (a) the Sr concentration in the pre-reconnection Neoeuxine Lake was 3–4 times higher than in modern Danube River water, or (b) the water column of the lake was strongly stratified during first entry of saline water. The second alternative is very unlikely because of seasonal vertical mixing (downwelling/upwelling) in what was then a rather homogeneous temperate-climate lake. Catastrophic flooding of a lowstand lake would require an average discharge through the Strait of Bosphorus of ~9500 m^3 s^{-1}, whereas entry of saline Mediterranean water as an underflow into an already high lake could reproduce the first stage of $^{87}Sr/^{86}Sr$ increase with an average discharge as low as ~2200 m^3 s^{-1}. Because the M02-45 site is 50 m above the Late Pleistocene lowstand shoreline and contains sediments with $^{87}Sr/^{86}Sr$ values that record the first entry of saline water into the Neoeuxine Lake, below storm wave base (Hiscott et al., 2007b), the surface of the lake must have been significantly higher than −70 m at the time of the reconnection (Fig. 21b).

Ankindinova et al. (2019a) documented that $^{87}Sr/^{86}Sr$ isotopic values in composite core M02-45 conform perfectly to the coarser Sr-isotopic trends published in Major et al (2006) and Yanchilina et al. (2017), firmly establishing that the shells extracted from core M02-45 must have being living in water with the same evolving chemistry as water in the open Neoeuxine Lake. Clearly this core site had to be on the margin of the lake itself, and base level cannot have been below the contemporary shelf edge as required by the Flood Hypothesis.

7.4. Faunal and floral data

Faunal and floral data reveal an internally consistent post-glacial salination history for the southwestern Black Sea (Fig. 29). Coccoliths are only present in allosubunit 1d within the upper

270 cm of composite core M02-45 (Fig. 29). The flora are dominated by *Emiliania huxleyi* with very minor and sporadic occurrences of *Thorachosphaera* spp., *Reticulofenestra* spp. and *Cyclococcolithus leptoporus*. Clone cultures in strains of *E. huxleyi* reveal that this species can tolerate surface water salinities of 15–17; however, under such conditions the organism displays strongly depressed calcification (Paasche et al., 1996; Saruwatari et al., 2016). The sustained occurrence of *E. huxleyi* in the southwestern Black Sea suggests that surface water salinities exceeded 15 since ~2.0 cal ka, possibly as early as ~5.5 cal ka (Fig. 29).

Calcareous benthic foraminifera are present in allosubunit 1d, but are abundant and diverse below the hiatus at α2 in the lower portion of allosubunit 1c and the upper portion of allosubunit 1b (Fig. 29; Hiscott et al., 2007b). They are absent in sediments older than ~9.3 cal ka (i.e., below 650 cm depth) in composite core M02-45. The fauna are overwhelmingly dominated by *Ammonia compacta* and *Ammonia tepida* with lesser numbers of *Porosononion subgranosus mediterranicus*. These species prefer shallow littoral and neritic environments and are tolerant of lower salinities and relatively high sedimentation rates (Debenay et al., 1998). They are reported to thrive on labile organic carbon produced by abundant phytoplankton fertilised by nutrients in the fluvial discharge along the western Black Sea off the mouth of the Danube River (Yanko-Hombach et al., 2017a). *A. tepida* dominates the fauna in allosubunit 1c, whereas *A. compacta* and *A. tepida* co-dominate the fauna in allosubunit 1d (Fig. 29). Smaller percentages of marine species *Haynesina depressula*, *H. germanica*, *Gavelinopsis praegeri*, *Elphidium* spp., *Eggerelloides scabrus*, *Ammomarginulina* spp., *Reophax* spp. and Lagenids and Miliolids (mostly *Triloculina* spp.) are also noted in allosubunit 1d (Hiscott et al., 2007b). Previous studies have shown that an assemblage dominated by *A. tepida* (without lagenids) today characterises areas of the inner continental shelf off Bulgaria where salinity values are in the range 17–19. *A. compacta* is a relatively deep-water form which characterises areas deeper than –70 m on the modern Bulgarian outer shelf; there, the salinity is 21–22 (Yanko, 1990).

Ostracods are ubiquitous in the southwestern Black Sea (Williams et al., 2018). From 11.9 cal ka to 7.3 cal ka (see Supplementary material 2 for calibration), the ostracod assemblage is dominated by Ponto-Caspian species, mainly *Loxoconcha sublepida*, *L. lepida* and *Tyrrhenocythere amnicola donetziensis* (Fig. 29; Williams et al., 2018). From 7.3 cal ka to 6.2 cal ka the assemblage consists of nearly equal abundances of Mediterranean species and Ponto-Caspian species. After 6.2 cal ka to the tops of MUN cores, the assemblage is dominated by Mediterranean species, including *Palmoconcha agilis*, *Carinocythereis carinata*, *Hiltermannicythere rubra* and *Pterygocythereis jonesii* (Fig. 29; Williams et al., 2018). These data indicate that environmental changes were progressive on the southwestern Black Sea shelf from at least 7.3 cal ka to the present. The first hint of changing conditions at 7.3 cal ka lags the initial reconnection to the Mediterranean Sea through the Strait of Bosphorus by ~2000 years (cf. Aksu et al., 2016 and Williams et al., 2018), demonstrating that Black Sea salinity increased slowly and took that long to reach values tolerable to marine ostracod immigrants. Widespread colonisation by Mediterranean species took even longer, ~3000 years from the time of the initial reconnection.

Two studies have provided salinity estimates using the process length of the dinoflagellate cyst *Lingulodinium machaerophorum* (Mudie et al., 2007; Mertens et al., 2012). Mudie et al. (2007) used dinocyst assemblages to show that variability in process length marks low diversity pleni-glacial–early Holocene *Spiniferites cruciformis* assemblages, suggesting fluctuating salinity similar to the modern Caspian Sea, with brackish to saline conditions with salinities of 5–16. Based on the distributions of euryhaline cysts *Spiniferites mirabilis* and *Spiniferites* *bentorii* these authors have shown that the Aegean and Marmara seas were already connected by 12.5 cal ka (11 ^{14}C ka) and linked to the Black Sea basin by 10.3 cal ka (9.3 ^{14}C ka). Furthermore, Mertens et al. (2012) calibrated summer surface-water salinity in the Black Sea, Sea of Azov and Caspian Sea with the process lengths of the dinoflagellate cyst *L. machaerophorum*. These authors then applied this calibration equation to the Black Sea, documenting a very gradual change of salinity from ~14 around 9.7 cal ka to a minimum 12.3 around 8.5 cal ka, reaching current salinities of 17.1 around 3.9 cal ka. The ~250 year resolution of their sampling failed to reveal a catastrophic salination event at 9.5–9.0 cal ka advocated by other researchers. Finally, the freshwater algae *Pediastrum* and *Botrycoccus* are only significant below a depth of 510 cm in composite core M02-45 (7.9 cal ka; Mudie et al., 2007). In the same interval and upward to a depth of 460 cm in core M02-45 (6.9 cal ka), a dinocyst assemblage dominated by *Spiniferites cruciformis* and *Pyxidinopsis psilata* indicates brackish waters with salinities of 3–12 (Fig. 29; Hiscott et al., 2007b). Minor amounts of euryhaline Mediterranean species in the same interval indicate periodically increased salinity. Along with Mudie et al. (2007), we interpret the overlap of *Pediastrum* and the *S. cruciformis* assemblage (*S. cruciformis*, *S. inaequalis* and *Pyxidinopsis psilata*) to indicate brackish conditions throughout allounit 1b, with the freshwater species washed in from rivers or nearby coastal areas. Mediterranean dinocysts *S. belerius*, *S. bentorii*, *S. mirabilis*, *S. ramosus* and *Operculodinium centrocarpum* first appear in a persistent way at a depth of 510 cm in core M02-45 (7.9 cal ka), reaching their highest relative proportions in the lower part of allosubunit 1c (Fig. 29; Mudie et al., 2007). These species require salinities above 12; abundance peaks of these taxa indicate sea surface salinities of at least 20. The overlapping occurrences of these Mediterranean species with the *S. cruciformis* assemblage and ostracods with Ponto–Caspian (brackish) affinities indicate lower salinities in nearshore areas including the middle shelf, and more influence of Mediterranean waters farther offshore. *Lingulodinium machaerophorum* (Fig. 29) can tolerate salinities as low as 3, but becomes abundant at salinities >10. Its acme is confined to core depths shallower than 475 cm in core M02-45 (7.1 cal ka), essentially coincident with the proliferation in allosubunit 1c of Mediterranean species of molluscs, ostracods and dinocysts (Hiscott et al., 2007b). These palynological publications demonstrate that the surface salinities of the Neoeuxine Lake during the early Holocene ranged between 7 and 13, then gradually increased to the present day values of 17. An essentially coincident transition from brackish to more salinity-tolerant dinocysts has also been reported for cores collected in coastal areas and the Black Sea shelf off Bulgaria (Filipova-Marinova and Bozilova, 2002; Filipova-Marinova, 2003; Filipova-Marinova et al., 2004).

Recently, Huang et al. (2021) used alkenones from a core recovered at –971 m elevation to show a salinity rise from ~2 to ~6 between ~13 cal ka and ~9.5 cal ka, with no evidence for a discontinuity at the time of first entry of Mediterranean waters. These values are lower than those obtained using *L. machaerophorum* process lengths, but show a similar climb in values preceding and through the time of reconnection. Huang et al. (2021) attribute the salinity rise before reconnection to a negative water balance in the Neoeuxine Lake, but it should be noted that this situation does not require a base-level fall, but only that all river water entering the basin is unable to escape, so the annual inputs (R+P) are balanced by evaporation (E) leading to concentration of dissolved components. For example, consider a 16 cal ka lake at –55 m elevation (Fig. 36a) and salinity S=3.0 being evaporated to –110 m with no river supply. The volume would change from 517010 km^3 to 497940 km^3, so the salinity would only increase to ~3.1. Now consider a lake with average volume of 522500 km^3 (so ~ –40 m elevation) and initial S=3.0, experiencing 6000 yr of river input (e.g., 15.5–9.5 cal ka after meltwater influx) at today's 350 km^3 yr^{-1} (reasonable for a rising lake and early Holocene climate; cf. Radoane, 2021), with river salinity S=0.45 (from Stankovic, 2006, Danube conductivity = 900 µS cm^{-1}). The resultant salinity would be ~4.8, so a far larger gain at constant base level than through evaporative drawdown, which alone has little impact. Of course base level is believed to have dropped to ~ –110 m before rising again to the sill depth in the Strait of Bosphorus, but that would not have seriously affected salinity based on scenarios like those described above (i.e., subtracting then adding river water augmented by variable precipitation over the lake). Short of introducing high-salinity seawater or brines from compacting substrata, the key to salinity changes in a closed basin is long-term concentration through evaporation of incoming river water.

Proxy data from cores across the northeastern Marmara Sea shelf provide further evidence for events in the Neoeuxine Lake and Black Sea described above. The most critical of these data are oxygen ($\delta^{18}O$) and carbon ($\delta^{13}C$) isotopic data from benthic foraminifera *Neocarinata crassa* and the faunal and floral characteristics of Marmara Sea allosubunit 1b (Fig. 30; Aksu et al., 2002b). Allosubunit 1b (i.e., seismic stratigraphic subunit 1b) represents the early Holocene mid-shelf delta Δ1, deposited from 11.1–10.2 cal ka (Figs. 13, 15; Aksu et al., 2016). The allosubunit is characterised by a *S. cruciformis* dinocyst assemblage with low percentages of *L. machaerophorum*, a Polypodiaceae and shrub pollen assemblage with low pine pollen percentages and the absence of coccoliths and planktonic foraminifera (Fig. 30; Aksu et al., 2002b). The benthic foraminifera consist of a low diversity fauna dominated by brackish water species (i.e., *Ammonia beccarii*, *A. tepida*, *A. compacta*). These fauna indicate oxic bottom waters (Kaiho, 1994). During the deposition of allosubunit 1b, the Marmara Sea was already connected to the global ocean—the breach of the sill in the Strait of Dardanelles occurred at 13.8 cal ka (Aksu et al., 2016), and the bottom water mass (thus most of the water volume) had originated by inflow from the Aegean Sea. Therefore, the brackish water mass which was introduced during the early Holocene, with fern and shrub pollen and a low-salinity *S. cruciformis* dinocyst assemblage can only be explained by Neoeuxine Lake outflow into the Marmara Sea. The $\delta^{18}O$ data of benthic foraminifera *N. crassa* in allosubunit 1b are characterised by depleted (<2‰) isotopic values, gradually becoming enriched toward the allosubunit 1b–1c transition (Fig. 30). This isotopic signal strongly suggests that the shelf waters during the deposition of the allosubunit had low salinity, gradually increasing toward the allosubunit 1b–1c transition. The $\delta^{13}C$ data for *N. crassa* show a nearly reciprocal relationship to the $\delta^{18}O$ record, with slight enrichment in allosubunit 1b, most likely reflecting the carbon isotopic composition of the DIC of the seawater in which the foraminiferal calcite was secreted (e.g., Ravelo and Hillaire-Marcel, 2007). The low abundance of opaline silica and the low concentrations of TOC further suggest that the surface waters did not have high biological productivity (Fig. 30).

Following the abandonment of delta Δ1, the northeastern Marmara Sea shelf transitioned into a marine environment. Kaminski et al., 2002) showed that at ~9.65 cal ka the abundance of the benthic foraminiferal genus *Ammonia* rapidly declined (Fig. 30) and planktonic foraminifera and coccoliths appeared, indicating that fresh-water outflow from the strait had declined to the point that more stenohaline species could establish themselves (Aksu et al., 2002b). Shortly before 9.65 cal ka, benthic foraminifera of Mediterranean origin colonised the prodelta fringe (dominated by *Brizaliana* spp, *Bulimina elongate*, *B. marginata*, *B. aculeate* and *B. costata*), suggesting that a salt wedge or estuarine-type flow had been established during the latter phases of Δ1 advance (Fig. 30; Kaminski et al., 2002). An enriched $\delta^{18}O$ record throughout allosubunit 1c suggests that increased salinities prevailed across the northeastern Marmara Sea shelf since the transition from allosubunit 1b to 1c (Fig. 30). The increased abundances of opaline silica and TOC, together with high concentrations of coccoliths and planktonic foraminifera, signal the establishment of more fully marine conditions in the area.

7.5. Linked sapropel deposition across the Marmara Sea (M1) and Aegean Sea (S1)

Across the eastern Mediterranean Sea, the development of sapropels has been linked to density stratification in the water column, which leads to weakening of vertical mixing and oceanic ventilation, severely reducing the advection of oxygen-rich surface waters into basinal depths (e.g., Rohling et al., 2015). Reduction in the rate of bottom water formation (or its cessation) leads to stagnation of bottom waters. Dysoxia/anoxia quickly follows, which in turn creates greater potential for the burial and preservation of the organic carbon settling to the seabed.

There are two different views on how water-column stratification developed in the Aegean Sea: (a) some researchers have advocated that the stratification occurred in near synchroneity with a similar development in the eastern Mediterranean Sea, which was triggered by an increase in African monsoonal run-off primarily through the Nile River associated with the 19–21 kyr precessional cycles of Earth's orbit (e.g., Rossignol-Strick, 1985; Scrivner et al., 2004; Rohling et al., 2015; Grant et al., 2016) and (b) others have argued that the morphology of the Aegean Sea as an archipelago dotted with hundreds of islands is much too restrictive for the fluvial discharges from the Nile River to reach the central and northern Aegean Sea basins and that increased fluvial discharge into the northern Aegean Sea by rivers draining Eastern Europe, and glacial and fluvial run-off into the Black Sea and subsequent outflow into the Aegean Sea through the Marmara Sea Gateway induced water column stratification across the Aegean Sea (Aksu et al., 1995b; İşler et al. 2016b). Herrle et al. (2018) record a broad depression in sea surface salinity (SSS) from ~10–6.5 cal ka in the northern Aegean Sea as well as two particularly strong reductions at ~8.3 cal ka and 7.6 cal ka, and attribute these latter events to pulses of Black Sea outflow induced by global steps in base-level rise after meltwater discharges in North America, leading to rapid expulsion of Black Sea surface waters. The timing of Holocene Neoeuxine Lake and Black Sea outflow fits nicely with the timing of S1 development, but not well for M1 in the Marmara Sea, which was initiated ~1700 years before the outflow responsible for the development of delta Δ1 south of the Bosphorus exit (Fig. 31).

Aksu et al. (2002b, 2016) and Hiscott et al. (2007a, 2017, 2021) proposed that outflow of large quantities of brackish water from the Black Sea basin across the Strait of Bosphorus during the early Holocene created the necessary conditions for sapropel M1 deposition across the Marmara Sea as originally proposed by Çağatay et al. (2000). However, the onset of M1 deposition pre-dates the outflow recorded by Δ1, so other explanations are required. Alternative 1 is that the initiation of Δ1 might have lagged the start of brackish-water export along the Strait of Bosphorus, as this outflow strengthened to a level sufficient to transport bedload material. Constantinescu et al. (2015) propose that transgression of the Neoeuxine Lake shelves began ~11.7 cal ka; delta Δ1 started to prograde into the Marmara Sea at ~11.1 cal ka, so it is not unreasonable to propose that brackish-water outflow began ~11.5 cal ka, contributing to water column stratification, although still not being early enough to trigger the original stratification required for M1 onset. Alternative 2 has been provided by Çağatay et al. (2009, 2015) and Liu et al. (2021). They suggested that the advection and subsequent sinking of saline Mediterranean water during the post-LGM reconnection of the Marmara Sea with the Aegean Sea (at 13.8 cal ka according to Aksu et al., 2016) forced the less dense lake water to the surface. These upwelling waters would have been rich in nutrients, increasing primary and secondary biological productivity across the Marmara Sea. At the same time, the bottom waters became dysoxic or anoxic through oxidation of the incoming biomass, thus triggering sapropel formation. Other workers have provided support for this suggestion using SST and SSS estimates derived from alkenone biomarkers and oxygen isotopic variations (Sperling et al., 2003; Vidal et al., 2010). For example, Vidal et al. (2010) stated that SSS actually increased during the deposition of the lower portion of sapropel M1, suggesting a weak or no outflow from the Neoeuxine Lake.

A major problem with the alternative 2 mechanism advocated by Çağatay et al. (2009, 2015) and Liu et al. (2021) is that the volume of the Marmara basin is extremely small compared with reasonable rates of inflow of Aegean water during the 13.8 cal ka reconnection event. Hiscott et al. (2021) estimate that full replacement of fresh/brackish water originally present in the Propontis Lake would have been complete by ~13.2 cal ka. This would leave no mechanism to maintain stratification for ~1700 years until it could be reinforced by outflow from the Neoeuxine Lake beginning at ~11.5 cal ka. Nevertheless, the initial elevation of brackish water to the surface is a reasonable explanation for the onset of M1 development, even if not a viable explanation for its longer term persistence. Regarding the speed of conversion of the Propontis Lake to a fully marine embayment of the Aegean Sea, Çağatay et al. (2009) dated a *Mytilus edulis* shell from a bioherm on the northern shelf, at ~15 m paleo-water depth, to 13.1 cal ka, and we have dated *Parvicardium exiguum* and *Mytilus galloprovincialis* shells from similar paleo-water depths to 12.8 cal ka and 13.0 cal ka, respectively (cores M02-103P and M02-111P; Table 2). A slightly older specimen of the fresh/brackish-dwelling gastropod *Euxinipyrgula lincta* from MUN core M14-03P (~10 m paleo-water depth) has an age of 13.35 cal ka, indicating that marine euryhaline fauna populated even surface waters of the Marmara Sea sometime between 13.35 cal ka and 13.1 cal ka.

Between the final expulsion of relict Propontis Lake water from the Marmara Sea basin at ~13.2 cal ka and the onset of significant Neoeuxine Lake outflow at ~11.5 cal ka, we propose an alternative 3: that the Marmara Sea deep water remained stagnant and thereby depleted in oxygen as a consequence of negligible current activity and no driving mechanism for upwelling/downwelling to improve ventilation. During this period, there would have been (a) little exchange with the northern Aegean Sea because of no remaining salinity differences and (b) insufficient discharge from local rivers (e.g., Kocasu River; Fig. 3) to do more than perhaps balance evaporation over the sea surface. Analogy can be made with the smaller scale Saanish Inlet in western Canada, which has a history of sapropel accumulation even though fully marine, simply because of near-isolation of its bottom waters from the open ocean and no deep-water circulation (Bornhold et al., 1998). This situation could explain the elevated rather than depressed SSS estimates of Sperling et al. (2003) and Vidal et al. (2010), particularly for the earlier stages of M1 development.

By 11.1 cal ka (or perhaps 11.5 cal ka), Neoeuxine Lake sustained outflow would have re-introduced a low salinity lid across the Marmara Sea, further preventing the ventilation of the bottom waters. However, the contribution of the outflow at this time to stratification might have been less than we have previously claimed, because there is no perceptible effect on SSS (Vidal et al., 2010) and there was no northward-directed counter-flow of saline water into the Black Sea basin to boost the discharge of the outward stream. Today, if there were no exchange along the Strait of Bosphorus, the annual amount of surplus water in the Black Sea budget (i.e., R+P-E) would be ~300 km^3 (Oğuz et al. 2004), about half of today's outflow. Clearly, a significant amount of today's outflow results from a density-driven exchange: entry of denser Mediterranean water at depth and complementary expulsion of brackish water toward the surface. There is no strait-exit delta today, not because of weaker outflow, but because the modern outflow is detached from the floor of the strait so does not transport bedload to its southern exit.

A combination of persistent stagnant bottom waters and an evolving fresher surface layer due to outflow likely allowed M1 sapropel to continue accumulation until the establishment of strong and persistent two-way exchange through the gateway between ~9.0–8.0 cal ka. Vidal et al. (2010, their §6.2.4) stated that "*...a significant outflow of Black seawater in the Sea of Marmara started again at approximately* [the time of initial entry of Mediterranean water into the Black Sea basin]*, as indicated by the salinity decrease possibly due to an increase in regional precipitation ...*". Although this enhanced volume of outflow more firmly established a brackish-water cap over the Marmara Sea, the increased volume of saline deep water transiting the Marmara central basins disrupted their earlier stagnant condition and probably accounts for the short residence times of the deep water today (~12–19 years; Lee et al., 2002). Since the Marmara deep water enters that small sea via the relatively shallow Strait of Dardanelles, it is oxygenated at entry, which diminishes any prospect of maintaining deep-water anoxia and conditions for sapropel development. Hence, M1 accumulation stopped by ~6.6 cal ka (Fig. 31). Sperling et al. (2003, their figure 4) initially proposed a similar reason for M1 termination.

Aegean Sea sapropel S1 was deposited during 10.75–6.9 cal ka (İşler et al., 2016b) beneath isotopically depleted, relatively cool and lower salinity surface waters (Fig. 32; Aksu et al., 1995b,c; İşler et al., 2016a,b; Herrle et al., 2018). Microfaunal and microfloral data indicate a major reduction in SSS, and oxygen isotopic data show a northerly fresh water source (Aksu et al., 1995b,c; İşler et al., 2016a,b). Relatively light $\delta^{13}C_{org}$ and high pollen-spore concentrations in S1 suggest increased influx of terrestrial organic carbon, probably supplied by major rivers draining into the northern Aegean Sea (Aksu et al., 1995c; İşler et al., 2016a,b). Benthic foraminifera indicate high-nutrient, oxygen-poor bottom waters for S1, yet based on the presence of silt-sized hematite and manganese coatings the seafloor nevertheless remained oxygenated (Aksu et al., 1995b,c; İşler et al., 2016a,b). Visual and XRD evidence of pyrite in S1, together with enrichments in S, Cu, Zn, As, Ni, Cr and Fe suggest that conditions below the sediment-water interface were sufficiently reducing for SO_4^{2-} reduction to occur, probably by diffusion from surface oxic into subsurface anoxic sediments. Palynological data show large increases in terrestrial pollen and spores across sapropel S1, with the floral assemblage indicating significant influx from northern European rivers, but with minor African components associated with increased summer monsoonal rain (Aksu et al., 1995b,c). The latter authors further showed that there was some increase in primary productivity during the deposition of S1, but no evidence for upwelling; a conclusion also reached by İşler et al. (2016a,b). In shallow basins with a thin surface layer, stratification can be broken during intense storms, which would cause the thermocline/nutricline to rise well into the surface mixed layer. As a result, nutrient-rich waters would increase the rate of photosynthesis, enhancing primary production. İşler et al. (2016b) suggested that sapropel S1 across the Aegean Sea was deposited in the absence of a deep chlorophyll maximum layer, so that the water column lacked a deep phytoplankton assemblage. Under such conditions, oxygen advection via intermediate water flow must have been significantly reduced, which implies significant stagnation.

Sapropel S1 coincided with maximum depletions in $\delta^{13}C$ and lowest SST values. Its formation is attributed to intense fresh/brackish water input, which resulted in strong stratification and the near stagnation of the bottom water (Fig. 32; İşler et al., 2016a,b). İşler et al. (2016b) also suggested that during the deposition of sapropel S1 the pycnocline significantly weakened across the Aegean Sea associated with the cessation of the formation of Mediterranean Intermediate Water in the region. Depletions in the $\delta^{13}C$ values of the TOC during the deposition of sapropel S1 further suggest significant inputs of fresh and/or brackish water. The close temporal association between brackish-water outflow from the Black Sea and sapropel deposition in the Marmara and Aegean Seas (Fig. 31) has been suggested by earlier studies (e.g., Aksu et al., 1995b,c; Hiscott et al., 2007a, 2007b). Thom (2010) modeled the hydrological budget of the Black Sea through the Late Quaternary and concluded that the Black Sea must have been exporting water to the world ocean during S1 time.

In summary, the origin of sapropel M1, in particular, likely involved a sequence of different mechanisms promoting bottom-water isolation: (a) lifting of relict Propontis Lake water as Aegean Sea water filled the deeper portions of the Marmara Sea (~13.8–13.2 cal ka) → 1.5–2.0% sapropelic mud; (b) stagnation of deep waters when the sea was a marine embayment devoid of bottom currents and with limited exchange (~13.2–11.5 cal ka) → sapropelic mud and sapropel; (c) continued stagnation but with introduction of a brackish surface layer to further impede ventilation (~11.5–9.5 cal ka) → sapropel; (d) decay of bottom-water stagnation eventually leading to termination of M1 because of active replenishment and northeastward flow of saline waters *en route* to the Black Sea (~9.5–6.6 cal ka) → sapropel giving way to sapropelic mud (~6.6–6.2 cal ka). This review provides an internally consistent interpretation for the origins of largely contemporaneous sapropels M1 and S1, rather than needing fully independent mechanisms for similar and near synchronous organic-rich deposits in such close geographic proximity.

7.6. Late activation of a saline inflow channel network

A prominent anastomosed channel network (herein called the Saline Channel; Fig. 33) crosses the southwestern Black Sea shelf linking the northern exit of the Strait of Bosphorus with a number of canyon heads that are cut into the shelf-edge (Di Iorio et al., 1996, 1999; Özsoy et al., 2001; Flood et al., 2009; Hiscott et al., 2013; Ankindinova et al., 2020). The main channel is ~20 m deep immediately north of the Bosphorus exit, but progressively becomes shallower (~5 m deep) toward the outer shelf, and is locally flanked on its western side by low-angle (2º–5º) lateral-accretion deposits indicating lateral infilling of the channel by detritus advected eastwards by the Rim Current (Hiscott et al., 2013). A number of muddy in-channel barforms and a variety of sediment waves adorn both the channel floors and bar crests (Fig. 33), and there are crevasse channels entering the overbank area, and levée/overbank deposits. Between water depths of 80–100 m, numerous conical mounds, some with what appear to be central "vents" indicate fluid seepage along linear fractures, or perhaps extrusion of fluid mud (Flood et al., 2009). These mounds exhibit streamlined leeside tails ascribed to winnowing and deposition associated with the eastward-flowing Rim Current (Flood et al., 2009). All these sedimentary features are radiocarbon-dated in numerous cores to be younger than 8–8.4 cal ka (Flood et al., 2009; Hiscott et al., 2013; see Table 2 and Supplementary material 2 for calibrations).

Ryan et al. (2014) suggested that the Saline Channel (they referred to it as a "depositional fan") was constructed following the erosive, rapid entry of saline Mediterranean water through the Strait of Bosphorus. They say (p. 22) "*it* [is] *likely that the outburst phase was rich in sediment scoured from the entry portal* [i.e., the Strait of Bosphorus] *and delivered to an apron on the shelf in sheets of chaotic debris*". In support for their arguments they pointed to the presence of a basal deposit of pebbly glacial/post-glacial shell debris with pebbles identical in "*composition to quartzite and gabbro recovered in drill cores from the Bosporus Strait*". A similar interpretation was subsequently published by Lericolais et al. (2019) who called the depositional fan of Ryan et al. (2014) a "shallow fan delta", and proposed that it was likely formed by a single event following relatively strong Mediterranean-originated northerly flow onto a subaerially exposed shelf before ~9.3 cal ka (8.5 ^{14}C ka; Lericolais et al., 2019). These authors further suggested that the original wedge of sediments was subsequently reworked during the Holocene into the current channel configuration by the saline undercurrent.

Ryan et al. (2014) and Lericolais et al. (2019) provide no chronostratigraphy for the sediments in the vicinity of the Saline Channel, particularly above the shelf-crossing unconformity α. We know, however, that the oldest allosubunit 1b was deposited between 12.3 cal ka and 7.2 cal ka, with a somewhat older contact with allosubunit 1c in the Saline Channel area, where allosubunit 1c is as old as ~8.2 cal ka (Fig. 15). Allosubunit 1b consists of sub-horizontal, parallel reflectors which define basin-fill morphology with progressive onlap over the irregular surface created by the shelf-crossing α unconformity (Supplementary material 3; Ankindinova et al., 2020). Allosubunit 1b is not part of the saline channel deposit, but underlies it. It is allosubunits 1c and 1d which were created and molded by the northward-flowing saline undercurrent exiting the Strait of Bosphorus (Flood et al., 2009; Hiscott et al., 2013; Ankindinova et al., 2020). Allosubunit 1c occurs between the α1 and α2 unconformities/correlative conformities dated by their first overlying deposits to (α1) ~7.2 cal ka where conformable near the Bulgarian border (M02-45; Fig. 15) to ~8.2 cal ka in the vicinity of the Saline Channel and (α2) ~5.5 cal ka where conformable near the Saline Channel to as young as ~2.0 cal ka in the west. Allosubunit 1d occurs above the α2 unconformity/correlative conformity so is everywhere younger than ~5.5 cal ka (Ankindinova et al., 2020). All of these deposits are younger than ~8.2 cal ka so cannot be related to a ~9.5 cal ka catastrophic flooding of the Black Sea.

Bedrock across the northeastern sector of the Istanbul Peninsula and the northwestern sector of the Kocaeli Peninsula is composed of Upper Cretaceous mafic volcanics and intrusive rocks of the Sarıyer Formation (Özgül et al., 2005). Very fine sand samples from the streams draining these rocks contain chromite, cummingtonite, staurolite, celadonite, ilmenite, serpentine, riebeckite and rutile, clearly representing a mixed mafic volcanic and metamorphic source (Hiscott et al., 2017). Thus, the presence of mafic rock fragments on the adjacent shelf cannot be used as evidence for catastrophic and deep erosion of the Bosphorus valley. There is no reason that material of this composition (including gravel) could not have been transported onto the lowstand coastal plain during the Pleistocene. Streams and small rivers in the area today carry such bedload seaward (e.g., Riva River near the strait exit; Fig. 2), and even at lowstands there could have been northward fluvial transport along the Bosphorus valley and onto the coastal plain from watersheds like the modern Göksu stream (Fig. 2).

Ryan et al. (2014, p. 11) and Lericolais et al. (2019) used a Gökaşan et al. (2005) volume estimate of 2×10^8 m^3 for the sediment excavated from an inner channel along the Strait of Bosphorus to compare with the volume of their so-called depositional fan/shallow fan delta. Ryan et al. (2014) concluded that "*the volume of the chaotic interior of the fan is comparable in magnitude to the volume excavated from the floor of the Bosporus Strait*". A very tight grid of high-resolution seismic reflection lines with 200–300 m line spacing across the entire Saline Channel area (Flood et al., 2009; Hiscott et al., 2013), and a solid chronostratigraphy with 57 radiocarbon dates in nine key cores (Ankindinova et al., 2020) allow calculation of the volume of sediments across the Saline channel area. The total volume of sediments above the α1 unconformity in allosubunits 1c+1d is 1.77×10^{10} m^3, which is ~90 times the estimated volume of sediments excavated from the floor of the Strait of Bosphorus by Gökaşan et al.(2005). Interpreted cross sections in Ryan et al. (2014) indicate that they included almost all deposits above α1 in their so-called "chaotic interior". Clearly the volume of sediments in the Saline Channel area violates any claim that it might compare well with potential erosion products from a putative catastrophic flood.

8. Discussion

8.1. Outflow versus Flood

The Outflow Hypothesis originally proposed by Aksu et al. (2002c) passes its two most critical tests: (a) there is compelling evidence that the Neoeuxine Lake had transgressed the marginal shelves of the Black Sea basin centuries before entry of saline Mediterranean waters, and (b) there is a clear record of discharge through the Strait of Bosphorus, Marmara Sea and Strait of Dardanelles during the same time interval preceding first penetration of saline waters through the strait. A pre-11 cal ka (and probably pre-12 cal ka) transgression of the shelves of the Neoeuxine Lake is conclusively indicated by at least four independent lines of evidence: (1) calcareous silty muds, deposited below storm wave base (at least 40–50 m today), are widely distributed on the southwestern shelf at paleo-elevations as shallow as –70 m (Hiscott and Aksu, 2002, their figure 16b; Fig. 22), (2) earliest Holocene lobes of the Danube Delta, deposited at a base level of –30 to –40 m, developed several hundred years before initial entry of saline waters (Giosan et al., 2009); (3) delivery by turbidity currents of sandy detritus to the Danube deep-sea fan ceased at ~11.7 cal ka because of transgression of the outer shelf to an elevation of –70 m or shallower, after which base level remained higher (Constantinescu et al., 2015); (4) alongshore growth of a ~9–9.5 km-long and ~0.9–1.1 km-wide recurved spit at –30 to –35 m elevation south of Cape Emine (Fig. 18; Ankindinova et al., 2020, their figure 25) requires a stillstand for centuries, which is only possible if the Neoeuxine Lake was temporarily pinned to the spill depth at the Bosphorus exit; if base level was instead controlled by rise of the global ocean after catastrophic entry of Mediterranean waters, the surface of the Black Sea would have climbed continuously at a rate of ~10 m kyr^{-1} (e.g., Lambeck et al., 2007). Rejection of a dramatically lower lake level before reconnection is supported by chronological arguments. For example, the presence of relict aeolian dunes on the modern Romanian shelf is not disputed here, but there is no reason to believe these are Holocene because of dependence on short, low-resolution cores (Lericolais et al., 2011). Likewise, a claim by Yanchilina et al. (2017) that the α1 unconformity developed beyond a –95 m lowstand shoreline after the Younger Dryas indicates that those authors miscorrelated an older surface in their seismic profiles to α1 as defined by Aksu et al. (2002) from the southwestern shelf, where the hiatus locally spans ~11.0–8.3 cal ka, but is also locally conformable.

In the Marmara Sea, evidence for earliest Holocene discharge through the Strait of Bosphorus, coincident with the rise of the Neoeuxine Lake to –30 to –40 m elevation, is found in the 11.1–10.2 cal ka Δ1 delta: its alignment with the strait, composition incompatible with local small streams, and remarkable climb into a rising sea flag this delta lobe as a unique product of outflow from the Neoeuxine Lake. The complete absence of (a) a precursor shelf-edge delta and (b) a younger lobe in the same area prove that Δ1 records a unique event. This lobe likely started to advance several decades (or longer) after outward spilling from the highstand Neoeuxine Lake began, when the outflow became strong enough to transport bedload. Δ1 is believed to have been abandoned when more dense saline water occupying the Marmara basin penetrated into the strait as a semi-permanent salt wedge, effectively lifting the outflow away from the floor of the strait so that bedload could no longer be transported to the delta front. This would have happened when the discharge and velocity of the outflow decreased and could no longer hold back the intrusion of denser saline water into the strait and across its shallow sill.

One would expect that the floor of the Strait of Bosphorus would retain evidence of south-direct outflow associated with Δ1, even though today the floor of the strait experiences north-directed flow of saline water as part of two-way exchange through the strait. Other authors (e.g., Gökaşan et al., 2005b; Ryan et al., 2014) have argued for deep erosion of the floor and walls of the strait by a deluge of saline water during a catastrophic flood into an evaporatively depressed Neoeuxine Lake (at –100 to –120 m), but such a deluge would have travelled north. However, Aksu et al. (2016) have described and illustrated southward-pointing giant megaflutes along the centreline of the strait at latitude 41°10.5' N, as well as ~6 m-high south-dipping clinoforms associated with a prominent northeast–southwest-elongated ridge in the vicinity of the sill near the southern end of the strait (Fig. 34). The ridge is delineated by the present-day –38 to –29 m isobaths as a southwest-facing streamlined seafloor feature. A northeast–southwest-running Uniboom seismic reflection profile collected across the central axis of the ridge (Alavi et al., 1989) shows two overlapping southwest-prograded oblique clinoform successions, immediately below a very thin surface unit (Fig. 34). These two clinoform successions are separated from one another by a prominent reflector. They constitute Unit B of Alavi et al. (1989). Two prominent reflectors bound the top and base of this unit, which are respectively correlated with the β1 and β2 reflectors of the NE Marmara Sea shelf (Aksu at al., 2016). A northwest–southeast-running multichannel seismic reflection profile intersecting the Uniboom profile reveals that Unit B of Alavi et al. (1989), particularly the upper clinoform unit, tapers toward the southeast and northwest (Fig. 35). The streamlined external shape, the width:length ratio of 0.27

(800 m × 3000 m), which falls squarely on the regression line for width:length ratios in fluvial barforms (e.g., Haltzweber et al., 2014), and the clearly oblique progradational internal architecture collectively indicate that the ridge is a streamlined barform, most probably a mid-channel bar, showing low-angle accretion/progradation on a downstream lee face inclined at 1.5º–2.5º (Fig. 34). Alavi et al. (1989, p. 201) interpreted the ridge as a sedimentary body created by the "*early Holocene spillover currents from the Black Sea before the establishment of the salt-wedge estuary across the southern sector of the Strait of Bosphorus*". Aksu at al. (2016) suggested that this southwest-prograded succession across the southern Strait of Bosphorus is genetically related to the early Holocene delta (i.e., Δ1). These features (i.e., the megaflutes and the southwest-prograded clinoform successions) have not been overprinted by indicators of north-directed flow, so appear to document the last strong discharge, capable of moving bedload along the floor of the strait. Of course if the depth of outflow above the –37 m sill was only 5–10 m, then the flow velocity and competence would have been significantly higher than today.

The elevation of the sill in the Strait of Bosphorus at the time of reconnection to the global ocean is controversial. We have assumed little difference from today, so a sill at –37 m elevation (e.g., Fig. 34). This is because the youngest topset-to-foreset transition of Δ1 is at –40 m elevation (Hiscott et al., 2002; Aksu et al., 2016) and the sill elevation at the time of salt-wedge penetration into the strait should have been similar, allowing for perhaps 5 m of water over both the delta top and the sill itself. The sill is very close to the Δ1 lobe, so little differential isostatic uplift or subsidence between the two is expected. Goldberg et al. (2016) highlighted how water loads might have influenced sill height, particularly if the Black Sea basin was suddenly subjected to a 100 m-thick additional water load. However, their modelling did not consider that base level in the Neoeuxine Lake might have been at the sill elevation for perhaps 2–3 kyr before entry of saline water. Nor did their approach consider that the lake was probably at this same high level several times during an extended deglaciation (17.2–15.7 cal ka; Tudryn et al., 2016), or when pulses of meltwater from the collapse of ice-dammed lakes in central Asia might have transited the gateway (Grosswald and Rudoy, 1996; Carling et al., 2002). Further consideration of water loads is not possible at this time without a fuller understanding of the entire Late Quaternary history, and even with such knowledge is not a simple task given the complex local geology, variable crustal thicknesses and rigidities, and crust/lithosphere-penetrating strike-slip faults in the area.

Ryan et al. (1997) originally proposed catastrophic entry of Mediterranean water into a low Neoeuxine Lake at ~7.5 cal ka, which would have required a much shallower sill since base level in the Marmara Sea was ~ –10 m at that time (Lambeck et al., 2007). Aksu et al. (2002c) called this hypothetical shallow barrier a sediment dam. The requirement for such a shallow sill disappeared with revision of the time of reconnection to ~9.1 cal ka (Ryan et al., 2003), but proponents of the Flood Hypothesis still advocate deep erosion along the floor of the strait (Ryan et al., 2014; Lericolais et al., 2019) which surely would have cut deeply into the area around the sill because it is underlain by sediment, not bedrock (Fig. 35). The south-directed clinoforms in the vicinity of the sill (Fig. 34) argue against substantial erosion after their development, as does the preservation and elevation of the β1 reflector, suggesting little erosion into the sedimentary fill in the same area (Fig. 35). Any northerly-directed flow over the sill heading downslope into a lowstand Neoeuxine Lake would have achieved higher velocity than the modern northerly-directed saline underflow because the former would have been driven by the density difference between the water and the atmosphere ($\Delta\rho = 1.0$ g cm^{-3}), whereas the latter is driven by the much smaller density difference between the outgoing and incoming water masses ($\Delta\rho \sim 0.01$ g cm^{-3}; Flood et al., 2009), and must also overcome interfacial friction at the top of the underflow.

Farther down the gateway, in the northern Aegean Sea, the primary potential link to early–middle Holocene outflow from the Black Sea basin is sapropel S1, if indeed its origin depended on a low-salinity surface layer advected from the Neoeuxine Lake, through the Marmara Sea and Strait of Dardanelles. The time of S1 initiation is consistent with outflow from the Neoeuxine Lake recorded by Δ1 progradation in the northeastern Marmara Sea (Fig. 31).

A unresolved issue for the Outflow Hypothesis is apparent incompatibility with some proxy values for paleo-salinity of the Marmara Sea surface waters during sapropel M1 and S1 deposition. Sperling et al. (2003) and Vidal et al. (2010) have used alkenone unsaturation ratios ($U_{37}^{k'}$) and the $\delta^{18}O$ record of the planktonic foraminifera *Turborotalia quinqueloba* to estimate variations in past sea surface salinity (SSS), and have concluded that SSS was higher than today throughout M1 accumulation, by up to four salinity units. This conclusion is opposite to that of Aksu et al. (2002b) who used a foraminiferal transfer function to estimate a lower SSS of 15–17, consistent with the presence of a brackish-water surface layer. This issue is partially rendered moot by our belief that processes other than outflow might have initiated and helped maintain oxygen-poor bottom waters in the Marmara Sea until ~8 cal ka when effective two-way exchange increased the vigour of deep circulation in the Marmara Sea, ending stagnant conditions inherited from an earlier time when it was a semi-isolated embayment of the Aegean Sea (Fig. 31 and associated text). Aksu et al. (2016) also suggested that very low salinity outflow from the Neoeuxine Lake might have been undetected by the methods used by Sperling et al. (2003) and Vidal et al. (2010) because planktonic foraminifera and other marine organisms could not have populated a surface water layer with low salinity (7–13; §7.4) to leave a record of its characteristics.

8.2. Water sources for pre-reconnection transgression in the Neoeuxine Lake

In several places, we have suggested that the level of the Neoeuxine Lake rose from ~ –110 m to –40 m from ~13.5–11.5 cal ka (Fig. 15), although the starting date for the transgression is poorly constrained. For this scenario to have occurred, $\Delta V = R+P-E$ would need to have become positive following an earlier evaporative drawdown. The required volume change is ~24675 km^3, so ~12.3 km^3 yr^{-1}. This is a very small fraction of modern annual inputs and losses, mostly in the range 300–350 km^3 yr^{-1} (Oğuz et al., 2004). Hence an increase in runoff (or decrease in evaporation) of perhaps 50 km^3 yr^{-1} would have been sufficient to overcome the pre-existing negative water balance and turn it well into positive territory. The first impression is that an increase in precipitation and runoff is contrary to what is known about the European climate in the Younger Dryas (~12.9–11.7 cal ka). This assessment is evident in regional palynology studies (e.g., Mudie et al., 2002b, 2007; Filipova-Marinova et al., 2004; Valsecchi et al., 2012; Popescu et al., 2021). However, Radoane (2021) turns this assessment on its head by looking in detail at changes in fluvial drainage entering the Black Sea, mostly from its European shores. She documents coarse-grained braided channel networks during the earliest post-LGM meltwater phase, giving way to large-scale meander belts along tributaries of major rivers like the Danube starting ~14 cal ka and continuing into the Holocene when runoff certainly became sufficient to raise and maintain a high Neoeuxine Lake level. Surface runoff from eastern European rivers into the Black Sea was higher during the Younger Dryas than in the Bølling-Allerød or Holocene (Radoane, 2021, her figures 7 & 10) at an average of ~225 km^3 yr^{-1}. These estimates are based on channel morphologies, dimensions and bed materials to reconstruct paleo-hydrological characteristics. This demonstrates that the quantity of precipitation alone does not dictate runoff, but other factors are important (e.g., soil absorbancy, bursts of heavy rainfall, type of vegetation cover, evapo-transpiration level). Importantly, Radoane (2021, p. 103) states that "... *available hydrological reconstructions reviewed in this study provide no support for the "flood hypothesis" which asserts that BS sea water level was –120 m lower prior to the connection with the Mediterranean Sea (at ca. 9.4 [cal] ka)*".

Today, the Danube, Dnieper, Dniester and Southern Bug Rivers deliver 265 $km^3 yr^{-1}$ to the Black Sea (Jaoshvili, 2002). Hence an input of ~225 $km^3 yr^{-1}$ would have been more than sufficient to create a positive hydrological balance, like today. Ignoring exchanges with the global ocean through the Strait of Bosphorus and inserting estimates from Oğuz et al. (2004), today's $\Delta V = R+P–E = 350+ 300-350 = 300$ $km^3 yr^{-1}$.

One study mentioned by Radoane (2021) requires comment. In describing and interpreting terraces along the flanks of the Sakarya River valley, Erturaç et al. (2019) concluded that development of their terrace T2 was triggered by an abrupt base-level rise at ~9 cal ka, which they implied confirmed the Flood Hypothesis. However, the oldest luminescence date from terrace T2 comes from its floodplain (overbank) deposits and not from its channel gravels. As Erturaç et al. (2019) state correctly in their interpretation of the older terrace T3, a sample immediately above the bedload facies only provides a minimum estimate for the age of that particular valley-fill succession; its initiation can be older by an unknown amount. Hence the ~9 cal ka date surely post-dates the base-level rise responsible for the adjustment of the floodplain to a new, higher profile. Furthermore, such changes in river gradient are known to propagate upstream from the new river mouth or perhaps the landward shoreline of a flooded estuary (i.e., drowned valley) after base-level rise, introducing an additional lag which was not accounted for (cf. Mackin, 1948).

Rarely during the Late Pleistocene, there have been catastrophic outburst floods generated by collapses of ice dams which had been holding back ephemeral lakes in central Asia (Rudoy and Baker 1993; Grosswald and Rudoy, 1996; Rudoy, 1998, 2002, 2005; Carling et al., 2002, 2011; Herget, 2005; Reuther et al., 2006; Bohorquez et al., 2016; Komatsu et al., 2016). Floodwaters from regions like the Altay Mountains escaped westward through a series of lakes and spillways into the Caspian and Black Sea basins, arriving in the latter area via the Manych spillway. Proposed ages of some events are as young as 16–9 cal ka (Reuther et al., 2006; Carling et al., 2011). Examples of volumes impounded by the largest of these lakes are in the range 595 km^3 (Carling et al., 2011) to 3500 km^3 (Rudoy, 2002). The volume of water reaching the Neoeuxine Lake might have greatly exceeded the volume released by any single ice-dam failure, because the surging floodwaters are documented to have cut deep gorges at the bedrock outlets of downstream glacial lakes (Rudoy, 2005, his figures 24, 30), inducing a chain reaction of catastrophic lake drainage (Komatsu et al., 2016). Hence, an initial outburst flood would have acted as a catalyst for a much more widespread and voluminous drainage of a string of pro-glacial lakes.

From a lowstand at –110 m, the sudden introduction of 3500 km^3 of water would have raised the level of the Neoeuxine Lake by ~10 m. Clearly an event of this magnitude would contribute to base-level rise, but could not be the dominant factor. However, a succession of such events over several thousand years, or a larger megaflood created by the draining of a string of lakes along a single pathway might have had a greater influence, and might help account for the rugose nature of salinity variations recorded by alkenone data in the period ~13–16 cal ka (Huang et al., 2021).

8.3. Archaeological implications

Investigations across the present-day circum-Black Sea shelves show that the occupation, subsistence and social dynamics of humans since early prehistoric times were directly and profoundly affected by changes in regional climate, the associated changes in vegetation, and very critically by the post-glacial rise in base level of adjacent seas (e.g., Dolukhanov and Shilik, 2007; Anthony 2007; Dergachev and Dolukhanov, 2007). The latest Pleistocene–Holocene is one of the most critical intervals of the Quaternary during which these key environmental factors have noticeably varied in the region. Because the Black Sea (and its more isolated version the Neoeuxine Lake) is largely a landlocked basin, some of these changes have often been greatly amplified, such as variations in the base level of the Neoeuxine Lake. Thus, understanding these environmental changes in space and time would provide much needed baseline data for detailed archaeological and anthropological interpretations.

There are critical archaeological and anthropological distinctions between the Flood and Outflow hypotheses. In the case of the Flood Hypothesis, the proposed rate of base-level change is so rapid, in fact catastrophic, that the Black Sea basin would have refilled from its lowstand of ~ –120 m during the Preboreal at ~ <10 cal ka to the breach depth of the Bosphorus sill at ~ –30 m by 9.47 cal ka, all within less than 40 years (Fig. 21; Ryan et al., 1997; Ryan and Pitman, 1998; Yanchilina et al., 2017). Coastal plains, grasslands, any farmlands or communities would have been destroyed within the memory of a single generation. Conversely, the Outflow Hypothesis presents a scenario where the rate of base-level rise is radically slower, rising from a low of ~ –110 m during the Bølling–Allerød, starting at perhaps 14–13 cal ka to ~5 m above the contemporary breach depth of the Strait of Bosphorus of ~ –40 m at ~11 cal ka in approximately 3000 years (Fig. 21; Hiscott et al., 2007a). If the refilling of the Neoeuxine basin occurred in 30–40 years, the Flood Hypothesis would require ~2.3–3.0 m yr^{-1} base-level rise. Across the northwestern and western sectors of the basin where the present-day slope of the continental shelf ranges between 0.05º and 0.06º this rate of base-level rise would translate to 2.2–3.4 km of annual transgression, which would only be sustainable for nomadic tribes intent on coastal habitation (e.g., for fishing), not Neolithic farmers. The Outflow Hypothesis suggests a distinctly slower rate of 2.5 cm yr^{-1} base-level rise, which would translate to 25–40 m annual transgression across the same terrain. Such a rate of transgression is not expected to severely alter population movements of any Mesolithic or early Neolithic farming communities living around the Neoeuxine Lake. The Outflow Hypothesis bases this slower rate of base-level rise on the elevation of radiocarbon-dated lacustrine/brackish-water shells in cores from the southwestern shelves of the Neoeuxine Lake which show that these regions were inundated as early as 13 cal ka and remained so until the initial marine inflow at ~9.47 cal ka (Fig. 22).

If there had been an extremely rapid inundation of coastal plains, the sedimentary archive would almost certainly contain enormous spikes in Gramineae, Cyperaceae and Compositae pollen from grasslands fringing the Neoeuxine Lake as they were destroyed and remnants dispersed by wave action (Mudie et al., 2002b), but composite core M02-45 and other Black Sea cores lack any evidence of this type at the appropriate levels (Mudie et al., 2007).

We are not aware of any archaeological evidence for urgent displacement and evacuation of humans from encroaching shoreline sites during the last transgression. Ballard et al. (2000) discovered wood fragments near what they interpreted as a drowned beach at ~ –150 m elevation off Sinop, central Anatolia. Radiocarbon age was ~3.4 cal ka. In the same area, Ballard et al.

(2001) mapped what they interpreted as a possible human habitation site at an elevation of ~ –100 m, but six samples of wood from the site all gave ages indistinguishable from modern. At this elevation, the site was likely somewhat inland from the lowstand shoreline of the Neoeuxine Lake, so it would only be of interest for discrimination between the Flood and Outflow hypotheses if samples in the age range 13–9.5 cal ka could be retrieved and shown to be *in situ* materials.

The Outflow Hypothesis is supported by some archaeological and anthropological data from the circum Black Sea region (e.g., Dolukhanov and Shilik, 2007; Anthony, 2007; Dergachev and Dolukhanov, 2007). For example, Dolukhanov and Shilik (2007) showed that Mesolithic groups of anatomically modern humans emerged between ~10.5 and 6.0 cal ka around the northern coastal zone of the Black Sea and that these groups were sustained by local resources during a gradual rise in base level. These authors concluded (p. 307) that "*there are no indications of major population movements or changes in subsistence that could suggest adjustment to the alleged flood at ca. 7400 cal BC* [= 9350 cal yrBP]". A similar conclusion is also reached by Anthony (2007, p. 345) who stated that "… a *review of Mesolithic and early Neolithic archaeological data in Ukraine provides little or no archaeological support for a sudden shift in human behavior at the time of the proposed flood*". Finally, Dergachev and Dolukhanov (2007) concluded that there is no evidence for catastrophic base-level rises that might have precipitated large-scale migrations of early farming groups across southeastern Europe and the Balkans. These authors (p. 509) indicated that "… *the alleged sea-level rise at ca. 8400* [^{14}C] *BP (~7400 cal BC* [= 9350 cal yrBP]*) in fact preceded the emergence of early farming communities in the Black Sea area. The Late Mesolithic groups that existed at the time were basically stable* ...".

In the remainder of the Discussion, we step through the latest Pleistocene and Holocene history of the Marmara Sea Gateway to show how the Outflow Hypothesis provides a consistent link between the events recorded in the three separate basinal areas (Black Sea, Marmara Sea and Aegean Sea).

8.4. Latest Pleistocene–Holocene paleoceanographic evolution

The relative sea-level curves of Lambeck et al. (2007) suggest that during the LGM the Marmara Sea (then the Propontis Lake) stood at –80 to –85 m. Lowstand terraces at 85 m water depth (Çağatay et al., 2009) and down-stepping of southern shelf-edge deltas to a topset-to-foreset transition at –90 m (Aksu et al., 1999) provide evidence that the lowest stand of the Propontis Lake must have been at an elevation no higher than –85 m (provided that the topset-to-foreset transition in the shelf-edge deltas occurred in 5 m of water). This level is 10–15 m below the –75 m LGM sill across the Strait of Dardanelles (Aksu et al., 2016), thus the lake was isolated from the Aegean Sea. Similarly, previous studies have shown that post-LGM lowstand shorelines, characterised by wave-cut terraces, occur around the Black Sea at depths from –110 m off Ukraine (Ryan et al., 1997), to –100 m on the Romanian shelf (Lericolais et al., 2007a,b), to –122 m on the Bulgarian shelf (Dimitrov, 1982), and possibly to –155 m off the very narrow Sinop shelf (Ballard et al., 2000). Hence the Strait of Bosphorus was subaerially exposed and the Black Sea basin (i.e., the Neoeuxine Lake) was completely isolated from the global ocean during the LGM. Tudryn et al. (2016) suggested that during the last deglaciation, through 17.2–15.7 cal ka, the Ponto-Caspian basin received large quantities of meltwater and fine-grained sediment from the southeastern margin of the Scandinavian Ice Sheet via the Dnieper and Volga rivers. During this period, the Neoeuxine Lake level rose to at least –55 m, draining into the Propontis Lake over a somewhat lower sill than today (Fig. 35, β2 elevation) and creating the older of two mid-shelf deltas (i.e., Δ2; Fig. 36a) in the northeastern Marmara Sea (Hiscott et al., 2002; Aksu et al., 2016). In response to this inflow, the level of the Propontis Lake rose to overtop the latest Pleistocene sill (–75 m) in the Strait of Dardanelles (Aksu et al., 2016), releasing meltwater into the northeastern Aegean Sea, which at that time was at a lowstand of ~ –110 m. The youngest topset-to-foreset elevation of Δ2 (–69 m) suggests perhaps 5–10 m-deep flow over the Dardanelles sill, although this estimate might depend on whether subsequent water-induced isostatic loading has changed the relative elevations of the northeastern and southeastern ends of the Marmara Sea. A drop of, say, 50 m along the 61 km Dardanelles would create an energy slope of ~ 0.0008, nearly identical to the modern Niagara River (without accounting for its waterfall).

Following the inflow of meltwater from the disintegrating Scandinavian Ice Sheet, the level of the Neoeuxine Lake fell to ~ –110 m by evaporative drawdown (Ryan et al., 2003; Major et al., 2006; Cohen et al., 2011). The Propontis Lake must also have experienced a deficit of freshwater from rivers and rainfall, likely falling at least to its spill depth of –75 m or lower. Whether the paleo-shoreline returned to its former ~ –84 m elevation is not known. However, at ~13.8 cal ka the rising global ocean reached the –75 m breach depth of the Strait of Dardanelles (Aksu et al., 2016), reconnecting the Propontis Lake (hereafter the Marmara Sea) with the Aegean Sea (Fig. 36b). Because of the small volume of the Marmara basin, equalisation of water levels would have been rapid, and intrusion of the amount of Aegean seawater needed to expel all lacustrine fresh/brackish water from the former lake basin would have been complete in a few hundred years (Hiscott et al., 2021).

From 13.8–11.1 cal ka, the Marmara Sea remained connected to the global ocean, and rose to –59 m by ~12.5 cal ka and –43 m by 11.1 cal ka (Figs. 37c,d; Lambeck et al., 2007). The level of the Black Sea also rose to an estimated –86 m by 12.5 cal ka and to ~ –40 m by 11.1 cal ka (5–7 m above the contemporary Bosphorus sill) so that it again began to spill outward into the still-lower Marmara Sea and onward to the Aegean Sea (Figs. 37c,d). Aksu et al. (2016) suggested that outburst floods created by cataclysmic emptying of ice-dammed lakes in the Altay and Sayan Mountains of Central Asia might have contributed to the rise of the Neoeuxine Lake level (§8.2). The –43 m water level across the Marmara Sea at 11.1 cal ka is supported by the oldest topset-to-foreset transition in the early Holocene Bosphorus delta (i.e., Δ1; Fig. 37d), which occurs at a modern elevation of –48 m (i.e., 5 m deeper than the contemporary base level based on water depths over other delta fronts in the region). Similarly, the youngest topset-to-foreset transition in the upper delta, well-dated at 10.2 cal ka (Aksu et al., 2016), occurs at a modern elevation of –40 m, consistent with a base level rise to –35 m. This ended an 8 m rise in the level of the Marmara Sea during 900 years of delta progradation (Fig. 25). It is at this time and for several thousand years afterward that brackish plumes carrying suspended sediment might have spread across the surface of large portions of the Marmara Sea, adding detritus to the evolving Holocene mud drape, both on newly transgressed shelves and in basinal areas (Hiscott et al., 2021). Continued southwestward escape of such brackish surface water through the Strait of Dardanelles could have contributed to stratification in the northern Aegean Sea, promoting development of sapropel S1 (Fig. 31).

Between 10.2 cal ka and the first entry of saline water into the Black Sea at ~9.5 cal ka (§7.3; Fig. 28; Yanchilina et al., 2017; Ankindinova et al., 2019), it is believed that a salt wedge advanced up the Strait of Bosphorus, lifting the Black Sea outflow off the floor of the strait and terminating southward bedload transport. Eventually, the tip of the salt wedge reached the northern end of the strait and sufficient Mediterranean water entered the Black Sea to affect the

$^{87}Sr/^{86}Sr$ ratio of shelf waters. If the Sr concentration in the Neoeuxine Lake was similar to that of modern large European rivers like the Danube, Ankindinova et al. (2019) estimated that ~8000 km^3 of Mediterranean seawater would have been required to shift the $^{87}Sr/^{86}Sr$ ratio in shells of the high-resolution composite core M02-45, in ~100 years, to values recorded soon after the first entry of saline water. This volume assumes good mixing of water masses in the lake. 80 km^3 yr^{-1} is significantly less than the discharge of saline water passing, at depth, through the modern Strait of Bosphorus, and the thickness of the initial saline inflow could have been similar to today because the strait is generally deeper than 60 m starting ~5 km north of the sill and continuing to its northern exit. For all scenarios considered in this review, sill height and base level are approximations with uncertainties of perhaps ±5 m. What is less uncertain, however, is the rate of early Holocene base-level rise (~10 m kyr^{-1}), so if intrusion of a salt wedge across the sill began at ~10.2 cal ka, then by ~9.5 cal ka the top of the saline underflow might have been ~7 m above the sill, whereas today it is on average ~10–12 m above the sill (Özsoy et al., 2001, their figure 4).

The weakening and eventual termination of outburst floods and enhanced river supply to the Black Sea by 10.2 cal ka (see also Radoane, 2021) and the continued rise of global sea level progressively deepened the waters across the Strait of Bosphorus, expanding the entry of saline water along the floor of the strait and allowing the development of persistent two-way flow by 8.0–7.5 cal ka (Figs. 38e,f), continuing to the present. Nevertheless, Black Sea outflow remained strong enough until ~6.0 cal ka to leave a mineralogical signature in the lower part of the mud drape on top of Δ1 (Figs. 38e,f; Hiscott et al., 2017), and perhaps to maintain sufficient water-column stratification in both the Marmara and Aegean Seas to extend accumulation of sapropels S1 and M1 (Fig. 31).

9. Conclusions

Data published by the authors and a number of other researchers since the late 1990's lend strong support to outflow of brackish water from the Black Sea basin starting ~11.5–11.1 cal ka and continuing to today, spanning the time of the first northward penetration of saline water along the Strait of Bosphorus and into the previously isolated Neoeuxine Lake. The Outflow Hypothesis of Aksu et al. (2002c) weaves these data into a single coherent narrative which can be applied from the Black Sea to the Aegean Sea. The timelines of events in each lake, sea and strait are consistent with one another. The hypothesis is supported by the following key observations and interpretations.

- Widespread uppermost Pleistocene to lower Holocene sediments (i.e., allosubunit 1b) across the southwestern Black Sea shelf (Ankindinova et al., 2020) shows that the level of the Neoeuxine Lake between 12.3 cal ka and ~11 cal ka (oldest allosubunit 1b) had risen high enough from its previous LGM lowstand to inundate the shelf to depths below storm wave base. Augmented surface runoff from surrounding drainage basins caused this latest transgression (Radoane, 2021).
- Paleobathymetric/paleotopographic maps constructed at the base and top of allosubunit 1b (this study; Ankindinova et al., 2020), Sr-isotopic (Ankindinova et al., 2019a) and provenance data (Lister et al., 2015) confirm that the uppermost Pleistocene to lower Holocene sediments were deposited in an open shelf environment, and not in isolated lagoons (or limans).
- An early Holocene delta (i.e., Δ1; 11.1–10.2 cal ka) on the northeastern Marmara Sea mid-shelf was sourced through the Strait of Bosphorus (Hiscott et al., 2002, 2021; Aksu

et al., 2016), and not by the small Kurbağalıdere stream which empties into the sea immediately east of the southern exit of the Strait of Bosphorus.

- Seismic profiles within the Strait of Bosphorus show southwest prograded clinoforms immediately below a thin veneer of sediments in the vicinity of the bathymetric sill at the southern end of the strait (Alavi et al., 1989). This clinoform unit correlates with the early Holocene delta (i.e., Δ1). Giant megaflutes farther north on the floor of the strait (Aksu et al., 2016) confirm that the most recent energetic flow was southward, not northward. Preservation of these relict features suggests little erosion of the floor of the strait during later entry of saline water into the Black Sea basin.
- Mineralogical data show that most of the detritus in the early Holocene delta likely comes from Oligo–Miocene successions which presently crop out along the shoreline immediately west of the northern exit of the Strait of Bosphorus (~50%), with a significant contribution from the Göksu stream which empties into the middle segment of the strait from the east plus minor amounts of detritus from various other sources, including the small Kurbağalıdere stream (Aksu et al., 2016; Hiscott et al., 2021).
- The early Holocene delta prograded 3.3 km into the Marmara Sea while its topset-to-foreset break climbed 8–9 m into the rising sea; such aggressive seaward progradation is unknown for true river deltas in the region (Hiscott et al., 2002, 2007a; Aksu et al., 2016). With no shelf-edge predecessor, this unique progradational lobe must record a defined, relatively short period of outflow from the Neoeuxine Lake rather than being tied to an established watershed and hinterland.
- The post-LGM reconnection of the Black Sea with the eastern Mediterranean occurred in a gradual fashion: first, a salt wedge lifted the 11.1–10.2 cal ka brackish outflow off the

floor of the strait; second, a more persistent density underflow introduced enough seawater strontium into the Black Sea to be noticed in shell calcite by ~9.5 cal ka, and finally a range of euryhaline marine organisms including molluscs and ostracods were able to replace lacustrine faunas when salinity levels became favourable by ~7.5 cal ka.

- Sapropel M1 was initiated across the Marmara Sea by stratification and nutrient enrichment caused by descent of saline Mediterranean water into the sea at 13.8 cal ka, which forced lower density, relict lacustrine waters to the surface and then out through the Strait of Dardanelles as suggested by Çağatay et al. (2015). Once the low-salinity cap was expelled, the deep waters of the fully saline Marmara Sea remained stagnant and sapropel accumulation continued. The beginning of Neoeuxine Lake outflow at 11.5–11.1 cal ka re-established water-column stratification across the Marmara Sea and created a low salinity lid across the northern sector of the Aegean Sea, initiating conditions favorable for sapropel S1 deposition. Today (and since ~6 cal ka), improved deep circulation and renewal of water masses on decadal time scales prevents the return of sapropel accumulation to the Marmara and Aegean Seas.

Acknowledgements

We thank the officers and crew of the RV *Koca Piri Reis*, particularly the former Captains Mehmet Özsaygılı and Kemal Dursun and the former Chief Engineers Bilâl Nuriler and Ömer Çubuk for their invaluable assistance during the 1991, 1995, 1997, 1998, 2000, 2002, 2003, 2005, 2008, 2011 and 2014 geophysical and coring operations. We further thank Dr. Doğan Yaşar of the Institute of Marine Sciences and Technology, Dokuz Eylül University for his role in facilitating these cruises and his assistance in the acquisition of the CTD profiles; Dr. Roger Flood of the School of Marine and Atmospheric Sciences, Stony Brook University for his contributions in the acquisition and preliminary processing of the multibeam data; Mr. Graham Standen of Geoforce Group Limited for his assistance in the acquisition of the Huntec DTS data; Dr. Vladimir Kostylev of Natural Resources Canada, Geological Survey of Canada-Atlantic for his assistance with mollusc identifications and ecology and the acquisition and processing of high-definition video images of the seafloor and Dr. Cenk Yaltırak of Istanbul Technical University for providing access to other seismic reflection and multibeam data from the Marmara Sea Gateway. We acknowledge research and shiptime funds from the Natural Sciences and Engineering Research Council of Canada (NSERC) to both AEA and RNH. Numerous discussions and two-way sharing of data with Dr. Petra Mudie of Natural Resources Canada, Geological Survey of Canada–Atlantic over the years have greatly improved our understanding of the Marmara Sea Gateway. We further acknowledge Mr. Peter Bruce (Memorial University CREAIT CSLV Facility) for his assistance in data management. Finally, we acknowledge and thank our students Neil Hackett, Sheldon Marsh, Michelle Alexander, Erin Lane, Krista Gammon, Jennifer Cranshaw, Renée Grant, Temilota Ogunniyi, Robyn Reynolds, Melanie Barnes, Joanne MacDonald, Kendra Power, Alycia MacDonald, Aaron Connolly, Laura Sinclair, Bursin İşler, Kahinde Adetona, Ayşe Çakıroğlu, Anna Linegar, Katey Roberts, Christopher Lister, Nicole Bursey, Lorna Williams and Olga Ankindinova for their contributions to the Marmara Sea Gateway Project during research for their theses. Journal reviewer Dr. Valentina Yanko-Hombach and an anonymous second reviewer are thanked for their helpful suggestions.

References

Abrajano, T., Aksu, A.E., Hiscott, R.N., Mudie, P.J., 2002. Aspect of carbon isotope biogeochemistry of Late Quaternary sediments from the Marmara Sea and Black Sea. Marine Geology 190, 151–164.

Aksu, A.E., Yaşar, D., Mudie, P.J., 1995a. Origin of late glacial - Holocene hemipelagic sediments in the Aegean Sea: clay mineralogy and carbonate cementation. Marine Geology 123, 33–59.

Aksu, A.E., Yaşar, D., Mudie, P.J., Gillespie, 1995b. Late glacial - Holocene paleoclimatic and paleoceanographic evolution of the Aegean Sea: micropaleontological and stable isotopic evidence. Marine Micropaleontology 25, 1–28.

Aksu, A.E., Yaşar, D., Mudie, P.J., 1995c. Paleoclimatic and paleoceanographic circumstances leading to the development of sapropel layer S1 in the Aegean Sea Basins. Palaeogeography, Palaeoclimatology, Palaeoecology 116, 71–101.

Aksu, A.E., Hiscott, R.N., Yaşar, D., 1999a. Oscillating Quaternary water levels of the Marmara Sea and vigorous outflow into the Aegean Sea from the Marmara Sea-Black Sea drainage corridor. Marine Geology 153, 275–302.

Aksu, A.E., Abrajano, T., Mudie, P.J., Yaşar, D., 1999b. Organic geochemical and palynological evidence for the Aegean Sea sapropel S1. Marine Geology 153, 303–318.

Aksu, A.E., Hiscott, R.N., Yaşar, D., Işler, F.I., Marsh, S, 2002a. Seismic stratigraphy of Late Quaternary deposits from the southwestern Black Sea shelf: evidence for non-catastrophic variations in sea-level during the last 10,000 years. Marine Geology 190, 61–94.

Aksu, A.E., Hiscott, R.N., Kaminski, M.A., Mudie, P.J., Gillespie, H., Abrajano, T., Yaşar, D., 2002b. Last glacial – Holocene paleoceanography of the Black Sea and Marmara Sea: stable isotopic, foraminiferal and coccolith evidence. Marine Geology 190, 119–149.

Aksu, A.E., Hiscott, R.N., Mudie, P.J., Rochon, A., Kaminski, M., Abrajano, T., Yaşar, D., 2002c. Persistent Holocene outflow from the Black Sea to the eastern Mediterranean contradicts Noah's Flood hypothesis. GSA Today, May 2002, 12, 4–10.

Aksu, A.E., Jenner, G.A. Hiscott, R.N., İşler, E.B., 2008. Occurrence, stratigraphy and geochemistry of Late Quaternary tephra layers in the Aegean Sea and the Marmara Sea. Marine Geology 252, 174–192.

Aksu, A.E., Hiscott, R.N., Yaltırak, C., 2016. Early Holocene age and provenance of a mid-shelf delta lobe south of the Strait of Bosphorus, Turkey, and its link to vigorous Black Sea outflow. Marine Geology 380, 113–137.

Aksu, A.E., Hiscott, R.N. Kostylev, V.E., Yaltırak, C., 2018. Organized patches of bioherm growth where the Strait of Dardanelles enters the Marmara Sea, Turkey. Palaeogeography, Palaeoclimatology, Palaeoecology 490, 325–346.

Alavi, S.N., Okyar, M., Timur, K., 1989. Late Quaternary sedimentation in the Strait of Bosporus: high-resolution seismic profiling. Marine Geology 89, 185–205.

Algan, O., Çağatay, N., Tchepalyga, A., Ongan, D., Eastoe, C., Gökaşan, E., 2001. Stratigraphy of the sediment infill in Bosphorus Strait: water exchange between the Black and Mediterranean Seas during the last glacial Holocene. Geo-Marine Letters 20, 209–218.

Algan, O., Ergin, M., Keskin, S., Gökaşan, E., Alpar, B., Ongan, D., Kırcı-Elmas, E., 2007. Sealevel changes during the Late Pleistocene-Holocene on the southern shelves of the Black Sea. *In*: V. Yanko-Hombach, A.S. Gilbert, N. Panin, P.M. Dolukhanov (Eds.), The

Black Sea Flood Question: Changes in Coastline, Climate, and Human Settlement. pp. 603–632. Springer, Dordrecht, 971 pp.

Alpar, B., Yüce, H., Doğan, E., 1996. Gas-charged Late Quaternary sediments in the Strait of Çanakkale (Dardanelles). Turkish Journal of Marine Sciences 2, 155–171.

Ankindinova, O., Hiscott, R.N., Aksu, A.E., Grimes, V, 2019a. Strontium isotopic composition of shells from the Black Sea and implications for the reconnection with the global ocean. Marine Geology, 407, 213–228.

Ankindinova, O., Aksu, A.E., Hiscott, R.N 2019b. Oxygen and carbon isotope and trace element/Ca ratios in Late Quaternary ostracodes *Loxoconcha lepida* and *Palmoconcha agilis* from the Black Sea: Holocene paleoclimatic and paleoceanographic implications. Palaeogeography, Palaeoclimatology, Palaeoecology 533, 109227.

Ankindinova, O., Aksu, A.E., Hiscott, R.N, 2020. Holocene sedimentation in the southwestern Black Sea: interplay between coastal eddies of the Rim Current, surface and internal waves, and saline underflow through the Strait of Bosphorus. Marine Geology 420, 106092.

Ashton, A.D., Nienhuis, J., Ells, K., 2016. On a neck, on a spit: controls on the shape of free spits. Earth Surface Dynamics 4, 193–210.

BBC [British Broadcasting Corporation], 1996. Noah's Flood, Season 33 Episode 8, 48:22 minutes. View at https://www.dailymotion.com/video/x223hpo (last screened by authors on 1 November, 2021).

Badertscher, S., Fleitmann, D., Cheng, H., Edwards, R.L., Göktürk, O.M., Zumbühl, A., Leuenberger, M., Tüysüz, O., 2011. Pleistocene water intrusions from the Mediterranean and Caspian seas into the Black Sea. Nature Geoscience 4, 236–239.

Badyukova, E. N. 2010. Evolution of the Northern Caspian Sea Region and the Volga delta in the Late Pleistocene–Holocene. Oceanology 50, 953–960.

Balabanov, I.P., 2007. Holocene sea-level changes of the Black Sea. *In*: V. Yanko-Hombach, A.S. Gilbert, N. Panin, P.M. Dolukhanov (Eds.), The Black Sea Flood Question. Springer, Dordrecht, pp. 711–730.

Balabanov, I.P., Kvirkveliya, B.D., Ostrovsky, A.B., 1981. Recent History of the Development of Engineering-Geological Conditions and Long-Time Forecast for the Coastal Zone of the Pitsunda Peninsula. Ministry of Geology of the USSR, Second Hydrological Division, Metanierba, Tbilisi, 202 pp. (in Russian)

Ballard, R.D., Coleman, D.F., Rosenberg, G. 2000. Further evidence of abrupt Holocene drowning of the Black Sea shelf. Marine Geology 170, 253–261.

Ballard, R.D., Hiebert, F.T., Coleman, D.F., Ward, C., Smith, J.S., Willis, K., Foley, B., Croff, K., Major, C., Torre, F., 2001. Deepwater archaeology of the Black Sea: the 2000 season at Sinop, Turkey. American Journal of Archaeology 105, 607–623.

Beşiktepe, Ş., Özsoy, E., Ünlüata, Ü., 1993. Filling of the Marmara Sea by the Dardanelles lower layer inflow. Deep-Sea Research I 40, 1815–1838.

Beşiktepe, Ş., Sur, H.I., Özsoy, E., Latif, M.A., Oğuz, T., Ünlüata, Ü., 1994. The circulation and hydrography of the Marmara Sea. Progress in Oceanography 34, 285–334.

Bhattacharya, J.P., 2001. Allostratigraphy versus sequence stratigraphy. *In*: APG Search and Discovery Article #90050. AAPG Hedberg Research Conference, Dallas, Texas, August 26–29, 2001.

Bhattacharya, J.P., Posamentier, H.W., 1994. Sequence stratigraphy and Allostratigraphic applications in the Alberta foreland basin. *In*: G.D. Mossop, I. Shetsen (Eds.), Geological

Atlas of the Western Canada Sedimentary Basin. Canadian Society of Petroleum Geologists and Alberta Research Council, pp. 407–412. https://ags.aer.ca/publications/chapter-25-sequence-and-allostratigraphic-applications.

Bohorquez, P., Carling, P.A., Herget, J., 2016. Dynamic simulation of catastrophic late Pleistocene glacial-lake drainage, Altai Mountains, central Asia. International Geology Review 58, 1795–1817. doi: 10.1080/00206814.2015.1046956.

Bornhold, B., Firth, J.V., et al., 1998. Proceedings of the Ocean Drilling Program, Initial Reports, Volume 169S, College Station, TX, doi:10.2973/odp.proc.ir.169s.1998

Bradley, L.R., Horne, D.J., Williams, L., Marret, F., Aksu, A.E., Hiscott. R., 2011. Salinity changes on the south-western shelf of the Black Sea during the Holocene. Joannea Geologie und Paläontologie 11, 30–33.

Bradley, L.R., Marret, F., Mudie, P.J., Aksu, A.E., Hiscott, R.N., 2012. Constraining Holocene sea-surface conditions in the southwestern Black Sea using dinoflagellate cysts. Journal of Quaternary Science 27, 835–843.

Brückner, H., Kelterbaum, D., Marunchak, O., Porotov, A., Vött, A., 2010. The Holocene sea level story since 7500 BP – Lessons from the Eastern Mediterranean, the Black and the Azov Seas. Quaternary International 225, 160–179.

Çağatay, M.N., Görür, N., Algan, O., Eastoe, C., Tchapalyga, A., Ongan, D., Kuşcu, I., 2000. Late glacial–Holocene palaeoceanography of the Sea of Marmara: timing of connections with the Mediterranean and the Black seas. Marine Geology 167, 191–206.

Çağatay, M.N., Görür, N., Polonia, A., Demirbağ, E., Sakınç, M., Cormier, M.H., Eriş, K., 2003. Sea-level changes and depositional environments in the Izmit Gulf, eastern Marmara Sea, during the late glacial–Holocene period. Marine Geology 202, 159–173.

Çağatay, M.N., Eriş , K., Ryan, W.B.F., Sancar, Ü., Polonia, A., Akçer, S., Bard, E., 2009. Late Pleistocene–Holocene evolution of the northern shelf of the Sea of Marmara. Marine Geology 265, 87–100.

Çağatay, M.N.,Wulf, S., Ümmühan, S., Özmaral, A., Vidal, L., Henry, P., Appelt, O., Gasperini, L., 2015. The tephra record from the Sea of Marmara for the last ca. 70 ka and its palaeoceanographic implications. Marine Geology 361, 96–110.

Çağatay, M.N., Eriş , K., Erdem, Z., 2021. Morphology and Late Pleistocene-Holocene sedimentation of the Strait of İstanbul (Bosphorus): A review. Geological Society of London, Special Publication 523, page numbers pending. doi.org/10.1144/SP523-2021-48.

Carling, P.A., Kirkbride, A.D., Parnachov, S., Borodavko, P.S., Berger, G.W., 2002. Late Quaternary catastrophic flooding in the Altai mountains of south-central Siberia: a synoptic overview and an introduction to flood deposits sedimentology. *In*: I.P. Martini, G. Garzon, V.R. Baker (Eds.), Flood and Megaflood Processes and Deposits: Recent and Ancient Examples. International Association of Sedimentologists, Special Publication 32. Blackwell Scientific, Oxford, pp. 17–35.

Carling, P.A., Knaapen, M., Borodavko, P., Herget, J., Koptev, I., Huggenberger, P., Parnachev, S., 2011. Palaeoshorelines of glacial lake Kuray–Chuja, south-central Siberia: Form, sediments and process. *In:* I.P. Martini, H.M. French, A. Pérez Alberti (Eds.), Ice-marginal and Periglacial Processes and Sediments. Geological Society, London, Special Publication 354, 111–128.

Catuneanu, O., 2020. Sequence stratigraphy. *In*: N. Scarselli, J. Adam, D. Chiarella, D.G. Roberts, A.W. Bally (Eds.), Regional Geology and Tectonics, Volume 1: Principles of Geological Analysis, Chapter 23, 605–686, 878 pp.

Chepalyga, (or Tchepalyga) A.L., 1984. Inland sea basins. *In*: W., Barnosky-Cathy (Ed.), Late Quaternary Environments of the Soviet Union. University of Minnesota Press, Minneapolis, MN, pp. 229–247.

Chepalyga (or Tchepalyga), A.L., 2002. The Black Sea. *In*: A.A., Velichko (Ed.), Dynamics of Terrestrial Landscape Components and Inner Marine Basins of Northern Eurasia during the Last 130,000 years. GEOS, Moscow, pp. 170–182. (in Russian)

Chepalyga (or Tchepalyga), A.L., 2007. The late glacial great flood in the Ponto-Caspian basin. *In*: V. Yanko-Hombach, A.S. Gilbert, N. Panin, P.M. Dolukhanov (Eds.), The Black Sea Flood Question: Changes in Coastline, Climate, and Human Settlement. Springer, Dordrecht, The Netherlands, 119–148.

Cohen, D.M., Ryan, W.B.F., Major, C.O., Goldstein, S.L., Pena, L.D., Dimitrov, P., Dimitrov, D., 2011. Post glacial evaporative drawdown of the Black Sea lake. *In*: 3rd International Symposium on the Geology of the Black Sea Region Bucharest, 1–10 October 2011, Abstracts, Supplement to Geo-Eco-Marina 17, 49–51.

Constantinescu, A.M., Toucanne, S., Dennielou, B., Jorry, S.J., Mulder, T., Lericolais, G., 2015. Evolution of the Danube deep-sea fan since the last glacial maximum: new insights into Black Sea water-level fluctuations. Marine Geology 367, 50–68.

Dean, W.E., Arthur, M.A., 2011. Geochemical characteristics of Holocene laminated sapropel (unit II) and underlying lacustrine unit III in the Black Sea: U.S. Geological Survey Open-File Report 2010–1323, 29 p.

Debenay, J-P., Bénéteau, E., Zhang, J., Stouff, V., Geslin, E., Redois, F., Fernandez-Gonzalez, M., 1998. *Ammonia beccarii* and *Ammonia tepida* (Foraminifera): morphofunctional arguments for their distinction. Marine Micropaleontology 34, 235–244.

Demirbağ, E., Gökaşan, E., Kurt, H., Tepe, C.M., 1998. Approaches about the formation of the NE of the Strait of the Çanakkale (in Turkish). *In*: Proceedings of the Marine Investigations in Turkey Workshop IV, 14–15 May 1998, İstanbul, pp 31–38.

Di Iorio, D., Akal, T., Sellschopp, J., Guerrini, P., Yüce, H., Gezgin, E., 1996. Oceanographic Measurements of the West Black Sea: November 26 to December 14, 1995. Web version developed by A. Cavanna; CD-ROM from SACLANTCEN; NATO, La Spezia.

Di Iorio, D., Akal, T., Guerrini, P., Yüce, H., Gezgin, E., Özsoy, E., 1999. Oceanographic Measurements of the West Black Sea: June 15 to July 5, 1996. Report SR-305, SACLANTCEN; NATO, La Spezia.

Dimitrov, P.S., 1982. Radiocarbon datings of bottom sediments from the Bulgarian Black Sea Shelf. Bulgarian Academy of Science, Oceanology 9, 45–53.

Dimitrov P., 2003. The Black Sea - a Clue to the Secret of World Flood. Oceanology, 4, 52-57.

Dimitrov, P., Dimitrov, D., 2004. The Black Sea, the Flood and the Ancient Myths. Slavena, Varna, Bulgaria, 103 pp.

EIE, 2011. Elektrik İşleri Etüt İdaresi Genel Direktörlüğü (The Turkish General Directorate of Waterworks). Water Year Discharges, Annual Catalogue 2011, 411 pp, Ankara, Turkey.

Eriksen, U., Friedrich,W.L., Buchardt, B., Tauber, H., Thomson, M.S., 1990. The Stronghyle Caldera: geological, paleontological and stable isotope evidence from radiocarbon dated stromatolites from Santorini. *In*: D.A. Hardy, J. Keller, V.P. Galanopoulos, N.C.

Flemming, T.H. Druitt (Eds.), Thera and the Aegean World III. Santorini, Greece, pp. 139–150.

Eriş, K.K., Ryan, W.B.F., Çağatay, M.N., Sancar, Ü., Lericolais, G., Ménot, G., Bard, E., 2007. The timing and evolution of the post-glacial transgression across the Sea of Marmara shelf south of İstanbul. Marine Geology 243, 57–76.

Eriş, K.K., Ryan, W.B.F., Çağatay, M.N., Lericolais, G., Sancar, Ü., Ménot, G., Bard, E., 2008. Reply to Comment on "The timing and evolution of the post-glacial transgression across the Sea of Marmara shelf south of İstanbul" by Hiscott et al., Marine Geology 248, 228–236. Marine Geology 254, 230–236.

Eriş, K.K., Çağatay, N., Akçer, S., Gaperini, L., Mart, Y., 2011. Late glacial to Holocene sea level changes in the Sea of Marmara: new evidence from high-resolution seismics and core studies. Geo-Marine Letters 31, 1–18.

Erol, O., 1992. Geomorphology and tectonics of the Çanakkale region. Bulletin of the Turkish Association of Petroleum Geologists 4, 147–165.

Erturaç, M.K., Şahiner, E., Zabcı, C., Okur, H., Polymeris, G.S., Meriç, N., İkiel, C., 2019. Fluvial response to rising levels of the Black Sea and to climate changes during the Holocene: Luminescence geochronology of the Sakarya terraces. The Holocene 29, 941–952. doi: 10.1177/0959683619831428.

Evsylekov, Y.D., Shimkus, KM., 1995. Geomorphological and neotectonic development of outer part of continental margin to the south of Kerch Strait. Oceanology 35, 623–628.

Facorellis, Y., Maniatis, Y., Kromer, B., 1998. Apparent ^{14}C ages of marine mollusks shells from a Greek island – calculation of the marine reservoir effect in the Aegean Sea. Radiocarbon 40, 963–974.

Federov, P.V., 1971. Postglacial transgression of the Black Sea. International Geology Review 14, 160–164.

Fedorov, P., 1982. Some controversial questions about the Pleistocene history of the Black Sea. Bulletin of the Moscow Society of Naturalists, Geological Department, 57, 108–117. (in Russian)

Filipova-Marinova, M., 2003. Paleoenvironmental changes along the Southern Black Sea Coast of Bulgaria during the last 29000 years. Phytologia Balcanica 9, 275–292.

Filipova-Marinova, M., 2007. Archaeological and paleontological evidence of climate dynamics, sea-level change, and coastline migration in the Bulgarian sector of the Circum-Pontic region. *In*: V. Yanko-Hombach, A.S. Gilbert, N. Panin, P.M. Dolukhanov (Eds.), The Black Sea Flood Question. Springer, Dordrecht, pp. 453–482.

Filipova-Marinova, M., Bozilova, E., 2002. Paleoecological conditions in the area of the prehistorical settlement in the Bay of Sozopol during the Eneolithic. Phytologia Balcanica 8, 133–143.

Filipova-Marinova, M., Christova, R., Bozilova, E., 2004. Palaeoeological conditions in the Bulgarian Black Sea area during the Quaternary. Journal of Environmental Micropaleontology, Microbiology and Meiobenthology 1, 135–154.

Flood, R.D., Hiscott, R.N., Aksu, A.E., 2009. Morphology and evolution of a channel system created by saline underflow into the Black Sea. Sedimentology 56, 87–839.

Fouache, E., Kelterbaum, D., Brückner, H., Lericolais, G., Porotov, A., Dikarev, V., 2012. The Late Holocene evolution of the Black Sea – a critical view on the so-called Phanagorian regression. Quaternary International 266, 162–174.

Frail-Gauthier, J., Mudie, P.J., 2014. Laboratory mesocosms and geological studies for monitoring wetlands diversity. *In*: P. Gâştescu, W. Marszelewski, P. Bretcan (Eds), 2nd International Conference – Water resources and wetlands. 11–13 September, 2014 Tulcea (Romania). http://www.limnology.ro/water2014/proceedings.html, ISSN: 2285-7923; p. 391–403;

Giamali, C., Koskeridou, E., Antonarakou, A. Ioakim, C., Kontakiotis, G., Karageorgis, A.P., Roussakis, G., Karakitsios, V., 2019. Multiproxy ecosystem response of abrupt Holocene climatic changes in the north–eastern Mediterranean sedimentary archive and hydrologic regime. Quaternary Research 92, 665–685.

Giosan, L., Donnelly, J.P., Vespremeanu, E., Bhattacharya, J.P., Olariu, C., Buonaiuto, F.S., 2005. River delta morphodynamics: examples from the Danube delta. *In*: L. Giosan, J.P. Bhattacharya (Eds.), River Deltas – Concepts, Models, and Examples. SEPM Special Publication No. 83, 393–412, 502 pp.

Giosan, L., Filip, F., Constatinescu, S., 2009. Was the Black Sea catastrophically flooded in the early Holocene? Quaternary Science Reviews 28, 1–6.

Goldberg, S., Lau, H.C.P., Mitrovica, J.X., Lathychev, K., 2016. The timing of the Black Sea flood event: Insights from modeling of glacial isostatic adjustment. Earth and Planetary Science Letters 452, 178–184.

Gökaşan, E., Algan, O., Tur, H., Meriç, E., Türker, A., Şimşek, M., 2005a. Delta formation at the southern entrance of Istanbul Strait (Marmara sea, Turkey): a new interpretation based on high-resolution seismic stratigraphy. Geo-Marine Letters 25, 370–377.

Gökaşan, E., Tur, H., Ecevitoğlu, B., Görüm, T., Türker, A., Tok, B., Çağlak, F., Birkan, H., Şimşek, M., 2005b. Evidence and implications of massive erosion along the Strait of İstanbul (Bosphorus). Geo-Marine Letters 25, 324–342.

Grant, K.M., Grimm, R., Mikolajewicz, U., Marino, G., Ziegler, M., Rohling, E.J., 2016. The timing of Mediterranean sapropel deposition relative to insolation, sea-level and African monsoon changes. Quaternary Science Reviews 140, 125–141.

Grosswald, M.G., Rudoy, A.N., 1996. Quaternary glacier-dammed lakes in the mountains of Siberia. Polar Geography 20, 180–198.

Heaton, T., Köhler, P., Butzin, M., Bard, E., Reimer, R., Austin, W., Bronk Ramsey, C., Grootes, P., Hughen, K., Kromer, B., Reimer, P., Adkins, J., Burke, A., Cook, M., Olsen, J., Skinner, L., 2020. Marine20 – the marine radiocarbon age calibration curve (0–55,000 cal BP). Radiocarbon 62, 779–820.

Herget, J., 2005. Reconstruction of ice-dammed lake outburst floods in the Altai mountains, Siberia. Geological Society of America, Special Paper 386, 118 p.

Herrle, J.O., Bollmann, J., Gebühr, C., Schulz, H., Sheward, R.M., Giesenberg, A., 2018. Black Sea outflow response to Holocene meltwater events. Nature Publishing Group Scientific Reports 8, 4081-6.

Hiscott, R.N., Aksu, A.E., 2002. Late Quaternary history of the Marmara Sea and Black Sea from high-resolution seismic and gravity core studies. Marine Geology 190, 261–282.

Hiscott, R.N., Aksu, A.E., Yaşar, D., Kaminski, M.A., Mudie, P.J., Kostylev, V., MacDonald, J., F.I. Işler, Lord, A.R., 2002. Deltas south of the Bosphorus Strait record persistent Black Sea outflow to the Marmara Sea since ~10 ka. Marine Geology 190, 95–118.

Hiscott, R.N., Aksu, A.E., Mudie, P.J., Kaminski, M.A., Abrajano, T., Yaşar, D. Rochon, A., 2007a. The Marmara Sea Gateway since ~16 ka: non-catastrophic causes of paleoceanographic events in the Black Sea at 8.4 ka and 7.15 ka. *In*: V. Yanko-Hombach, A.S. Gilbert, N. Panin, P.M. Dolukhanov (Eds.), The Black Sea Flood Question: Changes in Coastline, Climate, and Human Settlement, NATO Science Series IV-Earth and Environmental Sciences, Springer, Dordrecht, The Netherlands, p. 89–117.

Hiscott, R.N., Aksu, A.E., Mudie, P.J., Marret, F., Abrajano, T., Kaminski, M.A., Evans, J., Çakıroğlu, A., Yaşar, D., 2007b. A gradual drowning of the southwestern Black Sea shelf: evidence for a progressive rather than abrupt Holocene reconnection with the eastern Mediterranean Sea through the Marmara Sea Gateway. Quaternary International 167/8, 19–34.

Hiscott, R.N., Aksu, A.E., Mudie, P.J., 2008. Comment on ″The timing and evolution of post-glacial transgression across the Sea of Marmara shelf south of Istanbul″ by Eriş et al. [Marine Geology 243, 57–76]. Marine Geology 248, 228–236.

Hiscott, R.N., Aksu, A.E., Flood, R.D., Kostyley, V., Yaşar, D., 2013. Widespread overspill from a saline-density-current channel north of the Bosphorus Strait, and its role in generating topography on the SW Black Sea shelf. Sedimentology 60, 1639–1667.

Hiscott, R.N., Aksu, A.E., Yaltırak, C, 2017. Modelling the provenance of detritus flushed through the Strait of Bosphorus, Turkey, during early Holocene outflow from the Black Sea to the world ocean. Marine Geology 390, 147–169.

Hiscott, R.N., Aksu, A.E., Yaltırak, C, 2021. The uppermost Pleistocene–Holocene mud drape across the Marmara Sea: quantification of detrital supply from southern Marmara rivers. Sedimentary Geology 415, 105851.

Holzweber, B.I., Hartley, A.J., Weissmann, G.S., 2014. Scale invariance in fluvial barforms: implications for interpretation of fluvial systems in the rock record. Petroleum Geoscience 20, 211–224.

Intergovernmental Oceanographic Commission (IOC), 1981. International Bathymetric Chart of the Mediterranean. Head Department of Navigation and Oceanography, Russia (under the authority of IOC, 10 sheets).

İşler, E.B., Aksu, A.E., Hiscott, R.N., 2016a. Geochemistry of Aegean Sea sediments: implications for surface- and bottom-water conditions during sapropel deposition since MIS 5. Turkish Journal of Earth Sciences 25, 103–125.

İşler, E.B., Aksu, A.E., Hiscott, R.N., 2016b. Late Quaternary paleoceanographic evolution of the Aegean Sea: planktonic foraminifera and stable isotopes. Turkish Journal of Earth Sciences 25, 19–45.

İşler, E.B., Hiscott, R.N., Aksu, A.E., 2016c. Late Quaternary chronostratigraphy of the Aegean Sea sediments: special reference to the ages of sapropels S1–S5. Turkish Journal of Earth Sciences 25, 1–18.

Ivanova, E.V., Murdmaa, I.O., Chepalyga, A.L., Cronin, T.M., Pasechnik, I.V., Levchenko, O.V., Howe, S.S., Manushkina, A.V., Platonova, E.A., 2007. Holocene sea-level oscillations and environmental changes on the Eastern Black Sea shelf. Palaeogeography, Palaeoclimatology, Palaeoecology 246, 228–259.

Izmailov, Y.A., 2005. Evolutionary Geography of the Black Sea and Sea of Azov Coasts. T 1. (Anapa Sand Barrier). Lazarevskaya Polygrafiya, Sochi. 174 pp. (in Russian)

Jaoshvili, S., 2002. The Rivers of the Black Sea. European Environment Agency Technical Report 71, 58 pp.

Jipa, D.C., Panin, N., 2020. Narrow shelf canyons vs. wide shelf canyons: two distinct types of Black Sea submarine canyons. Quaternary International 540, 120–136.

Kaiho, K., 1994. Benthic foraminiferal dissolved-oxygen index and dissolved-oxygen levels in the modern ocean. Geology 22, 719–722.

Kaminski, M.A., Aksu, A.E., Hiscott, R.N., Box, M., Al-Salameen, M., Filipescu, S., 2002. Late glacial to Holocene benthic foraminifera in the Marmara Sea. Marine Geology 190, 165–202.

Kerey, I.E., Meriç , E., Tunoğlu, C., Kelling, G., Brenner, R.L., Doğan, A.U., 2004. Black Sea–Marmara Sea Quaternary connections: new data from the Bosphorus, İstanbul, Turkey. Palaeogeography, Palaeoclimatology, Palaeoecology 204, 277–295.

Komatsu, G., Baker, V.R., Arzhannikov, S.G., Gallagher, R., Arzhannikova, A.V., Murana, A., Oguchi, T., 2016. Catastrophic flooding, palaeolakes, and late Quaternary drainage reorganization in northern Eurasia. International Geology Review 58, 1693–1722. doi: 10.1080/00206814.2015.1048314.

Konikov, E.G., 2007. Sea-level fluctuations and coastline migration in the northwestern Black Sea area over the last 18 ky based on high-resolution lithological-genetic analysis of sediment architecture. *In*: V. Yanko-Hombach, A.S. Gilbert, N. Panin, P.M. Dolukhanov (Eds.), The Black Sea Flood Question: Changes in Coastline, Climate, and Human Settlement. Springer, Dordrecht, The Netherlands, pp. 405–435.

Konikov, E., Faschevsky, S., Pedan, G., 2009. Extreme fluctuations of the Black Sea level in Neoeuxine–Holocene as the alternative of catastrophic flood hypothesis. Geology and Mineral Resources of the World Ocean 3, 55–69. (in Russian)

Krastev, T., Grigoriev, A., Fedorov, P., 1990. Geological evolution of the western part of the Black Sea basin in Neogene-Quaternary time. Bulgarian Academy of Sciences 471, 340–348. (in Russian)

Kuprin, P.N., Sorokin, V.M., 2007. On the post-glacial changes in the level of the Black Sea. *In*: V. Yanko-Hombach, A.S. Gilbert, N. Panin, P.M. Dolukhanov (Eds.), The Black Sea Flood Question. Springer, Dordrecht, pp. 205–220.

Kuprin, P.N., Scherbakov, F.A., Morgunov, Ll., 1974. Correlation, age, and distribution of the postglacial continental terrace sediments of the Black Sea. Baltica 5, 241–249.

Kutterolf, S., Freundt, A., Druitt, T.H.,McPhie, J., Nomikou, P., Pank, K., Schindlbeck-Belo, J.C., Hansteen, T.H., Allen, S.R., 2021. The medial offshore record of explosive volcanism along the central to eastern Aegean Volcanic Arc: 2. Tephra ages and volumes, eruption magnitudes and marine sedimentation rate variations. Geochemistry, Geophysics, Geosystems 22, e2021GC010011. doi. org/10.1029/2021GC010011

Kwiecien, O., Arz, H., Lamy, F., Wulf, S., Bahr, A., Röhl, U., Haug, G.H., 2008. Estimated reservoir ages of the Black Sea since the last glacial. Radiocarbon 50, 99–118.

Lambeck, K., Sivan, D., Purcell, A., 2007. Timing of the last Mediterranean Sea–Black Sea connection from isostatic models and regional sea-level data. *In*: V. Yanko-Hombach, A.S. Gilbert, N. Panin, P.M. Dolukhanov (Eds.), The Black Sea Flood Question: Changes in Coastline, Climate and Human Settlement. Springer, The Netherlands, pp. 797–808.

Lambeck, K., Rouby, H., Purcell, A., Sun, Y., Sambridge, M., 2014. Sea level and global ice volumes from the Last Glacial Maximum to the Holocene. PNAS, Proceedings of the National Academy of Sciences of the United States of America 111, 15296–15303.

Larchenkov, E., Kadurin, S., 2011. Paleogeography of the Pontic Lowland and northwestern Black Sea shelf for the past 25 k.y. *In:* I.V. Buynevich, V. Yanko-Hombach, A.S. Gilbert, R.E. Martin (Eds.), Geology and Geoarchaeology of the Black Sea Region: Beyond the Flood Hypothesis. Geological Society of America Special Paper 473, p. 71–87.

Latif, M.L., Özsoy, E., Salihoğlu, I, Gaines, A.F., Baştürk, Ö., Yımaz, A., Tuğrul, S., 1992. Monitoring via Direct Measurements of the Modes of Mixing and Transport of Wastewater Discharges into the Bosphorus Underflow. Middle East Technical University, Institute of Marine Sciences, Technical Report No. 92–2, 98 pp.

Lee, B-S., Bullister, J.L., Murray, J.W., Sonnerup, R.E., 2002. Anthropogenic chlorofluorocarbons in the Black sea and the Sea of Marmara. Deep-Sea Research 49, 895-913.

Le Pichon, X., Şengör, A.M.C., Demirbağ, E., Rangin, C., İmren, C., Armijo, R., Görür, N., Çağatay, N., Mercier de Lepinay, B., Meyer, B., Saatçılar, R., Tok, B., 2001. The active Main Marmara Fault. Earth and Planetary Science Letters 192, 595–616.

Lericolais, G., Popescu, I., Guichard, F., Popescu, S.M., 2007a. A Black Sea lowstand at 8500yr B.P. indicated by a relict coastal dune system at a depth of 90m below sea level. *In*: J. Harff, W.W. Hay, D.M. Tetzlaff (Eds.), Coastline Changes: Interrelation of Climate and Geological Processes. GSA Books; Allen Press, Inc., Special Paper 426, pp. 171–188.

Lericolais, G., Popescu, I., Guichard, F., Popescu, S.M., Manolakakis, L., 2007b. Water-level fluctuations in the Black Sea since the Last Glacial Maximum. *In*: V. Yanko-Hombach, A.S. Gilbert, N. Panin, P.M. Dolukhanov (Eds.), The Black Sea Flood Question: Changes in Coastline, Climate, and Human Settlement. Springer, Dordrecht, The Netherlands, pp. 437–452.

Lericolais, G., Bulois, C., Gillet, H., Guichard, F., 2009. High frequency sea level fluctuations recorded in the Black Sea since the LGM. Global and Planetary Change 66, 65–75.

Lericolais, G., Guichard, F., Morigi, C., Minereau, A., Popescu, I., Radan, S., 2010. A post Younger Dryas Black Sea regression identified from sequence stratigraphy correlated to core analysis and dating. Quaternary International 225, 199–209.

Lericolais G, Guichard F, Morigi C, Popescu I, Bulois C, Gillet, H., Ryan, W.B.F., 2011. Assessment of Black Sea water-level fluctuations since the Last Glacial Maximum. *In*: I. Buynevich, V. Yanko-Hombach, A.S. Gilbert, R.E. Martin (Eds.), Geology and Geoarchaeology of the Black Sea Region: Beyond the Flood Hypothesis. The Geological Society of America, Special Paper 473, 33–50, Boulder, Colorado, USA.

Lericolais, G., Algan, O., Morigi, C., Okay, S., Kirci-Elmas, E., Çifçi, G., 2019. Overview of the Bosphorus Depositional Fan from data sets recovered on the Black Sea shelf off the Strait of Istanbul. International Journal of Environmental Sciences and Natural Resources 17, IJESNR.MS.ID.555959.

Lister, C.J., Hiscott, R.N., Aksu, A.E., Mudie, P.J., 2015. Compositional trends through the Holocene mud succession of the southwestern Black Sea shelf: implications for sedimentary provenance and water-level history. Sedimentary Geology 316, 13–25.

Liu, Y., Lu, X., Çağatay, N.M., Zhang, Y., Li, Y., Peng, Y., Ruffine, L., Lu, H., 2021. The organic, inorganic and isotope geochemistry of the holocene sapropel units in the sea of Marmara and their paleoceanographic significance. Marine and Petroleum Geology 129, 105094.

Lom, N., Ülgen, S.C., Sakınç, M., Şengör, A.M.C., 2016. Geology and stratigraphy of Istanbul region. *In*: S. Sen (Ed.), Late Miocene mammal locality of Küçükçekmece, European Turkey. Geodiversitas 38, 175–195.

Londeix, L., Herreyre, Y., Turon, J.-L., Fletcher, W., 2009. Last glacial to Holocene hydrology of the Marmara Sea inferred from a dinoflagellate cyst record. Review of Palaeobotany and Palynology 158, 52–71.

Mackin, J.H., 1948. Concept of the graded river. Geological Society of America Bulletin 59, 463–512.

Major, C.O., Ryan, W.B.F., Lericolais, G., Hajdas, I., 2002. Constraints on Black Sea outflow to the Sea of Marmara during the last glacial-interglacial transition. Marine Geology 190, 19–34.

Major, C., Goldstein, S., Ryan, W., Lericolais, G., Piotrowski, A.M., Hajdas, I., 2006. The coevolution of Black Sea level and composition through the last deglaciation and its paleoclimatic significance. Quaternary Science Reviews 25, 2031–2047.

Mangerud, J., Jakobsson, M., Alexanderson, H., Astakhov, V., Clarke, G.K.C., Henriksen, M., Hjort, C., Krinner, G., Lunkka, J.P., Möller, P., Murray, A., Nikolskaya, O., Saarnisto, M., Svendsen, J.I., 2004. Ice-dammed lakes and rerouting of the drainage of northern Eurasia during the Last Glaciation. Quaternary Science Reviews 23, 1313–1332.

Marret, F., Mudie, P.J., Aksu, A.E., Hiscott, R.N., 2009. A Holocene dinocyst record of a two step transformation of the Neoeuxinian brackish water lake into the Black Sea. Quaternary International 197, 72–86.

Meriç, E., 1995. İstanbul Boğazı öncesinde Marmara Denizi-Karadeniz bağlantısının İzmit Körfezi-Sakarya Vadisi boyunca gerçekleştiğinin ön bulguları [Preliminary findings suggesting the connection between Marmara Sea and Black Sea via Izmit Bay–Sakarya Valley prior to the development of the Strait of Bosphorus. GEOSOUND, Science and Technology Bulletin on Earth Science, Çukurova University, Adana, Turkey 27, 149–158. (in Turkish)

Mertens, K.N., Bradley, L.R., Takano, Y., Mudie, P.J., Marret, F., Aksu, A.E., Hiscott, R.N., Verleye, T.J., Mousing, E.A., Smyrnova, L.L., Bagheri, S., Mansor, M., Pospelova, V., Matsuoka, K., 2012. Quantitative estimation of Holocene surface salinity variation in the Black Sea using dinoflagellate cyst process length. Quaternary Science Reviews 39, 45–59.

Mudie, P.J., Aksu, A.E., Yaşar, D., 2001. Late Quaternary dinoflagellate cysts from the Black, Marmara and Aegean Seas: variations in assemblages, morphology and paleosalinity. Marine Micropaleontology 43, 155–178.

Mudie, P.J., Rochon, A., Aksu, A.E., Gillespie, H., 2002a. Dinoflagellate cysts and freshwater algae and fungal spores as salinity indicators in Late Quaternary cores from Marmara and Black Seas. Marine Geology 190, 203–231.

Mudie, P.J., Rochon, A., Aksu, A.E., 2002b. Pollen Stratigraphy of Late Quaternary cores from Marmara Sea: land-sea correlation and paleoclimatic history. Marine Geology 190, 233–260.

Mudie, P.J., Rochon, A.E., Aksu, A.E., Gillespie, H., 2004. Late glacial, Holocene and modern dinoflagellate cyst assemblages in the Aegean–Marmara–Black Sea corridor: statistical analysis and re-interpretation of the early Holocene Noah's Flood hypothesis. Review of Palaeobotany and Palynology 128, 143–167.

Mudie, P.J., Marret, F., Aksu, A.E., Hiscott, R.N., Gillespie, H., 2007. Palynological evidence for climate change, anthropogenic activity and outflow of Black Sea water during the late Pleistocene and Holocene: centennial- to decadal-scale records from the Black and Marmara Seas. Quaternary International 167/8, 73–90.

Myers, K.J., Milton, N.J., 1996. Concepts and principles of sequence stratigraphy. *In:* Emery, D., Myers, K.J. (Eds.), Sequence Stratigraphy. Blackwell Science, Oxford, pp. 11–44.

Nevesskaya, L.A., 1965. Late Quatemary bivalve mollusks of the Black Sea: Their systematics and ecology. Akad. Nauk S.S.S.R. Paleontol. Inst. Tr. (Proceeding of the USSR Academy of Sciences; Paleontological Institute) 105, 1–390.

Nevesskaya, L.A., 1970. On the classification of enclosed and semi-enclosed basins based on their fauna characteristics. *In*: D.B., Obruchev, V.N., Shimansky (Eds.), Modern Problems of Paleontology. Nauka, Moscow, pp. 258–278 (in Russian)

Nicholas, W.A., Chivas, A.R., Murray-Wallace, C.V., Fink, D., 2011. Prompt transgression and gradual salinisation of the Black Sea during the early Holocene constrained by amino acid racemization and radiocarbon dating. Quaternary Science Reviews 30, 3769–3790.

North American Commission on Stratigraphic Nomenclature, 2005. North American stratigraphic code. American Association of Petroleum Geologists, Bulletin 89, 1547–1591.

Oğuz, T., Latun, V.S., Latif, M.A., Vladimirov, V.V., Sur, H.I., Markov, A.A., Özsoy, E., Kotovshchikov, B.B., Eremeev, V.V., Ünlüata, Ü., 1993. Circulation in the surface and intermediate layers of the Black Sea. Deep-Sea Research I 40, 1597–1612.

Oğuz T., Tuğrul S., Kideys A.E., Ediger V. and Kubilay N., 2004. Physical and biogeochemical characteristics of the Black Sea. *In*: A.R. Robinson, K.H. Brink (Eds.), The Sea volume 14, Chapter 33, Harvard University Press, pp. 1331–1336.

Oktay, F.Y., Gökaşan, E., Sakınç, M., Yaltırak, C., İmren, C., Demirbağ, E., 2002. The effects of the North Anatolian Fault Zone on the latest connection between Black Sea and Sea of Marmara. Marine Geology 190, 367–382.

Olson, D.B., Kourafalou, V.H., Johns, W.E., Samuels, G., Veneziani, M., 2007. Aegean Surface circulation from a satellite-tracked drifter array. Journal of Physical Oceanography 37, 1898–1917.

Ostrovsky, A.B., Izmailov, Y.A., Balabanov, I.P., Skiba, S.I., Skryabina, N.G., Arslanov, S.A., Gey, N.A., Suprunova, N.I., 1977. New data on the paleohydrological regime of the Black Sea in the Upper Pleistocene and Holocene. *In*: P.A. Kaplin, F.A. Shcherbakov (Eds.), Pleistocene Paleogeography and Sediments of the Southern Seas of the USSR. Nauka, Moscow, pp. 131–140. (in Russian)

Özgül, N., Üner, K., Akmeşe, İ., Bilgin, İ., Kokuz, R., Özcan, İ., Yıldız, Z., Yıldırım, Ü., Akdağ, Ö., Tekin, M., 2005. İstanbul İl Alanının Genel Jeoloji Özellikleri (General Geological Properties of the Istanbul County Area). İstanbul Büyükşehir Belediyesi (Istanbul Metropolitan Municipality), 79 pp. (in Turkish)

Özsoy, E., Top, Z, White, G., Murray, J.W., 1991. Double diffusive intrusions, mixing and deep convective processes in the Black Sea. *In*: E. Izdar, J.M. Murray (Eds.), The Black Sea Oceanography. NATO/AS1 Series C. Vol. 35 1, Kluwer. Dordrecht, pp. 17–42.

Özsoy, E., Latif, M.A., Tuğrul, S., Ünlüata, Ü., 1995. Exchanges with the Mediterranean, fluxes and boundary mixing processes in the Black Sea. *In*: F. Briand (Ed.), Mediterranean

Tributary Seas. Bulletin de l'Institut Océanographique, Monaco, Special No. 15, CIESME Science Series 1, pp. 1–25.

Özsoy, E., Latif, M.A., Sur, H.I., Goryachkin, Y., 1996. A review of the exchange flow regimes and mixing in the Bosphorus Strait. *In*: F. Briand (Ed.), Mediterranean Tributary Seas. Bulletin de l'Institut Océanographique, Monaco, Special No. 17, CIESME Science Series 2, pp. 187–204.

Özsoy, E., Di Iorio, D., Gregg, M., Backhaus, J.O., 2001. Mixing in the Bosphorus Strait and the Black Sea continental shelf: observations and a model of the dense water outflow. Journal of Marine Systems 31, 99–135.

Paasche, E., Brubak, S., Skattebøl, S., Young, J.R., Green, J.C., 1996. Growth and calcification in the coccolithophorid *Emiliania huxleyi* (Haptophyceae) at low salinities. Phycologia 35, 394–403.

Panin, A.V., Sidorchuk, A.Yu., Borisov, O.K., 2007. River runoff into the Black and Caspian Seas in the end of OIS-2. *In*: V. Yanko-Hombach, I. Buinevich, P. Dolukhanov, A. Gilbert, R. Martin, M. McGann, P. Mudie (Eds), Extended abstracts of the Joint Plenary Meeting and Field Trip of IGCP 521 "Black Sea–Mediterranean corridor during the last 30 ky: Sea-level change and human adaptation" and IGCP 481 "Dating Caspian Sea Level Change", 8–17 September 2007. Gelendzhik (Russia) – Kerch (Ukraine), Southern Branch of the Institute of Oceanology, Russian Academy of Sciences and Demetra Beneficient Foundation, p. 127–129.

Panin, N., 1989, Danube delta, genesis, evolution and sedimentology. Revue Roumaine Géologie, Géophysique et Géographie 33, 25–36.

Pfannensteil, M., 1944. Die Diluvialen Entwicklungsstadien und die Urgeschicthe von Dardanellen, Marmarameer und Bosphorus: Diluvial-Geologie und Klima. Geologische Rundschau 3–4, 324–434.

Pichler, H., Friederich, W., 1976. Radiocarbon dates of the Santorini volcanics. Nature 262, 373–374.

Polat, Ç., Tuğrul, S., 1996. Chemical exchange between the Mediterranean and Black Sea via the Turkish Straits. *In*: F. Briand (Ed.), Dynamics of Mediterranean Straits and Channels. Bulletin de l'Institut Océanographique, Monaco, Special No. 17, CIESME Science Series 2, 167–186.

Popescu, I., Lericolais, G., Panin, N., Normand, A., Dinu, C., Le Drezen, E., 2004. The Danube submarine canyon (Black Sea): morphology and sedimentary processes. Marine Geology 206, 249–265.

Popescu, S-M., Jiménez-Moreno, G., Klotz, S., Lericolais, G., Guichard, F., Çağatay, M.N., Giosan, L., Calleja, M., Fauquette, S., Suc, J-P., 2021. Late Quaternary vegetation and climate of SE Europe–NW Asia according to pollen records in three offshore cores from the Black and Marmara seas. Palaeobiodiversity and Palaeoenvironments 101, 197–212. doi: 10.1007/s12549-020-00464-x.

Popov, G.I., 1973. New data on the stratigraphy of Quaternary marine sediments of the Kerch Strait. Dokl. Akad. Nauk S.S.S.R. (Proceeding of the USSR Academy of Sciences) 213, 84–86.

Posamentier, H.W., Jervey, M.T., Vail, P.R., 1988. Eustatic controls on clastic deposition. I, Conceptual framework. *In*: C.K. Wilgus, B.S. Hastings, C.G.St.C. Kendall, H.W.

Posamentier, C.A. Ross, J.C. Van Wagner (Eds.), Sea Level Changes – An Integrated Approach, SEPM Special Publications 42, 110–124.

Rădoane, M., 2021. A history of the circum-pontic river channels marked by climate and sea level changes during the Late Quaternary (25–8 ka BP). Revista de Geomorfologie 23, 91–120. doi: 10.21094/rg.2021.141.

Rangin, C., Demirbağ, E., Imren, C., Crusson, A., Normand, A., Le Drezen, E., Le Bot, A., 2001. Marine Atlas of the Sea of Marmara (Turkey). Ifremer Brest Technology Center, 11 Plates and 1 Booklet 2-84433-068-1.

Ravelo, A.C., Hillaire-Marcel, C., 2007. The use of oxygen and carbon isotopes of foraminifera in paleoceanography. *In*: C. Hillaire-Marcel, A. de Vernal (Eds.), Proxies in Late Cenozoic Paleoceanography, Developments in Marine Geology, Volume 1, Chapter 18, 735–764, 844 pp.

Reuther, A.U., Herget, J., Ivy-Ochs, S., Borodavko, P., Kubik, P.W., Heine, K., 2006. Constraining the timing of the most recent cataclysmic flood event from ice-dammed lakes in the Russian Altai Mountains, Siberia, using cosmogenic in situ ^{10}Be. Geology 34, 913–916. doi: 10.1130/G22755A.1.

Rohling, E.J., Marino, G., Grant, K.M., 2015. Mediterranean climate and oceanography, and the periodic development of anoxic events (sapropels). Earth-Science Reviews 143, 62–97.

Rossignol-Strick, M., 1985. Mediterranean Quaternary sapropels, an immediate response of the African monsoon to variation of insolation. Palaeogeography, Palaeoclimatology, Palaeoecology 49, 237–263.

Rudoy, A.N., 1998. Mountain ice-dammed lakes of southern Siberia and their influence on the development and regime of the intracontinental runoff systems of north Asia in the Late

Pleistocene. *In*: G. Benito, V.R. Baker, K.J. Gregory (Eds.), Palaeohydrology and Environmental Change. John Wiley & Sons Ltd., New York, 215–234, 368 pp.

Rudoy, A.N., 2002. Glacier-dammed lakes and geological work of glacial superfloods in the Late Pleistocene, southern Siberia, Altay Mountains. Quaternary International 87, 119–140.

Rudoy, A.N., Baker, V.R., 1993. Sedimentary effects of cataclysmic late Pleistocene glacial outburst flooding, Altay Mountains, Siberia. Sedimentary Geology 85, 53–62.

Rudoy, A.N., 2005. Giant Current Ripples (history of the research, their diagnostics and palaeogeographical significance). Tomsk, Publishing House of Tomsk State University, Russia (in Russian with extended English summary and captions), 223 pp.

Ryan, W.B.F., 2007. Status of the Black Sea flood hypothesis. *In:* V. Yanko-Hombach, A.S. Gilbert, N. Panin, P.M. Dolukhanov (Eds.), The Black Sea Flood Question: Changes in Coastline, Climate, and Human Settlement. Springer, Dordrecht, 63–88.

Ryan, W.B.F., Pitman, W.C., III, 1998. Noah's Flood: The New Scientific Discoveries about the Event that Changed History. Simon and Schuster, New York, 319 pp.

Ryan, W.B.F., Pitman, W.C., III, Major, C.O., Shimkus, K.S., Moscalenko, V., Jones, G.A., Dimitrov, P., Görür, N., Sakınç, M., Yüce, S.H., 1997. An abrupt drowning of the Black Sea shelf. Marine Geology 138, 119–126.

Ryan, W.B.F., Major, C.O., Lericolais, G., Goldstein, S.L., 2003. Catastrophic flooding of the Black Sea. Annual Review of Earth and Planetary Sciences 31, 525–554.

Ryan, W.B.F., Carbotte, S.M., Coplan, J.O., O'Hara, S., Melkonian, A., Arko, R., Weissel, R.A., Ferrini, V., Goodwillie, A., Nitsche, F., Bonczkowski, J., Zemsky, R., 2009. Global multiresolution topography synthesis. Geochemistry, Geophysics, Geosystems 10, Q03014. http://dx.doi.org/10.1029/2008GC002332.

Ryan, W.B.F., Vachtman, D., McHugh, C., Çağatay, M.N., Mart, Y., 2014. A channeled shelf fan initiated by flooding of the Black Sea. *In*: S. Goffredo, Z. Dubinsky (Eds.), The Mediterranean Sea: Its history and present challenges, 11 DOI 10.1007/978-94-007-6704-1_2, Springer Science + Business Media Dordrecht, pp. 11–27.

Saruwatari, K., Satoh, M., Harada, N., Suzuki, I., Shiraiwa, Y., 2016. Change in coccolith size and morphology due to response to temperature and salinity in coccolithophore *Emiliania huxleyi* (Haptophyta) isolated from the Bering and Chukchi seas. Biogeosciences 13, 2743–2755.

Scrivner, A.E., Vance, D., Rohling, E.J., 2004. New neodymium isotope data quantify Nile involvement in Mediterranean anoxic episodes. Geology 32, 565–568.

Shimkus, K.M., Emelyanov, E.M., Trimonis, E.S., 1975. Seafloor sediments and the late Quaternary history of the Black Sea. In: The Earth's Crust and the History of Development of the Black Sea Basin. Nauka, Moscow, pp. 138–162.

Shmuratko, V.I., 2007. The post-glacial transgression of the Black Sea. *In*: V. Yanko-Hombach, A.S. Gilbert, N. Panin, P.M. Dolukhanov (Eds.), The Black Sea Flood Question. Springer, Dordrecht, pp. 221–250.

Shuisky, Y., 2007. Climate dynamics, sea-level change, and shoreline migration in the Ukrainian sector of the Circum-Pontic Region. *In*: V. Yanko-Hombach, A.S. Gilbert, N. Panin, P.M. Dolukhanov (Eds.), The Black Sea Flood Question. Springer, Dordrecht, pp. 251–278.

Siani, G., Paterne, M., Arnold, M., Bard, E., Métiver, B., Tisnerat, N., Bassinot, F., 2000. Radiocarbon reservoir ages in the Mediterranean Sea and Black Sea. Radiocarbon 42, 271–280.

Skiba, S.I., Scherbakov, F.A., Kuprin, P.N., 1975. On paleogeography of the Kerch-Taman region in late Pleistocene and Holocene. Oceanologia 15, 862–867.

Soulet, G., Ménot, G., Lericolais, G., Bard, E., 2011. A revised calendar age for the last reconnection of the Black Sea to the global ocean. Quaternary Science Reviews 30, 1019–1026.

Sperling, M., Schmiedl, G., Hemleben, C., Emeis, K.C., Erlenkeuser, H., Grootes, P.M., 2003. Black Sea impact on the formation of eastern Mediterranean sapropel S1? Evidence from the Marmara Sea. Palaeogeography, Palaeoclimatology, Palaeoecology 190, 9–21.

Stuiver, M., Braziunas, T.F., 1993. Modelling atmospheric ^{14}C influences and ^{14}C ages of marine samples to 10,000 BC. Radiocarbon 35, 137–189.

Svendsen, J., Alexanderson, H., Astakhov, V., Demidov, I., Dowdeswell, J., Funder, S., Gataullin, V., Henriksen, M., Hjort, C., Houmark-Nielsen, M., Hubberten, Ó., Ingólfson, O., Jakobsson, M., Kjar, K., Larsen, E., Lokrantz, H., Lunkka, J., Lyså, A., Mangerud, J., Matiouchkov, A., Murray, A., Möller, P., Niessen, F., Nikolskaya, O., Polyak, P., Saarnisto, M., Siegert, C., Siegert, M., Spielhagen, R., Stein, R., 2004. Late Quaternary ice sheet history of Northern Eurasia. Quaternary Science Reviews 23, 1229–1271.

Syvitski, J.P.M., Milliman, J.D., 2007. Geology, geography, and humans battle for dominance over the delivery of fluvial sediment to the coastal ocean. Journal of Geology 115, 1–19.

Thom, N., 2010. A hydrological model of the Black and Caspian Seas in the late Pleistocene and early-middle Holocene. Quaternary Science Reviews 29, 2989–2995.

Triantaphyllou, M.V., Antonarakou, A., Kouli, K., Dimiza, M., Kontakiotis, G., Papanikolaou, M.D., Ziveri, P., Mortyn, P.G., Lianou, V., Lykousis, V., Dermitzakis, M.D., 2009. Late

Glacial–Holocene ecostratigraphy of the south-eastern Aegean Sea based on plankton and pollen assemblages. Geo-Marine Letters 29, 249–267.

Tudryn, A., Leroy, S.A.G., Toucanne, S., Gibert-Brunet, E., Tucholka, P., Lavrushin, Y.A., Dufaure, Olivier, D., Serge M., Germain, B., 2016. The Ponto-Caspian basin as a final trap for southeastern Scandinavian Ice-Sheet meltwater. Quaternary Science Reviews 148, 29–43.

Ünlüata, Ü., Oğuz, T., Latif, M.A., Özsoy, E., 1990. On the physical oceanography of the Turkish Straits. *In*: J. Pratt (Ed.), The Physical Oceanography of Sea Straits. NATO-ASI series, Kluwer Academic, Dordrecht, The Netherlands, pp. 25–60.

Valsecchi, V., Sanchez Goñi, M.F., Londeix, L., 2012. Vegetation dynamics in the Northeastern Mediterranean region during the past 23 000 yr: insights from a new pollen record from the Sea of Marmara. Climate of the Past 8, 1941–1956. doi:10.5194/cp-8-1941-2012.

Vidal, L., Ménot, G., Joly, C., Bruneton, H., Rostek, F., Çağatay, M.N., Major, C., Bard, E., 2010. Hydrology in the Sea of Marmara during the last 23 ka: implications for timing of Black Sea connections and sapropel deposition. Paleoceanography 25, PA1205. http://dx.doi. org/10.1029/2009PA001735.

Voskoboinikov, V.M., Kotar', M.F., Konikov, E.G., 1982. Relationship between the rhythmic composition of thick Holocene layers of the Black Sea region lagoons and the oscillatory level regime of the Black Sea. *In*: P.A. Kaplin, R.K. Klige, A.I. Chepalyga (Eds.), Sea Level Fluctuations. Moscow State University, pp. 264–274. (in Russian)

Wessel, P., Smith, W.H.F. 1996. A global, self-consistent, hierarchical, high-resolution shoreline database. Journal of Geophysical Research 101(B4), 8741–8743.

Williams, R.H., Hiscott, R.N., Aksu, A.E. Bradley, L.R., Horne, D., Stoica, M., 2018. Holocene paleoecology and paleoceanography of the southwestern Black Sea shelf delineated by ostracod assemblages. Marine Micropaleontology 142, 48–66.

Yaltırak, C., Alpar, B., Yüce, H., 1998. Tectonic elements controlling the evolution of the Gulf of Saros (northeastern Aegean Sea, Turkey). Tectonophysics 300, 227–248.

Yaltırak, C., Alpar, B., Sakınç, M., Yüce, H., 2000. Origin of the Strait of Çanakkale (Dardanelles): regional tectonics and the Mediterranean-Marmara incursion. Marine Geology 164, 139–159.

Yaltırak, C., Sakınç, M., Aksu, A.E., Hiscott, R.N., Galleb, B., Ulgen, U.B., 2002. Late Pleistocene uplift history along the southwestern Marmara Sea determined from raised coastal deposits and global sea-level variations. Marine Geology 190, 283–305.

Yanchilina, A.G., Ryan, W.B.F., McManus, J.F., Dimitrov, P., Dimitrov, D., Slavova, K.A., Filipova-Marinova, M., 2017. Compilation of geophysical, geochronological, and geochemical evidence indicates a rapid Mediterranean-derived submergence of the Black Sea's shelf and subsequent substantial salinification in the early Holocene. Marine Geology 383, 14–34.

Yanchilina, A.G., Ryan, W.B.F. Kenna, T.C., McManus, J.F., 2019. Meltwater floods into the Black and Caspian Seas during Heinrich Stadial. Earth-Science Reviews 198, 102931.

Yanko, V., 1990. Stratigraphy and palaeogeography of marine Pleistocene and Holocene deposits of the southern seas of the USSR: Memorie - Società Geologica Italiana 44, 167–187.

Yanko-Hombach, V., 2006. Transformation of the Neoeuxinian Lake into the Black Sea: evidence from benthic foraminifera. *In*: IGCP 521 Second Plenary Meeting, Odessa, Ukraine, 20–28 August, Abstracts volume, pp. 171–173.

Yanko-Hombach, V., Motnenko, I., 2011. Pleistocene water intrusions from the Mediterranean and Caspian Seas into the Black Sea: Reconstructions based on foraminifera. *In*: Yanko-Hombach V. & Gilbert A. (Eds). Abstract Volume of the Seventh Plenary Meeting and Field Trip of INQUA 501. 21st - 28th August 2011, Odessa, Ukraine, pp. 187–194.

Yanko-Hombach, V., Gilbert, A.S., Dolukhanov, P., 2007. Controversy over the great flood hypotheses in the Black Sea in light of geological, paleontological, and archaeological evidence. Quaternary International 167–168, 91–113.

Yanko-Hombach, V., Mudie, P., and Gilbert, A.S., 2011. Was the Black Sea catastrophically flooded during the post-glacial? Geological evidence and impacts. *In*: J. Benjamin, C. Bonsall, C. Pickard, A. Fischer (Eds.), Submerged Prehistory, Oxbow Books, pp. 245–262.

Yanko-Hombach, V., Mudie P. J., Kadurin S., Larchenkov E. 2013. Holocene marine transgression in the Black Sea: New evidence from the northwestern Black Sea shelf. Quaternary International 345, 100–118.

Yanko-Hombach, V., Mudies, P.J., Kadurin, S., Larchenkov, E., 2014. Holocene marine transgression in the Black Sea: New evidence from the northwestern Black Sea shelf. Quaternary International 345, 100–118.

Yanko-Hombach, V., Kondariuk, T., Motnenko, I., 2017a. Benthic foraminifera indicate environmental stress from river discharge to marine ecosystems: example from the Black Sea. Journal of Foraminiferal Research 47, 70–92.

Yanko-Hombach, V., Schnyukov, E., Pasynkov, A., Sorokin,, V., Kuprin, P., Maslakov, N., Motnenko, I., Smyntyna, O., 2017b. Geological and geomorphological factors and marine conditions of the Azov–Black Sea Basin and coastal characteristics as they determine prospecting for seabed prehistoric sites on the continental shelf. *In:* N.C. Flemming, J. Harff, D. Moura, A. Burgess, G.N. Bailey (Eds.), Submerged Landscapes of the European Continental Shelf: Quaternary Paleoenvironments, John Wiley & Sons, 431–478.

Yilmaz, Ö., Özyalvac, M., Duman, F., Catakli, M., Polat, Z., 2018. Offshore high-resolution seismic survey for a subsea tunnel across the Bosphorus Waterway, Istanbul, Turkey. The Leading Edge, Special Section: Infrastructure Assessment, 732–738. https://doi.org/10.1190/tle37100732.1.

Figure Captions

Figure 1. (a) Regional map of the eastern Mediterranean Sea and Black Sea, showing the setting for this review and prominent rivers (white lettering with blue outline) discussed in the text. (b) Map showing the location of the Marmara Sea Gateway linking the Black Sea with the Aegean Sea through the Straits of Bosphorus and Dardanelles and the intervening Marmara Sea. In both (a) and (b) the topography is compiled using data from GeoMapApp (Ryan et al., 2009), the bathymetry is compiled using data from EMODnet (http://www.emodnet-hydrography.eu/) and Rangin et al. (2001), and shaded in Global Mapper™. Coastline, rivers and lakes are from NOAA National Geophysical Data Center, extracted from http://www.ngdc.noaa.gov/mgg/shorelines/ (Wessel and Smith, 1996). White-filled circles with black lettering = M91 cores, red-filled circles with red lettering = M03 cores.

Figure 2. (a) Bathymetry of the Strait of Bosphorus, and the regions immediately south in the northeast Marmara Sea and the north in the southwest Black Sea, compiled using the multibeam surveys carried by the authors in 2005, 2008 and 2011 across the Strait of Bosphorus and southwestern Black Sea and multibeam data from the Turkish Navy, Office of Navigation, Hydrography and Oceanography (SHOD) in the vicinity of the southern exit of the Strait of Bosphorus, and contoured and shaded using Global Mapper™. The coastline is digitised using Google Earth Pro™. Note that the present-day sill occurs at –37 m depth across the southern sector of the strait. Streams and small rivers: Gö= Göksu, Ka= Kağıthane, Ku= Kurbağalıdere, Kü= Küçüksu, Ri= Riva. Oligo–Miocene outcrops and the Saline and NE Marmara channels are discussed in the

text. (b) Simplified model showing the evolution of the Strait of Bosphorus during the Late Pleistocene (adapted from Okay et al., 2002).

Figure 3. Bathymetry of the Marmara Sea and a small portion of the southwestern Black Sea compiled using the multibeam data of Rangin et al. (2001) and bathymetry data extracted from GeoMapApp (Ryan et al., 2009), respectively, and shaded in Global Mapper^{TM}. Tekirdağ, Central, Kumburgaz and Çınarcık are deep-water basins, whereas İmralı Basin is perched along the southern continental slope of the Çınarcık Basin. Sakarya and Kocasu rivers are discussed in the text. Coastline, rivers and lakes are from NOAA National Geophysical Data Center, extracted from http://www.ngdc.noaa.gov/mgg/shorelines/ (Wessel and Smith, 1996). The –100 m isobath shows the approximate position of the present-day shelf edge. Red dashed line shows the position of the purported Sakarya Bosphorus.

Figure 4. Bathymetry of the Strait of Dardanelles and the regions immediately east in the southwestern Marmara Sea and west in the northeastern Aegean Sea, compiled using a multibeam survey carried by the authors in 2011 across the southwestern Marmara Sea and multibeam data from the Turkish Navy, Office of Navigation, Hydrography and Oceanography (SHOD) across the northeastern Aegean Sea and southwestern Marmara Sea, and contoured using Global Mapper^{TM}. The coastline is digitised using Google Earth Pro^{TM}. Note that the present-day sill occurs at –63 m across the southern sector of the eastern exit of the strait; the basement sill in the same region is at –75 m elevation (Aksu et al., 2016).

Figure 5. Surface (red lines with white outline) and bottom (blue lines with white outline) water circulation patterns across the Marmara Sea Gateway. Black Sea surface and bottom

water circulations are from Oğuz et al. (1993) and Özsoy et al. (1991), respectively. Water circulation patterns across the Marmara Sea and the Aegean Sea are adopted from Beşiktepe et al. (1994) and Olson et al. (2007), respectively. Note that two-way flow dominates the circulation across the Straits of Bosphorus and Dardanelles; the centrelines of the opposing currents are nearly directly one above the other but are shown in the enlarged views with laterally separated paths for clarity. Background topography is compiled using data from GeoMapApp (Ryan et al., 2009). The multibeam bathymetry is compiled using data from Rangin et al. (2001) for the deep Marmara Sea basins, from the Turkish Navy, Office of Navigation, Hydrography and Oceanography for the northeast and southwest Marmara Sea shelves and the northeast Aegean Sea shelf and authors' data across the regions north of the Strait of Bosphorus and east of the Strait of Dardanelles, placed over bathymetry extracted from EMODnet data (http://www.emodnet-hydrography.eu/) for the Aegean Sea and Black Sea. Coastline, rivers and lakes are from NOAA National Geophysical Data Center, extracted from http://www.ngdc.noaa.gov/mgg/shorelines/ (Wessel and Smith, 1996). The map is compiled and shaded using Global Mapper^{TM}.

Figure 6. Latest Pleistocene–Holocene base-level curves compiled for the Black Sea basin, showing the inconsistencies in both timing (in ^{14}C years) and magnitude of variations. The Marmara Sea curve (gray band with maximum and minimum estimates, from Lambeck et al., 2007) is shown for comparison. Sill depth at reconnection of the Marmara Sea with the Aegean Sea and the present-day sill depth in the Strait of Dardanelles are from Aksu et al. (2016), whereas elevation of the Bosphorus sill is documented later in this review.

Figure 7. Map of the Marmara Sea Gateway showing the locations of author high-resolution seismic reflection profiles, high-resolution multibeam and dual frequency (Simrad) echosounder profiles and cores considered in this review. These data were collected by the authors during eleven cruises of the RV *Koca Piri Reis* of the Institute of Marine Sciences and Technology, Dokuz Eylül University between 1991 and 2014. Background topography is compiled using data from GeoMapApp (Ryan et al., 2009). The multibeam bathymetry is compiled using data from Rangin et al. (2001) for the deep Marmara Sea basins, from the Turkish Navy, Office of Navigation, Hydrography and Oceanography for the northeastern and southwestern Marmara Sea shelves and the northeastern Aegean Sea shelf and authors' data across the regions north of the Strait of Bosphorus and east of the Strait of Dardanelles, placed over bathymetry extracted from EMODnet data (http://www.emodnet-hydrography.eu/) for the Aegean Sea and Black Sea. Coastline, rivers and lakes are from NOAA National Geophysical Data Center, extracted from http://www.ngdc.noaa.gov/mgg/shorelines/ (Wessel and Smith, 1996). The map is compiled using Global Mapper™.

Figure 8. Author-specified reservoir ages (R values, orange solid lines) for radiocarbon-dated shells younger than 24,000 cal yrBP from the Black (a) and Marmara (b) Seas, consistent with constraints in Table 3. ΔR values (blue solid lines) are fixed at –100 ^{14}C yr back to the time when marine conditions similar to today became established; before this, ΔR values are those required to adjust default Marine20 reservoir ages (from Heaton et al., 2020) to the author-specified R values. Solid points correspond to actual calibrations completed for this review (Table 2 and Supplementary material 2). R and ΔR values

employed before 24,000 cal yrBP can be determined from Table 3 and are listed for each calibrated date in Supplementary material 2.

Figure 9. (a) High-resolution Huntec DTS seismic reflection profile showing the seismic stratigraphic architecture of the latest Pleistocene–Holocene successions across the southwestern Black Sea shelf. Seismic markers α, α0, α1 and α2, seismic stratigraphic Units 1, 3, allostratigraphic Unit 1, and its allosubunits 1a, 1b, 1c and 1d are described in the text. The folded and relatively steeper dipping package highlighted in yellow below the α0 and/or α markers is Upper Miocene–Lower Pliocene successions (Aksu et al., 2002a). Small red half-arrows indicate onlap. Red ticks and numbers with F prefixes at the base of the profile are navigational fixes. Blue numbers in brackets next to fix numbers are water depths taken from the 2005 multibeam bathymetry. (b) Index map showing the position of the seismic profile. The map is compiled using data from GeoMapApp (Ryan et al., 2009), and also shows authors' M05 multibeam profiles.

Figure 10. (a) High-resolution Huntec DTS seismic reflection profile showing the seismic stratigraphic architecture of the latest Pleistocene–Holocene successions across the northeastern Marmara Sea shelf. Seismic markers β1–β5, seismic stratigraphic Units 1, 2, allostratigraphic Units 1, 2 and their allosubunits 1a, 1b, 1c and 2a, 2b, mid-shelf deltas Δ1 and Δ2 are explained in the text. Red ticks and numbers with F prefixes at the base of the profile are navigational fixes. Present water depths (blue letters in brackets next to fix numbers) are taken from 2011 multibeam bathymetry. White circles with blue numbers 1–5 are seismic stratigraphic units of Hiscott et al. (2002). (b) Index map showing the position of the seismic profile. The map is compiled using the topography data from

GeoMapApp (Ryan et al., 2009) and the SHOD multibeam mosaic for the northeastern Marmara Sea shelf (adopted from Aksu et al., 2016).

Figure 11. (a) High-resolution Huntec DTS seismic reflection profile showing the seismic stratigraphic architecture of the Pleistocene–Holocene successions across the southwestern Marmara Sea. Seismic markers α1, α2, α3, seismic stratigraphic Units 1–3, and allostratigraphic Units 1–3 are described in the text. Note that allounits 1 and 2 are not further subdivided across the southwestern Marmara Sea shelf. Red ticks and numbers with F prefixes at the base of the profile are navigational fixes. Present water depths (blue letters in brackets next to fix numbers) are taken from 2011 multibeam bathymetry. (b) Index map showing the position of the seismic profile. The map is compiled using the topography data from GeoMapApp (Ryan et al., 2009) and the authors' high-resolution multibeam data (Aksu et al., 2018) placed over the SHOD multibeam mosaic for the southwestern Marmara Sea.

Figure 12. Correlations between piston and gravity cores across the southwestern Black Sea shelf. All radiocarbon ages (red numbers with arrows) are calibrated to calendar years using the Marine20 curve and author-specified reservoir ages (Fig. 8, Table 3). Allosubunits 1a–1d are indicated next to the schematic core logs. The word "composite" below the core number indicates that any core-top loss is accounted for by correlating the piston and gravity cores at the same site and adjusting original depth assignments in the piston core. At each core site the depths of the seismic markers α, α0, α1 and α2 (described in the text) are determined using Huntec DTS profiles, and converted from milliseconds of two-way travel time (ms twt) to metres of sub-seabed depth (m) using a 1500 m s^{-1} interval velocity. Note that the α unconformity is synonymous with the L–TS

(highlighted by a thick purple line). Index map at bottom shows the core locations along a broadly WNW–ESE profile. The map is compiled using the topography and bathymetry data from GeoMapApp (Ryan et al., 2009) and the authors' high-resolution multibeam data (Flood et al., 2009; Hiscott et al., 2013) placed over the bathymetry data from GeoMapApp.

Figure 13. Correlations between piston and gravity cores across the northeastern Marmara Sea shelf. All radiocarbon ages (red numbers with arrows) are calibrated to calendar years using the Marine20 curve and author-specified reservoir ages (Fig. 8, Table 3). Allostratigraphic subunits 1a–1d are indicated next to the schematic core logs. The word "composite" below the core number indicates that any core-top loss is accounted for by correlating the piston and gravity cores at the same site. At each core site the depths of the seismic markers β1 through β3 (described in the text) are determined using Huntec DTS profiles, and converted from ms twt to m using a 1500 m s^{-1} interval velocity. Core-top losses for piston cores are consistent with magnetic susceptibility data, age models, and seismic ties for core M02-109P (see Aksu et al., 2016). Except for sapropel, most sediments are bioturbated. Note that the β3 unconformity is synonymous with the L–TS (highlighted by a thick purple line). Except for core MD04-2750, logs are simplified from author core-table descriptions. The MD04-2750 log is based on the unpublished IFREMER report for cruise "Marmara VT/Marmacore 2" (co-chiefs G. Lericolais and P. Henry; describer M. Muret). Δ2 and Δ1 are the late Pleistocene and early Holocene deltas, respectively (described in the text). Index map at bottom right shows the core locations along a broadly NW–SE profile. The map is compiled using the topography

data from GeoMapApp (Ryan et al., 2009) and the SHOD multibeam mosaic for the northeastern Marmara Sea shelf (adopted from Aksu et al., 2016).

Figure 14. Correlations between piston and gravity cores across the southwestern Marmara Sea shelf. All radiocarbon ages (red numbers with arrows) are calibrated to calendar years using the Marine20 curve and author-specified reservoir ages (Fig. 8, Table 3). Allostratigraphic units 1 and 2 are indicated next to the schematic core logs. The word "composite" below the core number indicates that the core-top loss is accounted for by correlating the piston and gravity cores at the same site. Note that the allounits 1 and 2 are not further subdivided for the southwestern Marmara Sea shelf. At each core site the depths of the seismic marker α1 (described in the text) are determined using Huntec DTS profiles, and converted from ms twt to m using a 1500 m s^{-1} interval velocity. Y2 = Cape Riva eruption, ca. 18.13 ^{14}C ka (21.05 cal ka; Aksu et al., 2008). Index map at bottom shows the core locations along a broadly W–E/E–W profile. The map is compiled using the topography data from GeoMapApp (Ryan et al., 2009) and the multibeam bathymetry compiled from Rangin et al. (2001) multibeam data for the deep water basins and the SHOD multibeam mosaic for the southwestern Marmara Sea.

Figure 15. Chronostratigraphic chart, representing the unconformity-bounded sequences across the southwestern Black Sea shelf. The time of reconnection at 9.47 cal ka is from Ankindinova et al. (2019a). The evaporative drawdown of the Neoeuxine Lake is from Ryan et al. (2003), Major et al. (2006) and Cohen et al. (2011). At 10.2 cal ka, a salt wedge penetrated sufficiently deeply into the southern end of the Strait of Bosphorus that bedload supply to the Holocene delta lobe in the northeastern Marmara Sea ceased (from Aksu et al., 2016). Blue letters below the core labels are present-day water depths at core

sites determined using the multibeam data collected during the M05, M08 and M11 cruises. Ages of allosubunit 1a are conjectural. Pre-B = Preboreal (11.7–9.3 cal ka); YD = Younger Dryas (12.9–11.7 cal ka); BA = Bølling–Allerød (14.8–12.9 cal ka). Index map at top shows the core locations along a broadly WNW–ESE transect. The map is compiled using the topography and bathymetry data from GeoMapApp (Ryan et al., 2009) and the authors' high-resolution multibeam data (Flood et al., 2009; Hiscott et al., 2013) placed over bathymetry data from GeoMapApp.

Figure 16. Chronostratigraphic chart, representing the unconformity-bounded sequences across the northeastern Marmara Sea shelf. Base-level curves for the Propontis Lake (subsequently the Marmara Sea) at the Bosphorus sill (maximum and minimum) are from Lambeck et al. (2007). The onsets of Black Sea outflow at ~17.2 cal ka and 11.1 cal ka, resulting in the development of two mid-shelf strait deltas (i.e., Δ1 and Δ2), are from Aksu et al. (2016). Blue letters below the core labels are present-day water depths at core sites, determined using the multibeam data collected during the M11 cruise. Pre-B = Preboreal; YD = Younger Dryas; BA = Bølling–Allerød. Index map at top shows the core locations along a broadly NW–SE transect. The map is compiled using the topography data from GeoMapApp (Ryan et al., 2009) and the SHOD multibeam mosaic for the northeastern Marmara Sea shelf (adopted from Aksu et al., 2016).

Figure 17. Chronostratigraphic chart, representing the unconformity-bounded sequences across the southwestern Marmara shelf. Base-level curves for the Propontis Lake (subsequently the Marmara Sea) at the Dardanelles sill (maximum and minimum) are from Lambeck et al. (2007). Reconnection of the Propontis Lake with the Aegean Sea at 13.8 cal ka is from Aksu et al. (2016). Blue letters below the core labels are present-day water depths

at core sites, determined using the multibeam data collected during the M11 cruise. Pre-B = Preboreal; YD = Younger Dryas; BA = Bølling–Allerød. Index map at top shows the core locations along a broadly W–E/E–W transect. The map is compiled using the topography data from GeoMapApp (Ryan et al., 2009) and multibeam bathymetry compiled from Rangin et al. (2001) multibeam data for the deep water basins and the SHOD multibeam mosaic for the southwestern Marmara Sea.

Figure 18. Map showing the Cape Emine region, western Black Sea, and an abandoned recurved spit inferred to have developed by sustained south-directed longshore transport when base level was at a stillstand of ~ –30 to –35 m during the early Holocene. The gridded xyz data for the multibeam mosaic were downloaded from the EMODnet Bathymetry Consortium site (http://doi.org/10.12770/18ff0d48-b203-4a65-94a9-5fd8b0ec35f6), and displayed and contoured using Global Mapper™. The topography and −110 m isobath are extracted from GeoMapApp (Ryan et al., 2009), and compiled using Global Mapper™. Coastline is from NOAA National Geophysical Data Center (http://www.ngdc.noaa.gov/mgg/shorelines/ shorelines.html).

Figure 19. (a) High-resolution Huntec DTS seismic reflection profile showing the shelf-crossing unconformities across the northeastern Marmara Sea shelf. Seismic markers β1–β6, and mid-shelf delta Δ1 are explained in the text. Note the development of prominent unconformities β3 and β5 best imaged across the shelf-edge. The β6 unconformity is interpreted to be much older as it cuts a well-bedded, southerly-tilted succession. Note the absence of shelf-edge deltas seaward of the early Holocene mid-shelf delta (Δ1). Red ticks and numbers with F prefixes at the base of the profile are navigational fixes. Present water depths (blue letters in brackets next to fix numbers) are taken from 2011

multibeam bathymetry. (b) Index map showing the position of the seismic profile, compiled using the topography data from GeoMapApp (Ryan et al., 2009) and the SHOD multibeam mosaic for the northeastern Marmara Sea.

Figure 20. (a) Isopach (in milliseconds of twt) of the early Holocene delta (Δ1). The thickest deposits (36 ms = 27 m) form an elongate tongue which extends seaward from the exit of the Strait of Bosphorus, and not from the mouth of the Kurbağalıdere stream. (b) Isopach (in milliseconds of twt) of the Late Pleistocene delta (Δ2). The position of a delta-top feeder channel is marked by the white dashed line. Figures are adapted from Aksu et al. (2016, their figures 16 and 17).

Figure 21. Schematic water-level histories of the Black Sea, Marmara Sea and the Aegean Sea according to the Flood Hypothesis (a: Ryan et al., 1997, 2003; Yanchilina et al., 2017) and the Outflow Hypothesis (b: Hiscott et al., 2002, 2007a,b, 2017; Aksu et al., 2002a,b, 2016; Ankindinova et al., 2020). When the Mediterranean and Marmara curves are superimposed but before the start of outflow from the Neoeuxine Lake (i.e., ~13.8–11.5 cal ka), the Marmara Sea was a rather stagnant embayment of the Mediterranean Sea. According to the Flood Hypothesis, saline Marmara and Mediterranean waters catastrophically flooded into the depressed Black Sea basin, and only afterwards did Black Sea surface waters begin to flow outward across the gateway. The Flood Hypothesis predicts a homogeneous Marmara Sea water column until ~9.5 cal ka with a final turbulent stirring and flushing in of Mediterranean fauna and flora in the subsequent torrent crossing the gateway. According to the Outflow Hypothesis, the surface of the rising Neoeuxine Lake reached the shallow sill (likely ~ –45 m) toward the southern end of the Strait of Bosphorus first, triggering a downslope cascade into the rising Marmara

Sea as the overspill depth reached, perhaps, –40 m or less—building the delta illustrated in Figure 19. The Outflow Hypothesis predicts stratification and low oxygen conditions in the Marmara Sea since ~11.5 cal ka, similar to today. Pre-B = Preboreal; YD = Younger Dryas; BA = Bølling–Allerød.

Figure 22. Plot of calibrated radiocarbon age versus the depositional elevation (relative to modern sea level) of 40 dated shells extracted from Memorial University of Newfoundland cores raised from the southwestern Black Sea shelf. Thirteen calibrated ages of lacustrine/brackish gastropods and bivalves (red-filled circles) indicate that the southwestern Black Sea shelf was inundated between ~16.5 and 11 cal ka, within a period when Ryan et al. (1997) and Yanchilina et al. (2017) suggested that the Neoeuxine Lake level was between –150 and <–120 m. Fourteen calibrated ages of lacustrine/brackish molluscs (yellow-filled circles) between 11 and ~9.2 cal ka indicate that the Neoeuxine Lake remained high prior to the purported catastrophic flooding of these latter authors.

Figure 23. Isopach map (in ms twt) of the lower Holocene seismic stratigraphic subunit 1b (corresponding to sedimentary allosubunit 1b) across the southwestern Black Sea. The data are contoured using Global Mapper™. Coastline is from NOAA National Geophysical Data Center (http://www.ngdc.noaa.gov/mgg/shorelines/shorelines.html). The −50 m and −100 m isobaths are from Intergovernmental Oceanographic Commission (1981). Black dotted line shows the area underlain by gas-charged sediments (cf. Fig. 9). Map is adapted from Ankindinova et al. (2020).

Figure 24. Paleobathymetry/paleotopography maps (in 5 m contour intervals) showing the effects of the latest Pleistocene–early Holocene transgression across the southwestern Black Sea shelf. Panels a–f (here and Figs. 25, 26) were constructed assuming a constant

rate of sedimentation between 12.5 cal ka and 7.5 cal ka, and that base levels were at –75 m, –65 m, –35 m, –30 m, –20 m and –10 m at 12.5 cal ka, 11.5 cal ka, 10.5 cal ka, 9.5 cal ka, 8.5 cal ka and 7.5 cal ka, respectively. At ~12.5 cal ka (i.e., reflector α time; panel a), part of allosubunit 1a (50% assumed) and all of allosubunits 1b–1d had not yet been deposited. Hence, the water depth at every fix point on the map was calculated by subtracting 75 m from today's depth, then adding the combined thicknesses of 50% of allosubunits 1a and 100% of 1b–1d (panel a). For panel b (i.e., ~11.5 cal ka), water depth at every fix point on the map was calculated by subtracting 65 m from today's depth, then adding the combined thicknesses of allosubunits 1b, 1c and 1d to extend the paleo-water depth downward from the modern seabed to the base of subunit 1b. The maps were then compiled, colour-shaded and contoured using Global Mapper^{TM}. Present-day coastline is from NOAA National Geophysical Data Center (http://www.ngdc.noaa.gov/mgg/shorelines/shorelines.html). The datum for each map is the contemporary local base level. Paleo-shoreline (base level) assumed.

Figure 25. Paleobathymetry/paleotopography maps (in 5 m contour intervals) showing the effects of the latest Pleistocene–early Holocene transgression across the southwestern Black Sea shelf. See the Figure 24 caption for more details. For panel c (i.e., ~10.5 cal ka), water depth at every fix point on the map was calculated by subtracting 35 m from today's depth, then adding the combined thicknesses of 4/5 of allosubunit 1b, and all of allosubunits 1c and 1d. For panel d (i.e., ~9.5 cal ka), water depth at every fix point on the map was calculated by subtracting 30 m from today's depth, then adding the combined thicknesses of 3/5 of allosubunit 1b, and all of allosubunits 1c and 1d. The different fractions used are based on the chronology of the various allosubunits deduced

from core records (Fig. 12). The datum for each map is the contemporary local base level. Paleo-shoreline (base level) assumed.

Figure 26. Paleobathymetry/paleotopography maps (in 5 m contour intervals) showing the effects of the latest Pleistocene–early Holocene transgression across the southwestern Black Sea shelf. See the Figure 22 caption for more details. For panel e (i.e., ~8.5 cal ka), water depth at every fix point on the map was calculated by subtracting 20 m from today's depth, then adding the combined thicknesses of 2/3 of allosubunit 1b, and all of allosubunits 1c and 1d. At 7.5 cal ka (i.e., ~α1 time; panel f) sea level was 10 m lower than today (Lambeck et al., 2007; Fig. 21), but allosubunits 1d and 1c had not yet been deposited. Hence, the water depth at every fix point on the map was calculated by subtracting 10 m from today's depth, then adding the combined thicknesses of allosubunits 1d and 1c. The different fractions used are based on the chronology of the various allosubunits deduced from core records (Fig. 12). The pale pink mask over the saline channel demarcates the region where the modern seafloor has been eroded below the α1 level (to α or α0), creating a morphology that did not exist during α time, but started to develop immediately prior to α1 time. The datum for each map is the contemporary local base level. Paleo-shoreline (base level) assumed.

Figure 27. (a) High-resolution Huntec DTS seismic reflection profile showing >3 km of delta-front progradation during a base-level rise of at least 8 m, but likely >8 m to explain the eventually abandonment of the lobe as it was overtaken by the water-level rise. This situation is unexpected for river deltas (see the text for further explanation). The blue-highlighted delta-top wedge accumulated while the lobe was prograding seaward, so is interpreted as fluvial and floodplain facies. Seismic markers β1, β5, and mid-shelf delta

Δ1 are explained in the text. Red ticks and numbers with F prefixes at the base of the profile are navigational fixes. Present water depths (blue letters in brackets next to fix numbers) are taken from 2011 multibeam bathymetry. (**b**) Index map showing the position of the seismic profile, compiled using topography data from GeoMapApp (Ryan et al., 2009) and the SHOD multibeam mosaic for the northeastern Marmara Sea. (**c**) Mouth of the Kurbağalıdere stream downloaded from https://www.diken.com.tr/wp-content/uploads/2015/11/kurbagali-dere-kadikoy4.jpg.

Figure 28. (a) Detail of 8–11 cal ka portion of the $^{87}Sr/^{86}Sr$ data of Ankindinova et al. (2019a) to better portray the initial sharp rise in the isotopic ratio and the character of the older "plateau" (flagged by a red bar) used in modelling exercises. One data point (*) falls off the smoothed trend and is considered an outlier. A–D segments of the plot are alternately coloured and are explained as evolutionary stages in the text. (b) Full M02-45 $^{87}Sr/^{86}Sr$ data (blue points; 1σ error bars = ±0.000014) of Ankindinova et al. (2019a) compared with Major et al. (2006) and Yanchilina et al. (2017) data mostly from coquina layers. Bold orange line represents smoothed $^{87}Sr/^{86}Sr$ evolution of basin water, and is the basis of interpretation in this review.

Figure 29. Plots for Black Sea composite core M02-45 of benthic foraminifera *Ammonia compacta* and *A. tepida*, *Porosononion* spp., Coccolith *Emiliania huxleyi*, freshwater algae *Pediastrum* and *Botrycoccus*, Ponto-Caspian ostracods (sum of *Tyrrhenocythere amnicola*, *Candona schweyeri*, *Loxoconcha lepida* and *L. sublipida*, and *Amnicythere olive*) and Mediterranean ostracods (sum of *Palomochonca agilis*, *Hiltermanicythere rubra*, *Carinocythereis carinata*, and *Leptocythere* spp.), dinoflagellate cysts *Spiniferites cruciformis*, *Lingulodinium machaerophorum* (sensu lato) and Mediterranean dinocysts

(sum of *S. belerius*, *Operculodinium centrocarpum*, *S. bentorii*, *S. mirabilis* and *S. ramosus*), all expressed as percentages of the total respective faunal/floral assemblages. The depth-to-age conversion was made using 16 radiocarbon ages, calibrated to calendar years. Blue dashed lines indicate the depths of dated shells. Original data are largely from Hiscott et al. (2007a).

Figure 30. Plots for Marmara Sea core M98-09 of brackish benthic foraminifera (sum of *Ammonia compacta*, *A. beccarii*, *A. tepida*), marine benthic foraminifera (sum of *Breziliana* spp., *Bulemina elongate*, *B. marginata*, *B. aculeate*, *B. costata*), oxic bottom water indicator benthic foraminifera (sum of *Ammonia compacta*, *A. beccarii*, *A. tepida*, *Hyalina balthica*, *Quinqueloculina* spp., *Biloculinella* spp., *Sigmoilinita tenuis*, *Lagena striata*, *Lagena semistriata*, *Discorbinella bertheloti*, *Lobatula lobatula*, *Globocassidulina subglobosa*, *Valvulina* spp., *Cibicides* spp., *Rosalina* spp., *Spiroloculina excavate*, *Gavelinopsis praegeri*, *Planorbulina medIterranea*), dysoxic bottom water indicator benthic foraminifera (sum of *Breziliana* spp., *Bulemina elongate*, *B. marginata*, *B. aculeate*, *Bolivina* spp., *Astigerinata mammilla*, *Chilostomella* spp., *Cassidulina carinata*, *C. crassa*, *Globobulimina* spp., *Fursinkoina acuta*), Coccolith *Emiliania huxleyi*, dinoflagellate cysts *Spiniferites cruciformis*, *Lingulodinium machaerophorum* (sensu lato), *Pinus*, *Polypodiaceae* and shrubs, and planktonic foraminifera (sum of *Turborotalia quinqueloba*, *Globigerina bulloides* and *Neogloboquadrina pachyderma*), all expressed as percentages of the total respective faunal/floral assemblages. The depth-to-age conversion was made using 6 radiocarbon ages, calibrated to calendar years. Also shown are the oxygen and carbon isotopic compositions in benthic foraminifera *Neocarinata crassa*, total organic carbon (TOC)

and the abundance of opaline silica fractions in the core. Blue dashed lines indicate the depths of dated shells. Original data are largely from Aksu et al. (2002b). Distinction of lower and upper mud drape from Hiscott et al. (2017).

Figure 31. Summary of paleoceanographic conditions believed to be responsible for sapropel development in the Aegean and Marmara Seas: S1 and M1 respectively. See text for details.

Figure 32. Spatiotemporal distribution of (a) winter sea surface oxygen isotopic composition (δ^{18}Ow), (b) winter sea surface salinity (SSSw) and (c) winter sea surface temperature (SSTw) across the Aegean Sea since 16 cal ka. SSSw and SSTw are extracted from the Mediterranean-based planktonic foraminiferal transfer function results published in Aksu et al. (1995b) and İşler et al. (2016b). The δ^{18}Ow estimates for the M91 cores are adopted from Aksu et al. (1995c), whereas those for the M03 cores are calculated for this review using the procedure explained in Aksu et al. (1995c). Note that these estimates reflect first-order variations of the surface water oxygen isotopic composition, but not absolute values. The age models of Aksu et al. (1995c) and İşler et al. (2016b) were used to obtain calibrated ages for the data points, which were then re-contoured for this manuscript using Global Mapper™. The gray shade represents sapropel S1. Core locations are shown in Fig. 1.

Figure 33. (a) Bathymetric map of the saline channel area in the southwestern Black Sea. Multibeam bathymetry, collected during M05, M08 and M11 cruises (Flood et al., 2009; Hiscott et al., 2013; Ankindinova et al., 2020), is superimposed on bathymetry extracted from EMODnet data (http://www.emodnet-hydrography.eu/) for the Black Sea (Ryan et al., 2009). (b) Saline bottom water dispersal pathways are highlighted in red.

Figure 34. Maps showing (a) Turkish Navy, Office of Navigation, Hydrography and Oceanography multibeam imagery over the southern sector of the Strait of Bosphorus and its shallowest sill, (b) the same area contoured with 1 m spacing, (c) a simplified view showing locations of deepest points along two corridors across the –37 to –38 m sill, (d) a longitudinal seismic reflection profile (located in map a) showing a southwest-prograded clinoform succession immediately below the β1 reflector. The profile is adopted from Alavi et al. (1998). Correlations with β1, β2 and Δ1 are from Aksu et al. (2016). Location is shown in panel (a).

Figure 35. (a) High resolution multichannel seismic reflection profile across the southern sector of the Strait of Bosphorus and (b) interpretation of the seismic reflection profile (both adopted from Yilmaz et al., 2018) showing a thick sedimentary fill deposited over the Carboniferous Trakya Formation ([illegible] et al., 2016). β1 and β2 are prominent reflectors defined by Aksu et al. (2016), and transferred from the crossing seismic profile in Figure 34. Δ1= early Holocene delta and correlative units. DS02–DS12 are engineering boreholes. Location is shown in panel (a) of Figure 34.

Figure 36. (a) Map showing the inferred paleogeography of the Marmara Sea (Propontis Lake), southwestern Black Sea (Neoeuxine Lake) and northeastern Aegean Sea at 16.5 cal ka (17.2–15.7 cal ka). The Neoeuxine Lake was swollen by meltwaters originating from deglaciation of the southeastern margin of the Scandinavian Ice Sheet and was discharging into the isolated Propontis Lake, raising its base level to at least –68 m (above the top of outflow delta Δ2). The Propontis Lake emptied through the Strait of Dardanelles into the Aegean Sea (i.e., global ocean) which stood at ~ –100 m (Lambeck et al., 2014). (b) Map for 13.8 cal ka when saline waters of the Aegean Sea began to

enter the Propontis Lake. Between 15.7 cal ka and 13.8 cal ka both the Propontis and Neoeuxine Lakes experienced evaporative drawdown, which caused their base levels to stand at ~ –73 m and –110 m, respectively. The rise of global sea level to the breach depth of the Strait of Dardanelles at –75 m (Aksu et al., 2016) allowed reconnection between the Aegean Sea and the Propontis Lake, creating the Marmara Sea embayment with quick salination due to its small volume. The region occupied by the Strait of Bosphorus was subaerially exposed during this time.

Figure 37. Maps showing the paleogeography of the Marmara Sea, southwestern Black Sea (Neoeuxine Lake) and northeastern Aegean Sea during (c) 12.5 cal ka when the Marmara Sea was saline but without driving forces to create deep circulation, and (d) at 11.1 cal ka after the Neoeuxine Lake had risen 5–10 m above the breach depth of the Bosphorus sill at ~ −45 m and vigorous outflow into the Marmara Sea had started (yellow arrow). The Marmara and Aegean Seas both stood at ~ –43 m but by 10.2 cal ka had climbed to ~ –35 m. Outflow from the Neoeuxine Lake continued into the Aegean Sea, maintaining water-column stratification in the Marmara Sea.

Figure 38. (e) Map showing the paleogeography of the Marmara Sea, southwestern Black Sea (Neoeuxine Lake) and northeastern Aegean Sea during ~9.5 cal ka when the surface outflow from the Strait of Bosphorus had diminished enough to allow the initial penetration of saline water into the lake as an underflow, resulting in its progressive salination and conversion to what we know as the Black Sea. Complementary two-way flow grew in importance across the Strait of Dardanelles. (f) Map for 8.0 cal ka when global sea level reached –15 m. This shortly follows the establishment of robust and continuous two-way flow across both the straits of Bosphorus and Dardanelles. Saline

inflow redistributed fine-grained sands and silts on the shelf beyond the northern exit of the Strait of Bosphorus to sweep clean the floors of a network of channels and to build levées of the Saline Channel system. The sediment itself was largely advected into the area from the west by the Rim Current (Hiscott et al., 2013).

Table 1. Coordinates, core lengths and water depths of cores used in this study. G= independent gravity core, P= piston core, T= trigger weight core.

Core identifier	Latitude	Longitude	Core length (cm)	Water depth (m)
SW Black Sea shelf				
M02-45T	41° 41.170' N	28° 19.080' E	183	–69
M02-45P	41° 41.170' N	28° 19.080' E	851	–69
M05-03P	41° 40.878' N	28° 19.024' E	588	–68
M05-04G	41° 09.947' N	31° 07.715' E	171	–75
M05-05G	41° 13.105' N	31° 16.432' E	230	–77
M05-07P	41° 13.028' N	31° 16.373' E	890	–77
M05-13P	41° 09.987' N	31° 07.686' E	813	–75
M05-19P	41° 33.948' N	28° 53.670' E	960	–94
M05-19G	41° 33.961' N	28° 53.719' E	168	–94
M05-22P	41° 32.416' N	28° 48.854' E	666	–86
M05-22T	41° 32.416' N	28° 48.854' E	210	–86
M05-44P	41° 27.529' N	29° 10.004' E	925	–82
M05-44G	41° 27.529' N	29° 10.004' E	208	–82
M05-50P	41° 29.634' N	29° 04.445' E	760	–91
M05-51G	41° 29.471' N	29° 04.393' E	159	–93
M11-08T	41° 22.787' N	29° 01.047' E	272	–77
M11-09T	41° 21.123' N	29° 01.018' E	190	–76
M11-15G	41° 22.657' N	29° 11.122' E	251	–71
M11-16P	41° 22.663' N	29° 11.115' E	735	–70
M11-22P	41° 21.118' N	29° 00.983' E	299	–75
M11-23P	41° 22.784' N	29° 01.060' E	517	–77
M11-29G	41° 30.007' N	28° 56.160' E	216	–83
M11-30P	41° 29.978' N	28° 56.188' E	673	–83
NE Marmara Sea shelf				
M98-07G	40° 50.977' N	29° 00.983' E	238	–95
M98-09G	40° 55.357' N	28° 56.803' E	130	–64
M02-109P	40° 55.490' N	28° 57.109' E	200	–62
M02-110P	40° 55.605' N	28° 57.100' E	309	–62
M02-111P	40° 55.306' N	28° 56.125' E	409	–72
M08-18G	40° 56.707' N	28° 56.155' E	146	–67
M08-19G	40° 55.305' N	28° 56.122' E	161	–73
M08-20G	40° 55.585' N	28° 57.107' E	152	–62
M11-032P	40° 56.685' N	28° 56.141' E	525	–62
M11-031G	40° 56.703' N	28° 56.151' E	137	–62
M11-033G	40° 55.562' N	28° 58.682' E	180	–47
M11-034P	40° 55.560' N	28° 58.675' E	571	–47
M11-040G	40° 56.470' N	28° 56.414' E	153	–60
M11-041P	40° 56.487' N	28° 56.411' E	345	–60

S and SW Marmara Sea				
M97-11G	40° 39.200' N	28° 22.670' E	237	–111
M02-088P	40° 37.989' N	28° 50.848' E	682	–354
M02-089P	40° 40.303' N	28° 51.389' E	806	–257
M02-090P	40° 49.520' N	28° 16.975' E	852	–635
M02-102P	40° 50.187' N	27° 45.439' E	969	–567
M02-103P	40° 34.852' N	27° 27.810' E	440	–72
M02-106P	40° 27.216' N	27° 02.334' E	593	–61
M14-16P	40° 39.219' N	28° 22.724' E	668	–112
M14-21G	40° 34.868' N	27° 27.823' E	153	–73
M14-26G	40° 27.228' N	27° 02.367' E	149	–61
Aegean Sea				
M91-03G	40° 08.100' N	24° 51.160' E	150	–685
M91-05G	37° 19.020' N	26° 06.080' E	165	–430
M91-19G	39° 16.030' N	24° 50.030' E	145	–380
M91-20G	38° 26.120' N	24° 58.100' E	150	–630
M91-22G	35° 45.150' N	26° 45.190' E	135	–820
M03-02P	38° 03.970' N	26° 22.300' E	813	–398
M03-03P	37° 51.720' N	25° 49.170' E	604	–720
M03-25P	37° 10.360' N	26° 26.5[illegible]0' E	629	–494
M03-27P	38° 18.680' N	25° 18.970' E	1032	–651
M03-28P	39° 01.020' N	25° 01.480' E	826	–453

Table 2. Accelerator mass-spectrometer (AMS) 14C dates (±1σ) and calibrated equivalents as calendar years (±1σ) for shells from the cores used in this study. Calibration uses the Marine20 curve of Heaton et al. (2020) with reservoir values (R) and local departures from default reservoir values (ΔR) provided in Table 3 and Figure 8 and justified both in the text and in Williams et al. (2018). TO = IsoTrace Radiocarbon Laboratory Accelerator Mass Spectrometry Facility University of Toronto; UCIAMS = Radiocarbon Dating Laboratory Université Laval via KECK Carbon Cycle AMS Facility University of California Irvine; BETA = Beta Analytic Inc., Miami Florida, USA. G= gravity core P= piston core, T= trigger weight core. Dates with SACA and OS laboratory numbers in core MD04-2750 are from Eriş et al. (2007). * = articulated shell; ** = composite core (discussed in the text; also see Ankindinova et al., 2020); *** = these dates are used together with the age of the Z2 tephra at 3.6 cal ka in the development of age models for the Aegean Sea cores.

Core Identifier	**Depth (cm)**		**Dated material**	**uncalibrated**		**calibrated**		**ΔR**	**Lab number**
	core	**true**		**^{14}C yr BP**		**cal yr BP**		**Marine20**	
SW Black Sea shelf									
M02-45 (M02-45T + M02-45P + M05-03P)**									
M02-45T	92	92	*Spisula subtruncata*	730	± 50	290	± 90	–100	TO-11433
M02-45T	145	145	*Spisula subtruncata*	770	± 50	330	± 80	–100	TO-11434
M02-45P	33	143	*Spisula subtruncata*	730	± 40	295	± 85	–100	TO-11435
M02-45P	158	268	*Mytilus edulis*	2400	± 60	1985	± 105	–100	TO-11006
M02-45P	174	284	*Mytilus galloprovincialis*	5115	± 20	5385	± 70	–100	UCIAMS-85907
M02-45P	220	330	*Mytilus edulis*	5190	± 50	5460	± 85	–100	TO-11436
M02-45P	302	412	*Mytilus galloprovincialis*	5900	± 60	6225	± 95	–100	TO-11437
M02-45P	406	516	*Monodacna pontica.*	7560	± 60	8020	± 90	–175	TO-11438
M02-45P	495	605	*Euxinipyrgula* sp.	8380	± 70	9025	± 125	–200	TO-11142
M02-45P	569	679	*Didacna ?praetrigonoides*	8570	± 70	9415	± 90	–340	TO-11439

M02-45P	639	749	*Didacna* spp.	8620	± 70	9455	± 95	–335	TO-11440
M02-45P	754	864	*Dreissena rostiformis*	8840	± 70	9590	± 110	–230	TO-11441
M02-45P	810	920	*Dreissena rostiformis*	9370	± 70	10390	± 120	–305	TO-11007
M02-45P	822	932	*Dreissena polymorpha*	9340	± 70	10355	± 115	–300	TO-11442
M02-45P	835	945	*Theodoxus* spp.	9070	± 70	9985	± 135	–260	TO-11443
M05-03P	183	485	*Cardium edule*	6810	± 25	7225	± 75	–100	UCIAMS-85908
M05-03P	226	528	*Adacna ?laeviuscula*	7785	± 25	8275	± 110	–145	UCIAMS-85911
M05-03P	342	644	*Monodacna caspia*	8340	± 25	9020	± 80	–230	UCIAMS-85910
M05-03P	678	980	*Dreissena* spp.	9510	± 25	10585	± 80	–295	UCIAMS-85909
M05-03P	712	1014	*Dreissena* spp.	10475	± 30	12130	± 80	–385	UCIAMS-85912
M05-07 (M05-05G + M05-07P)**									
M05-07P	706	716	*Turricaspia spica*	8870	± 60	9625	± 105	–230	TO-12718
M05-07P	748	758	*Turricaspia spica*	10370	± 80	11990	± 165	–400	TO-12832
M05-07P	792	802	*Turricaspia spica*	14770	± 90	16190	± 155	685	TO-12833
M05-07P	851	861	*Turricaspia spica*	14300	± 90	15635	± 165	645	TO-12719
M05-13P (M05-04G + M05-13P)**									
M05-13P	647	687	bivalve fragments	7020	± 100	7425	± 110	–100	TO-12912
M05-13P	696	736	*Turricaspia spica*	8740	± 70	9540	± 80	–290	TO-12834
M05-13P	757	797	*Turricaspia spica*	11560	± 41	12930	± 44	–20	TO-12835

					0		5		
M05-13P	784	804	bivalve fragments	9870	±90	11215	±90	–380	TO-12835
M05-19 (M05-19G + M05-19P)**									
M05-19G	31	31	*Cerastoderma lamarcki*	2230	±60	1775	±100	–100	TO-12722
M05-19G	132	132	*Mactra corallina*	4390	±50	4485	±105	–100	TO-12723
M05-19P	36	36	*Cerastoderma lamarcki*	2880	±50	2580	±95	–100	TO-12725
M05-19P	149	149	*Mactra corallina*	4960	±60	5190	±115	–100	TO-12724
M05-19P	211	211	white mussels	8070	±60	8555	±110	–180	TO-12726
M05-19P	318	318	*Dreissena r. distincta*	32360	±290	36640	±340	–644	TO-12727

M05-19P	445	445	*Dreissena r. distincta*	36590	± 440	41490	± 295	–1215	TO-12728
M05-19P	556	556	bivalve fragments	32040	± 280	36365	± 310	–675	TO-12729
M05-19P	685	685	*Dreissena r. distincta*	37260	± 430	41985	± 225	–1430	TO-12723
M05-22 (M05-22T + M05-22P)**									
M05-22P	669	730	White mussel	9290	± 60	10280	± 100	–280	TO-12914
M05-50 (M05-51G + M05-50P)**									
M05-50P	44	94	*Mytilus galloprovincialis*	2590	± 90	2220	± 135	–100	TO-13095
M05-50P	180	230	*Mytilus galloprovincialis*	3240	± 50	3010	± 100	–100	TO-13096
M05-50P	200	250	*Mytilus galloprovincialis*	3590	± 15	3440	± 70	–100	UCIAMS-96128
M05-50P	279	329	*Mytilus galloprovincialis*	3250	± 70	3025	± 115	–100	TO-13097
M05-50P	310	360	*Mytilus galloprovincialis*	4130	± 20	4135	± 85	–100	UCIAMS-96127
M05-	340	390	*Mytilus*	4320	±	438	±	–100	TO-13098

50P			*galloprovincialis*		60	5	115		
M05-50P	435	485	*Mytilus galloprovincialis*	5330	± 70	5615	± 105	–100	TO-13099
M05-50P	550	600	foraminifera/ostracod	7710	± 40	8190	± 90	–180	BETA305920
M05-50P	620	670	foraminifera/ostracod	8540	± 50	9330	± 90	–275	BETA305921
M05-50P	625	675	foraminifera/ostracod	7570	± 40	8020	± 80	–170	BETA307981
M05-50P	670	720	*Dreissena polymorpha*	9880	± 110	11235	± 165	–380	TO-13100
M05-50P	737	785	*Dreissena* spp.	10270	± 90	11880	± 175	–430	TO-12915
M05-51G	145	145	*Mytilus galloprovincialis*	3280	± 60	3060	± 105	–100	TO-13101
M11-16 (M11-15G + M11-16P)**									
M11-15G	223	223	*Mytilus galloprovincialis*	2955	± 15	2675	± 70	–100	UCIAMS-116467
M11-16P	68	208	*Mytilus galloprovincialis*	2865	± 10	2570	± 80	–100	UCIAMS-116468
M11-16P	689	829	*Mytilus galloprovincialis*	5510	± 20	5800	± 75	–100	UCIAMS-116469
M11-22 (M11-09T + M11-22P)**									
M11-09T	117	117	*Cyclopes spp?*	6470	± 20	6850	± 80	–100	UCIAMS-116459
M11-22P	51	91	*Spisula subtruncata*	3990	± 20	3950	± 80	–100	UCIAMS-116470
M11-22P	239	279	*Dreissena rostiformis*	10670	± 251	12355	± 315	–390	UCIAMS-116471
M11-23 (M11-08T + M11-23P)**									
M11-08T	178	178	*Abra alba*	1130	± 20	625	± 55	–100	UCIAMS-209113
M11-08T	227	227	*Cyclope donovania*	1445	± 20	930	± 70	–100	UCIAMS-209114
M11-08T	253	253	*Nuculana commutata*	3910	± 15	3840	± 80	–100	UCIAMS-209117
M11-	264	264	*Monodacna*	7870	±	835	±	–210	UCIAMS-

08T			*pontica*		20	0	60		116458
M11-23P	45	170	*Cyclopes* spp?	990	± 25	525	± 60	–100	UCIAMS-116472
M11-23P	270	395	*Cyclopes* spp?	9190	± 256	10225	± 370	–345	UCIAMS-116473
M11-23P	366	491	*Dreissena polymorpha*	9105	± 25	10075	± 80	–290	UCIAMS-209118
M11-23P	464	589	*Dreissena polymorpha*	10555	± 25	12285	± 120	–387	UCIAMS-116474
Other cores									
M00-06G	124	124	*Mytilus* spp.	7770	± 70	8220	± 100	–150	TO-9138
M05-10P	46	96	*Mytilus galloprovincialis*	6970	± 60	7375	± 85	185	TO-12720
M05-41G	150	150	white mussels	9150	± 110	10200	± 170	–355	TO-12837
M08-09G	126	126	*Dreissena polymorpha*	10045	± 25	11380	± 105	–350	UCIAMS-72971
M08-12G	140	140	*Spisula subtruncata*	7305	± 20	8220	± 65	–100	TO-9138
M11-07P	142	387	*Monodacna pontica*	7805	± 25	8335	± 65	–230	UCIAMS-116456
M11-07P	272	387	*Dreissena rostiformis*	10650	± 25	12475	± 90	–430	UCIAMS-116457
M11-11P	358	438	*Dreissena rostiformis*	11215	± 25	12755	± 60	–210	UCIAMS-116466
NE Marmara Sea shelf									
M98-07									
M98-07G	72	72	White mussel	15210	± 100	17330	± 185	195	TO-7785
M98-07G	95	95	*Dreissena r. distincta*	43550	± 790	45955	± 755	–820	TO-8455
M98-07G	119	119	White mussel	41480	± 610	44465	± 490	–1055	TO-7786
M98-07G	180	180	White mussel	41900	± 610	44690	± 475	–925	TO-7787

M98-07G	217	217	White mussel	40460	± 590	43435	± 475	–785	TO-7788
M98-09									
M98-09G	35	35	*Anomia* spp.	4500	± 60	4625	± 110	–100	TO-7789
M98-09G	42	42	*Nuclea nucleus*	6120	± 70	6460	± 105	–100	TO-8455
M98-09G	52	52	*Varicorbula gibba*	8810	± 100	9410	± 135	–100	TO-8456
M98-09G	60	60	*Turritella* spp.	9070	± 70	9735	± 130	–100	TO-7790
M98-09G	94	94	*Turritella* spp.	9840	± 80	10805	± 150	–100	TO-7791
M98-09G	113	113	*Mytilus* spp.	10220	± 70	11325	± 125	–100	TO-7792
M02-109 (M08-20G + M02-109P)**									
M02-109P	152	287	*Mytilus galloprovincialis*	10220	± 90	11335	± 150	–100	TO-11655
M02-109P	164	299	Bivalve	14520	± 110	16290	± 180	350	TO-11656
M08-20G	77	77	*Nucula* spp.	5255	± 15	5525	± 70	–100	UCIAMS-66263
M08-20G	97	97	*Abra alba*	8670	± 15	9265	± 80	–100	UCIAMS-66264
M08-20G	121	121	*Spisula* spp.	9095	± 20	9755	± 95	–100	UCIAMS-66262
M02-110 (M08-20G + M02-110P)**									
M02-110P	67	102	*Dosinia lupines, C. gibba*	5280	± 50	5555	± 90	–100	TO-12707
M02-110P	117	157	*Varicorbula gibba*	6760	± 60	7170	± 95	–100	TO-12708
M02-110P	148	188	*D.lupinus, Corbula gibba*	9110	± 70	9790	± 135	–100	TO-12709
M02-110P	186	226	*Turritella* spp.	9480	± 60	10300	± 10	–100	TO-12710

							5		
M02-110P	223	263	*Turritella* spp.	9650	± 60	10505	± 120	–100	TO-12711
M02-110P	275	315	*Cardium edule*	10580	± 100	11855	± 195	–100	TO-11149
M08-19G	46	46	*Turritella* spp.	9480	± 25	10290	± 75	–100	UCIAMS-61352
M08-19G	100	100	*Mytilus galloprovincialis*	10660	± 25	11980	± 115	–100	UCIAMS-61345
M08-19G	156	156	*Acanthocardium* spp.*	10650	± 25	11965	± 115	–100	UCIAMS-61356
M02-111 (M08-19G + M02-111P**									
M02-111P	16	66	*Turritella* spp.	9455	± 25	10260	± 75	–100	UCIAMS-61349
M02-111P	71	121	*Mytilus galloprovincialis*	10520	± 90	11750	± 180	–100	TO-11657
M02-111P	127	177	*Parvicardium exiguum*	10460	± 90	11655	± 175	–100	TO-11658
M02-111P	284	334	*Cardium edule**	10950	± 100	12375	± 160	–100	TO-11150
M02-111P	156	406	*Mytilus galloprovincialis*	11560	± 90	12975	± 110	–100	TO-11659
M11-34 (M11-33T + M11-34P)**									
M11-33G	145	160	*Turritella* spp.	5340	± 20	5620	± 75	–100	UCIAMS-129795
M11-34P	157	212	*Corbula gibba**	6815	± 20	7230	± 70	–100	UCIAMS-129796
M11-34P	246	301	*Corbula gibba**	8365	± 20	8860	± 85	–100	UCIAMS-129797
M11-34P	359	414	*Corbula gibba**	8910	± 25	9520	± 65	–100	UCIAMS-129798
M11-34P	530	585	*Mytilus galloprovincialis*	9845	± 25	10810	± 110	–100	UCIAMS-129806
M11-41 (M11-40T + M11-41P)**									
M11-40G	112	112	*Spisula subtruncata*	8890	± 25	9495	± 65	–100	UCIAMS-116475
M11-	88	145	*Spisula*	9240	±	998	±	–100	UCIAMS-

41P			*subtruncata*		25	5	95		116476
M11-41P	190	247	*Turritella* spp.	9970	± 25	10980	± 100	–100	UCIAMS-116477
M11-41P	207	264	*Monodacna pontica*	10645	± 25	11955	± 110	–100	UCIAMS-116478
M11-41P	333	390	bivalves/ostracods	11690	± 25	13110	± 70	–100	BETA335441
MD04-2750									
MD04-2750	327	327	Bivalve	5770	± 60	6085	± 95	–100	SACA-002573
MD04-2750	356	356	Bivalve	6460	± 55	6840	± 100	–100	OS-50131
MD04-2750	590	590	Bivalve	8380	± 70	6875	± 125	–100	SACA-002574
MD04-2750	940	940	Bivalve	9820	± 80	10780	± 150	–100	SACA-002575
MD04-2750	1126	1126	Bivalve	10450	± 50	11640	± 130	–100	OS-53538
MD04-2750	1236	1236	Bivalve	10900	± 65	12325	± 135	–100	OS-50130
S and SW Marmara Sea									
M97-11 & M14-16P									
M97-11G	79	79	*Turritella* spp.	10790	± 70	12180	± 150	–100	TO-7774
M97-11G	92	92	*Dreissena* spp.	12970	± 80	13855	± 130	526	TO-7775
M97-11G	174	174	Small oyster	14940	± 90	17000	± 155	215	TO-7776
M97-11G	204	204	*Dreissena* spp.	15590	± 90	17920	± 155	135	TO-7777
M14-16P	586	586	*Dreissena rostriformis*	18915	± 40	22055	± 110	–50	UCIAMS 166908
M02-88									
M02-	43	43	*Brysopsis*	1065	±	580	±	–100	UCIAMS 78276

88P					15		50		
M02-88P	663	663	*Brysopsis*	5935	± 15	6265	± 70	–100	UCIAMS 78277
M02-89									
M02-89P	10	10	bivalve fragments	7775	± 15	8160	± 75	–100	UCIAMS 78269
M02-89P	255	255	bivalve fragments	12920	± 110	13770	± 165	526	TO 11147
M02-89P	270	270	*Dreissena polymorpha*	15005	± 30	17050	± 115	235	UCIAMS 78270
M02-89P	290	290	*Dreissena polymorpha*	16085	± 30	18325	± 125	240	UCIAMS 78271
M02-89P	450	450	*Dreissena polymorpha*	16895	± 35	19260	± 120	180	UCIAMS 78272
M02-89P	490	490	*Dreissena polymorpha*	17570	± 35	20175	± 120	125	UCIAMS 78273
M02-89P	740	740	*Dreissena polymorpha*	23690	± 70	27795	± 110	–842	UCIAMS 78274
M02-89P	800	800	*Dreissena polymorpha*	25320	± 90	29675	± 160	–930	UCIAMS 78275
M02-90									
M02-90P	114	114	*Nucula* spp.	6760	± 15	7175	± 75	–100	UCIAMS 78278
M02-103 (M14-21T + M02-103P)**									
M14-21G	140	140	*Mytilus* spp.	4585	± 15	4720	± 75	–100	UCIAMS-187914
M02-103P	79	153	*Nucula sulcata*	4900	± 15	5125	± 90	–100	UCIAMS-187910
M02-103P	128	202	*Turritella* spp.	6080	± 80	6420	± 110	–100	TO 11148
M02-103P	224	298	*Turritella* spp.	8840	± 20	9445	± 60	–100	UCIAMS-187912
M02-103P	327	401	*Turritella* spp.	9270	± 20	10025	± 85	–100	UCIAMS-187911
M02-103P	358	432	*Parvicardium exiguum*	11340	± 80	12785	± 100	–100	TO 11011
M02-106 (M14-26T + M02-106P)**									

M14-26G	127	126	echinoderm plates	1820	± 15	1315	± 60	–100	UCIAMS-187908
M02-106P	10	46	*Nucula* spp.	895	± 15	435	± 60	–100	UCIAMS-187909
M02-106P	148	184	*Turritella* spp.	3125	± 15	2865	± 70	–100	UCIAMS-190395
M02-106P	308	344	*Turritella* spp.	6895	± 20	7310	± 65	–100	UCIAMS-190396
M02-106P	480	516	*Spisula* spp.	9115	± 20	9790	± 100	–100	UCIAMS-187913
Aegean Sea cores									
M91-03***	80	80	bulk foraminifera	9920	± 70	10780	± 140	0	TO-3739
M91-05***	90	90	bulk foraminifera	10190	± 70	11130	± 120	0	TO-3740
M91-19***	100	100	bulk foraminifera	10860	± 50	12140	± 160	0	TO-3741
M91-20***	120	120	bulk foraminifera	9830	± 70	10630	± 140	0	TO-3742
M91-22***	50	50	bulk foraminifera	9670	± 70	10405	± 115	0	TO-3743

Table 3. R and ΔR constraints employed for calibration of radiocarbon dates with the Marine20 curve. R values between these tie points are based on linear interpolation.

Age (cal yrBP)	R (^{14}C yr)	ΔR (^{14}C yr)	Explanation
Black Sea			
0–7400	default Marine20	–100	Average R built into the Marine20 curve over this interval is 515 ^{14}C yr, 100 yr more than Siani et al. (2000) estimate for the modern sea. Near-modern conditions began ~7400 cal yrBP.
7500	415	–188	Siani et al. (2000) modern R is imposed at 7500 cal yrBP; ΔR is the difference between this R and the default R provided by Heaton et al. (2020).
9450	200	–335	This tie point at initial marine entry falls between 7500 cal yrBP value and 11860 cal yrBP minimum needed to conform to Sofular cave data. ΔR is the difference between this R and the default R provided by Heaton et al. (2020).
11860 12610 13080 13830	50 250 700 1000	–440 –450 +50 +558	These four tie points are converted from raw radiocarbon tie points in Williams et al. (2018), used by them to shift the Yanchilina et al. (2017) δ^{13}C trend for mollusc shells to a best fit with stalagmite results from Sofular Cave. ΔR values are differences between the listed R values and default values from Heaton et al. (2020).
17300	1500	698	Consistent with Kwiecien et al. (2008).
22050	1670	800	These are required values to convert a Kwiecien et al. (2008) Y2 tephra radiocarbon date of 19760 ^{14}C yrBP to 22050 cal yrBP using the Marine20 curve. R is close to the difference between 19760 and the average Y2 radiocarbon date of 18130 ± 255 ^{14}C yrBP. ΔR is the difference between this R and the default R provided by Heaton et al. (2020).
28000	0	–765	Consistent with Soulet et al. (2011). ΔR is the difference between this R and the default R provided by Heaton et al. (2020).
Marmara Sea			
0–13500	default Marine20	–100	Average R built into Marine20 curve over this interval is 515 ^{14}C yr, 100 yr more than Siani et al. (2000) estimate for the modern sea. Near-modern conditions began ~13500 cal yrBP.
13800	1100	630	Vidal et al. (2010) place first penetration of Mediterranean water across ~ –75 m sill in Dardanelles at 13050 ± 75 ^{14}C yrBP. Lambeck et al. (2007) estimate base level in the Aegean Sea reached this elevation at ~13800 cal yrBP. ΔR listed here is required to calibrate the Vidal et al. (2010) date to 13800 cal yrBP.

22050	820	–50	These are required values to convert a MUN radiocarbon date of 18915 ± 40 ^{14}C yrBP just below the Y2 tephra in core M14-16P to 22050 cal yrBP using the Marine20 curve. R is close to the difference between 18915 and the average Y2 radiocarbon date of 18130 ± 255 14C yrBP. ΔR is the difference between this R and the default R provided by Heaton et al. (2020).
28000	0	–765	Consistent with reservoir ages in the Black Sea (Soulet et al., 2011). ΔR is the difference between this R and the default R provided by Heaton et al. (2020).

Declaration of interests

☒ The authors declare that they have no known competing financial interests or personal relationships that could have appeared to influence the work reported in this paper.

☐The authors declare the following financial interests/personal relationships which may be considered as potential competing interests:

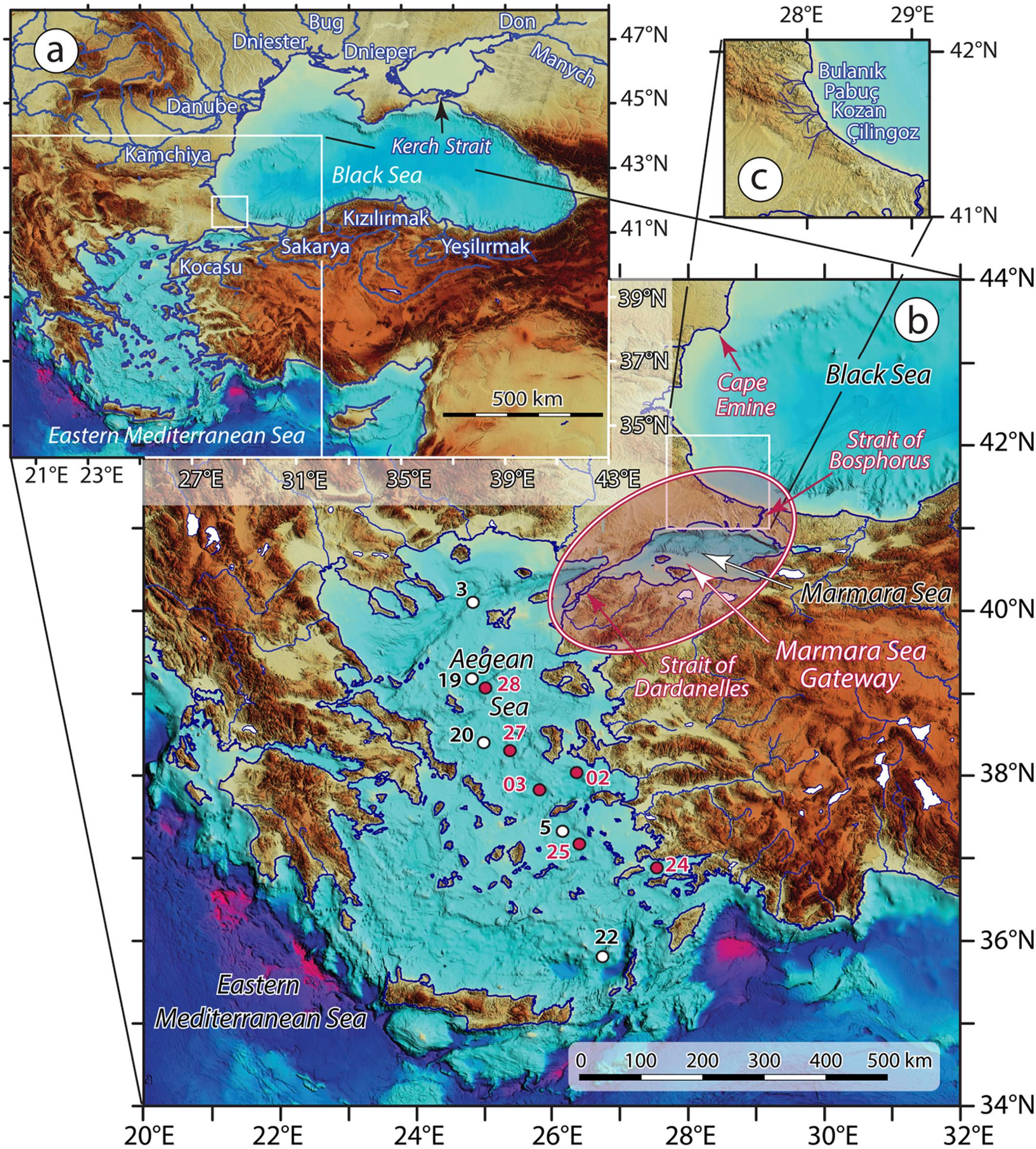

a
Bug
Don
Dniester
Dnieper
Manych
Danube
Kerch Strait
Kamchiya
Black Sea
Kızılırmak
Sakarya
Yeşilırmak
Kocasu
500 km
Eastern Mediterranean Sea
47°N
45°N
43°N
41°N
39°N
37°N
35°N
21°E
23°E
27°E
31°E
35°E
39°E
43°E
c
28°E
29°E
42°N
41°N
Bulanık
Pabuç
Kozan
Çilingoz
b
44°N
42°N
40°N
38°N
36°N
34°N
Cape Emine
Black Sea
Strait of Bosphorus
Marmara Sea
Marmara Sea Gateway
Strait of Dardanelles
Aegean Sea
3
19
28
20
27
03
02
5
25
24
22
Eastern Mediterranean Sea
0
100
200
300
400
500 km
20°E
22°E
24°E
26°E
28°E
30°E
32°E

Figure 1

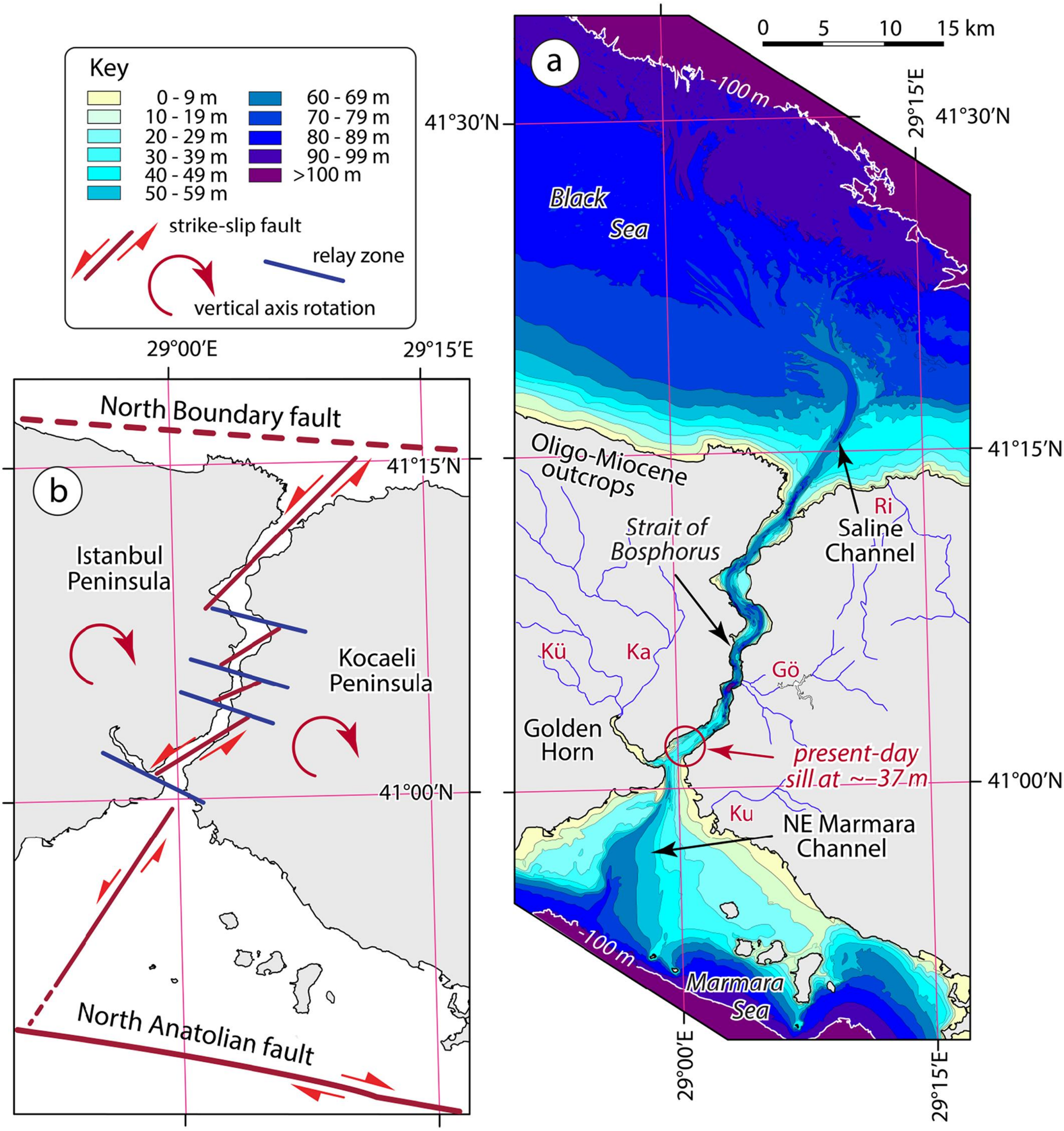

Key
0 - 9 m
10 - 19 m
20 - 29 m
30 - 39 m
40 - 49 m
50 - 59 m
60 - 69 m
70 - 79 m
80 - 89 m
90 - 99 m
>100 m
strike-slip fault
relay zone
vertical axis rotation
a
0 5 10 15 km
-100 m
41°30'N
29°15'E
41°30'N
Black Sea
Oligo-Miocene outcrops
41°15'N
Ri
Saline Channel
Strait of Bosphorus
Kü
Ka
Gö
Golden Horn
present-day sill at ~-37 m
41°00'N
Ku
NE Marmara Channel
-100 m
Marmara Sea
29°00'E
29°15'E
b
29°00'E
29°15'E
North Boundary fault
41°15'N
Istanbul Peninsula
Kocaeli Peninsula
41°00'N
North Anatolian fault

Figure 2

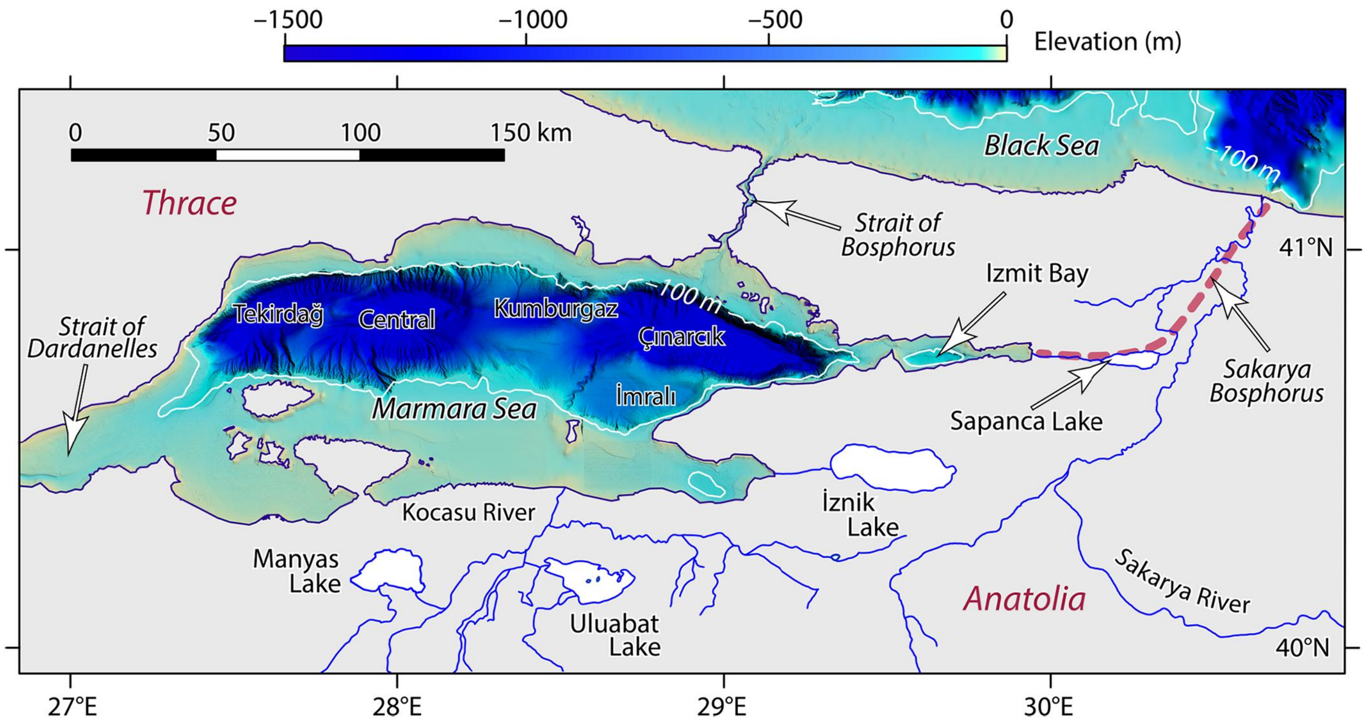
−1500
−1000
−500
0
Elevation (m)
0
50
100
150 km
Black Sea
−100 m
Thrace
Strait of Bosphorus
41°N
Izmit Bay
−100 m
Tekirdağ
Central
Kumburgaz
Çınarcık
Strait of Dardanelles
Marmara Sea
İmralı
Sapanca Lake
Sakarya Bosphorus
Kocasu River
İznik Lake
Manyas Lake
Uluabat Lake
Anatolia
Sakarya River
40°N
27°E
28°E
29°E
30°E

Figure 3

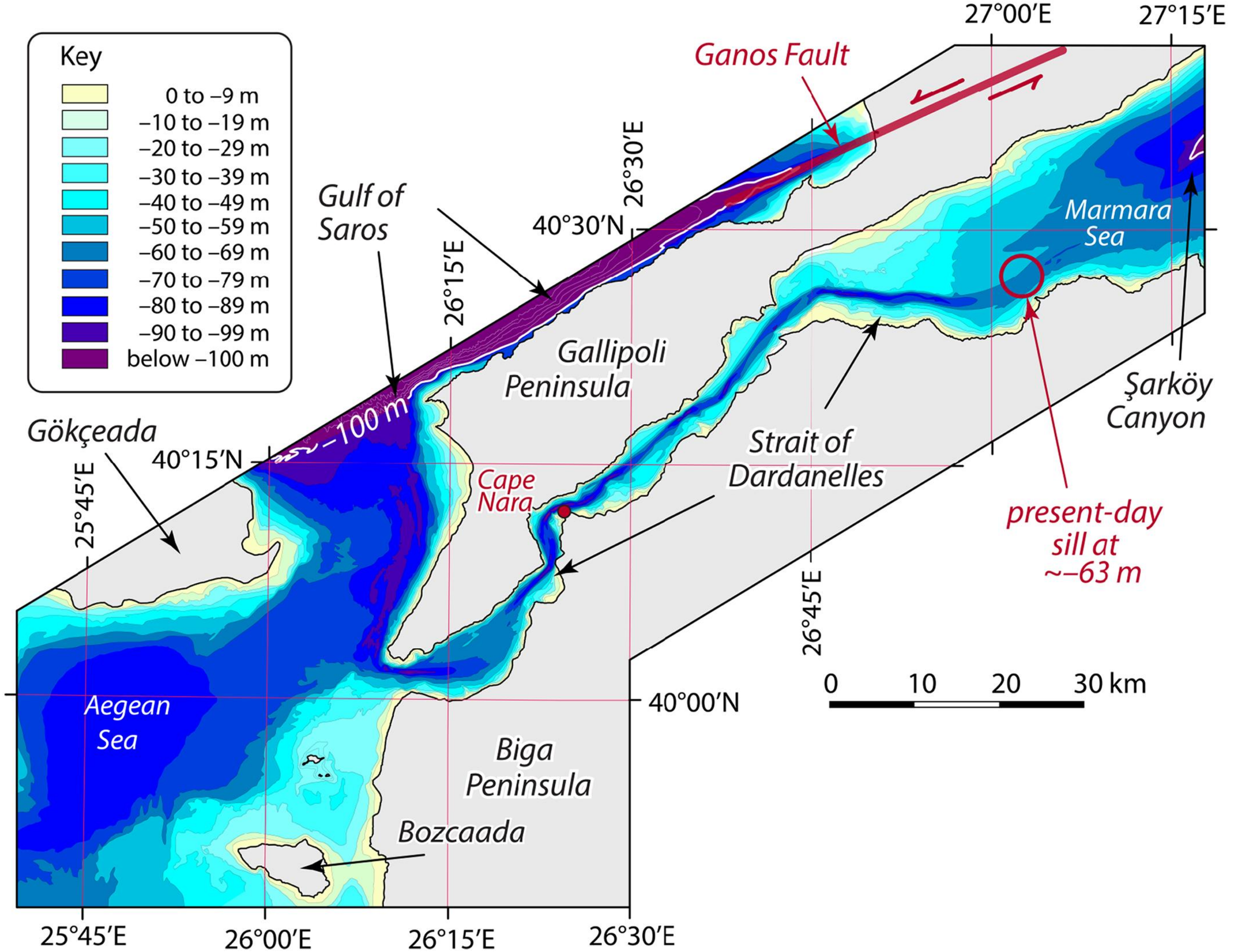
Key
0 to −9 m
−10 to −19 m
−20 to −29 m
−30 to −39 m
−40 to −49 m
−50 to −59 m
−60 to −69 m
−70 to −79 m
−80 to −89 m
−90 to −99 m
below −100 m
Ganos Fault
27°00′E
27°15′E
26°30′E
40°30′N
Gulf of Saros
26°15′E
Gallipoli Peninsula
Marmara Sea
Şarköy Canyon
Gökçeada
40°15′N
25°45′E
−100 m
Cape Nara
Strait of Dardanelles
present-day sill at ~−63 m
26°45′E
0
10
20
30 km
40°00′N
Aegean Sea
Biga Peninsula
Bozcaada
25°45′E
26°00′E
26°15′E
26°30′E

Figure 4

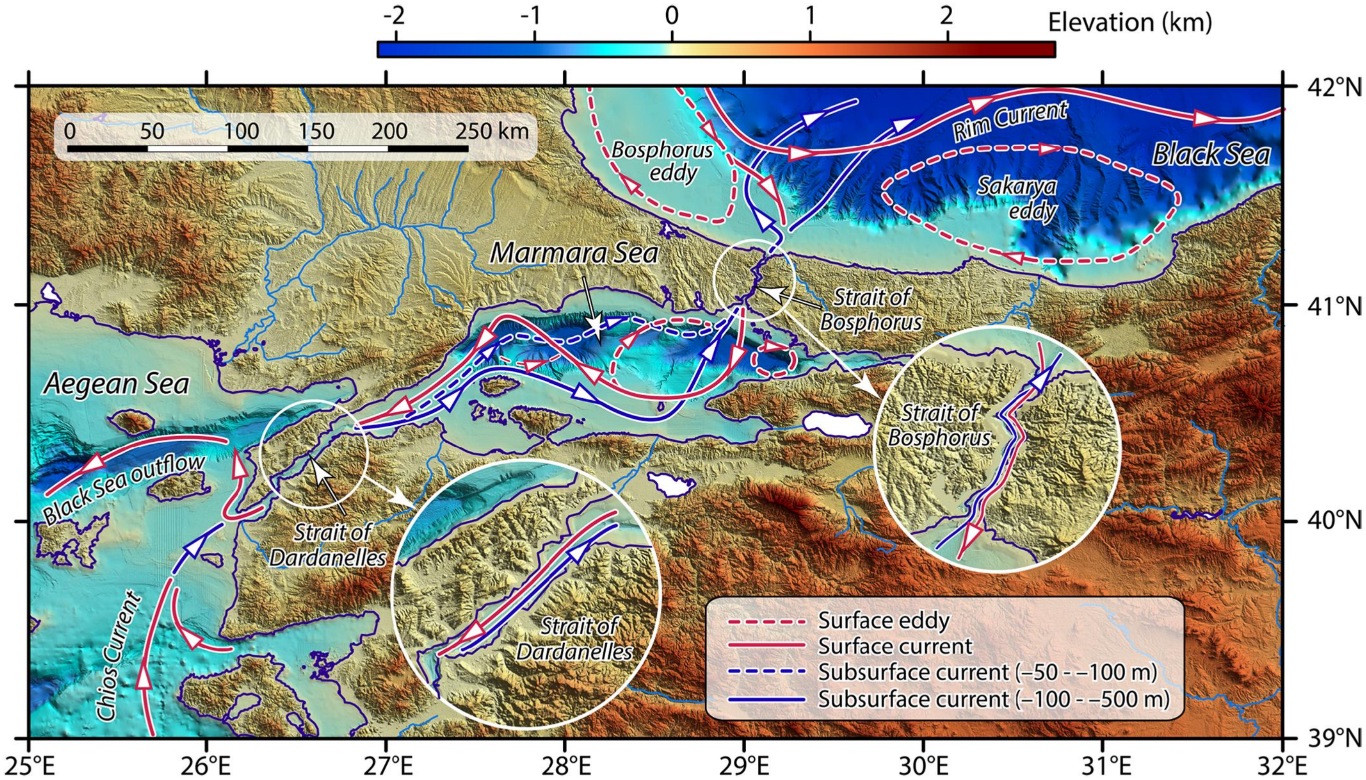
Elevation (km)
-2
-1
0
1
2
42°N
41°N
40°N
39°N
25°E
26°E
27°E
28°E
29°E
30°E
31°E
32°E
0
50
100
150
200
250 km
Black Sea
Rim Current
Sakarya eddy
Bosphorus eddy
Marmara Sea
Strait of Bosphorus
Aegean Sea
Black Sea outflow
Strait of Dardanelles
Chios Current
Strait of Bosphorus
Strait of Dardanelles
Surface eddy
Surface current
Subsurface current (–50 - –100 m)
Subsurface current (–100 - –500 m)

Figure 5

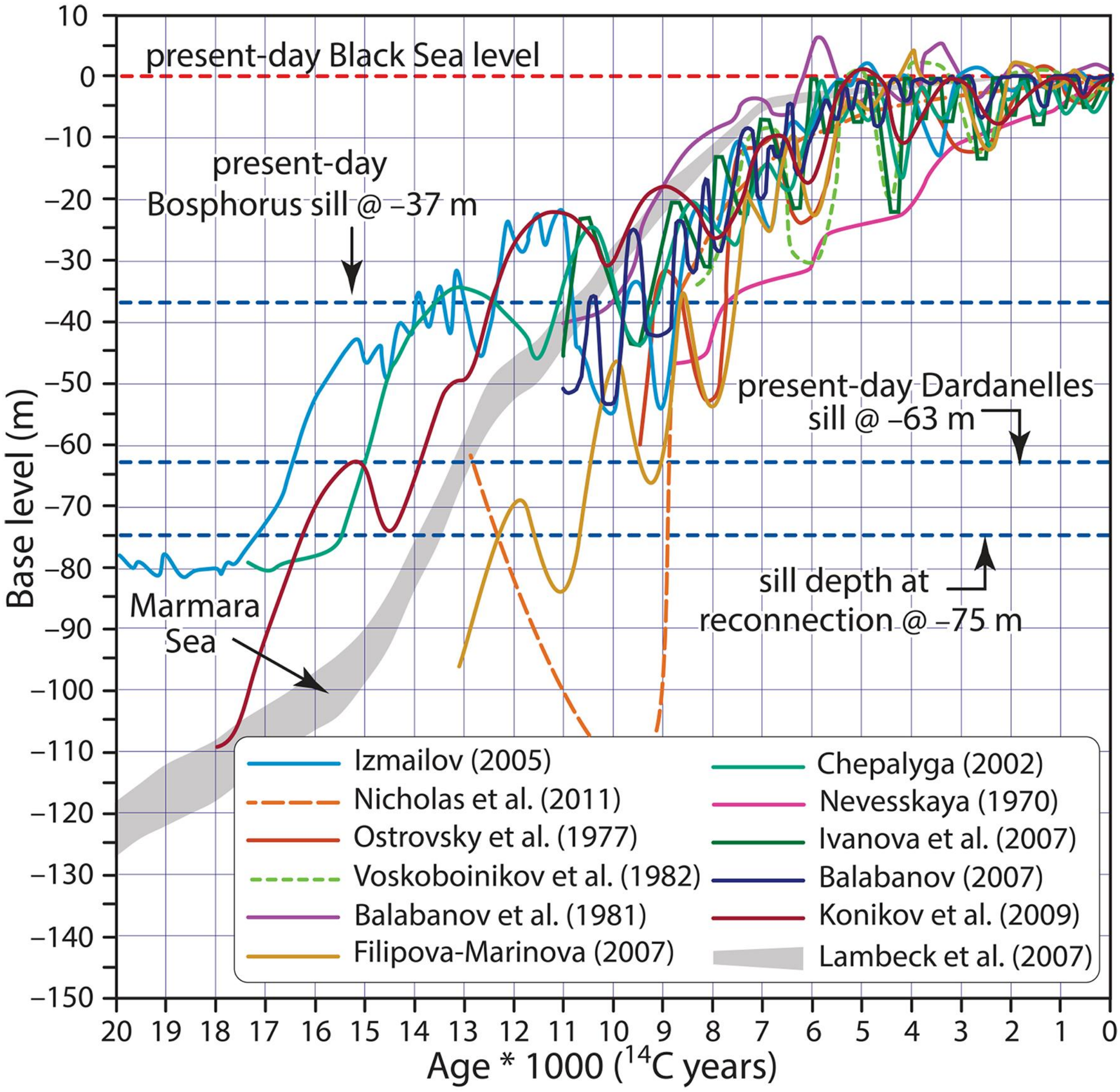

present-day Black Sea level
present-day Bosphorus sill @ –37 m
present-day Dardanelles sill @ –63 m
sill depth at reconnection @ –75 m
Marmara Sea
Base level (m)
Age * 1000 (14C years)
10
0
−10
−20
−30
−40
−50
−60
−70
−80
−90
−100
−110
−120
−130
−140
−150
20 19 18 17 16 15 14 13 12 11 10 9 8 7 6 5 4 3 2 1 0
Izmailov (2005)
Nicholas et al. (2011)
Ostrovsky et al. (1977)
Voskoboinikov et al. (1982)
Balabanov et al. (1981)
Filipova-Marinova (2007)
Chepalyga (2002)
Nevesskaya (1970)
Ivanova et al. (2007)
Balabanov (2007)
Konikov et al. (2009)
Lambeck et al. (2007)

Figure 6

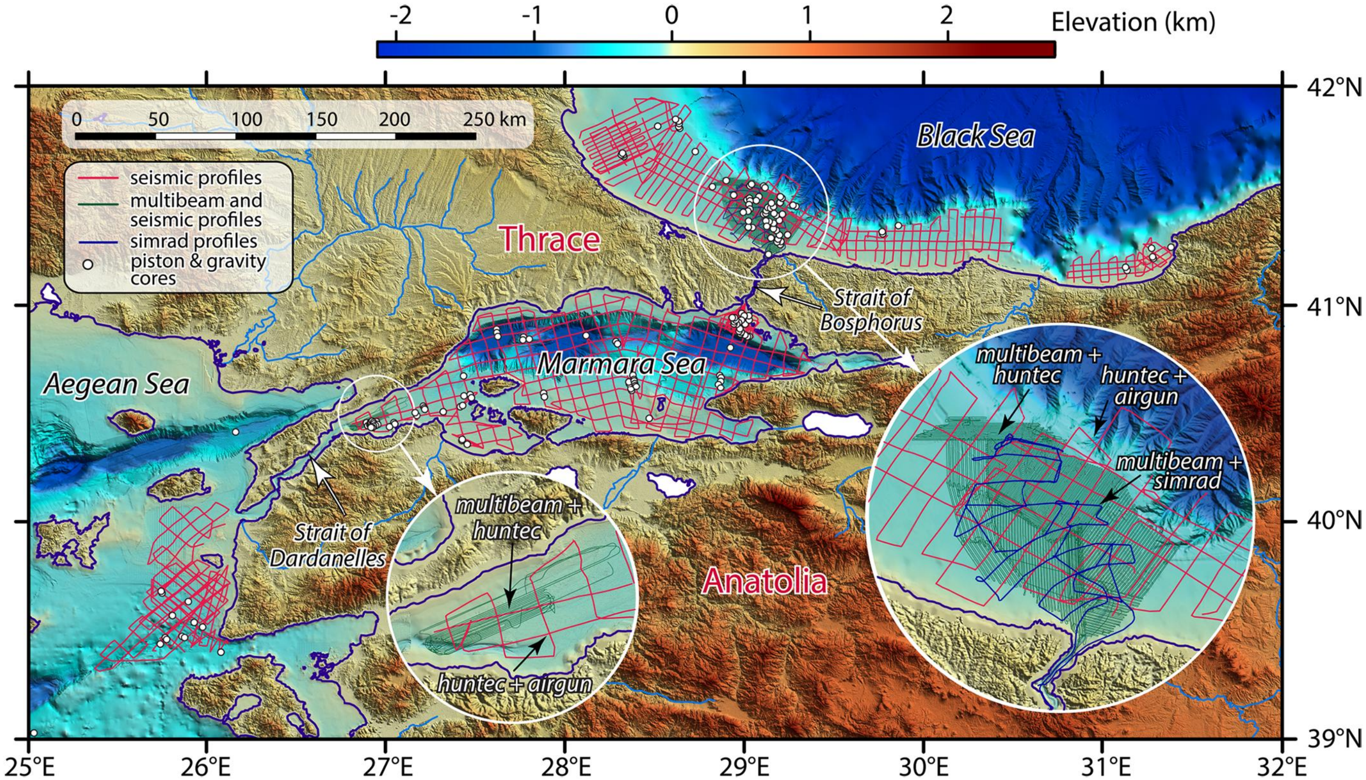
Elevation (km)
-2
-1
0
1
2
0
50
100
150
200
250 km
seismic profiles
multibeam and seismic profiles
simrad profiles
piston & gravity cores
Black Sea
Thrace
Strait of Bosphorus
Marmara Sea
Aegean Sea
Strait of Dardanelles
Anatolia
multibeam + huntec
huntec + airgun
multibeam + simrad
multibeam + huntec
huntec + airgun
42°N
41°N
40°N
39°N
25°E
26°E
27°E
28°E
29°E
30°E
31°E
32°E

Figure 7

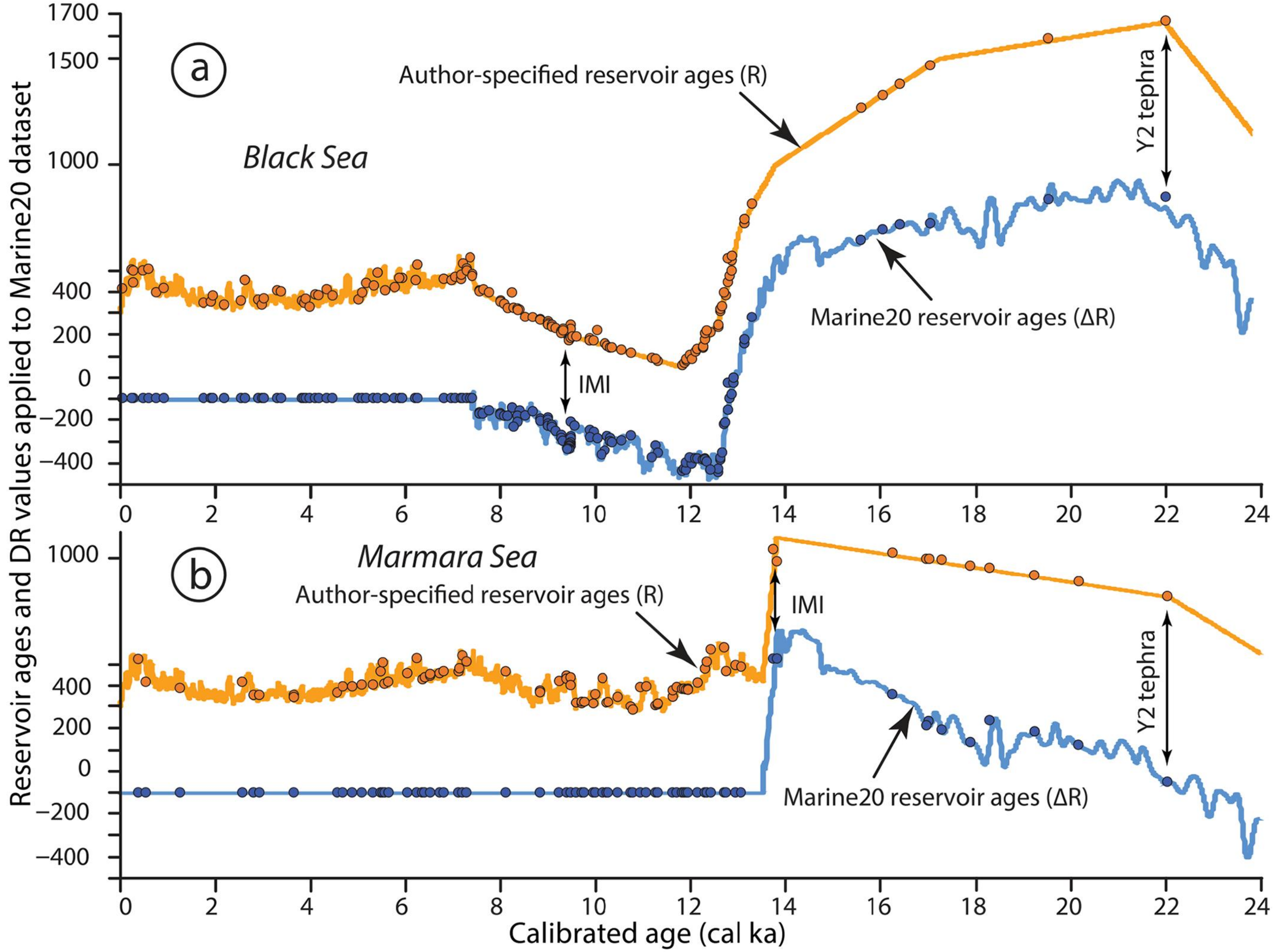
a
Black Sea
Author-specified reservoir ages (R)
Marine20 reservoir ages (ΔR)
IMI
Y2 tephra
b
Marmara Sea
Author-specified reservoir ages (R)
Marine20 reservoir ages (ΔR)
IMI
Y2 tephra
Reservoir ages and DR values applied to Marine20 dataset
Calibrated age (cal ka)
1700
1500
1000
400
200
0
−200
−400
0
2
4
6
8
10
12
14
16
18
20
22
24

Figure 8

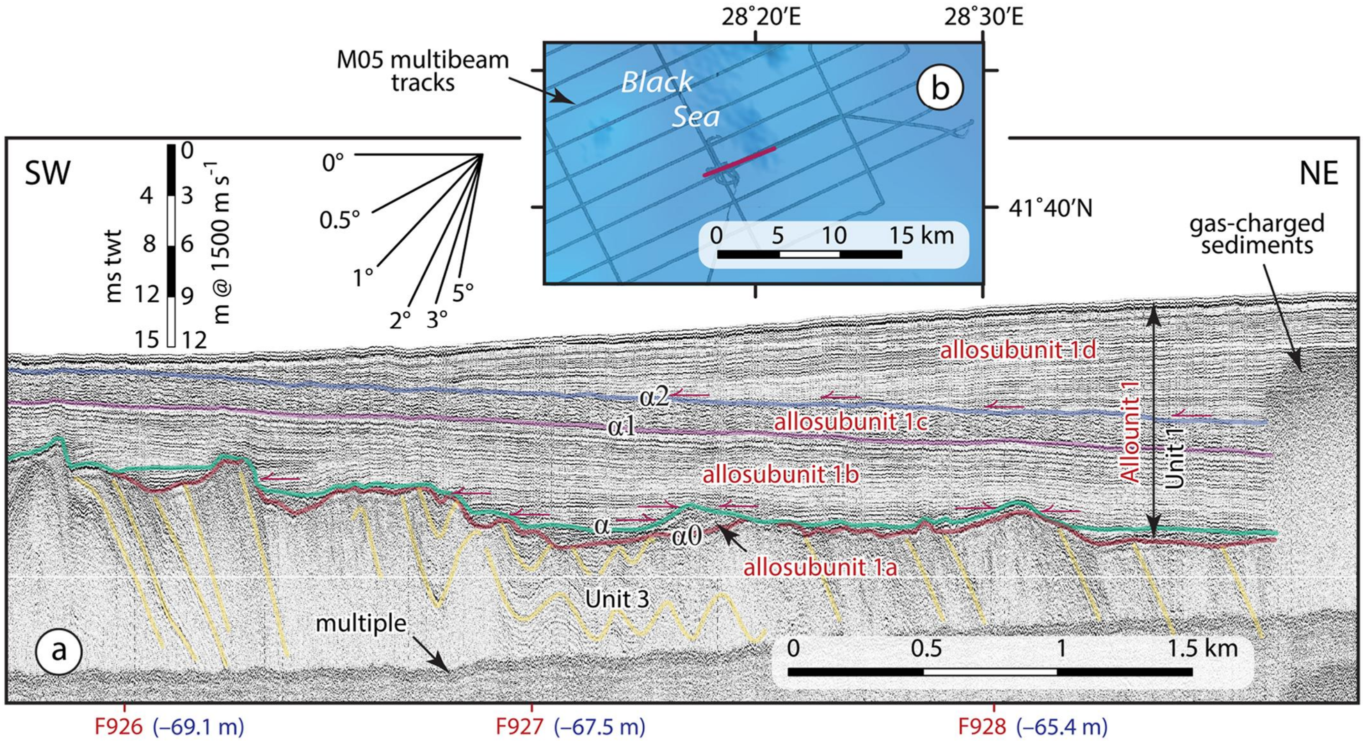
28°20′E
28°30′E
M05 multibeam tracks
Black Sea
b
41°40′N
0 5 10 15 km
SW
NE
ms twt
m @ 1500 m s-1
0 4 8 12 15
0 3 6 9 12
0° 0.5° 1° 2° 3° 5°
gas-charged sediments
allosubunit 1d
allosubunit 1c
allosubunit 1b
allosubunit 1a
α2
α1
α
α0
Allounit 1
Unit 1
Unit 3
multiple
a
0 0.5 1 1.5 km
F926 (–69.1 m)
F927 (–67.5 m)
F928 (–65.4 m)

Figure 9

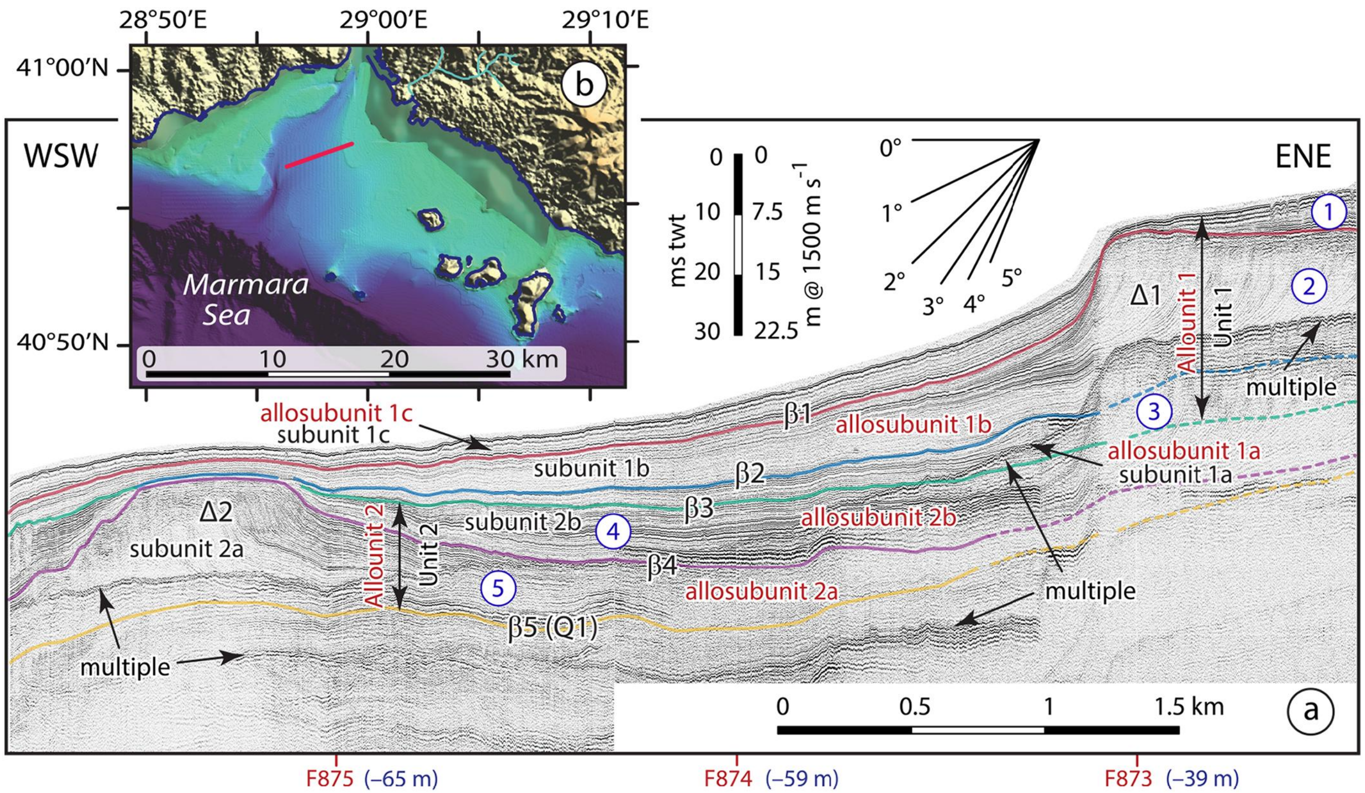

28°50′E
29°00′E
29°10′E
41°00′N
40°50′N
Marmara Sea
0 10 20 30 km
b
WSW
ENE
ms twt
m @ 1500 m s-1
0 10 20 30
0 7.5 15 22.5
0° 1° 2° 3° 4° 5°
allosubunit 1c
subunit 1c
subunit 1b
β1
allosubunit 1b
β2
β3
Δ1
Allounit 1
Unit 1
multiple
allosubunit 1a
subunit 1a
Δ2
subunit 2a
subunit 2b
allosubunit 2b
Allounit 2
Unit 2
β4
allosubunit 2a
β5 (Q1)
multiple
multiple
1
2
3
4
5
0 0.5 1 1.5 km
a
F875 (–65 m)
F874 (–59 m)
F873 (–39 m)

Figure 10

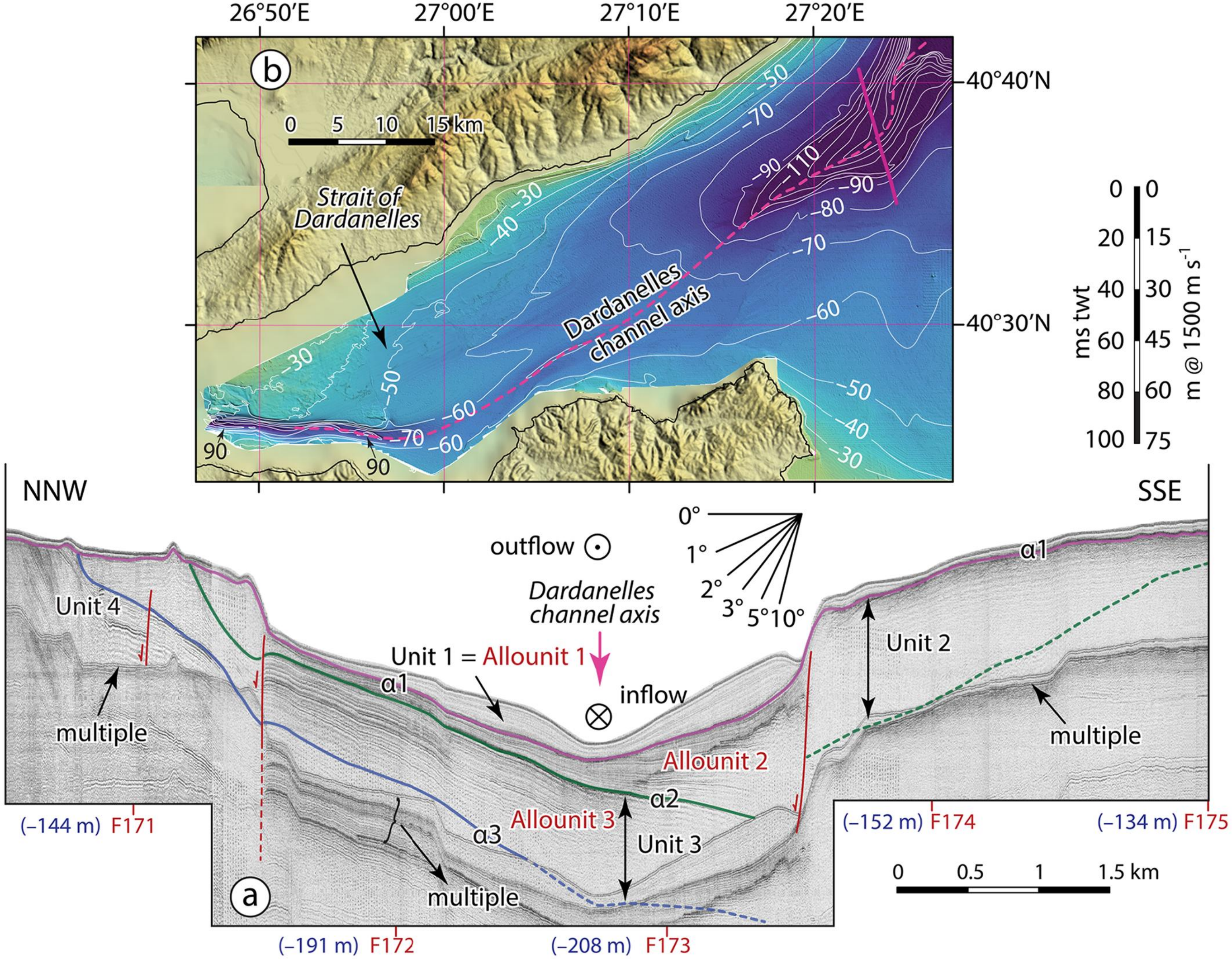
26°50'E
27°00'E
27°10'E
27°20'E
40°40'N
40°30'N
b
0 5 10 15 km
Strait of Dardanelles
Dardanelles channel axis
–30
–40
–50
–60
–70
–80
–90
–110
90
ms twt
m @ 1500 m s-1
0 20 40 60 80 100
0 15 30 45 60 75
NNW
SSE
outflow
Dardanelles channel axis
inflow
0° 1° 2° 3° 5° 10°
Unit 1 = Allounit 1
Allounit 2
Allounit 3
Unit 2
Unit 3
Unit 4
α1
α2
α3
multiple
(–144 m) F171
(–191 m) F172
(–208 m) F173
(–152 m) F174
(–134 m) F175
0 0.5 1 1.5 km
a

Figure 11

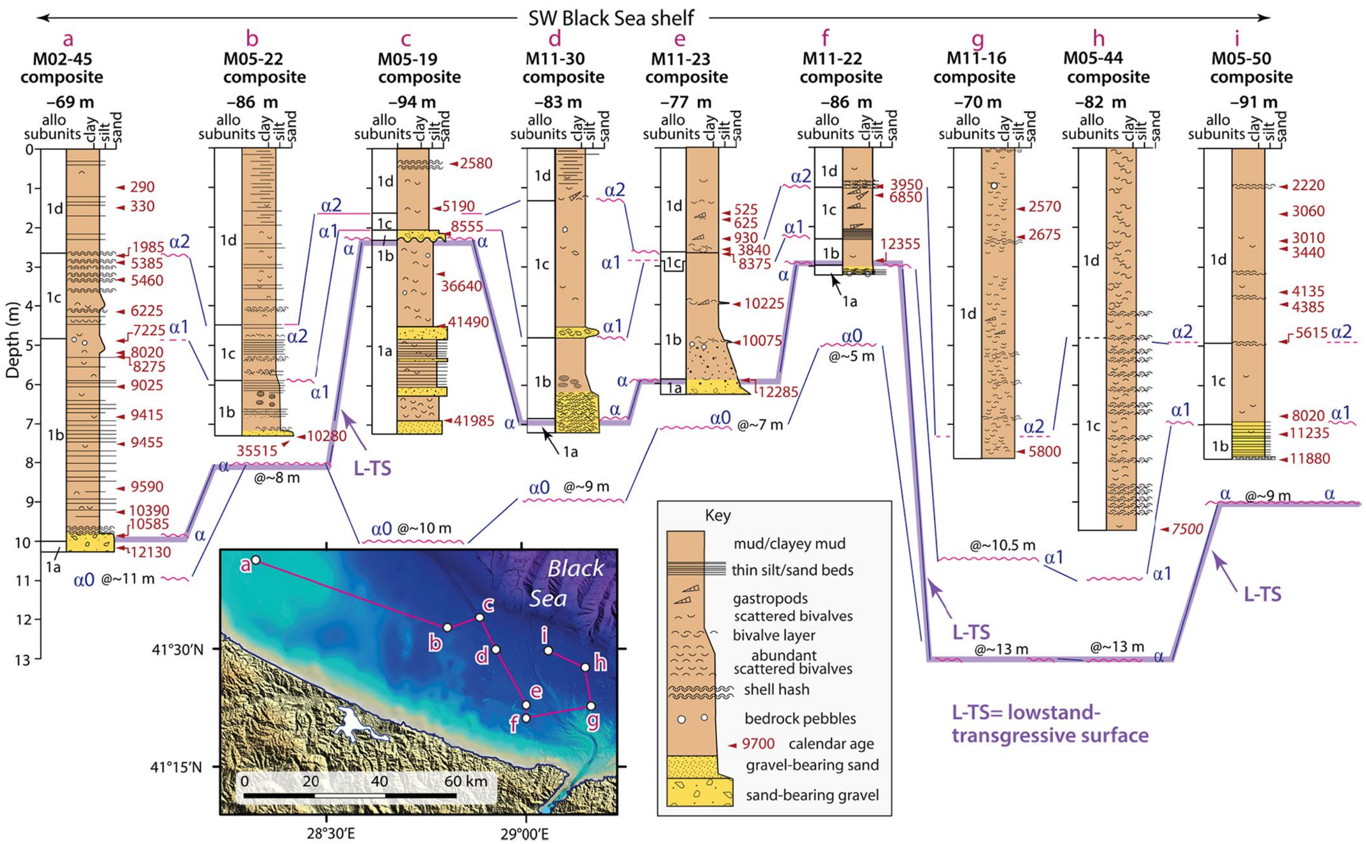

SW Black Sea shelf
a M02-45 composite −69 m
b M05-22 composite −86 m
c M05-19 composite −94 m
d M11-30 composite −83 m
e M11-23 composite −77 m
f M11-22 composite −86 m
g M11-16 composite −70 m
h M05-44 composite −82 m
i M05-50 composite −91 m
allo subunits
clay
silt
sand
Depth (m)
L-TS
@~11 m
@~8 m
@~10 m
@~9 m
@~7 m
@~5 m
@~10.5 m
@~13 m
L-TS= lowstand-transgressive surface
Black Sea
41°30'N
41°15'N
28°30'E
29°00'E
0 20 40 60 km
Key
mud/clayey mud
thin silt/sand beds
gastropods
scattered bivalves
bivalve layer
abundant scattered bivalves
shell hash
bedrock pebbles
9700 calendar age
gravel-bearing sand
sand-bearing gravel

Figure 12

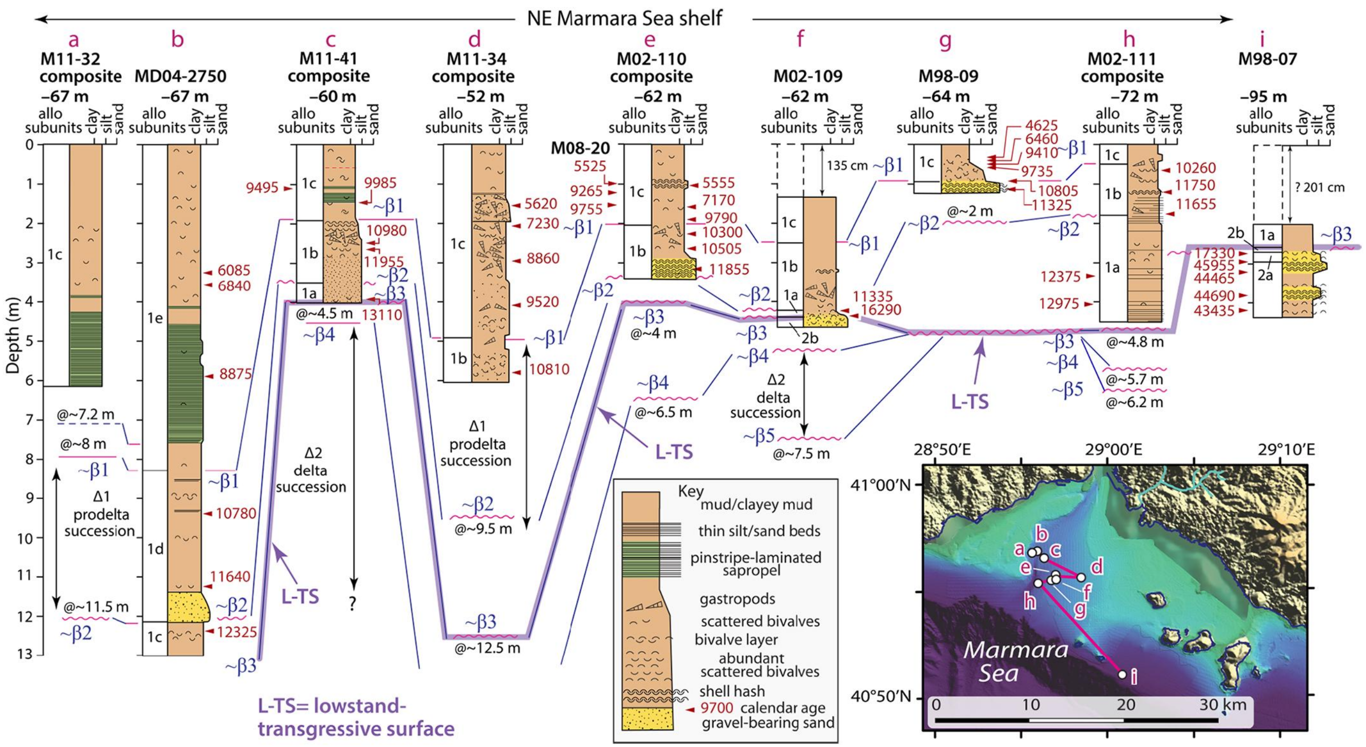

NE Marmara Sea shelf
a M11-32 composite −67 m
b MD04-2750 −67 m
c M11-41 composite −60 m
d M11-34 composite −52 m
e M02-110 composite −62 m
f M02-109 −62 m
g M98-09 −64 m
h M02-111 composite −72 m
i M98-07 −95 m
allo subunits
clay silt sand
Depth (m)
M08-20
Δ1 prodelta succession
Δ2 delta succession
L-TS
L-TS= lowstand-transgressive surface
Key
mud/clayey mud
thin silt/sand beds
pinstripe-laminated sapropel
gastropods
scattered bivalves
bivalve layer
abundant scattered bivalves
shell hash
9700 calendar age
gravel-bearing sand
28°50'E
29°00'E
29°10'E
41°00'N
40°50'N
Marmara Sea
0 10 20 30 km

Figure 13

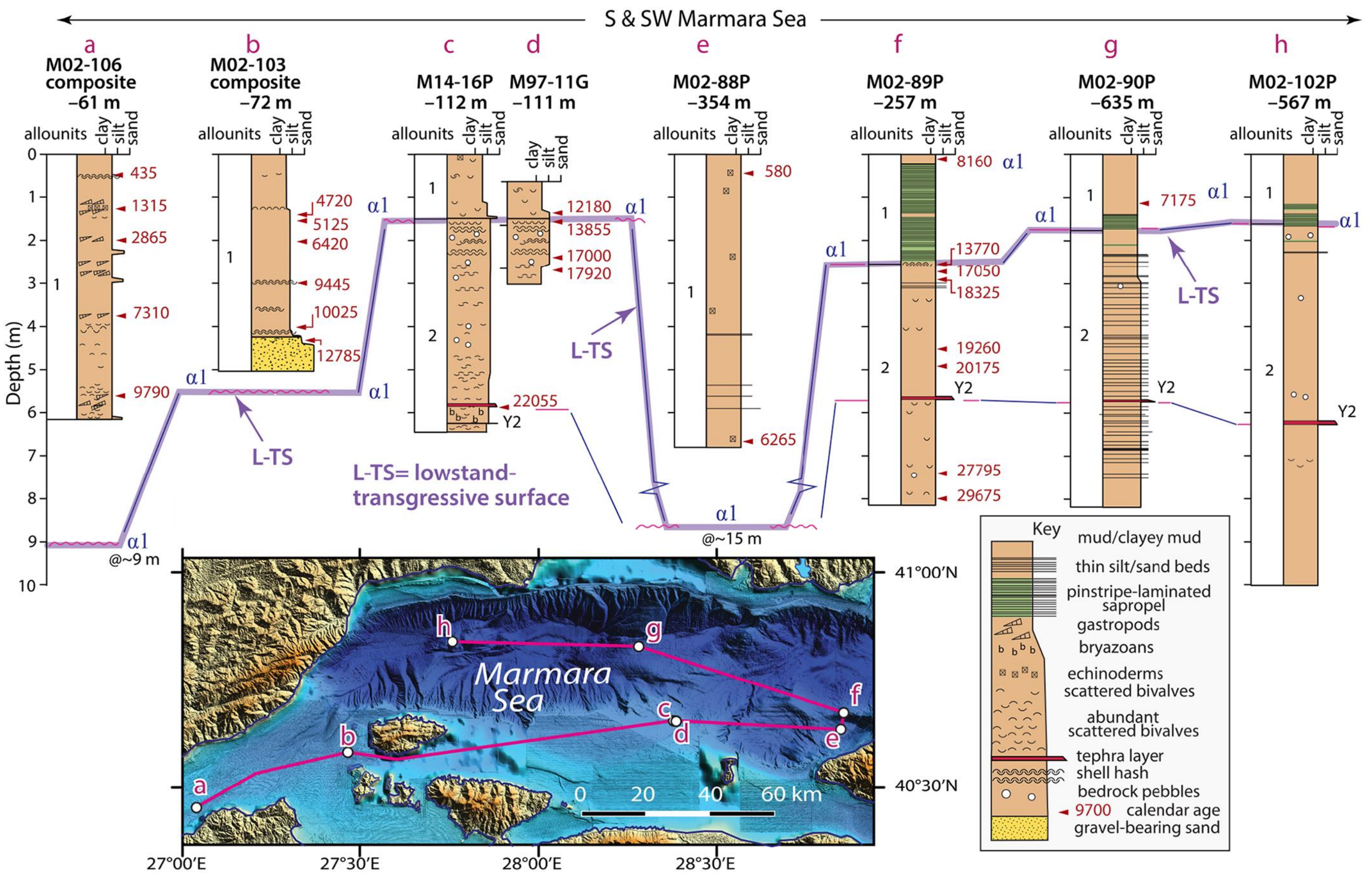
S & SW Marmara Sea
a M02-106 composite −61 m
b M02-103 composite −72 m
c M14-16P −112 m
d M97-11G −111 m
e M02-88P −354 m
f M02-89P −257 m
g M02-90P −635 m
h M02-102P −567 m
allounits
clay silt sand
Depth (m)
L-TS
L-TS= lowstand-transgressive surface
α1
@~9 m
@~15 m
Y2
Marmara Sea
0 20 40 60 km
41°00′N
40°30′N
27°00′E
27°30′E
28°00′E
28°30′E
Key
mud/clayey mud
thin silt/sand beds
pinstripe-laminated sapropel
gastropods
bryazoans
echinoderms
scattered bivalves
abundant scattered bivalves
tephra layer
shell hash
bedrock pebbles
9700 calendar age
gravel-bearing sand

Figure 14

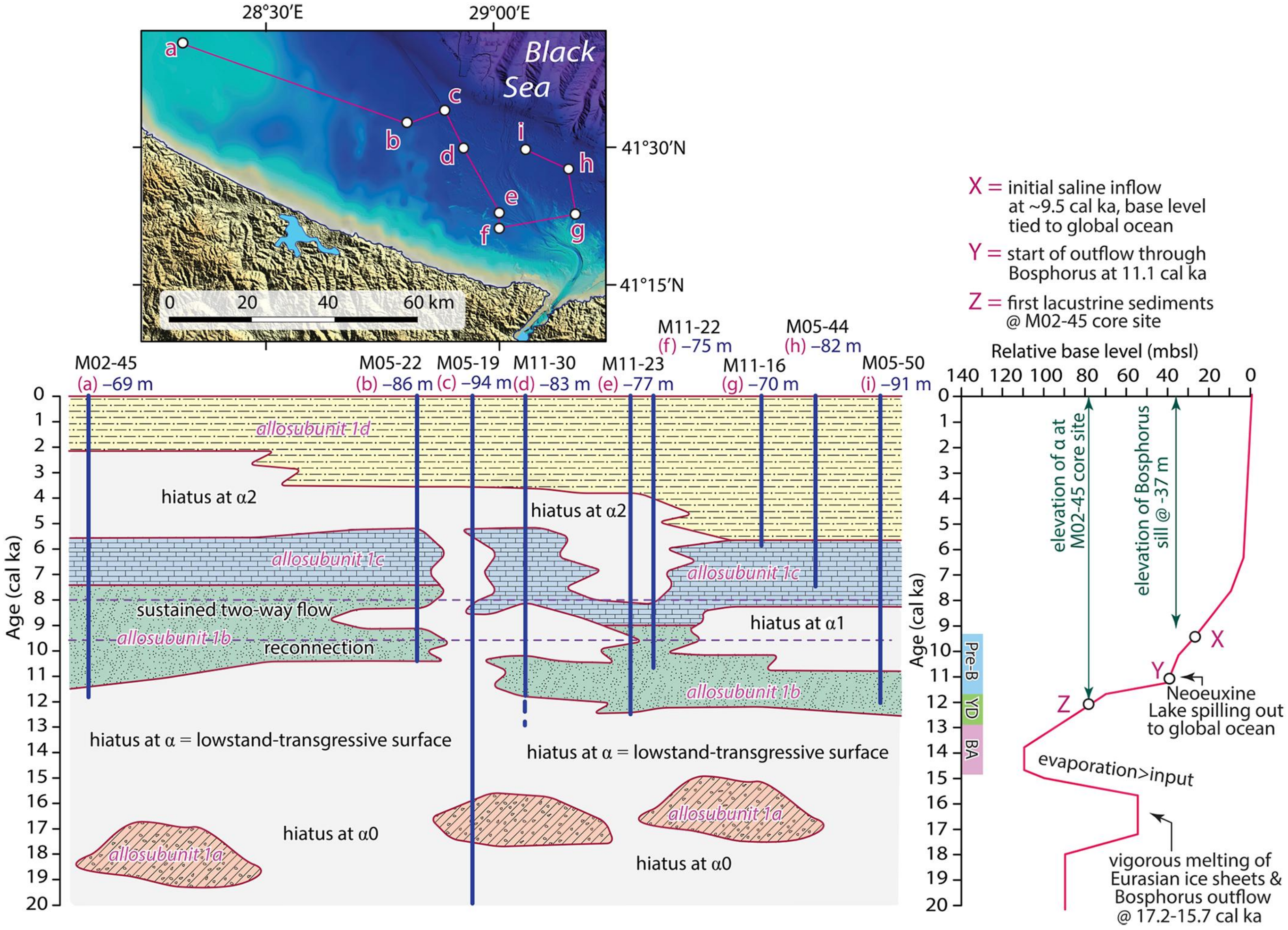

28°30′E
29°00′E
Black Sea
41°30′N
41°15′N
0 20 40 60 km
a b c d e f g h i
M02-45 (a) −69 m
M05-22 (b) −86 m
M05-19 (c) −94 m
M11-30 (d) −83 m
M11-23 (e) −77 m
M11-22 (f) −75 m
M11-16 (g) −70 m
M05-44 (h) −82 m
M05-50 (i) −91 m
Age (cal ka)
allosubunit 1d
hiatus at α2
allosubunit 1c
sustained two-way flow
allosubunit 1b
reconnection
hiatus at α1
hiatus at α = lowstand-transgressive surface
allosubunit 1a
hiatus at α0
X = initial saline inflow at ~9.5 cal ka, base level tied to global ocean
Y = start of outflow through Bosphorus at 11.1 cal ka
Z = first lacustrine sediments @ M02-45 core site
Relative base level (mbsl)
elevation of α at M02-45 core site
elevation of Bosphorus sill @ -37 m
Pre-B
YD
BA
Neoeuxine Lake spilling out to global ocean
evaporation>input
vigorous melting of Eurasian ice sheets & Bosphorus outflow @ 17.2-15.7 cal ka

Figure 15

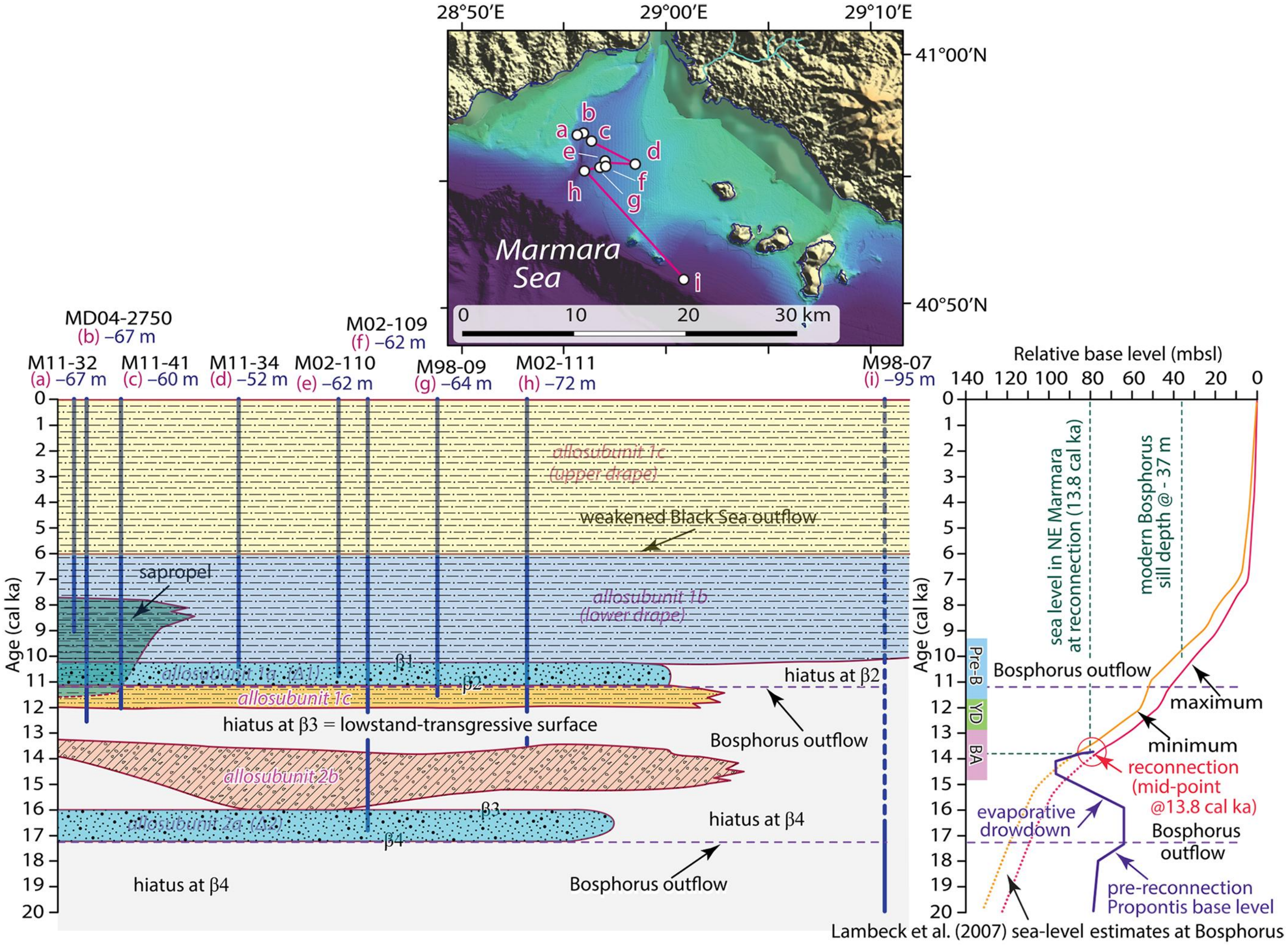

28°50'E
29°00'E
29°10'E
41°00'N
40°50'N
Marmara Sea
0 10 20 30 km
MD04-2750 (b) −67 m
M02-109 (f) −62 m
M11-32 (a) −67 m
M11-41 (c) −60 m
M11-34 (d) −52 m
M02-110 (e) −62 m
M98-09 (g) −64 m
M02-111 (h) −72 m
M98-07 (i) −95 m
Age (cal ka)
allosubunit 1c (upper drape)
weakened Black Sea outflow
sapropel
allosubunit 1b (lower drape)
hiatus at β2
allosubunit 1c
hiatus at β3 = lowstand-transgressive surface
Bosphorus outflow
allosubunit 2b
hiatus at β4
hiatus at β4
Bosphorus outflow
β1
β2
β3
β4
Relative base level (mbsl)
sea level in NE Marmara at reconnection (13.8 cal ka)
modern Bosphorus sill depth @ - 37 m
Pre-B
YD
BA
Bosphorus outflow
maximum
minimum
reconnection (mid-point @13.8 cal ka)
evaporative drowdown
Bosphorus outflow
pre-reconnection Propontis base level
Lambeck et al. (2007) sea-level estimates at Bosphorus

Figure 16

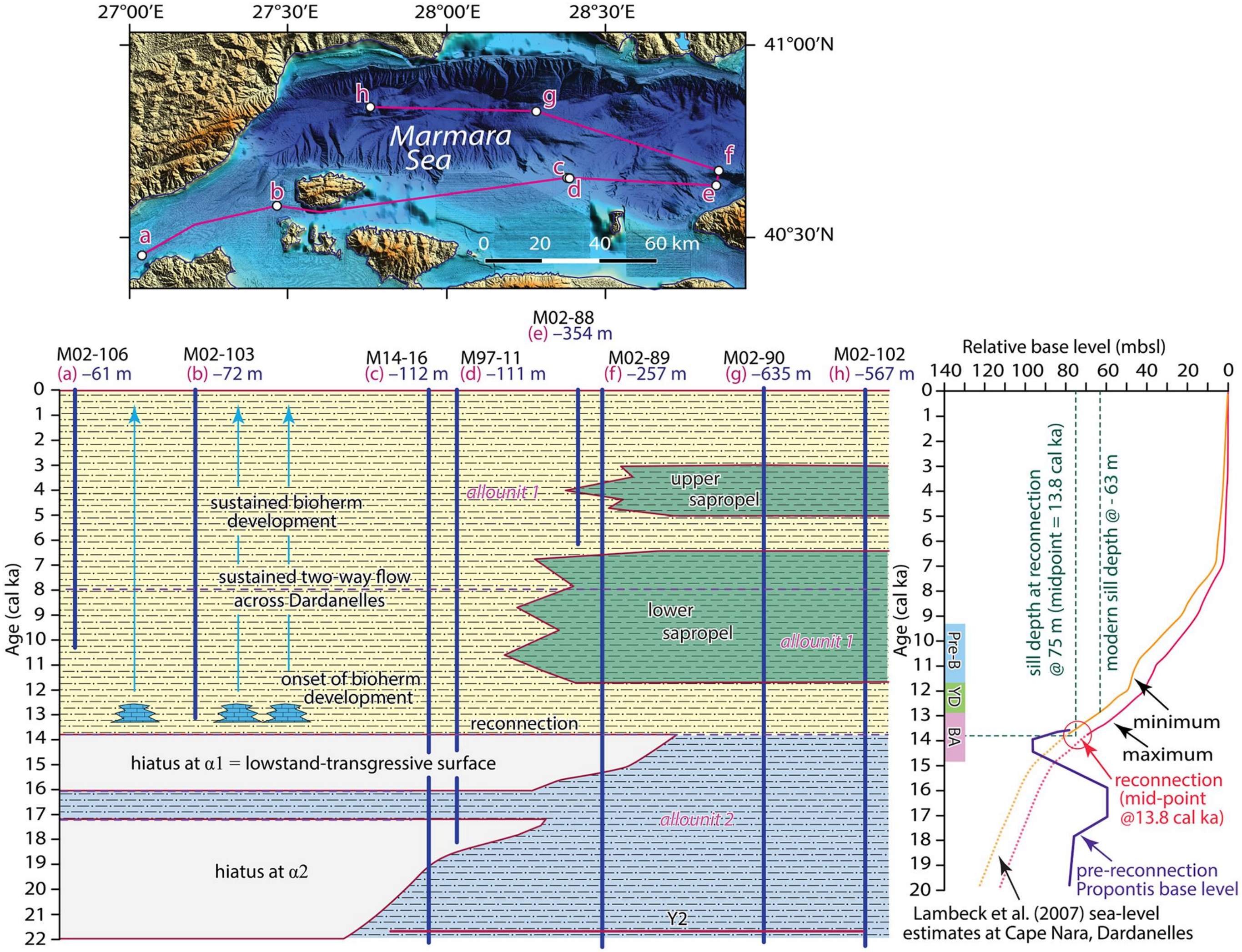
27°00′E
27°30′E
28°00′E
28°30′E
41°00′N
40°30′N
Marmara Sea
0 20 40 60 km
M02-106 (a) −61 m
M02-103 (b) −72 m
M14-16 (c) −112 m
M97-11 (d) −111 m
M02-88 (e) −354 m
M02-89 (f) −257 m
M02-90 (g) −635 m
M02-102 (h) −567 m
Age (cal ka)
sustained bioherm development
sustained two-way flow across Dardanelles
onset of bioherm development
reconnection
allounit 1
upper sapropel
lower sapropel
hiatus at α1 = lowstand-transgressive surface
allounit 2
hiatus at α2
Y2
Relative base level (mbsl)
sill depth at reconnection @ 75 m (midpoint = 13.8 cal ka)
modern sill depth @ - 63 m
Pre-B
YD
BA
minimum
maximum
reconnection (mid-point @13.8 cal ka)
pre-reconnection Propontis base level
Lambeck et al. (2007) sea-level estimates at Cape Nara, Dardanelles

Figure 17

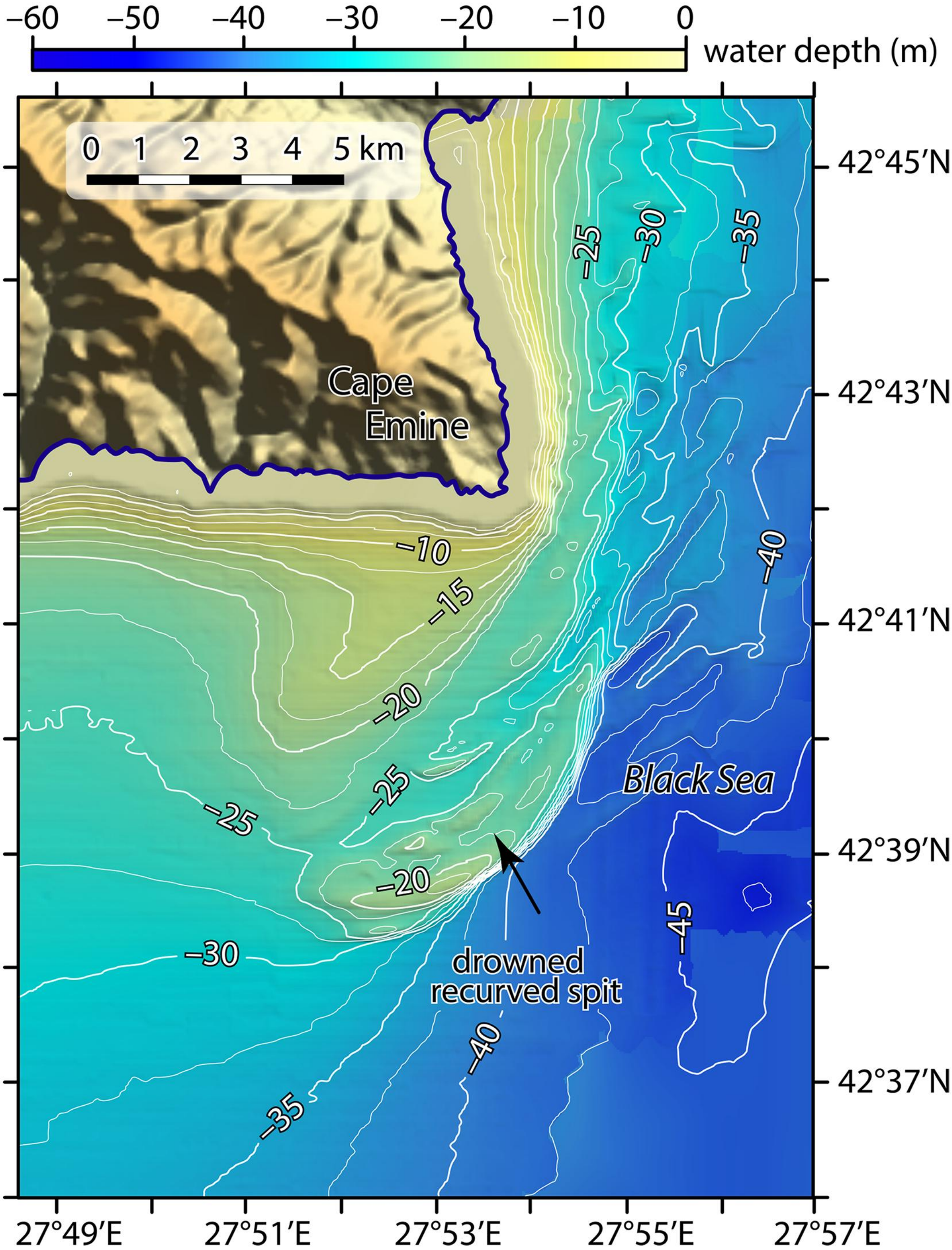
−60 −50 −40 −30 −20 −10 0
water depth (m)
0 1 2 3 4 5 km
Cape Emine
Black Sea
drowned recurved spit
−10
−15
−20
−25
−30
−35
−40
−45
42°45′N
42°43′N
42°41′N
42°39′N
42°37′N
27°49′E
27°51′E
27°53′E
27°55′E
27°57′E

Figure 18

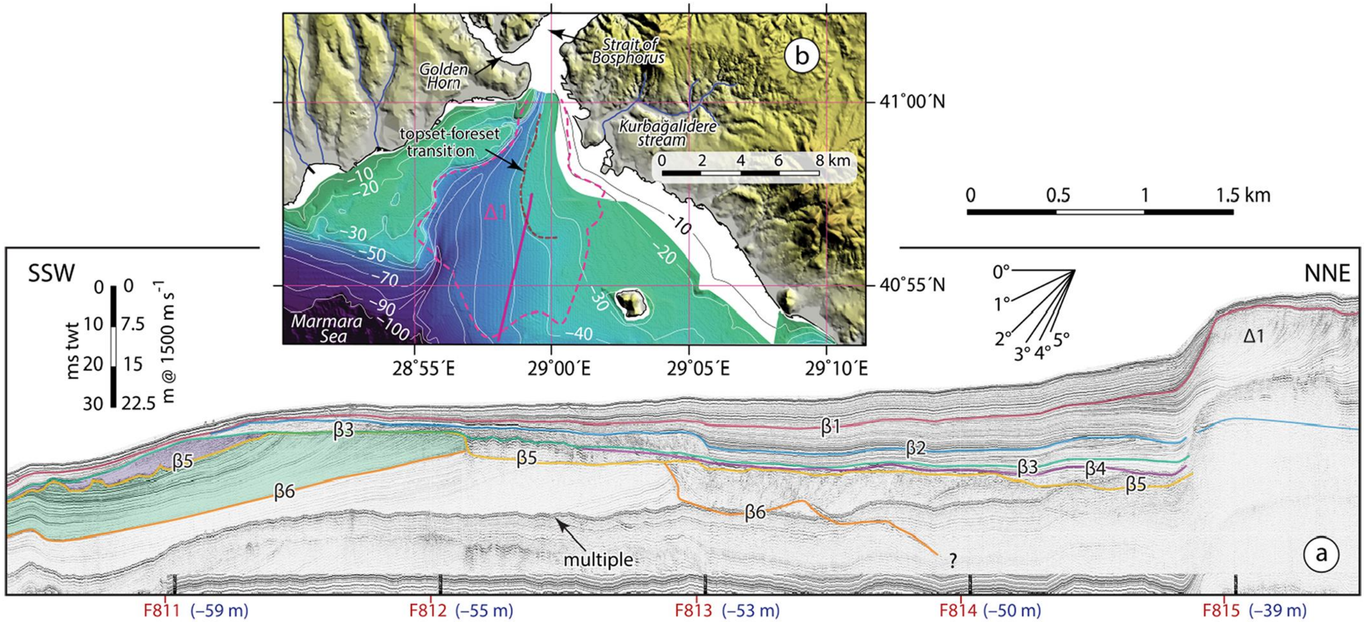
b
Golden Horn
Strait of Bosphorus
Kurbağalidere stream
topset-foreset transition
Δ1
Marmara Sea
0 2 4 6 8 km
−10
−20
−30
−40
−50
−70
−90
−100
41°00´N
40°55´N
28°55´E
29°00´E
29°05´E
29°10´E
0 0.5 1 1.5 km
SSW
NNE
ms twt
m @ 1500 m s−1
0 10 20 30
0 7.5 15 22.5
0° 1° 2° 3° 4° 5°
Δ1
β1
β2
β3
β4
β5
β6
multiple
?
a
F811 (−59 m)
F812 (−55 m)
F813 (−53 m)
F814 (−50 m)
F815 (−39 m)

Figure 19

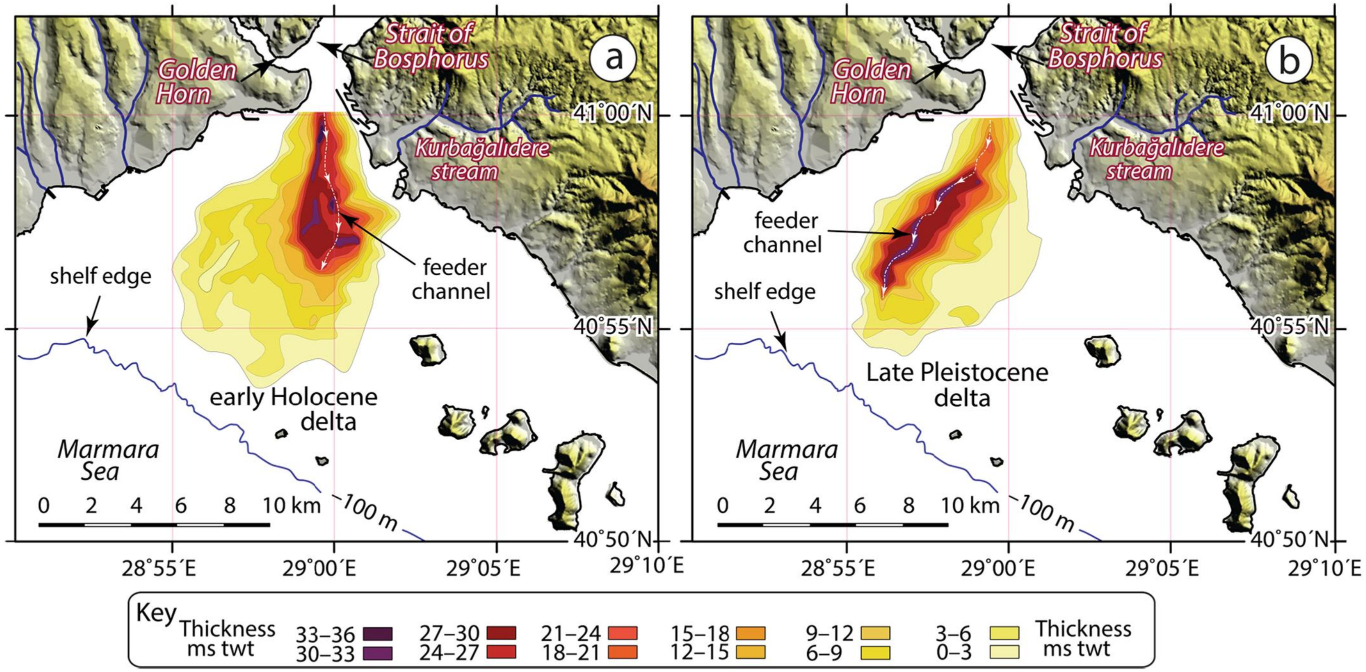

a
b
Golden Horn
Strait of Bosphorus
Kurbağalıdere stream
41°00´N
40°55´N
40°50´N
feeder channel
shelf edge
early Holocene delta
Late Pleistocene delta
Marmara Sea
0 2 4 6 8 10 km
100 m
28°55´E
29°00´E
29°05´E
29°10´E
Key
Thickness ms twt
33–36
30–33
27–30
24–27
21–24
18–21
15–18
12–15
9–12
6–9
3–6
0–3

Figure 20

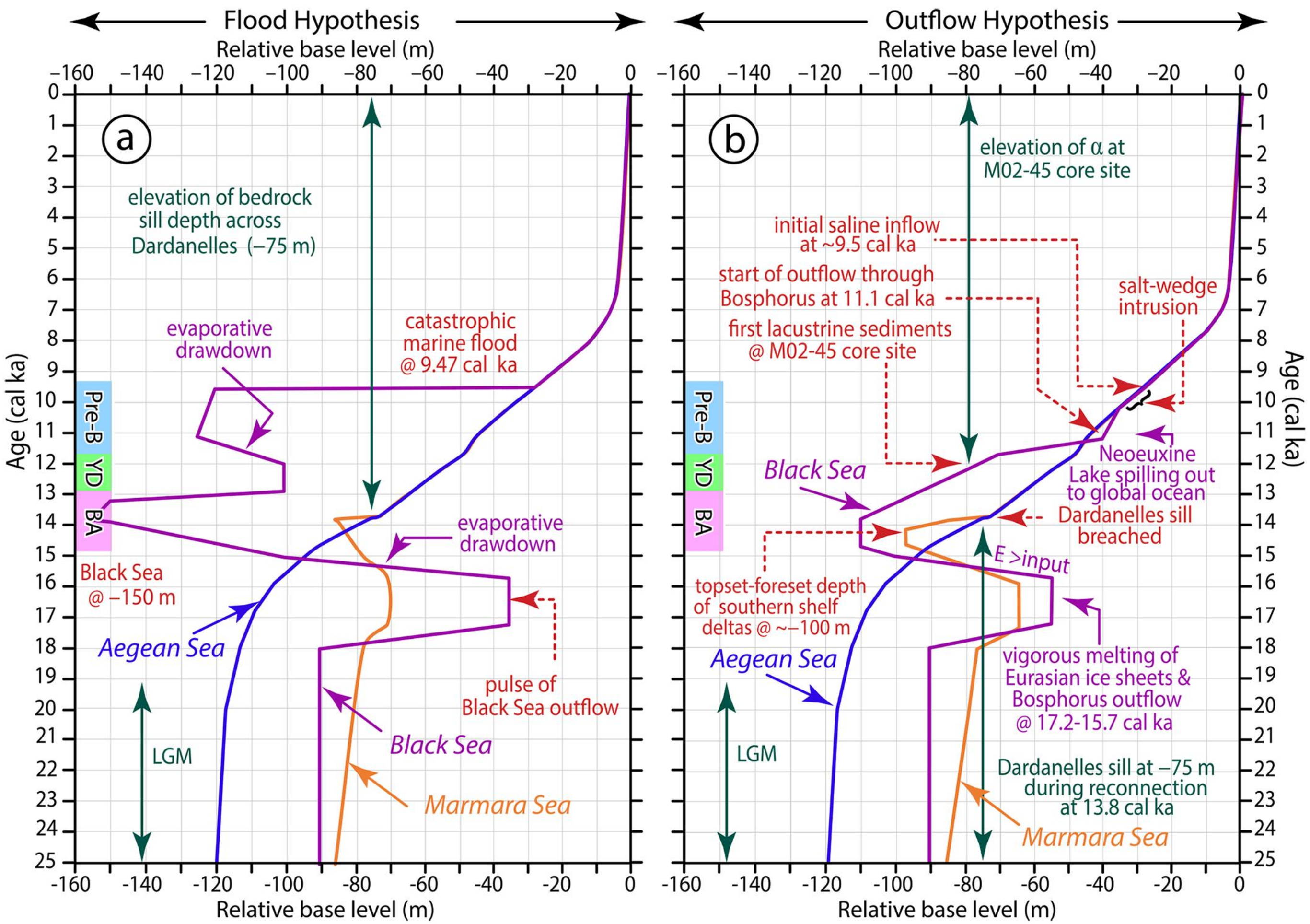

Flood Hypothesis
Outflow Hypothesis
Relative base level (m)
Age (cal ka)
a
b
elevation of bedrock sill depth across Dardanelles (−75 m)
evaporative drawdown
catastrophic marine flood @ 9.47 cal ka
evaporative drawdown
Pre-B
YD
BA
Black Sea @ −150 m
Aegean Sea
pulse of Black Sea outflow
LGM
Black Sea
Marmara Sea
elevation of α at M02-45 core site
initial saline inflow at ~9.5 cal ka
start of outflow through Bosphorus at 11.1 cal ka
salt-wedge intrusion
first lacustrine sediments @ M02-45 core site
Neoeuxine Lake spilling out to global ocean
Dardanelles sill breached
E >input
topset-foreset depth of southern shelf deltas @ ~−100 m
vigorous melting of Eurasian ice sheets & Bosphorus outflow @ 17.2-15.7 cal ka
Dardanelles sill at −75 m during reconnection at 13.8 cal ka

Figure 21

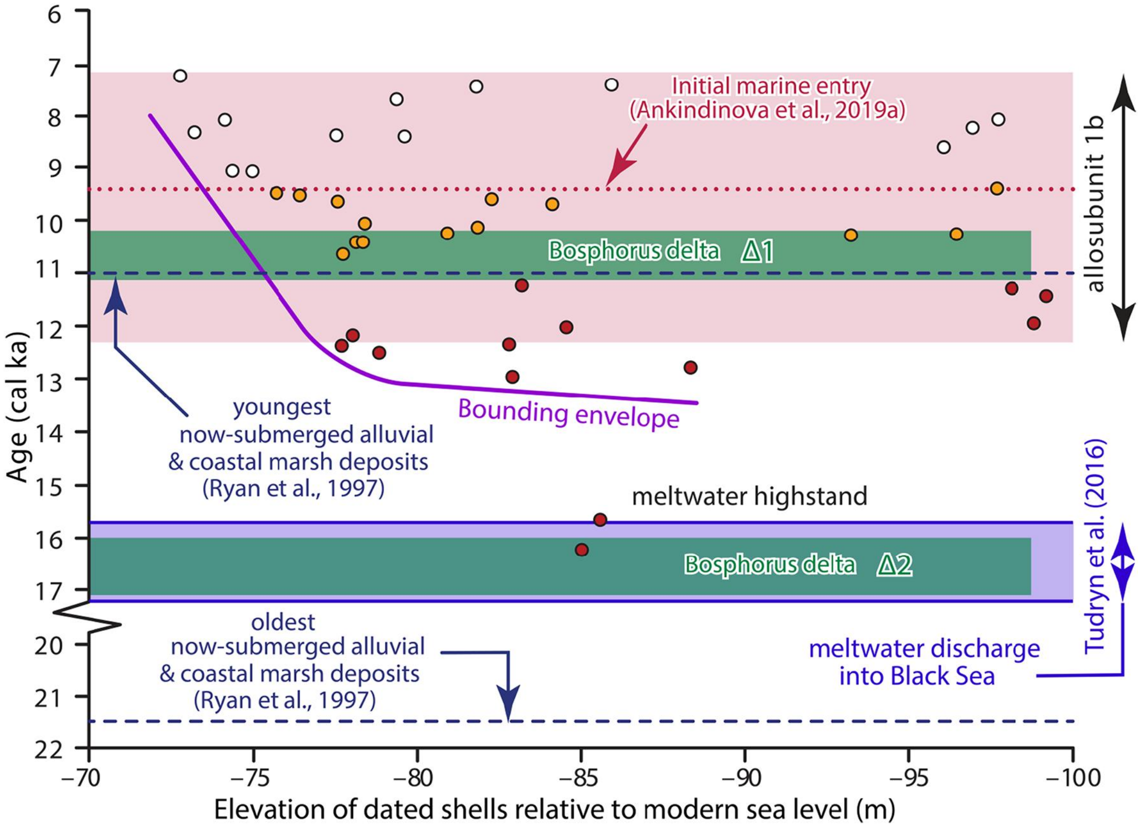
Initial marine entry
(Ankindinova et al., 2019a)
Bosphorus delta Δ1
allosubunit 1b
youngest
now-submerged alluvial
& coastal marsh deposits
(Ryan et al., 1997)
Bounding envelope
meltwater highstand
Bosphorus delta Δ2
Tudryn et al. (2016)
oldest
now-submerged alluvial
& coastal marsh deposits
(Ryan et al., 1997)
meltwater discharge
into Black Sea
Age (cal ka)
Elevation of dated shells relative to modern sea level (m)

Figure 22

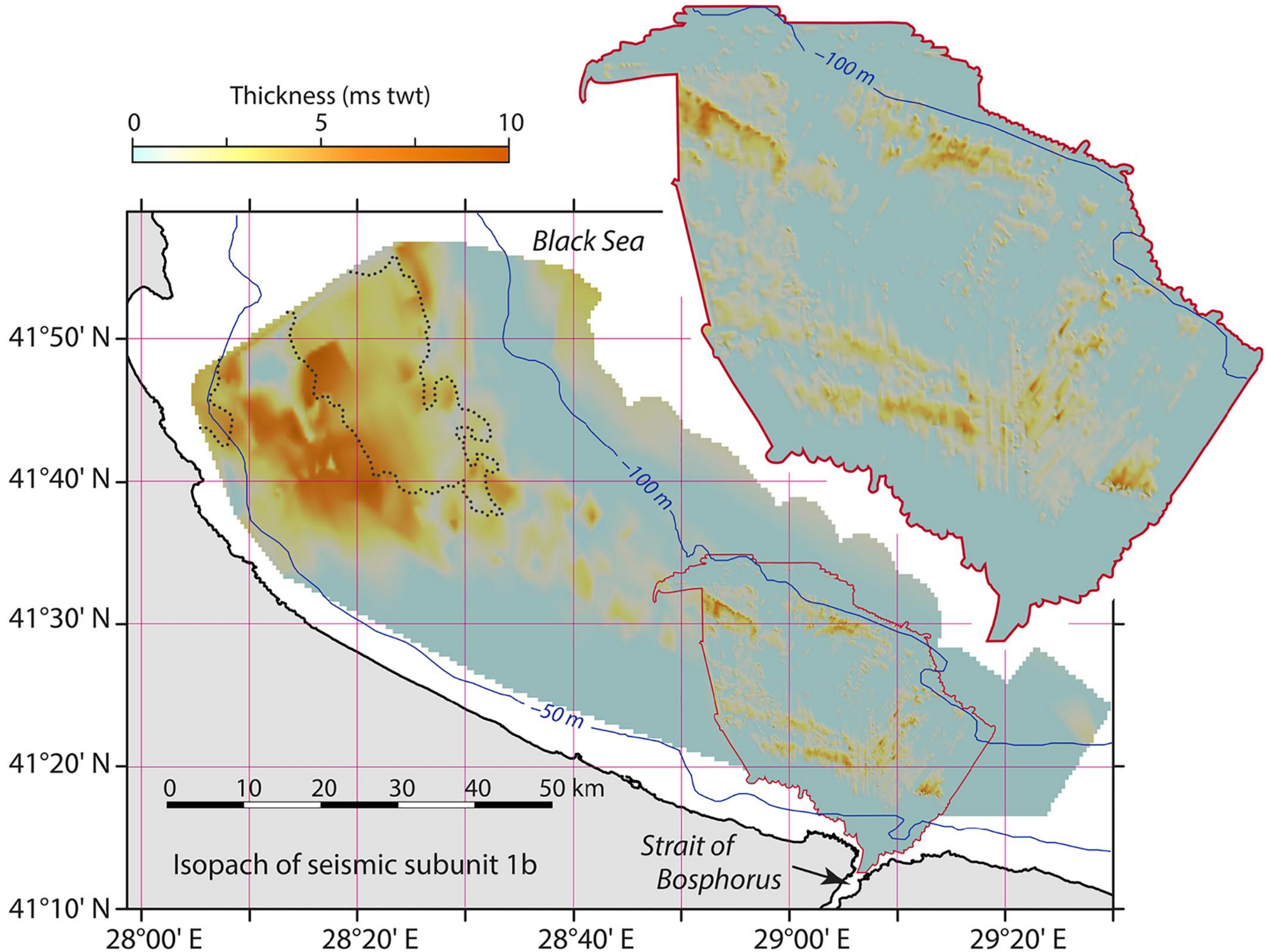
Thickness (ms twt)
0
5
10
Black Sea
−100 m
−100 m
−50 m
41°50' N
41°40' N
41°30' N
41°20' N
41°10' N
28°00' E
28°20' E
28°40' E
29°00' E
29°20' E
0
10
20
30
40
50 km
Isopach of seismic subunit 1b
Strait of
Bosphorus

Figure 23

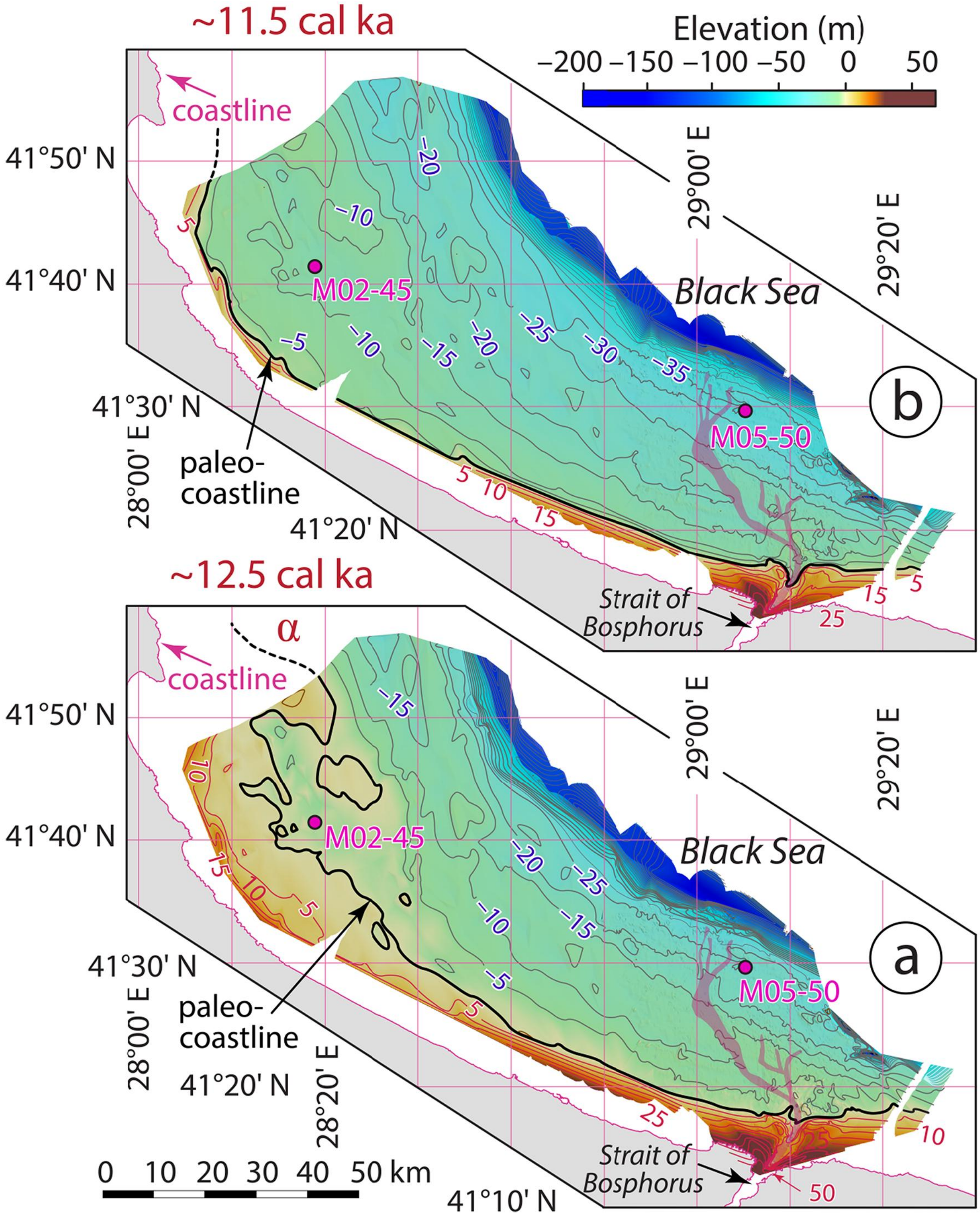

~11.5 cal ka
Elevation (m)
−200 −150 −100 −50 0 50
coastline
41°50' N
41°40' N
41°30' N
41°20' N
28°00' E
29°00' E
29°20' E
M02-45
M05-50
Black Sea
paleo-
coastline
Strait of
Bosphorus
b
~12.5 cal ka
α
28°20' E
41°10' N
a
0 10 20 30 40 50 km

Figure 24

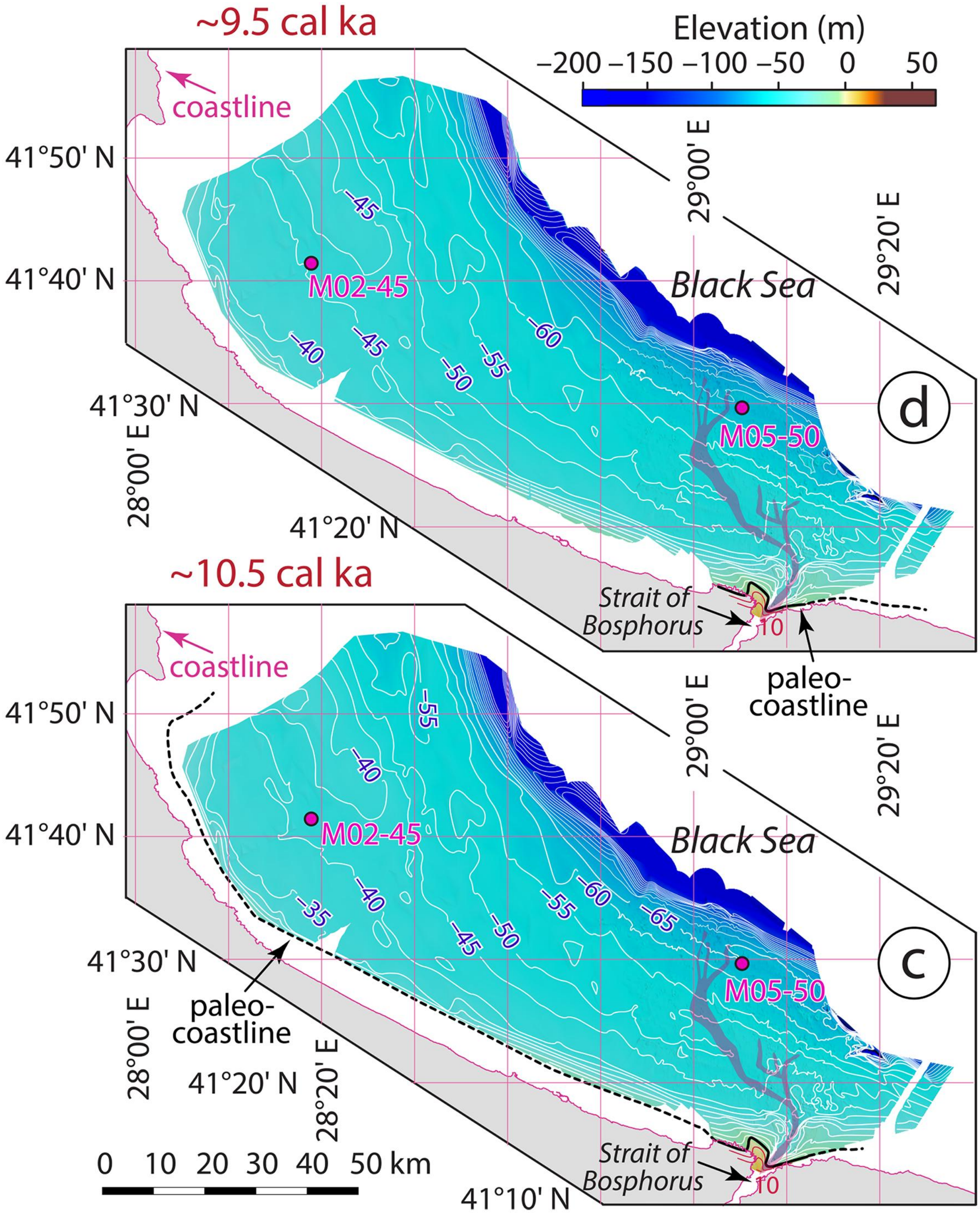
~9.5 cal ka
Elevation (m)
−200 −150 −100 −50 0 50
coastline
41°50' N
41°40' N
41°30' N
41°20' N
28°00' E
29°00' E
29°20' E
M02-45
M05-50
Black Sea
−45
−40
−45
−50
−55
−60
d
Strait of Bosphorus
10
paleo-coastline
~10.5 cal ka
coastline
41°50' N
41°40' N
41°30' N
41°20' N
41°10' N
28°00' E
28°20' E
29°00' E
29°20' E
M02-45
M05-50
Black Sea
−55
−40
−35
−40
−45
−50
−55
−60
−65
c
paleo-coastline
Strait of Bosphorus
10
0 10 20 30 40 50 km

Figure 25

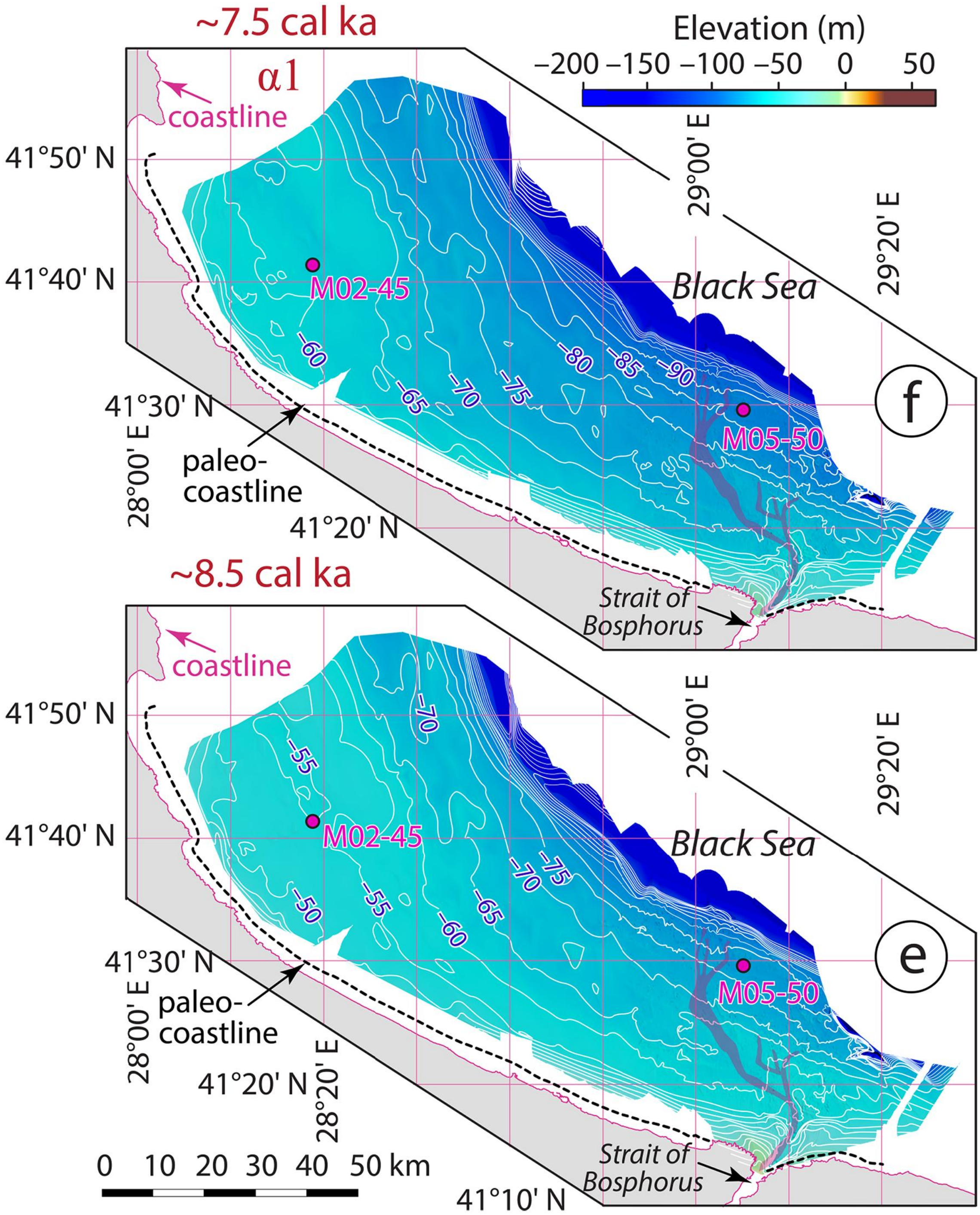
~7.5 cal ka
α1
Elevation (m)
−200 −150 −100 −50 0 50
coastline
41°50' N
41°40' N
41°30' N
41°20' N
28°00' E
29°00' E
29°20' E
M02-45
M05-50
Black Sea
−60
−65
−70
−75
−80
−85
−90
f
paleo-coastline
Strait of Bosphorus
~8.5 cal ka
coastline
41°50' N
41°40' N
41°30' N
41°20' N
41°10' N
28°00' E
28°20' E
29°00' E
29°20' E
M02-45
M05-50
Black Sea
−50
−55
−60
−65
−70
−75
e
paleo-coastline
Strait of Bosphorus
0 10 20 30 40 50 km

Figure 26

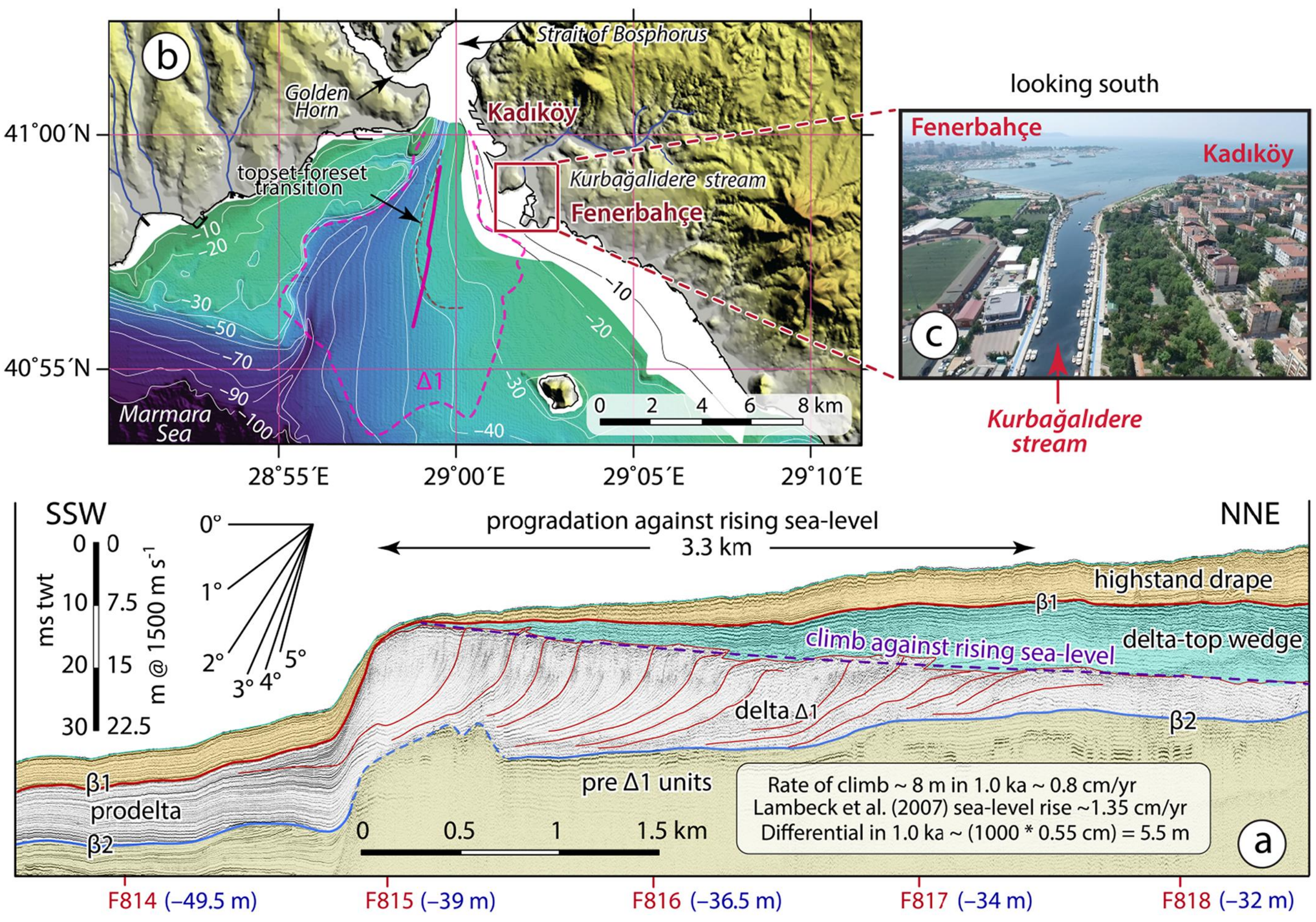
b
Strait of Bosphorus
Golden Horn
Kadıköy
Kurbağalıdere stream
Fenerbahçe
topset-foreset transition
41°00´N
40°55´N
28°55´E
29°00´E
29°05´E
29°10´E
Δ1
Marmara Sea
−10
−20
−30
−40
−50
−70
−90
−100
0 2 4 6 8 km
looking south
Fenerbahçe
Kadıköy
c
Kurbağalıdere stream
SSW
NNE
ms twt
m @ 1500 m s-1
0 10 20 30
0 7.5 15 22.5
0° 1° 2° 3° 4° 5°
progradation against rising sea-level
3.3 km
highstand drape
β1
climb against rising sea-level
delta-top wedge
delta Δ1
β2
pre Δ1 units
prodelta
0 0.5 1 1.5 km
Rate of climb ~ 8 m in 1.0 ka ~ 0.8 cm/yr
Lambeck et al. (2007) sea-level rise ~1.35 cm/yr
Differential in 1.0 ka ~ (1000 * 0.55 cm) = 5.5 m
a
F814 (−49.5 m)
F815 (−39 m)
F816 (−36.5 m)
F817 (−34 m)
F818 (−32 m)

Figure 27

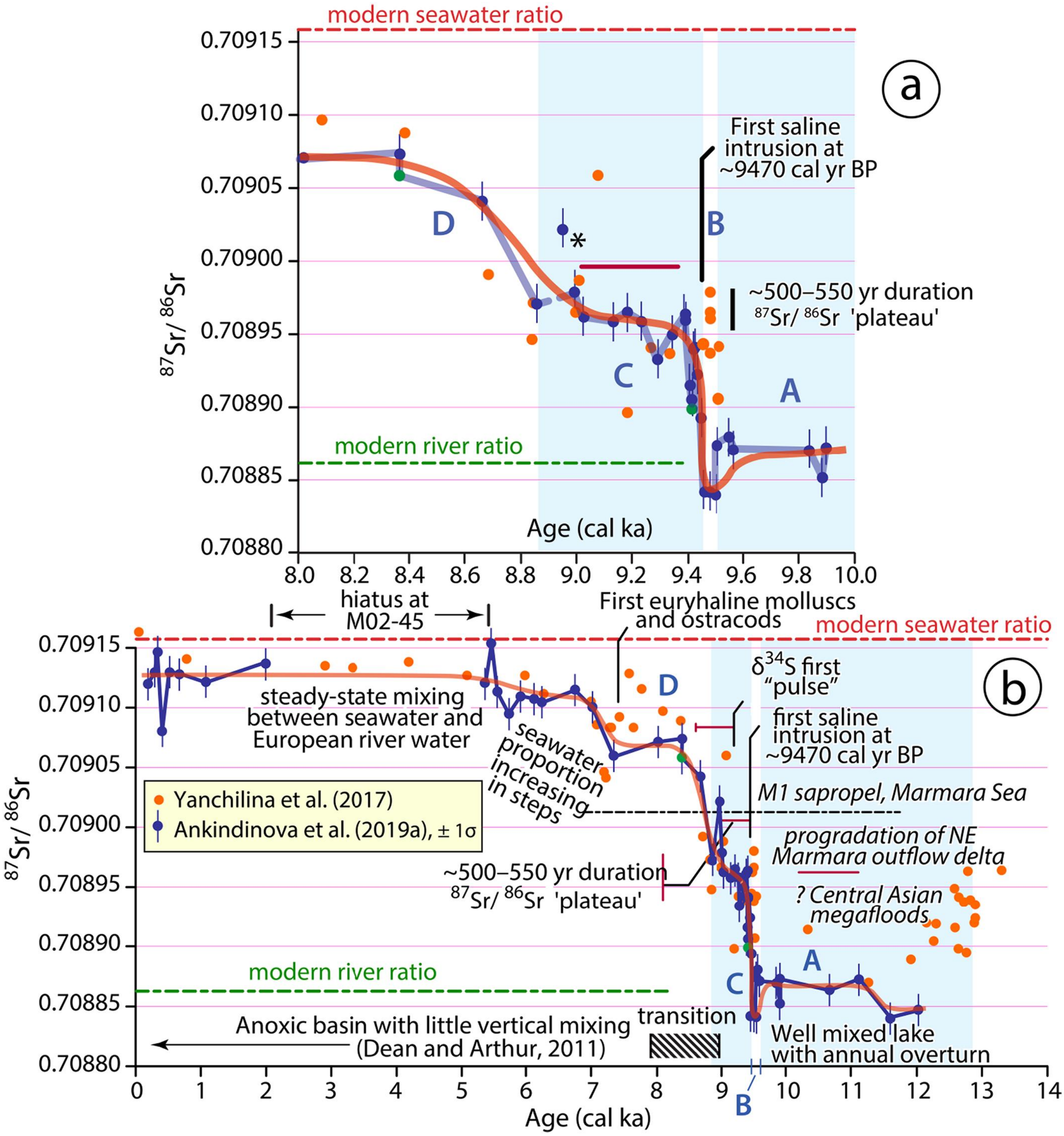

modern seawater ratio
a
First saline intrusion at ~9470 cal yr BP
D
B
*
~500–550 yr duration 87Sr/86Sr 'plateau'
C
A
modern river ratio
Age (cal ka)
87Sr/86Sr
0.70915
0.70910
0.70905
0.70900
0.70895
0.70890
0.70885
0.70880
8.0 8.2 8.4 8.6 8.8 9.0 9.2 9.4 9.6 9.8 10.0
hiatus at M02-45
First euryhaline molluscs and ostracods
modern seawater ratio
δ34S first "pulse"
b
steady-state mixing between seawater and European river water
seawater proportion increasing in steps
first saline intrusion at ~9470 cal yr BP
M1 sapropel, Marmara Sea
Yanchilina et al. (2017)
Ankindinova et al. (2019a), ± 1σ
progradation of NE Marmara outflow delta
~500–550 yr duration 87Sr/86Sr 'plateau'
? Central Asian megafloods
modern river ratio
Anoxic basin with little vertical mixing (Dean and Arthur, 2011)
transition
Well mixed lake with annual overturn
Age (cal ka)
0 1 2 3 4 5 6 7 8 9 10 11 12 13 14

Figure 28

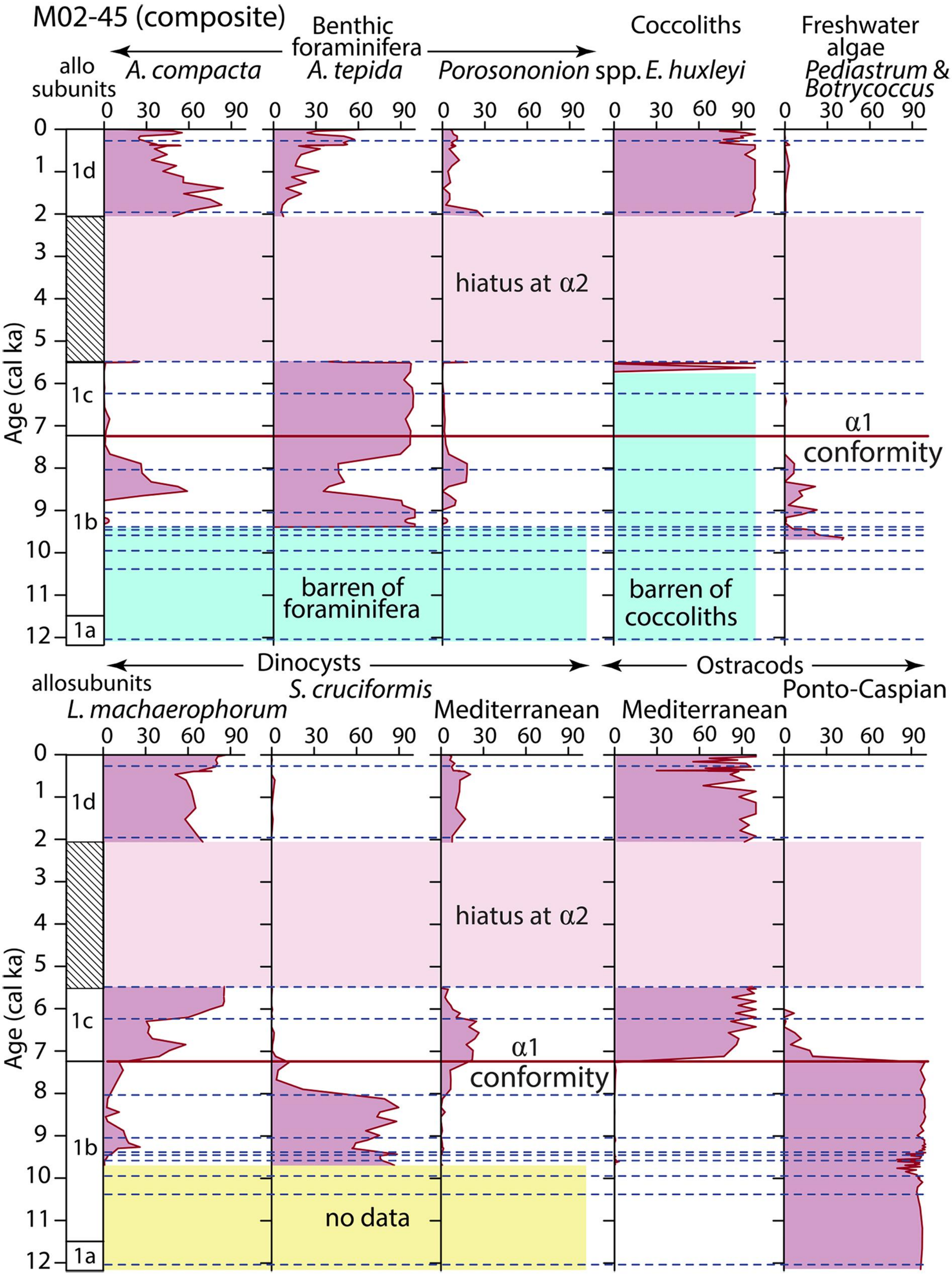
M02-45 (composite)
Benthic foraminifera
Coccoliths
Freshwater algae
allo subunits
A. compacta
A. tepida
Porosononion spp.
E. huxleyi
Pediastrum & Botrycoccus
Age (cal ka)
1d
1c
1b
1a
hiatus at α2
α1 conformity
barren of foraminifera
barren of coccoliths
Dinocysts
Ostracods
allosubunits
L. machaerophorum
S. cruciformis
Mediterranean
Mediterranean
Ponto-Caspian
no data

Figure 29

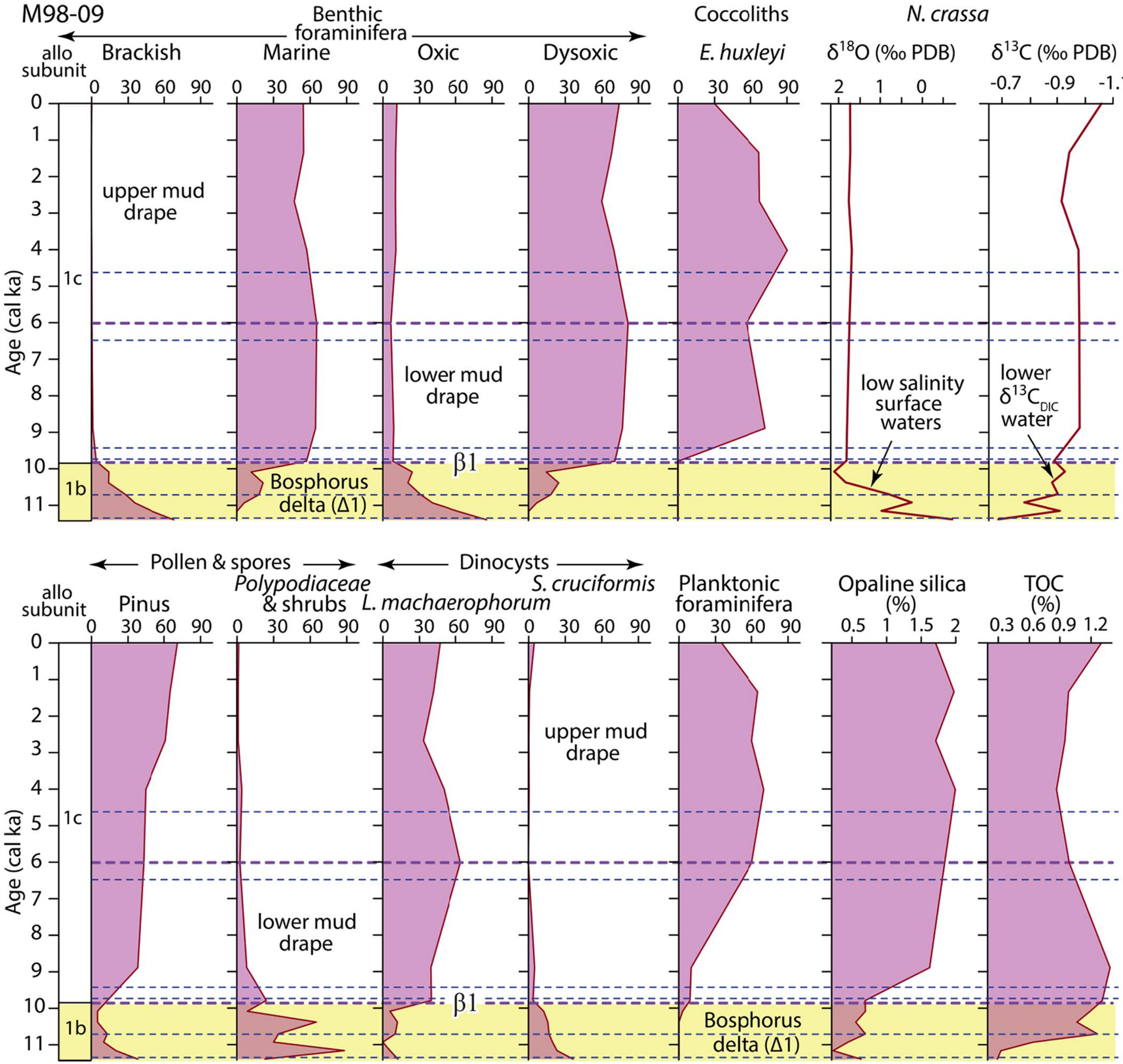
M98-09
Benthic foraminifera
Brackish
Marine
Oxic
Dysoxic
Coccoliths
E. huxleyi
N. crassa
δ18O (‰ PDB)
δ13C (‰ PDB)
allo subunit
Age (cal ka)
upper mud drape
lower mud drape
low salinity surface waters
lower δ13C DIC water
β1
Bosphorus delta (Δ1)
1c
1b
Pollen & spores
Pinus
Polypodiaceae & shrubs
Dinocysts
L. machaerophorum
S. cruciformis
Planktonic foraminifera
Opaline silica (%)
TOC (%)

Figure 30

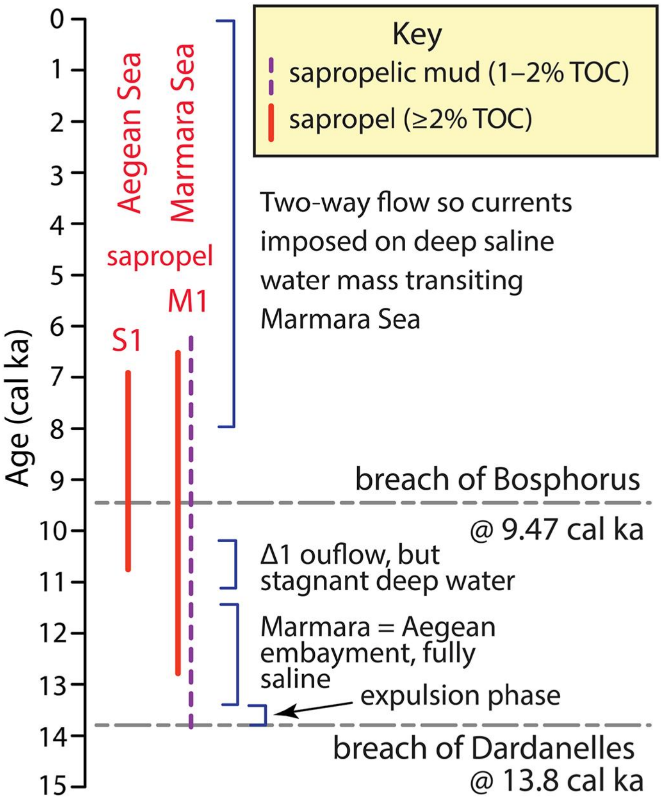

Key
sapropelic mud (1–2% TOC)
sapropel (≥2% TOC)
Aegean Sea
Marmara Sea
sapropel
S1
M1
Age (cal ka)
0
1
2
3
4
5
6
7
8
9
10
11
12
13
14
15
Two-way flow so currents imposed on deep saline water mass transiting Marmara Sea
breach of Bosphorus
@ 9.47 cal ka
Δ1 ouflow, but stagnant deep water
Marmara = Aegean embayment, fully saline
expulsion phase
breach of Dardanelles
@ 13.8 cal ka

Figure 31

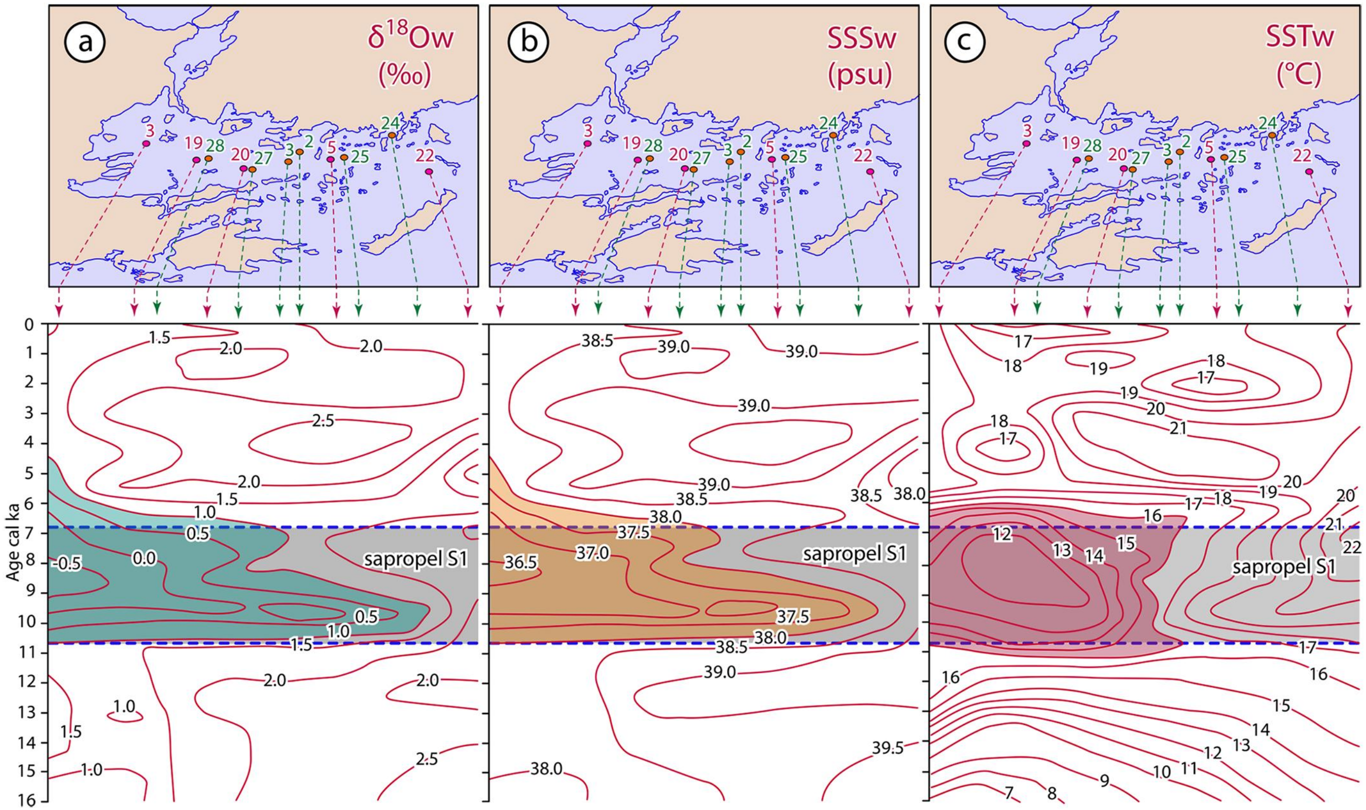
a
δ18Ow
(‰)
b
SSSw
(psu)
c
SSTw
(°C)
Age cal ka
sapropel S1
sapropel S1
sapropel S1

Figure 32

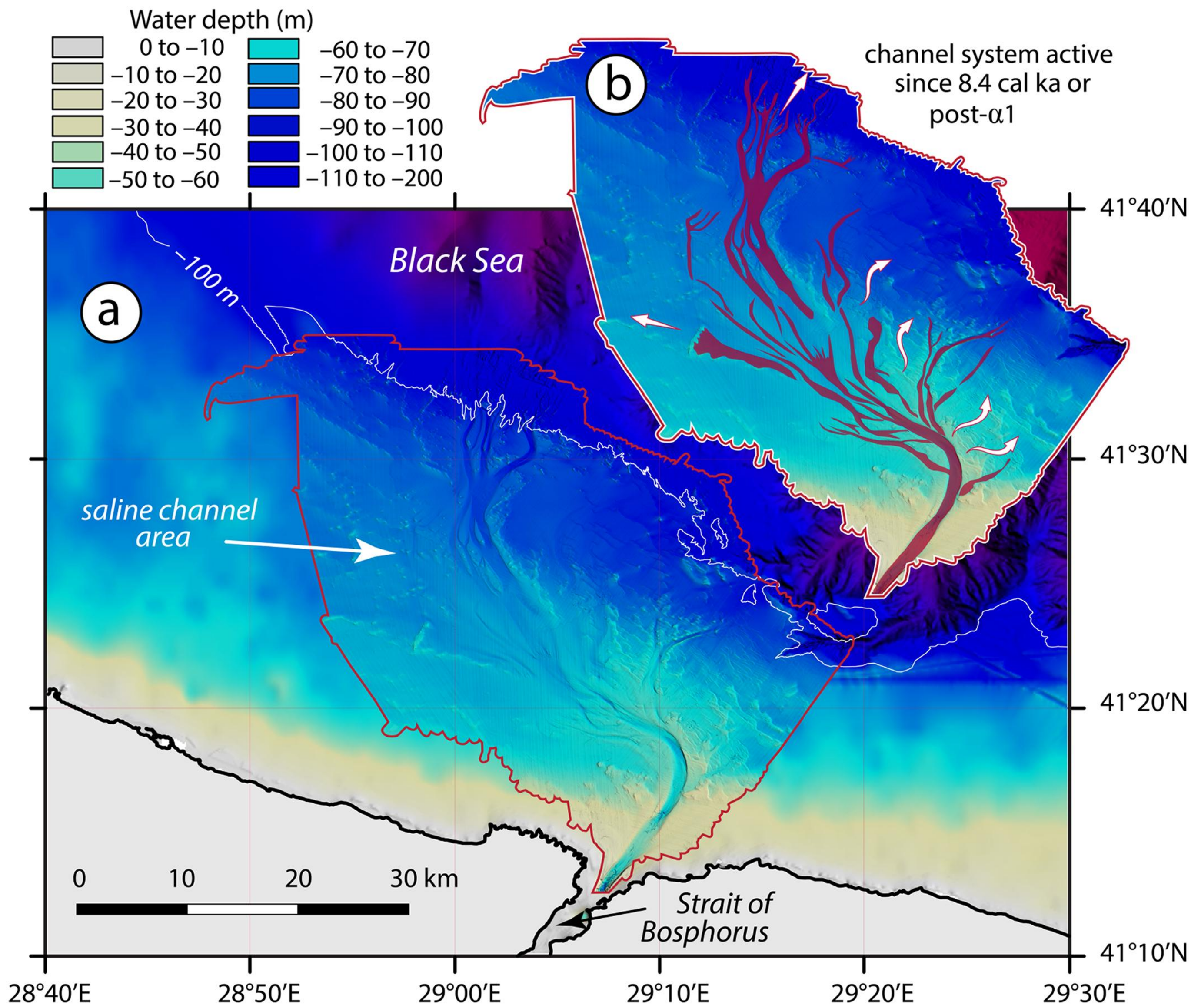

Water depth (m)
0 to −10
−10 to −20
−20 to −30
−30 to −40
−40 to −50
−50 to −60
−60 to −70
−70 to −80
−80 to −90
−90 to −100
−100 to −110
−110 to −200
b
channel system active since 8.4 cal ka or post-α1
a
−100 m
Black Sea
saline channel area
0
10
20
30 km
Strait of Bosphorus
41°40′N
41°30′N
41°20′N
41°10′N
28°40′E
28°50′E
29°00′E
29°10′E
29°20′E
29°30′E

Figure 33

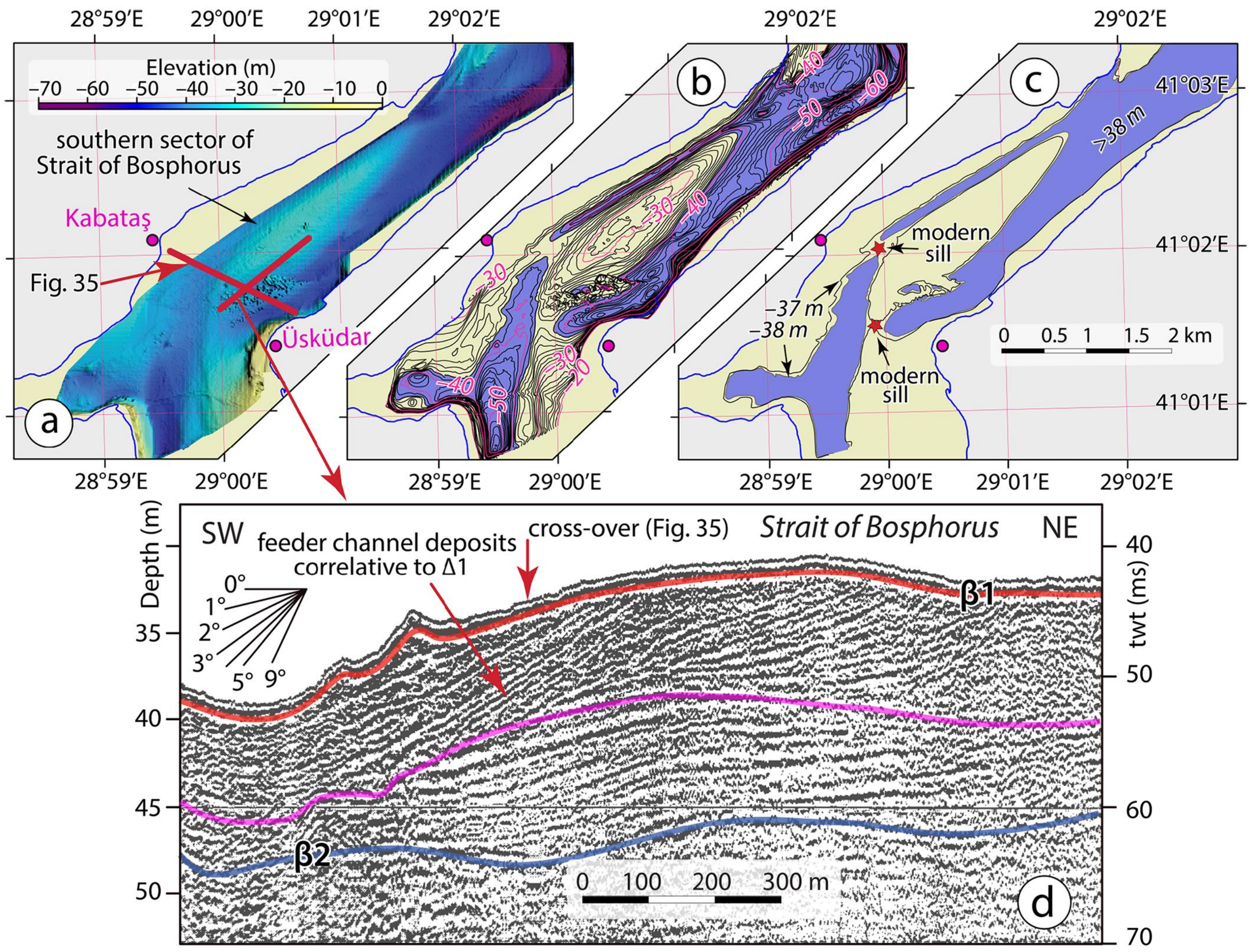

a
b
c
d
Elevation (m)
−70 −60 −50 −40 −30 −20 −10 0
southern sector of
Strait of Bosphorus
Kabataş
Üsküdar
Fig. 35
28°59′E
29°00′E
29°01′E
29°02′E
41°03′E
41°02′E
41°01′E
modern sill
modern sill
−37 m
−38 m
>38 m
0 0.5 1 1.5 2 km
SW
NE
Strait of Bosphorus
feeder channel deposits
correlative to Δ1
cross-over (Fig. 35)
β1
β2
Depth (m)
twt (ms)
0° 1° 2° 3° 5° 9°
0 100 200 300 m

Figure 34

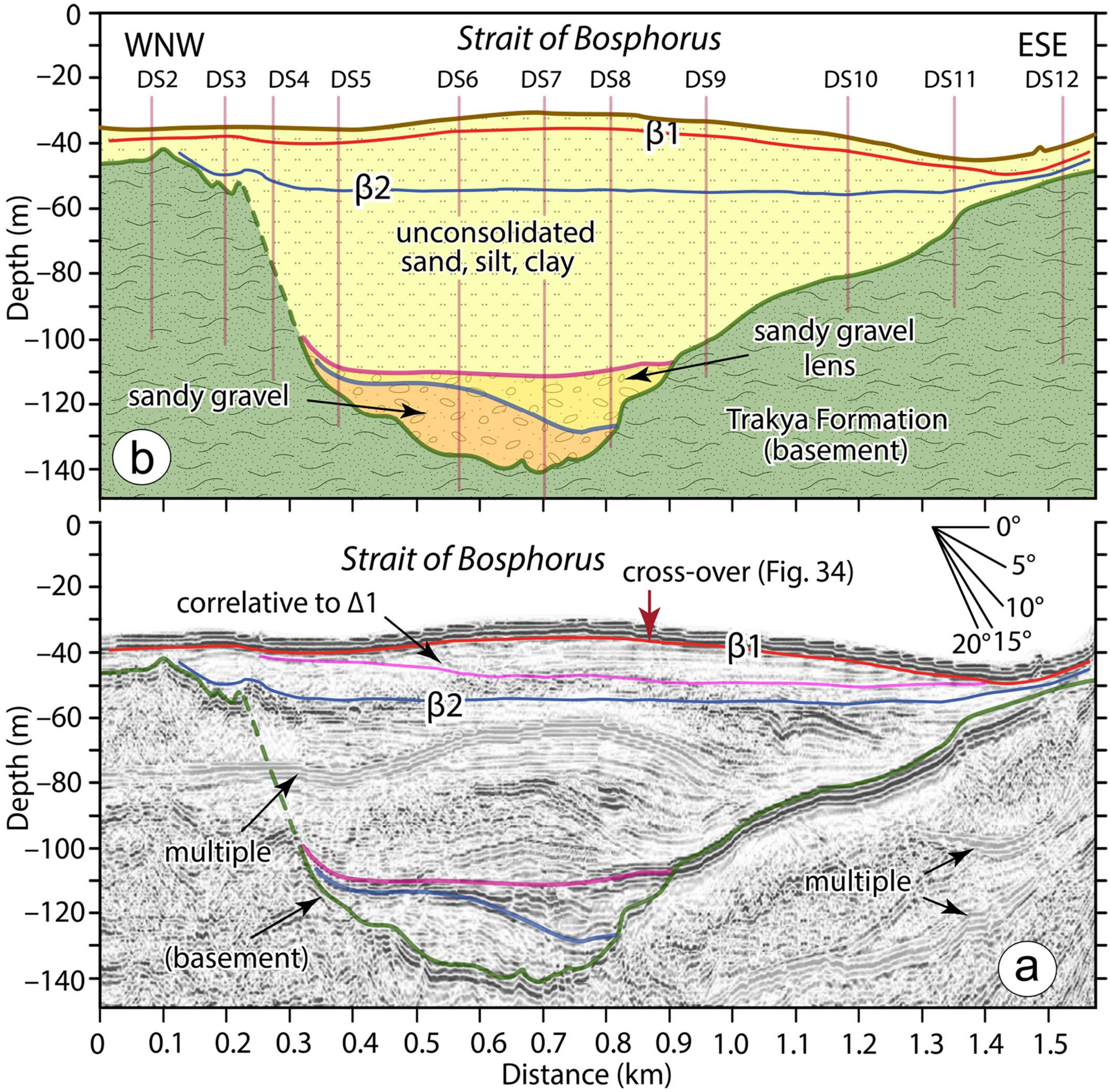

WNW
Strait of Bosphorus
ESE
DS2
DS3
DS4
DS5
DS6
DS7
DS8
DS9
DS10
DS11
DS12
β1
β2
unconsolidated sand, silt, clay
sandy gravel lens
sandy gravel
Trakya Formation (basement)
b
Depth (m)
Strait of Bosphorus
cross-over (Fig. 34)
correlative to Δ1
β1
β2
0°
5°
10°
20°15°
multiple
(basement)
multiple
a
Distance (km)

Figure 35

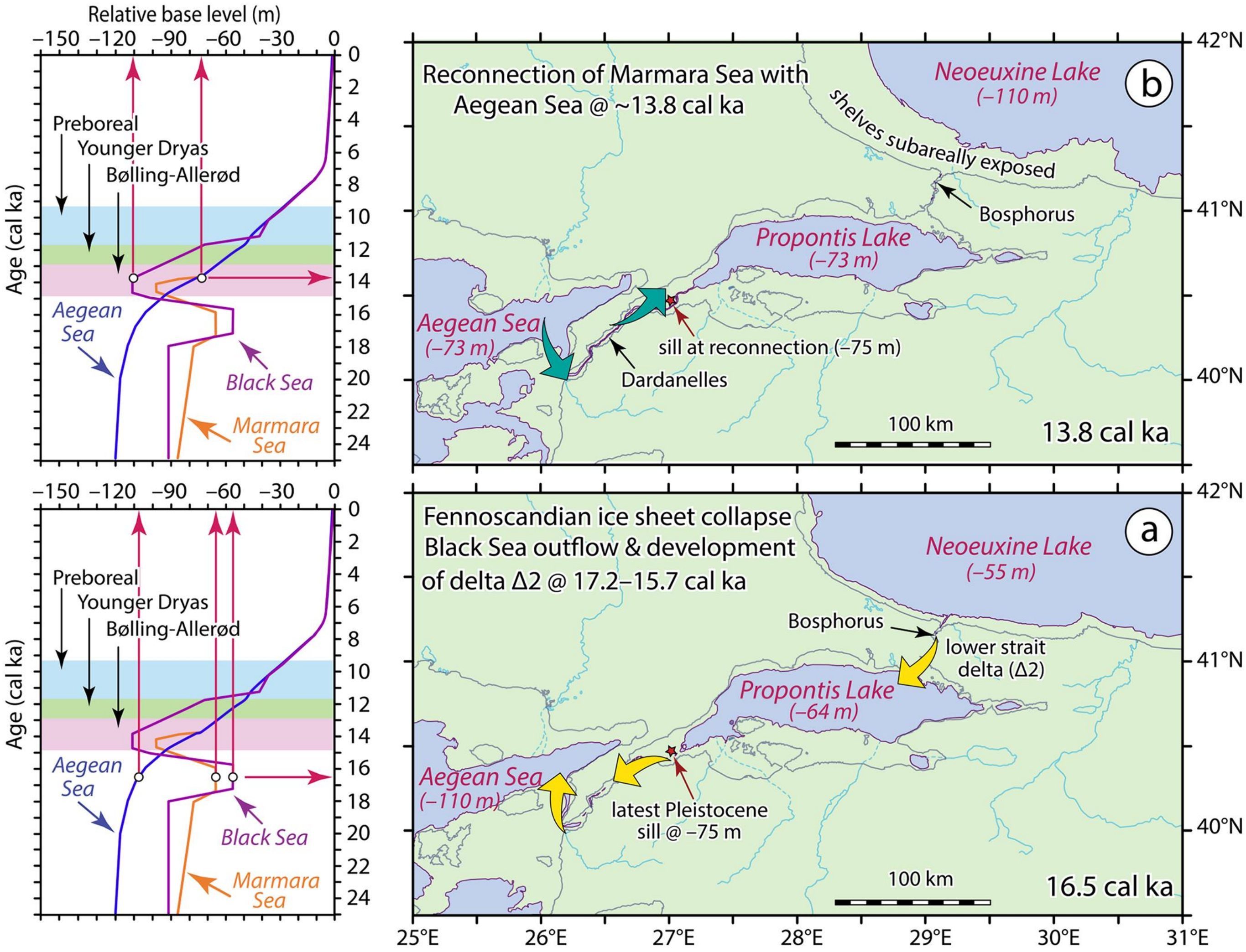
Relative base level (m)
Age (cal ka)
Preboreal
Younger Dryas
Bølling-Allerød
Aegean Sea
Black Sea
Marmara Sea
Reconnection of Marmara Sea with Aegean Sea @ ~13.8 cal ka
Neoeuxine Lake (−110 m)
shelves subareally exposed
Bosphorus
Propontis Lake (−73 m)
Aegean Sea (−73 m)
sill at reconnection (−75 m)
Dardanelles
100 km
13.8 cal ka
b
Fennoscandian ice sheet collapse Black Sea outflow & development of delta Δ2 @ 17.2–15.7 cal ka
Neoeuxine Lake (−55 m)
Bosphorus
lower strait delta (Δ2)
Propontis Lake (−64 m)
Aegean Sea (−110 m)
latest Pleistocene sill @ −75 m
100 km
16.5 cal ka
a

Figure 36

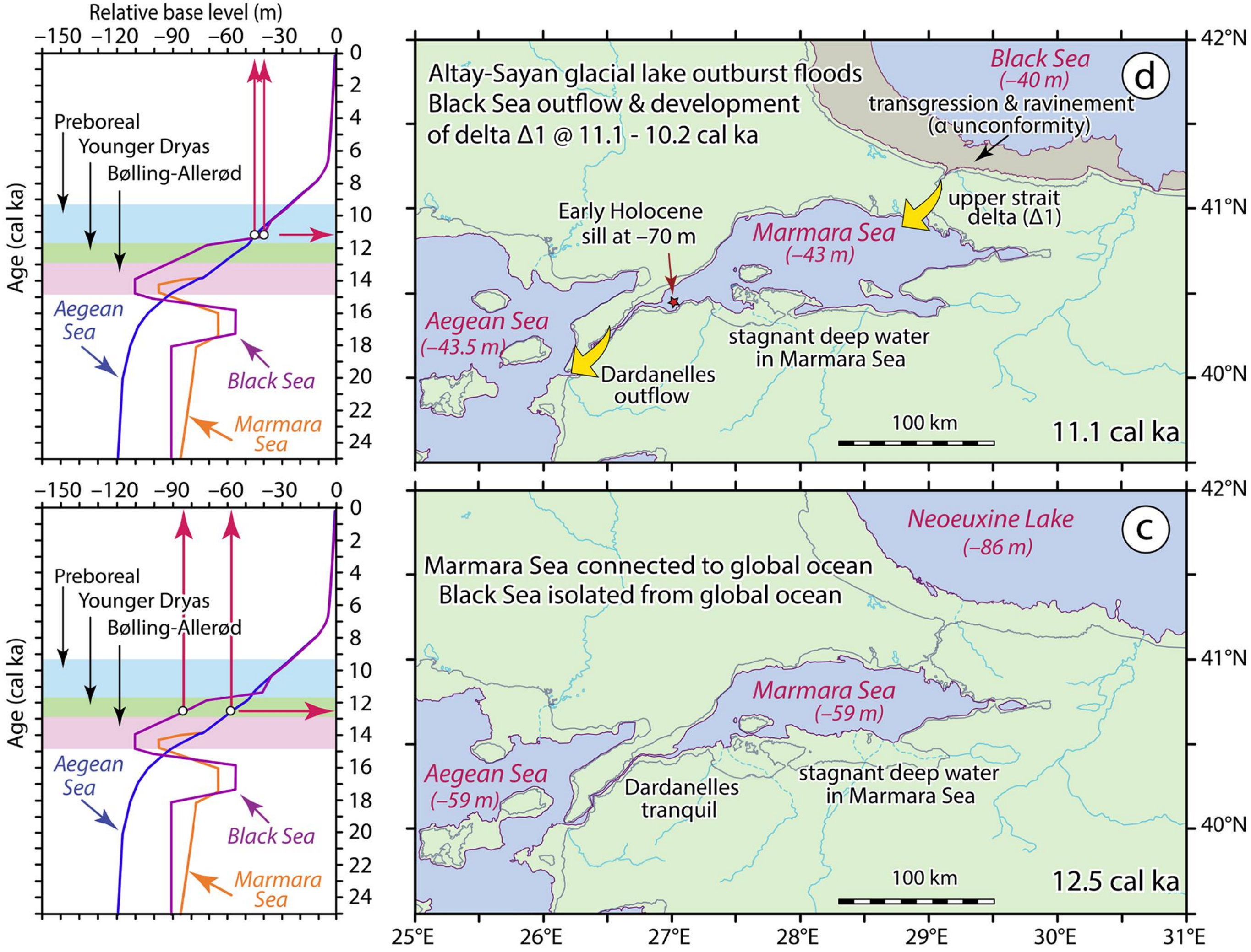
Relative base level (m)
−150 −120 −90 −60 −30 0
Age (cal ka)
Preboreal
Younger Dryas
Bølling-Allerød
Aegean Sea
Black Sea
Marmara Sea
Altay-Sayan glacial lake outburst floods
Black Sea outflow & development
of delta Δ1 @ 11.1 - 10.2 cal ka
Black Sea
(−40 m)
d
transgression & ravinement
(α unconformity)
upper strait
delta (Δ1)
Early Holocene
sill at −70 m
Marmara Sea
(−43 m)
Aegean Sea
(−43.5 m)
stagnant deep water
in Marmara Sea
Dardanelles
outflow
100 km
11.1 cal ka
Neoeuxine Lake
(−86 m)
c
Marmara Sea connected to global ocean
Black Sea isolated from global ocean
Marmara Sea
(−59 m)
Aegean Sea
(−59 m)
Dardanelles
tranquil
stagnant deep water
in Marmara Sea
100 km
12.5 cal ka
25°E 26°E 27°E 28°E 29°E 30°E 31°E
42°N 41°N 40°N

Figure 37

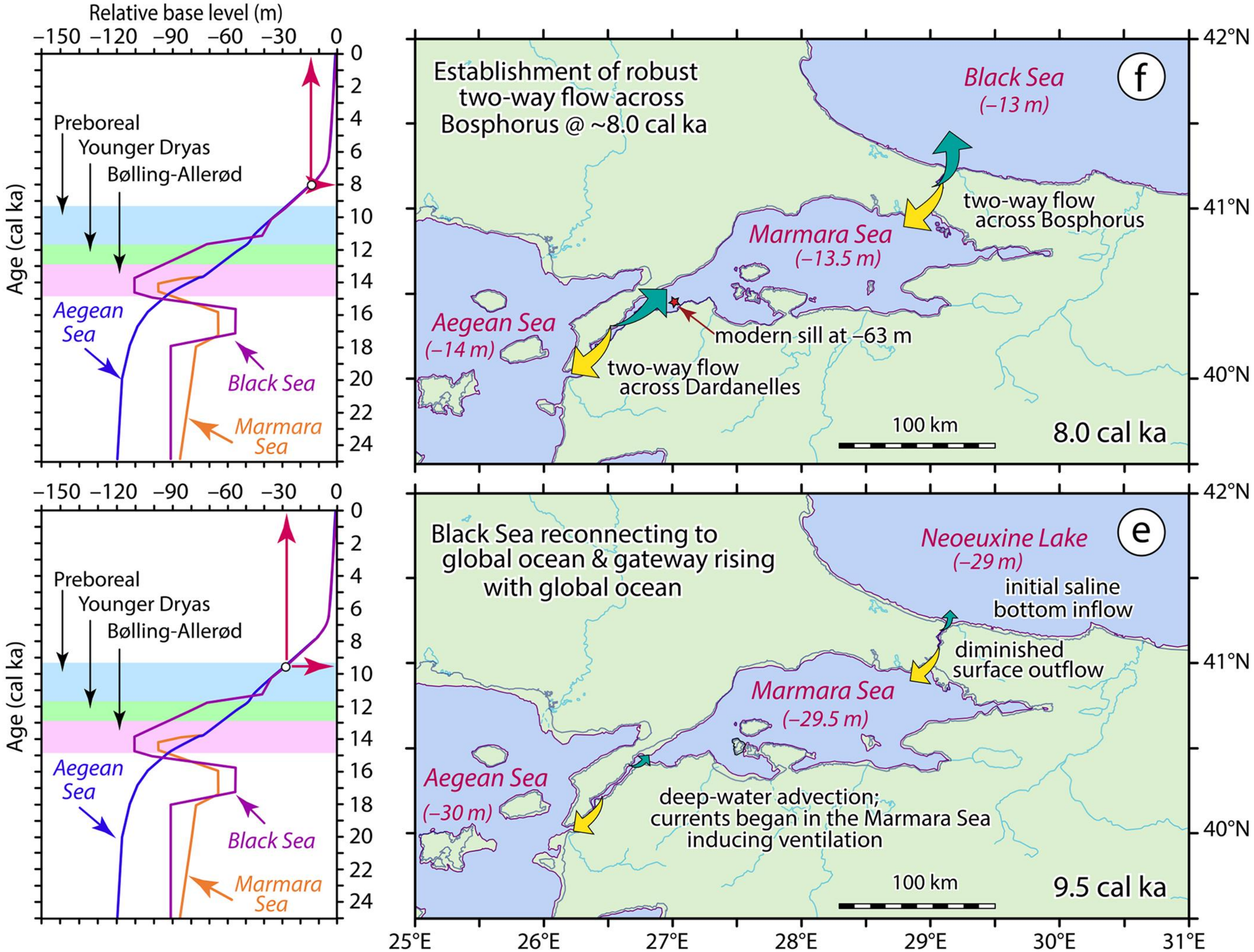

Relative base level (m)
−150 −120 −90 −60 −30 0
Age (cal ka)
Preboreal
Younger Dryas
Bølling-Allerød
Aegean Sea
Black Sea
Marmara Sea
Establishment of robust two-way flow across Bosphorus @ ~8.0 cal ka
f
Black Sea (−13 m)
two-way flow across Bosphorus
Marmara Sea (−13.5 m)
Aegean Sea (−14 m)
modern sill at −63 m
two-way flow across Dardanelles
100 km
8.0 cal ka
Black Sea reconnecting to global ocean & gateway rising with global ocean
e
Neoeuxine Lake (−29 m)
initial saline bottom inflow
diminished surface outflow
Marmara Sea (−29.5 m)
Aegean Sea (−30 m)
deep-water advection; currents began in the Marmara Sea inducing ventilation
100 km
9.5 cal ka
25°E 26°E 27°E 28°E 29°E 30°E 31°E
42°N 41°N 40°N

Figure 38